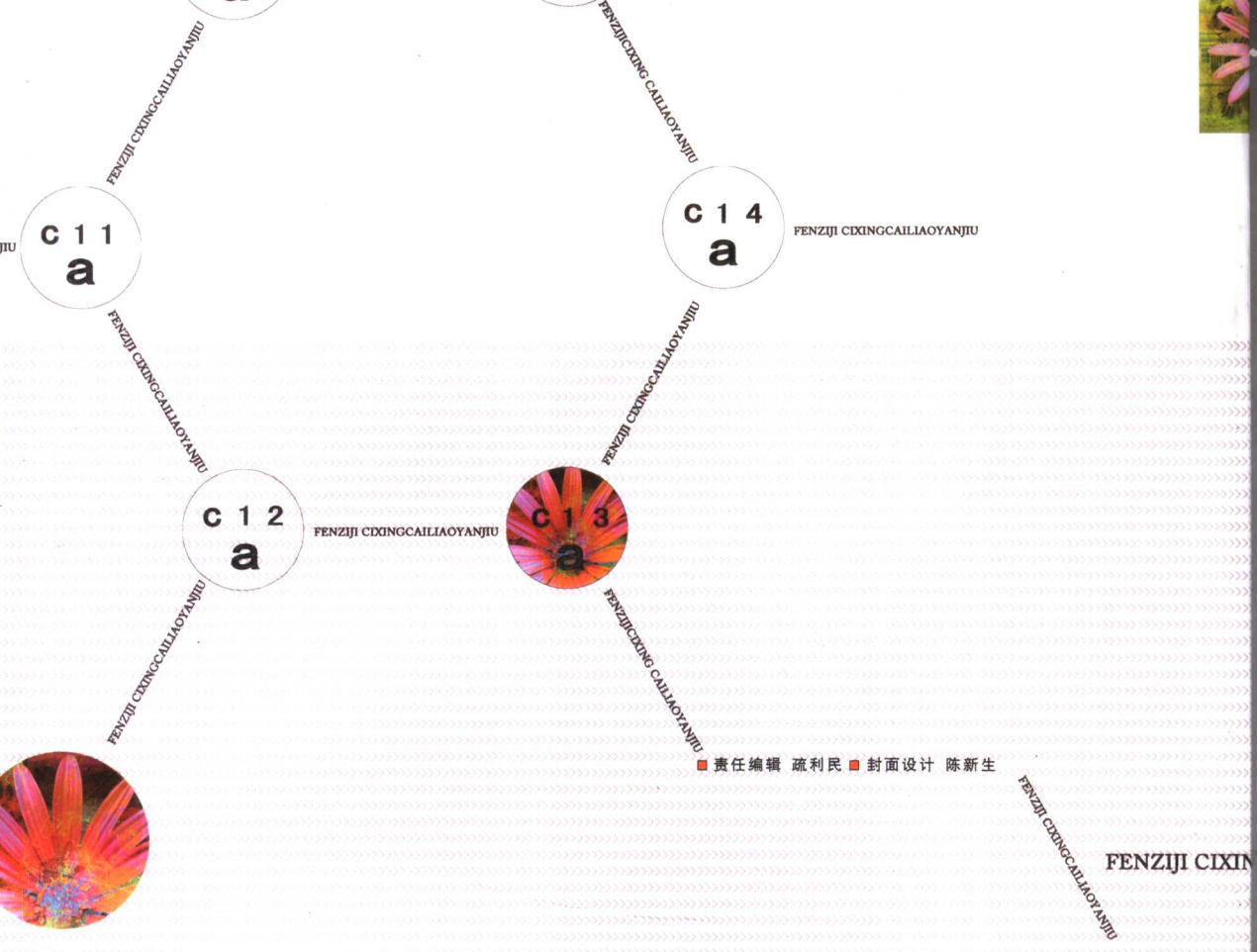


陈友存 | 著

FENZIJI CIXINGCAILIAOYANJIU

分子基磁性材料研究

合肥工业大学出版社



■ 责任编辑 疏利民 ■ 封面设计 陈新生

ISBN 7-81093-508-9

9 787810 935081 >

ISBN 7-81093-508-9/ TM · 5

定价：25.00 元

本书由安庆师范学院出版基金资助出版

分子基磁性材料研究

陈友存　著

合肥工业大学出版社

图书在版编目(CIP)数据

分子基磁性材料研究/陈友存著. —合肥:合肥工业大学出版社,2006.11

ISBN 7-81093-508-9

Ⅰ.分… Ⅱ.陈… Ⅲ.磁性材料—研究 Ⅳ.TM271

中国版本图书馆 CIP 数据核字(2006)第 139302 号

分子基磁性材料研究

陈友存 著　　责任编辑 疏利民

出　版	合肥工业大学出版社	版　次	2006 年 11 月第 1 版
地　址	合肥市屯溪路 193 号	印　次	2006 年 11 月第 1 次印刷
邮　编	230009	开　本	710×1000　1/16
电　话	总编室:0551-2903038	印　张	12.5
	发行部:0551-2903198	字　数	204 千字
网　址	www.hfutpress.com.cn	印　刷	中国科学技术大学印刷厂
E-mail	press@hfutpress.com.cn	发　行	全国新华书店

ISBN 7-81093-508-9/TM·5　　定价:25.00 元

如果有影响阅读的印装质量问题,请与出版社发行部联系调换。

前　言

由于电子器件、电子线路、信息存储介质等材料科学迅速发展的需要，分子组装磁性材料（分子基磁体）的研究成为当代科学研究中最具挑战性的前沿领域之一。分子基磁体在分子水平上的热开关、光开关、新型存储介质等材料方面具有潜在的应用前景。世界各国，特别是美、法、德、日、英等发达国家对该领域的研究十分重视，并投入大量的人力和物力开展该领域的研究工作。分子基磁体的分子设计、合成、性质研究和功能性开发等方面的研究工作已成为当前化学家、物理学家、材料科学家等共同感兴趣的焦点。

我们对分子基磁性材料的研究得到两项国家自然科学基金、安徽省科技厅“十五”科技攻关项目和安徽省教育厅自然科学基金重点项目的资助，在该领域研究中顺利地完成了课题计划，取得了一定的成果，并获得安徽省高等学校省级优秀科技成果二等奖。

本文集收录了我在此研究领域中的主要科研成果，分为三个专题，第一专题：二维磁性可调配位聚合物；第二专题：自旋双稳分子磁体；第三专题：分子自旋梯磁体。共计收录了25篇专题学术论文，已全部在国内外出版物上公开发表。在此研究领域中，课题组研究成员任小明教授、刘光祥副教授、徐衡副教授等做了大量研究工作，在此表示感谢！

需要说明的是，本文集收录了本人作为第一作者或通迅联系人发表的论文，并未收录该课题组在此研究领域的全部成果以及本人在其他研究领域的成果。

出版本文集的目的，一是总结本人此研究领域中的成果，为学校学科建设做出贡献，二是由于本人与众多的同行相比，相距甚远，以便向众多同行请教。

本文集收录的论文和文集的编辑难免存在错误，不当之处，欢迎读者批评指正，不胜感谢。

本文集的出版得到安庆师范学院学科建设基金的资助，在此表示感谢！

作　者

2006年9月8日于安庆师范学院

目 录

前 言 …… (1)

第一专题

二维磁性可调配位聚合物

硫氮西夫碱配体及其金属配合物的合成与表征 …… (3)

双金属层状配位聚合物{[NO_2BzQI][MCr(ox)$_3$]}$_\infty$的合成、光谱表征和磁性研究 …… (7)

双金属层状配位聚合物{[ML][$Fe^{II}Fe^{III}$(ox)$_3$]·1.5H_2O}$_\infty$的合成和波谱表征…… (14)

自旋交叉配合现象与分子电子器件…… (22)

一种新的席夫碱配合物的合成、结构和磁性研究 …… (31)

配位聚合物{[CoL]$Fe^{II}Fe^{III}$(ox)$_3$·1.5H_2O}$_\infty$的合成、波谱表征和磁学性质…… (33)

双金属层状配位聚合物{[ML][$Fe^{II}Fe^{III}$(ox)$_3$]·H_2O}$_\infty$的合成和波谱表征…… (42)

多维分子基铁磁体 $Co(phen)_3[LiFe(ox)_3]$的合成与光谱表征 …… (50)
基于席夫碱配合物的分子磁体:合成、结构和磁学性质…… (56)

第二专题

自旋双稳分子磁体

Molecule - Based Magnets with 1D Chain Structure of Bifurcated H-Bonding: Syntheses, Structure, and Magnetic Properties[1] …… (67)

Spontaneous magnetization below 7.7 K based on an extended 3 - D H-bonding network material: synthesis, crystal structure and magnetic properties …… (77)

The 1 : 2 Bis(maleonitriledithiolato)- palladium(II) Complex of the N -(2 - fluoro - 4 - bromobenzyl) Pyridinium Cation …… (89)

3D H-bonding Networks Self - assembly from Pyridinium Derivatives and Bis (maleonitriledithiolato) Zincate(II) …… (96)

两种新型电荷转移盐的合成和光谱研究 …… (107)

β - Phase of 1 -(4 - bromobenzyl)Pyridinium Bis(1,2 - dicyanoethene - 1,2 - dithiolato - κ^2S,S')Platinate(III) …… (114)

An Ion - pair Complex Composed of Two N -(4 - Cyanobenzyl)Quinolinium Cations, Two 7,7,8,8 - Tetracyanoquinodimethane Anions and One neutral 7,7,8,8 - tetracyanoquinodimethane Molecule …… (121)

Mixed - valence Molecular Magnets Based on $[TCNQ]_3^{2-}$ Building Block: Structures, Magnetic Properties and DFT Analyses …… (127)

具有分子双稳性的一维自由基磁相变材料的研究 …… (129)

Mixed-valence Molecular Magnets Based on $[TCNQ]_3^{2-}$ Building Block: Structures, Magnetic Properties and DFT Analyses …… (138)

第三专题

分子自旋梯磁体

八面体配合物取代反应的反应动力学 …… (155)

双-(2,2′-联吡啶)和二硫烯钌(Ⅱ)混配配合物合成、光谱表征和电化学性质 …… (164)

分子基磁体[NCBzPy][$Ni(dmit)_2$]的合成、表征和磁学性质 …… (170)

Self - assembly from 1D to 2D Molecular Magnets Based on $[Ni(dmit)_2]^-$ Building Blocks: Structures, Magnetic Properties and Spin Dimer Analyses …… (175)

一维链状配合物[BrBzPy][$Ni(dmit)_2$]的合成和红外光谱研究 …… (177)

Molecular spin ladders self - assembly from $[Ni(dmit)_2]^-$ building blocks: Syntheses, structures and magnetic properties …… (184)

第一专题

二维磁性可调配位聚合物

具有层状结构的化合物是备受材料学家青睐的物质之一。通过层间插入功能性分子，可赋予材料多功能性。我们开展了由草酸根桥连的、具有层状结构的一类分子基磁性材料的研究工作，草酸根具有独特的分子结构，可与过渡金属离子形成具有二维层状结构的配位聚合物。这类层状配位聚合物的磁性是可调的，即通过改变填充在阴离子层间的阳离子就能获得分子基铁磁体、亚铁磁体以及倾斜的反铁磁体；虽然这类分子基磁体的临界温度（T_c）较低（5K 到 44K 之间），但是矫顽力的大小可以从小于 10Oe 到大于 16kOe。人们对这类层状结构的配位聚合物的研究，仅限于阳离子是有机阳离子和$[FeCp2^*]^+$、$[CoCp2^*]^+$等金属茂类阳离子，而上述阳离子分子间只有弱的 van de Waals 力，因而限制了提高层状分子基磁体的维数。根据分子场理论，提高分子基材料的维数是提高 T_c 的有效途径之一。基于这种思想，我们已合成金属配合物阳离子 ML^+（其中 $M=Co^{2+}$，Ni^{2+}，Cu^{2+}等；L＝水杨醛和等摩尔的二乙撑三胺缩合的 Schiff 碱）。由于配体 L 上的活泼 H 原子有可能与草酸根上的 O 原子形成氢键，从而有望实现将此类分子基磁体的维数从二维扩展到三维，达到提高其 T_c 值的目的。上述工作在本部分中收录了发表的学术论文 9 篇，其中被 SCI 收录 4 篇。

硫氮西夫碱配体及其金属配合物的合成与表征

摘 要：合成了 1,7-二(2′-苯甲酰)-1,4,7-三氧庚烷双缩肼基二硫代甲酸苄酯西夫碱配体及其 Cu(Ⅱ),Ni(Ⅱ),Zn(Ⅱ)的配合物，并通过元素分析、IR 和 UV-vis 对其进行了表征。

关键词：西夫碱；过渡金属配合物；合成；表征

近年来，二硫代甲酸衍生物的西夫碱及其金属配合物由于具有抗菌、抗病毒和抗癌活性[1,2]引起了人们的极大兴趣。合成与检测此类西夫碱配合物对于寻求更高活性的抗癌药物有着重要意义，也成为配位化学工作者的研究热点[3,4]。我们合成了未见文献报道的 1,7-二(2′-苯甲酰)-1,4,7-三氧庚烷双缩肼基二硫代甲酸苄酯西夫碱配体(简记为 H_2L)及其 Cu(Ⅱ),Ni(Ⅱ),Zn(Ⅱ)的配合物，研究了它们的组成，IR 和 UV-vis 光谱性质以及配位模式。

1. 实验部分

1.1 仪器与试剂

PE-2400CHN 型自动元素分析仪；美国 Nicolet FT-IR 170SX 型傅里叶变换红外光谱仪(KBr 压片)；日本岛津 UV-260 型紫外可见分光光度计。1,7-二(2′-苯甲酰)-1,4,7-三氧庚烷按文献[5]方法合成，物理性质和文献值一致。所用其他试剂均为分析纯。

1.2 配体(H_2L)及配合物(ML)的合成

H_2L 的合成是在电磁搅拌下，将肼基二硫代甲酸苄酯 3.96g(20mmol)的无水乙醇溶液滴加到 1,7-二(2′-苯甲酰)-1,4,7-三氧庚烷 3.53g(10mmol)的无水乙醇溶液中，回流 3h，得黄色沉淀，趁热过滤，用热无水乙醇洗沉淀至洗涤液颜色很浅，干燥后即得黄色产物 H_2L 6.29g，产率 84.1%，m. p. 182℃。

ML 的合成将 $NiCl_2 \cdot 6H_2O$ 2.38g(10mmol)的乙醇溶液滴加到含等摩尔的 H_2L 乙醇-DMF 溶液($V_{乙醇} : V_{DMF} = 1 : 5$)中，回流即得棕色晶状固体，趁热过滤，用热乙醇洗涤、干燥，得配合物 NiL 6.56g。将沉淀溶解在 THF 中，室温缓慢挥发溶剂后得到 NiL 配合物(棕黑色单晶)。同法合成了配合物 CuL(红色单晶)和 ZnL(淡黄色单晶)。

2. 结果与讨论

H_2L 几乎不溶于水、甲醇和乙醇，但能溶于 DMF，DMSO，二氯甲烷和 THF 等试剂。NiL，CuL 和 ZnL 三种配合物都能培养出单晶，NiL 和 ZnL 配合物单晶在空气中稳定，但 CuL 配合物单晶在空气中风化。配合物晶体结构测定工作仍在继续。

实验结果列于表 1。从表 1 可以看出 Ni(Ⅱ)，Cu(Ⅱ)和 Zn(Ⅱ)与四齿配体 H_2L 形成 $mol_M : mol_L = 1 : 1$ 的配合物。元素分析结果与理论计算值一致。

表 1 产物的分析结果

Comp	Analysis(%)(Calcd)			IRυ(cm^{-1})				产率
	C	H	N	K—H	C=O	C=N	C=S	(%)
H_2L	54.7(55.2)	3.9(4.3)	8.3(8.0)	3112	1598	1522	1096	84.1
NiL	55.9(55.8)	4.4(4.7)	8.2(7.7)		1596	1496		95.0
CuL	55.6(55.5)	4.1(4.4)	7.4(7.6)		1597	1485		94.3
ZnL	54.3(55.5)	4.0(4.7)	7.1(7.6)		1597	1477		96.1

在合成西夫碱 H_2L 金属配合物时发现，H_2L 与金属离子配位反应速率与金属离子有关。Zn(Ⅱ)的反应速率比 Ni(Ⅱ)和 Cu(Ⅱ)快。

配合物的红外光谱很相似，各峰位移亦不大，但与配体 H_2L 的红外光谱有很大差异。有关振动频率及归属见表 1。在 H_2L 的红外光谱中，观察到了 N－H 和 C＝S 吸收带，在 2750cm^{-1}附近未见 S－H 吸收。而配合物 ML 的红外光谱中，N－H 和 C＝S 带消失，说明西夫碱 H_2L 在固态时主要以酮式结构存在。而 H_2L 与金属离子配位后烯醇结构比较稳定。H_2L 两种互变异构和配合物配位模式如图 1 所示。比较 H_2L 和 ML 的红外光谱，发现 C＝N 频率有下列规律：H_2L＞NiL＞CuL＞ZnL。ML 中由于形成了更大的共轭体系，导致了配合物的 $\mu_{C=N}$ 比 H_2L 的 $\mu_{C=N}$ 低。4 种化合物在 1597cm^{-1}处强红外吸收带受 M 影响很小，归属为芳环 $\mu_{C=C}$。

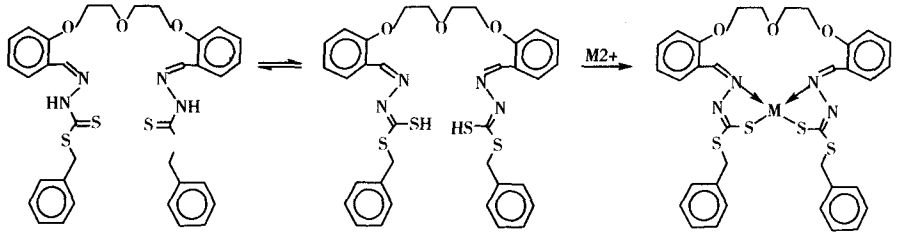


图 1　H_2L 两种互变异构体及 ML 配位模式

我们将 4 种化合物配制成浓度约为 10^{-5} mol·L^{-1}的二氯甲烷溶液，表 2 列出了在 200nm～700nm 的电子吸收光谱。H_2L 在此区间可能发生 π→π* 和 n→π* 电子跃迁，而 ML 的 UV－vis 光谱除配体内电子跃迁外，还可能发生金属离子 M^{2+} 的 d－d 跃迁及 M→L 或 L→M 电荷转移跃迁等。比较 UV－vis 光谱，3 种配合物 ML 光谱相似，H_2L 中不明显的肩峰在 3 种配合物的谱图中变得明显。

表 2　产物的二氯甲烷溶液 UV－vis 光谱数据

Comp	λ(nm)(lgε)			
	λ_{max}	λ_1	λ_2	λ_2
H_2L	226(4.40)		349(4.66)	
N_2L	214(4.45)	280(4.46)	340(4.30)	386(3.92)
CuL	228(4.37)	300Sh	323(4.55)	
ZnL	229(4.99)	302(4.80)	363(4.92)	

以上情况说明，1,7－二(2′－苯甲酰)－1,4,7－三氧庚烷双缩肼基二硫代

甲酸苄酯是一种良好的西夫碱配体，可与 Ni(Ⅱ)，Cu(Ⅱ)，Zn(Ⅱ)等金属离子形成稳定的配合物，其生物活性我们正在进一步研究。

参考文献

[1] Kirschner S. ,W ei Y. K. ,T rancis D. ,et al. . J. M ed. Chem. [J],1966, 9:369～370.

[2] Das M. ,L ivingstone S. E. . In org. Chim. Acta. [J],1976,19:5～7.

[3] Duan C. Y. , W u B. M. , M ak Thomas C. K. . J. Chem. Soc. Dolton Trans. [J],1996:3485～3486.

[4] Tian Y. P. , Duan C. Y. , L n Z. L. , et al. . Polyhedrou [J], 1996, 15 (13):2263～2264.

[5] Kenneth R. A. ,Anthony J. L. ,Leonard F. L. ,et al. . J. Am. Chem. Soc. [J],1983,105 (13):4645～4646.

Synthesis and Characterization of Schiff Base Containing N,S and It's Metal Complexes

Abstract: The novel schiff base ligand was prepared via the reaction of S－benzyl dithio carbazate with 1,7－bis (2′－form ylphenyl)－1,4,7－trioxahep tane in a 2∶1 molar ratio. Both the ligand and its complexes with copper (Ⅱ), nicke (Ⅱ), and zinc (Ⅱ) were characterized by elemental analysis, IR and UV－vis spectra. It was found that the schiff－base ligand acts as a doubly negatively－charged quaridentate.

Key Words: schiff－base; complex; synthesis; characterization

本文原载于《合成化学》2001 年第 9 卷第 1 期

双金属层状配位聚合物{[NO_2BzQl][$MCr(ox)_3$]}$_\infty$的合成、光谱表征和磁性研究

摘 要：合成了两种新的草酸根桥联的双金属层状配位聚合物，{[NO_2BzQl][$MCr(ox)_3$]}$_\infty$，其中[NO_2BzQl]$^+$为1-(*p*-nitrobenzyl)quinolinium，ox^{2-}为Oxalate，M为Ni^{2+}或Cu^{2+}，并经元素分析、红外光谱表征。变温磁化率测定结果表明，在这两种层状配位聚合物中，相邻的金属离子之间存在反铁磁偶合作用。应用Curie-Weiss公式拟合相应的变温磁化率数据为：$C=0.662$emu K/mol，$\theta=-1.658$K，$R=2.0\times10^{-5}$(Ni^{2+})；$C=0.17$emu K/mol，$\theta=-0.693$K，$R=1.86\times10^{-6}$(Cu^{2+})。

关键词：草酸根桥联；配位聚合物；合成；磁性

1. 前 言

由于电子器件、信息存储介质、热开关、光开关等材料科学迅速发展的需要，分子组装磁性材料(分子基磁体)的研究成为当代科学中的前沿领域[1]。具有高临界温度T_c和较大的矫顽性H_c的分子基铁磁体(molecule-based ferromagnet)是新型的信息存储介质。因此，设计、合成具有高T_c和大的H_c值的分子基铁磁体是分子基材料研究领域中最具挑战性的课题之一[2,3]。目前，这方面的研究工作主要集中在两方面：(1)设计和制备新的分子基铁磁体，研究新体系的磁性-结构相关性；(2)对已知的分子基铁磁体，通过调节分子结构，提高铁磁体的铁磁相变临界温度和增大矫顽性。理论上，

宏观铁磁性是铁磁性材料在三维空间长程磁有序的协同结果，因此，在设计新的分子基铁磁性体系时，力求增强分子间的相互作用。磁性配位聚合物能满足这一要求，因而，设计和合成磁性配位聚合物就成为分子基铁磁体研究的热点[2]。草酸根具有独特的分子结构，可与过渡金属离子形成具有二维层状结构的配位聚合物，近年来，草酸根桥联的异核过渡金属配位聚合物的磁性已引起了人们的极大兴趣[2,4-7]。本工作中，我们合成和表征了 CrNi 和 CrCu 两种双金属配位聚合物，研究了这两种配位聚合物的磁学性质。

2. 实　验

2.1　仪器和试剂

使用 Perkin - Elmer 240 型元素分析仪测定所合成的新化合物的 C、H、N 的质量分数。使用 Bruker 公司的 IFS66V 型 FT - IR 光谱仪，并用 KBr 压片法测定了两种配合物的红外光谱。使用 MagLab 2000 型磁强计测定了两种配合物的变温磁化率，并用 Pascal 常数对配合物的抗磁性进行了校正。所有试剂均为分析纯，使用前未作进一步纯化。

2.2　原料的制备

$K_3[Cr(ox)_3]\cdot 3H_2O$ 按文献[8]中的方法制备。

对-硝基苄基喹啉盐酸盐（$[NO_2BzQl]Cl$）的合成[9]：将 1.70g 对-硝基苄氯和 1.30g 喹啉溶解在 50mL 丙酮中，混合溶液回流 20min 后就有白色微晶生成。继续回流 40min，冷却后过滤。依次用少量丙酮、无水乙醚洗涤微晶状沉淀，真空干燥后，得产物 $[NO_2BzQl]Cl$ 2.76g（产率 92%）。元素分析结果：C，63.71；H，4.50；N，9.14。按分子式 $C_{16}H_{13}ClN_2O_2$ 计算的理论值：C，63.90；H，4.36；N，9.31。

2.3　配位聚合物的合成

$\{[NO_2BzQl][NiCr(ox)_3]\}_\infty$（A）的合成：用 487mg $K_3[Cr(ox)_3]\cdot 3H_2O$、240mg $NiCl_2\cdot 6H_2O$ 和 300mg $[NO_2BzQl]Cl$ 溶解在 30mL 水和甲醇（体积比为 1∶1）混合溶剂中，保温在 60℃，搅拌 0.5h 后即有绿色微晶生成。反应溶液冷却后过滤，用甲醇洗涤微晶状沉淀，真空干燥后，得产物 556mg

(产率 88%)。元素分析结果:C,40.88;H,2.42;N,4.21;按化学式 $CrNiC_{22}H_{13}N_2O_{14}$ 计算的理论值:C,41.29;H,2.05;N,4.38。红外光谱数据(KBr 压片法):1 644 和 815cm^{-1}。

{[NO_2BzQl][$CuCr(ox)_3$]}$_\infty$(B)的合成:用类似于制备 A 的方法合成 B,产率高于 84%。元素分析结果:C,40.69;H,2.35;N,4.18。按化学式 $Cr_2CuC_{22}H_{13}N_2O_{14}$ 计算的理论值:C,40.97;H,2.03;N,4.34。红外光谱数据 1 635 和 811cm^{-1}。

3. 结果与讨论

3.1 合成和光谱表征

在水和甲醇混合溶剂中,摩尔比为 1∶1∶1 的 $K_3[Cr(ox)_3]\cdot 3H_2O$、Ni^{2+} 或 Cu^{2+} 氯化物和对-硝基苄基喹啉盐酸盐一锅反应得到 A 和 B. A 和 B 的元素分析结果与分别按化学式 $CrNiC_{22}H_{13}N_2O_{14}$ 和 $CrCuC_{22}H_{13}N_2O_{14}$ 计算的结果一致,表明在这两种配位聚合物中,有机平衡阳离子([NO_2BzQl]$^+$)、Ni^{2+} 或 Cu^{2+} 与 Cr^{3+} 的摩尔比是 1∶1∶1,即两种配位聚合物分别可用结构简式[NO_2BzQl][$NiCr(ox)_3$]、[NO_2BzQl][$CuCr(ox)_3$]表示。

结构简式[cation]$^+$[$M^{(II)}M^{(III)}(ox)_3$]$^-$ 配合物为层状分子堆积结构,[$M^{(II)}M^{(III)}(ox)_3$]$^-$ 形成蜂巢状阴离子层,[cation]$^+$ 填充在阴离子层间[4]。此外,在草酸根配位的配合物中,草酸根的 υ_{as}(C=O)谱带和 δ(C=O)谱带的位置与其配位模式密切相关,因此,用红外光谱技术是研究草酸根的配位模式的有力手段。草酸根单螯合配位模式的 υ_{as}(C=O)、δ(C=O)谱带分别在 1 700、800cm^{-1} 左右有吸收[10];若草酸根作为四齿配体,即桥联配位模式与过渡金属离子配位,那么相应的 υ_{as}(C=O)谱带红移,而 δ(C=O)谱带蓝移[11]。在 A 和 B 的红外光谱图中,A 的 υ_{as}(C=O)、δ(C=O)分别在 1644 和 815cm^{-1},B 的 υ_{as}(C=O)、δ(C=O)分别在 1 635 和 811cm^{-1}。上述结果表明,A 和 B 中的草酸根都是桥式配位的,即草酸根与 Cr^{3+}、M^{2+}(Ni^{2+} 或 Cu^{2+})形成了双金属二维层状配位聚合物。

3.2 配位聚合物的磁性

我们分别测定了聚合物 A(2～300K)和 B(2～220K)的变温磁化率，经 Pascal 常数校正后的顺磁性磁化率按 Curie－Weiss 公式拟合，$\chi_m=\frac{C}{T-\theta}$式中，$\chi_m$为摩尔磁化率；$C$ 为 Curie－Weiss 常数；T 为绝对温度；θ 为 Curie 温度．实验数据和拟合结果分别示于图 1 和图 2。每个 MCr 单元的有效磁矩按方程 $\mu_{eff}=2.828(\chi_m T)1/2$ 计算，聚合物 A 中每个 CrNi 单元的室温有效磁矩 μ_{eff}为 3.15μ_B，其值高于 $S=1/2(S=S_{Cr}-S_{Ni})$的唯自旋值 1.732μ_B，低于 $S=5/2(S=S_{Cr}+S_{Ni})$的唯自旋值 5.916μ_B。随着温度降低，μ_{eff}减小，说明在配位聚合物层内，相邻的 Cr^{3+} 和 Ni^{2+} 之间存在反铁磁交换作用。当温度降至 4.8K 时，μ_{eff}值仍为 2.021μ_B；继续降低温度，μ_{eff}值急剧减小，到 2.0K 时，μ_{eff}值几乎为 0。这种现象可能是配位聚合物层间反铁磁合引起的，或者是 Ni^{2+} 的零场分裂造成的。聚合物 B 中的每个 CrCu 单元的室温有效磁矩是 2.94μ_B，其值略高于 $S=1(S=S_{Cr}-S_{Cu})$的唯自旋值 2.828μ_B，远低于 $S=2(S=S_{Cr}+S_{Cu})$的唯自旋值 4.899μ_B。当温度降至 2K 时，μ_{eff}降到 1.071μ_B。表明配合物 B 的层内和层间都存在反铁磁交换作用。应用 Curie－Weiss 公式，经非线性最小平方二乘法拟合两种配合物的变温磁化率数据，获得相应的参数值：A 的 $C=0.662$emu K/mol，$\theta=-1.658$K，一致性因子 $R=\frac{\sum_i(\chi^i_{exp}-\chi^i_{calc})^2}{\sum_i(\chi^i_{exp})^2}=2.0\times10^{-5}$，配合物 B 的 $C=0.170$emu K/mol，$\theta=-0.693$K，一致性因子 $R=1.86\times10^{-6}$。在[cation][$MCr(ox)_3$](M＝二价过渡金属离子)类二维层状分子基磁体中，通常得到的都是分子基铁磁体，或亚铁磁体。但是，配合物 A 和 B 的变温磁化率结果表明，配合物的层内和层间都存在着反铁磁相互作用，显然，阳离子对阴离子层间的磁相互作用有一定的影响。因此，研究这类二维层状分子基磁体的磁性和结构相关性，对研究新的二维层状分子基磁体是有意义的。

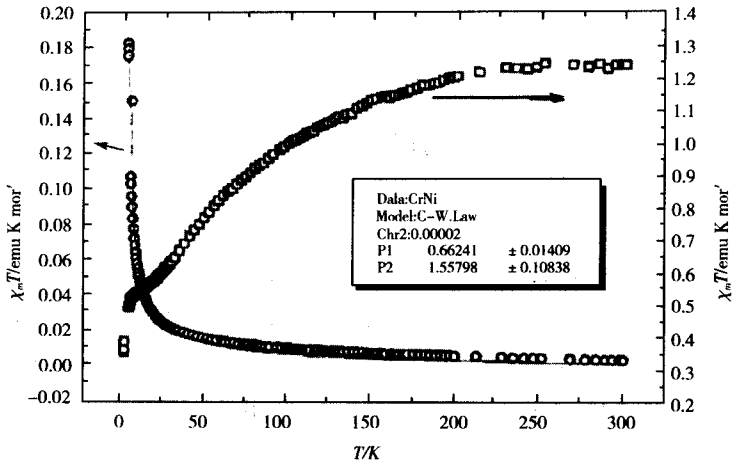


图 1　配合物 A 的 $\chi_m \sim T$ 和 $\chi_m T \sim T$ 曲线

Fig. 1　The plots of $\chi_m \sim T$ and $\chi_m T \sim T$ for A

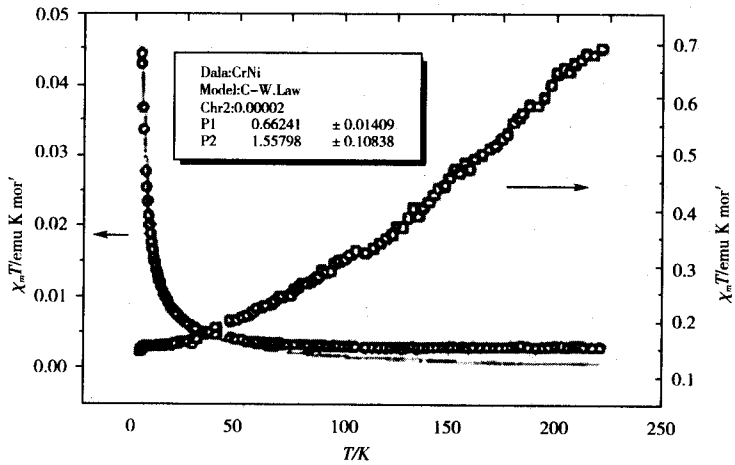


图 2　配合物 B 的 $\chi_m \sim T$ 和 $\chi_m T \sim T$ 曲线

Fig. 2　The plots of $\chi_m \sim T$ and $\chi_m T \sim T$ for B

参考文献

[1] Alivisatos A P, Barbara P F, et al. Adv. Mater., 1998, 10: 1297

[2] Tamaki H, Zhuang Z J, Matsumoto N, Kida S, Koikawa M, Achiwa N, Hashimoto Y,. Okawa H. J. A m. Chem. Soc., 1992, 114: 6974

[3] Stumpf H O, Ouabab L, Pei Y, Bergerat P, Kahn O. J. Am. Chem. Soc., 1994, 116: 3866

[4] (a) Bhattacharjee A, Miyazaki Y, Sorai M. Solid State Commun., 2000, 115: 639

(b) Coronado E, Galán - Mascarós J R, Gómez - García C J, Laukhin V. Nature, 2000, 408: 447

(c) Coronado E, Galán - Mascarós J R, Gómez - García CJ, Martínez - Agudo J M. Synthetic Metals, 2001, 122: 501, 507

[5] Pellaux R, Schmalle H W, Huber R, Fisher P, Hauss T, Ouladdiaf B, Decurtins S. Inorg. Chem., 1997, 36: 2301

[6] Ohba M, Tamaki H, Matsumoto N, Okawa H, Kida S. Chem. Lett., 1991: 1157

[7] Coronado E, Galán - Mascarós J R, Gómez - García C J, Martínez - Agudo J M. Inorg. Chem., 2001, 40: 113

[8] Bulgarevich S B, Bren D V, Movshovic D Y, Finocchiaro P, Failla S. J. Mol. Struct., 1994, 317: 147

[9] Baylar J C, Jones E M. Inorg. Synth., 1939, 1: 37

[10] Nakamoto K. Infrared Spectra of Inorganic and Coordination Compounds, 2nd Ed., Wiley - Interscience, New York, 1970. 244

[11] Zhuang J Z, Matsumoto N,. Okawa H, Kida S. Chem. Lett., 1990: 87

Bimetallic Coordination Polymers with Layer Structure $\{[NO_2BzQl][MCr(ox)_3]\}_\infty$: Syntheses, Spectra Characterization and Magnetic Properties

Abstract: Two new bimetallic coordination polymers, $\{[NO_2BzQl][MCr(ox)_3]\}_\infty$, where $[NO_2BzQl]^+$ = 1-(*p*-nitrobenzyl) quinolinium, ox^{2-} = oxalate, M = Ni^{2+} (A) or Cu^{2+} (B), were synthesized, and characterized by elemental analysis, infrared spectra. The bonds of υ as (C=O) 、δ(C=O) are at 1644 cm^{-1}、815 cm^{-1} for complex (A), and 1635 cm^{-1}、811 cm^{-1} for complex (B), respectively. The results of IR for (A) and (B) indicated that two complexes form 2-D layer structures in the solidstate. The results of the variable temperature magnetic susceptibilities for (A) and (B) revealed that there exists antiferromagnetically coupled interactions in both intra- and interlayer. The best fit parameters using Curie-Weiss formula are as follows: C = 0.662 emu K/ mol, θ = −1.658 K, and agreement factor $R = 2.0 \times 10^{-5}$ for (A). C = 0.17 emu K/ mol, θ = −0.693 K, and $R = 1.86 \times 10^{-6}$ for (B).

Key Words: bridging oxalate; coordination polymer; synthesis; magnetic properties

本文原载于《化学物理学报》2002 年第 15 卷第 2 期

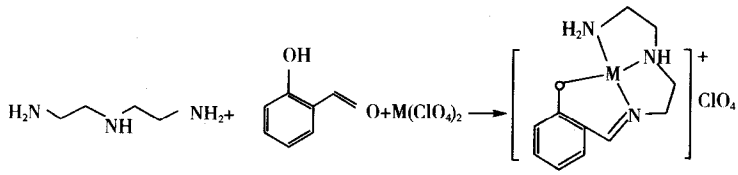
双金属层状配位聚合物 $\{[ML][Fe^{II}Fe^{III}(ox)_3]\cdot 1.5H_2O\}_\infty$ 的合成和波谱表征

摘　要：合成和表征了两种新的 Schiff 碱配合物 $[NiL(ClO_4)\cdot 3H_2O$ (1)和 $CuL(ClO_4)\cdot 4H_2O$(2)，其中 L 是由摩尔比为 1∶1 的水杨醛和二乙撑三胺缩合而成的 Schiff 碱。1(或 2)、$FeSO_4\cdot 7H_2O$ 和 $K_3[Fe(ox)_3]\cdot 3H_2O$ 进一步反应，生成了双金属层状配位聚合物 $\{[ML][Fe^{II}Fe^{III}(ox)_3]\cdot 1.5H_2O\}_\infty$，其中 $M^{2+}=Ni^{2+}$ (3)或 Cu^{2+} (4)。红外光谱和 Mössbauer 谱测定结果表明，3 和 4 具有二维层状结构，其阴离子层由 $[Fe^{II}Fe^{III}(ox)_3]^-$ 单元构成。

关键词：草酸根桥联；配位聚合物；合成；波谱表征

近年来，具有二维层状结构的配位聚合物 $A[Fe^{II}Fe^{III}(ox)_3]$(其中 A＝季胺盐、季膦盐)的磁学性质引起人们极大兴趣[1~5]。人们发现，这类层状配位聚合物的磁性是可调的，即通过改变填充在阴离子层间的阳离子就能获得分子基铁磁体、亚铁磁体以及倾斜的反铁磁体[6]；虽然这类分子基磁体的临界温度(T_c)较低(5K 到 44K 之间)，但是矫顽力的大小可以从小于 10Oe 到大于 1kOe[7]。文献检索的结果表明，人们对这类层状结构的配位聚合物的研究，仅限于阳离子是有机阳离子和 $[FeCp_2^*]^+$，$[CoCp_2^*]^+$ 等金属茂类阳离子[7]。最近，制备具有二维层状结构的多功能分子基材料成为化学、物理学和材料科学领域中的热点之一[8]。上述阳离子分子间只有弱的 Van de Waals 力，因而限制了提高层状分子基磁体的维数。根据分子场理论，提高分子基材料的维数是提高 T_c 的有效途径之一。基于这种思想，我们合成和表征了两种金属配合物阳离子 NiL^+ 和 CuL^+(其中 L＝水杨醛和等摩尔的

二乙撑三胺缩合的 Schiff 碱)。由于配体 L 上的活泼 H 原子有可能与草酸根上的 O 原子形成氢键,从而有望实现将此类分子基磁体的维数从二维扩展到三维,达到提高其 T_c 值的目的。为此,我们进一步合成和表征了 NiL^+ 和 CuL^+ 两种金属配合物阳离子与$[Fe^{II}Fe^{III}(ox)_3]^-$阴离子形成的双金属二维层状配位聚合物(见 Scheme),$\{[NiL][Fe^{II}Fe^{III}(ox)_3]\cdot 1.5H_2O\}_\infty$ 和 $\{[CuL][Fe^{II}Fe^{III}(ox)_3]\cdot 1.5H_2O\}_\infty$ ($M=Ni^{2+}$,Cu^{2+}),其配阳离子及层状配位聚合物的合成路线如下:



$$ML(ClO_4)+FeSO_4+K_3Fe(ox)_3 \longrightarrow (ML)FeFe(ox)_3$$

1. 实验部分

1.1 仪器和试剂

所有新化合物的 C,H,N 元素百分含量使用 Perkin－Elmer 240 型元素分析仪测定。红外光谱使用 Nicolet FTIR AVATAR 360 光谱仪测定,样品与 KBr 磨均后压片,测量范围为 400～4 000cm^{-1}。配位聚合物室温下的 Mössbauer 谱实验在等加速 Mössbauer 谱仪上进行,放射源为 20mCi^{57}Co(Pd),同质异能位移相对于 α－Fe 标定。所用试剂均为分析纯,使用前未作进一步纯化。

1.2 原料的制备

$K_3[Fe(ox)_3]\cdot 3H_2O$ 按照文献[9]中的方法制备。

1.3 $NiL(ClO_4)\cdot 3H_2O$(1)和 $CuL(ClO_4)\cdot 4H_2O$(2)的合成

在一只 100mL 的圆底烧瓶中,加 40mL 甲醇溶解 366mg$Ni(ClO_4)_2\cdot 6H_2O$,边搅拌边逐滴加入 103mg 二乙撑三胺,加热回流 20min 后,滴加 20mL 含 122mg 水杨醛的甲醇溶液。混合溶液回流近 30min 后就有深黄色

微晶生成。继续回流 40min，冷却后过滤。依次用少量甲醇、无水乙醚洗涤微晶状沉淀，真空干燥后，得产物 343mg（产率 82%）。元素分析结果：C，31.51%；H，5.31%；N，10.01%。按分子式 $C_{11}H_{22}N_3O_8ClNi$ 计算的理论值：C，31.57%；H，5.30%；N，10.04%。用类似于制备配合物(1)的方法和合成路线合成深蓝色配合物(2)。产率为 81%。元素分析结果：C，29.87%；H，5.51%；N，9.47%。按分子式 $C_{11}H_{24}N_3O_9ClCu$ 计算的理论值：C，29.94%；H，5.48%；N，9.52%。

1.4 配位聚合物的合成

$\{[NiL][Fe^{II}Fe^{III}(ox)_3]\cdot 1.5H_2O\}_n$（3）的合成：在 N_2 气氛下，492mg $K_3[Fe(ox)_3]\cdot 3H_2O$，278mg $FeSO_4\cdot 7H_2O$ 溶解在 30mL 水和甲醇（体积比为 1∶1）混合溶剂中，室温下搅拌 0.5h 后，逐滴加入 30mL 含 418mg 配合物 1 的甲醇溶液，立即有黄褐色沉淀生成。滴加完毕，反应溶液过滤，用甲醇洗涤沉淀，真空干燥后，得产物 567mg（产率 85%）。元素分析结果：C，30.52%；H，2.90%；N，6.27%；按化学式 $C_{17}H_{19}N_3O_{14.5}Fe_2Ni$ 计算的理论值：C，30.58%；H，2.87%；N，6.29%

$\{[CuL][Fe^{II}Fe^{III}(ox)_3]\cdot 1.5H_2O\}_n$（4）的合成：用类似于制备(3)的方法合成(4)，产率高于 80%。元素分析结果：C，30.29%；H，2.88%；N，6.21%。按化学式 $C_{17}H_{19}N_3O_{14.5}N_3Fe_2Cu$ 计算的理论值：C，30.36%；H，2.85%；N，6.25%。

2. 结果与讨论

2.1 配合物 1～4 的合成

将 $Ni(ClO_4)_2\cdot 3H_2O$（或 $Cu(ClO_4)_2\cdot 4H_2O$）溶解在热的甲醇中，然后依次滴加摩尔比为 1∶1∶1 的二乙撑三胺和水杨醛，回流过程中即得到深黄色（深蓝色）微晶，(1)和(2)的产率均高于 80%。元素分析结果与按分子式 $NiL(ClO_4)_2\cdot 3H_2O$（$CuL(ClO_4)_2\cdot 4H_2O$）的计算值一致。

在 N_2 气氛下，水和甲醇混合溶剂中，摩尔比为 1∶1∶1 的 $K_3[Fe(ox)_3]\cdot 3H_2O$，$FeSO_4\cdot 7H_2O$ 和(1)或(2)一锅反应得到(3)和(4)。元素分析结果与(3)、(4)分别按化学式 $C_{17}H_{19}N_3O_{14.5}Fe_2Ni$ 和 $C_{17}H_{19}N_3O_{14.5}N_3Fe_2Cu$

计算的结果一致，表明在配位聚合物(3)和(4)中，平衡阳离子$[NiL]^+$(或$[CuL]^+$)，Fe^{2+}与Fe^{3+}的摩尔比是1∶1∶1，即配位聚合物(3)和(4)分别可用结构简式$\{[NiL][Fe^{II}Fe^{III}(ox)_3]\cdot 1.5H_2O\}_\infty$，$\{[CuL][Fe^{II}Fe^{III}(ox)_3]\cdot 1.5H_2O\}_\infty$表示。

2.2 配合物1～4的IR光谱表征

配合物1～4的IR光谱图分别示于图1和图2，一些特征官能团的IR振动频率归纳在表1中。

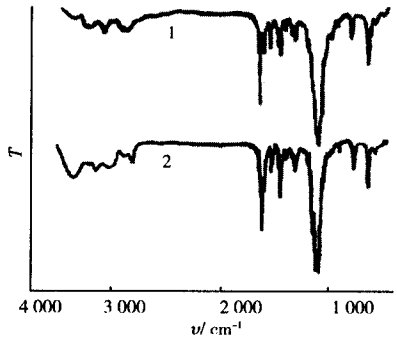


Fig. 1 The infrared spectra of (1) and (2)

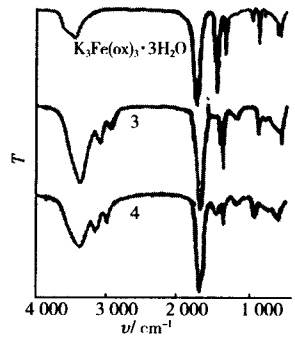


Fig. 2 The infrared spectra of (3)、(4) and $K_3Fe(ox)_3\cdot 3H_2O$

Tab. 1 The character vibrating frequencies for 1－4

IR振动频率/cm^{-1}	归属	IR振动频率/cm^{-1}	归属
1		2	
3 423,3 216(m)	υ_{N-H},υ_{O-H}	3 421,3 290 3 263(m)	υ_{N-H},υ_{O-H}
3 017(w)	苯环上的υ_{C-H}	3 039(w)	苯环上的υ_{C-H}
2 685(w)	烷环上的υ_{C-H}	2 956(w)	烷环上的υ_{C-H}
1 626(s)	υ_{C-H}	1 644(s)	υ_{C-H}
1 602～1 449(m)	苯环上的$\upsilon_{C=C}$	1 600～1 400(m)	苯环上的$\upsilon_{C=C}$
1 145,1 120,1 089(s)	ClO_4^-的特征峰	1 094(s)	ClO_4^-的特征峰
3		4	
3 368(m)	υ_{N-H},υ_{O-H}	3 359(m)	υ_{N-H},υ_{O-H}
3 021(w)	苯环上的υ_{C-H}	3 010(w)	苯环上的υ_{C-H}
2 865(w)	烷环上的υ_{C-H}	2 875(w)	烷环上的υ_{C-H}
1 654(s)	$\upsilon_{C=O}$	1 651(s)左右	$\upsilon_{C=O}$
1 612～1 452(m)	苯环上的$\upsilon_{C=C}$	1 611～1 445(m)	苯环上的$\upsilon_{C=C}$
814(m)	C=O伸缩振动	820(m)	C=O伸缩振动

图 1 中的结果清楚地呈现了苯环上的 υ_{C-H}、烷烃上亚甲基的 υ_{C-H}，Schiff 碱的 $\upsilon_{C=N}$特征峰，因而证明了配合物 1 和 2 中含二乙撑三胺和水杨醛形成的 Schiff 碱。在 1 100～1 140cm^{-1}的强吸收带归属为 ClO_4^- 的特征吸收带(υ_{Cl-O})。Ni^{2+} 和 Cu^{2+} 的配位数一般不超过 6，水杨醛的酚羟基配位时将失去质子，根据电荷平衡，在配合物(1)和(2)中，水杨醛和 ClO_4^- 的摩尔比只能是 1∶1。综上所述，Schiff 碱 L 是由 1∶1 摩尔比的二乙撑三胺和水杨醛缩合而成，而在配合物(1)和(2)中的 L 与 M(M=Ni^{2+} 和 Cu^{2+})的摩尔比也应是 1∶1。

结构简式为$[Cation]^+[M^{\text{Ⅱ}}M^{\text{Ⅲ}}(ox)_3]^-$ 的配合物，具有层状分子堆积结构，即$[[M^{\text{Ⅱ}}M^{\text{Ⅲ}}(ox)_3]^-$形成蜂巢状阴离子层，一阶阳离子$[Cation]^+$填充在阴离子层间[10]。此外，在草酸根配位的配合物中，草酸根的 $\upsilon_{as}(C=O)$ 谱带和 $\delta C=O$ 谱带的位置与其配位模式密切相关，因此，红外光谱技术是研究草酸根的配位模式的有力手段。草酸根单螯合配位模式的 $\upsilon_{as}(C=O)$ 谱带、$\delta C=O$ 谱带分别在 1 700，800cm^{-1}左右有吸收；若草酸根作为四齿配体，即桥联配位模式与过渡金属离子配位，那么相应的 $\upsilon_{as}(C=O)$ 谱带红移，而 $\delta C=O$ 谱带蓝移[11]。在(3)和(4)的红外光谱图中，(3)的 $\upsilon_{as}(C=O)$，$\delta C=O$ 分别在 1 626 和 814cm^{-1}，(4)的 $\upsilon_{as}(C=O)$，$\delta C=O$ 分别在 1 644 和 820cm^{-1}。上述结果表明，(3)和(4)中的草酸根都是桥式配位的，即草酸根与 Fe^{3+}，Fe^{2+} 形成了二维层状配位聚合物。

2.2 位聚合物(3)和(4)的 Mössbauer

^{57}Fe 的 Mössbauer 谱是研究 Fe 的价态和自旋态的最有效的方法之一[11]。为了确定二维层状配位聚合物(3)和(4)中含有 Fe^{3+}，Fe^{2+}，我们测定了(3)和(4)的室温 Mössbauer 谱，相应结果分别示于图 3 和图 4。显然，配合物(3)和(4)中都含有两种不同状态的铁离子。应用 Origin(Version 510) 软件，对配位聚合物(3)和(4)中重叠的峰进行分峰拟合，分别得到两组峰，即，配合物(3)：(Ⅰ)$\delta=0.49mm\cdot s^{-1}$，$\Delta E_Q=0.93mm\cdot s^{-1}$；(Ⅱ)$\delta=1.67mm\cdot s^{-1}$，$\Delta E_Q=2.46mm\cdot s^{-1}$。配合物(4)：(Ⅰ)$\delta=0.45mm\cdot s^{-1}$，$\Delta E_Q=0.25mm\cdot s^{-1}$；(Ⅱ)$\delta=1.69mm\cdot s^{-1}$，$\Delta E_Q=2.53mm\cdot s^{-1}$。第一组双峰具有较小的同质异能位移 δ 和较小的四极矩分裂 ΔE_Q，是高自旋 Fe^{3+} 离子的 Mössbauer 谱特征；第二组双峰具有较大的同质异能位移 δ 和较大的四极矩分裂 ΔE_Q，是高自旋 Fe^{2+} 离子的 Mössbauer 谱特征[11]。

3. 结 论

我们合成了两种 Schiff 碱配合物(1)和(2),元素分析和红外光谱测定结果表明 Schiff 碱 L 是由 1∶1 的水杨醛和二乙撑三胺缩合而成,(1)和(2)中 L 与 M(M=Ni^{2+} 和 Cu^{2+})的摩尔比也应是 1∶1。ML^{+}(M=Ni^{2+} 和 Cu^{2+})进一步与 Fe^{2+},$[Fe(ox)_3]^{3-}$ 反应得到(3)和(4),红外光谱测定结果表明它们具有二维层状结构,Mössbauer 谱清楚地表明配位聚合物(3)和(4)中都含有 Fe^{2+} 和 Fe^{3+} 离子。因此,(3)和(4)是双金属层状配位聚合物。

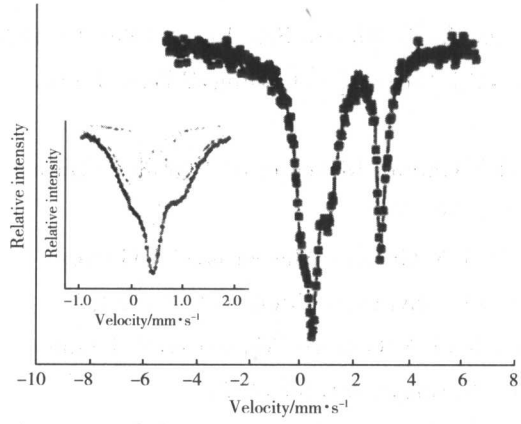


Fig. 3 The Mösshauer spectra of (3)

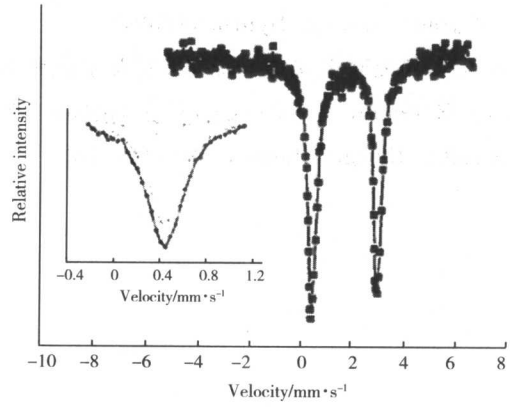


Fig. 4 The Mösshauer spectra of (4)

参考文献

[1] A Bhattacharjee, Y Miyazaki Y, M Sorail Solid State Commun., 2000, 115:639.

[2] A Bhattacharjee, Y Miyazaki, M Sorai. J. Phys. Soc. Jap., 2000, 69. 479.

[3] A Bhattacharjee, R Feyerherm, M Steiner. J. Phys. Soc. Jap., 1999, 68:1679.

[4] A Bhattacharjee A. J. Mat t. Sci. Lett., 1996, 15:102.

[5] C Mathoniere, C J Nuttal, S G Carling, P Day. Inorg. Chem., 1995, 35: 1201.

[6] E Coronado, J R Galán - Mascarós, C J Gómez - García. Synthetic Metals, 1999, 102:1459.

[7] E Coronado E, J R Galán - Mascarós, C J Gómez — - García, and J M Martínez - Agudo. Synthetic Metals, 2001, 122:50.

[8] (a) E Coronado, J R Galán - Mascarós, C J Gómez - García, and V Laukhin. Nature, 2000, 408:447;

(b) R Pellaux, H W Schmalle, R Huber, P Fisher, T Hauss, B Ouladdiaf, and S Decurtins. Inorg. Chem., 1997, 36:2301.

[9] J C Baylar, E M Jones. Inorg. Synth., 1939, 1:37.

[10] 唐恢同. 有机化合物光谱鉴定. 北京:北京大学出版社, 1992, 71

[11] E Coronado, J R Galán - Mascarós, C J Gómez - García, and J M Martínez—Agudo. Inorg. Chem., 2001, 40:113.

Bimetallic Coordination Polymers{[ML][$Fe^{II}Fe^{III}(ox)_3$]·1.5H_2O}$_\infty$ with Layer Structure Syntheses, Spectra Characterization

Abstract: Two new schiff base complexes, NiL(ClO_4)·3H_2O (1) and CuL(ClO_4)·4H_2O (2) {L was condensed from equation molar salicylaldehyde and diethylenetriamine} have been synthesized and characterized. Further, two new bimetallic coordination polymers, {[ML][$Fe^{II}Fe^{III}(ox)_3$]·1.5H_2O}$_\infty$ were synthesized and characterized, where ox^{2-} = oxalate, M = Ni^{2+} (3) or Cu^{2+} (4). The tested results of elementary analysis of coordination polymers (3) and (4) were according with the theoretical value, and the results of the IR indicated that the coordination of oxalate were bridge-type in compound (3) and (4). 2-layer coordination polymers were synthesized by oxalate and Fe^{3+}, Fe^{2+}. The result of Mössbauer spectra of (3) and (4) in room temperature revealed that two different postural ferric ions were found in coordination polymer (3) and (4), and anions layer was formed by $[Fe^{II}Fe^{III}(ox)_3]^-$ unit. The compounds of (3) and (4) were bimetallic coordination polymers.

Key Words: bridging oxalate; coordination polymer; synthesis; spectra characterization

本文原载于《光谱学与光谱分析》,2002 年第 22 卷第 5 期

自旋交叉配合现象与分子电子器件

摘　要：自旋交叉配合物在热、压力或光诱导自旋交叉现象的同时会伴随着其他一些协同效应，比如配合物颜色的改变、存在着大的热滞后效应等，这些协同效应是单个分子或分子集合体作为热开关、光开关和信息存储元件材料的基础。因此，自旋交叉配合物是开发新型的热开关、光开关和信息存储元件材料的理想分子体系。本文概述了自旋交叉现象的研究历史、现状和未来的发展趋势，讨论了影响配合物自旋交叉性质的各种内在的和外部的因素，总结了目前用于研究自旋交叉现象的各种现代测试技术。最后，展望了自旋交叉配合物在分子电子器件方面的应用前景。

关键词：自旋交叉配合物；分子电子器件；分子双稳定性

随着微电子的迅速发展，分子水平的电子器件材料的研究越来越受到人们的关注。分子双稳性与分子水平上的新型信息存储、光开关、热开关等分子电子器件材料密切相关，因而成为当前化学、物理和材料科学的研究热点之一[1,2]。著名的磁化学家 Kahn 曾对分子双稳性给出如下定义：分子双稳性是指在一定的外界条件下，分子存在两种稳定或介稳的电子状态。过渡金属配合物的自旋交叉现象是目前研究最为广泛而深入的分子双稳现象之一。

1. 自旋交叉配合物研究回顾和现状

自旋交叉现象的发现可追溯到 70 多年前。1931－1932 年 Cambi 在研究一类 Fe(Ⅲ)配合物时，发现其中一些配合物的磁矩随着温度的变化而发

生强烈的变化，这种奇特的现象意味着，在温度的变化过程中，这些配合物中心的金属离子，即 Fe(Ⅲ)离子的电子构型发生了变化[3,4]。20 世纪 80 年代以前，配合物的自旋交叉现象仅仅作为一种独特的磁现象被人们所认识。随着科学技术的发展，特别是许多新的测试技术的诞生，使得人们对物质世界的了解能够深入到分子和原子水平上，也使得人们更广泛而深入地认识自旋交叉现象。更为重要的是，信息科学、计算机科学的迅猛发展，刺激了新材料领域的研究工作。到了 80 年代中期，人们逐渐地认识到配合物的自旋交叉现象可能在未来的分子电子器件材料如分子开关、信息存储介质材料方面有着应用前景，于是，其研究得到了迅速发展。迄今为止，自旋交叉配合物体系已从最初的 Fe(Ⅲ)体系扩展到目前的 Cr(Ⅲ)、Mn(Ⅲ)、Fe(Ⅱ)、Co(Ⅱ)、Co(Ⅲ)和 Ni(Ⅱ)等过渡金属配合物体系；早期的研究仅限于单核自旋交叉配合物体系，如今向着多核配合物和配位聚合物方向发展；为应用方面的考虑，自旋交叉配合物的 LB 膜方面的研究也正在开展。1999 年，Fujita 等[2]报道了一种具有准一维堆积结构特征的 S、N 自由基分子体系在室温左右显示分子双稳性，这一重大发现揭示了低维磁学体系是潜在的具有分子双稳性的体系。最近，孟庆金等也发现了一类在结构上具有准一维性质的过渡金属配合物显示出分子水平上的热开关特征[5](图 1)。与自由基分子体系相比，过渡金属配合物具有许多优点：化学稳定性好，易于制备；可以通过改变配合物的中心离子、配体等以获得更广泛的分子双稳性体系。在新的具有分子双稳性的体系不断发现的同时，自旋交叉现象也呈现出多样性。从最先被发现的一步自旋状态的转换发展到近几年被认识的两步自旋状态的转换，自旋交叉现象和磁交换相互协同，自旋交叉过程伴随着热滞后效应等[5~10]。为使这类材料满足实用化的要求，科学工作者充分地发挥他们的聪明才智，巧妙地进行分子设计，不断地开发出新的呈现双稳性分子体系，同时也不断地改进这类材料的一些性能，比如调节高、低自旋态之间转变的温度，使 T_c 值接近室温，增大热滞后效应等。这方面的研究工作，Kahn 小组尤为卓越。他们在理论上提出，增大分子间的协同作用将有利于提高自旋交叉配合物的 T_c 值和增大热滞后效应，并已制备了多种具有自旋交叉性质的配位聚合物，而且，一些配位聚合物的 T_c 值已接近室温，相应的热滞环的 $T_c\uparrow - T_c\downarrow > 50K$。在此类材料的应用方面，尤其是在利用这类材料作为电子显示元件、热开关、光开关等分子电子器件方面，一些研究小组也提出了种种奇妙的设想。迄今为止，这一领域的研究差不多每

隔两年就有一篇综述性的文章发表[11~15]，其研究的活跃程度由此可见一斑。虽然国内在此方面的研究工作起步较晚，但是，近年来游效曾、孟庆金以及廖代正等分别在铁系自旋交叉配合物、低维分子间自旋交叉配合物的制备和自旋交叉性质研究方面都开展了卓有成效的工作。

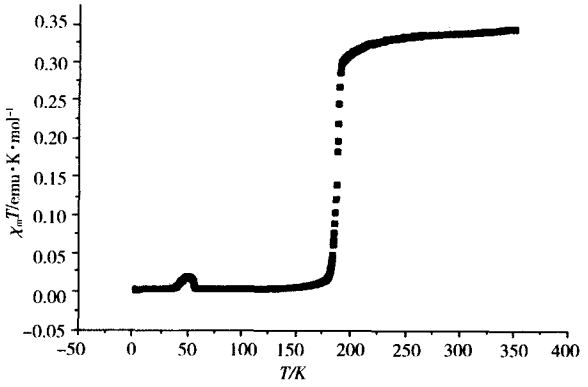


图 1　$\chi_m T-T$ 曲线[5]

Fig. 1　Plotof $\chi_m T-T$[5]在 184K 附近显示自旋开关特征

2. 自旋交叉配合物在高、低自旋状态时的电子排布

在正八面体配位场中，具有电子构型 $d^4 \sim d^7$ 的过渡金属离子可能有两种电子排布方式，即高自旋状态和低自旋状态。当配位场分裂能 Δ 和电子成对能 P 相近时，则电子排布方式就由外界条件如温度变化、压力变化、光辐射等来决定。因此，外界条件的变化可能引起中心金属离子 d 轨道上的电子重新排布，从而导致配合物中心离子的自旋状态转变，即产生自旋交叉现象。图 2 所示的是正八面体配位场中 d^6 电子组态的金属离子两种不同电子排布及其相互转换示意图。低自旋状态的电子组态是 $(t_{2g})^6(e_g)^0$（对应谱项 1A1g），高自旋状态的电子组态为 $(t_{2g})^4(e_g)^2$（对应谱项 $5T_{2g}$）。



图 2　在正八面体配位场中 d^6 电子组态的金属离子高、低自旋状态相互转换示意图

Fig. 2　LS and HS states for a molecular species formed by a electron configuration by six ligands situated at the corners of an octahedron

3. 自旋交叉现象的几种类型

自旋交叉配合物从高自旋状态向低自旋状态转变过程中，通常是利用配合物的高自旋状态的摩尔分数 $\gamma_{HS}(T)$ 来描述转变程度，$\gamma_{HS}(T)$ 定义如下：

$$\gamma_{HS}(T)=n_{HS}(T)/[n_{HS}(T)+n_{LS}(T)] \tag{1}$$

自旋交叉现象最常用的表征方法是测量配合物的变温磁化率，因此，公式(1)又可演变为：

$$\gamma_{HS}(T)=\{(\chi T)-(\chi T)_{LS}\}/\{(\chi T)_{HS}-(\chi T)_{LS}\} \tag{2}$$

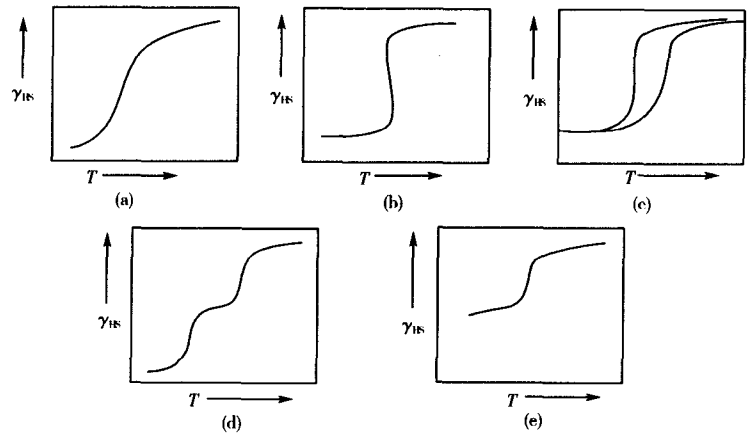


图 3　自旋交叉的五种类型

Fig. 3　Five types of of spin－crossover phenomena

根据 $\gamma HS(T)$ 对 T 的变化形态，自旋交叉现象可分为以上几类(图 3)：(a)渐变型；(b)突变型；(c)回滞型；(d)阶梯型；(e)不完全型。

4. 诱导自旋交叉的几种外部因素

4.1 热诱导自旋交叉

设 E_{HS}、E_{LS} 分别代表高自旋和低自旋的势能，则当满足 $\triangle E_{HL} \approx kT$ 时，就能产生热诱导自旋交叉现象。

4.2 压力诱导的自旋交叉[16]

自旋交叉过程常常伴随着中心金属离子和配体之间配位键键长的改变，因而导致配合物在高、低自旋状态时的固态堆积结构不同。当配合物所受的外部压力发生改变时，配合物的固态结构发生变化，因而配合物的自旋状态也随之改变，即压力诱导了自旋交叉效应。

4.3 光诱导自旋交叉[17]

自旋交叉配合物在高、低自旋状态时的电子结构不同，因此配合物在不同自旋状态时的电子光谱会有差异。通过不同波长的光激发高、低自旋状态，就可以调控配合物在高、低自旋状态之间的互换，即光诱导自旋交叉(LIESST)。

5. 影响自旋交叉性质的一些因素

影响配合物自旋交叉性质的因素非常多，总的来讲可分为两类：(1)来自化学方面的因素，即配体、溶剂以及平衡离子对配合物自旋交叉性质的影响。具体为：(a)配体替换和修饰的影响。配体不同，中心离子的配位场场强的大小被调节，从而配合物的自旋交叉性质受到影响；(b)在自旋交叉配合物的主晶格中掺杂其他离子形成分子合金对自旋交叉性质的影响；(c)未参

与配位的阴离子的影响。自旋交叉现象的产生是分子间协同作用的结果，自旋交叉体系中的平衡离子，比如，未配位阴离子是协同效应的来源之一，所以，非配位阴离子能强烈地影响自旋交叉的类型和性质[18]；(d)非配位溶剂分子的影响。和非配位阴离子一样，配合物中心离子的配位层外的溶剂分子也能通过影响晶格的变化来达到影响配合物自旋交叉的性质；(e)同位素效应。(2)来自物理方面的因素，即外界非化学方面因素产生的影响：(a)试样制备过程的影响。自旋交叉配合物制备中的反应速率，结晶过程等条件不同，往往会对配合物的自旋交叉性质造成影响。Haddad 等首次发现，研磨自旋交叉配合物将会导致配合物在低温时具有较高的高自旋成分残留[19]；(b)压力的影响。由于高自旋分子比低自旋分子体积要大，所以，可以预料当对自旋交叉配合物施加高压时，配合物将更容易从高自旋状态转化为低自旋状态。事实上，许多结果证明了这一点[16]；(c)磁场的影响。不同自旋状态具有不同的磁学性质，理论上，当外加磁场达到 100T 或以上时，高、低自旋状态相互转变温度(相变温度)会受到明显的影响[20]。但是，到目前为止，在实验室里尚无法获得如此强的磁场。

6. 研究自旋交叉现象的现代测试技术

自旋交叉现象是分子间各种协同效应相互影响的结果，因此，当自旋交叉配合物分别处于高、低自旋状态时，不仅中心金属离子的电子结构发生了变化，而且配体与中心离子之间的配位键键长也会有差别，这些差异同时会影响配体的分子结构(如配体的分子构象等)。因此，下列一些现代测试技术是研究自旋交叉现象的有力手段，比如，变温红外光谱、变温拉曼光谱、变温核磁共振谱、变温 EPR 波谱，尤其是变温 X 射线单晶结构的测定，有利于理解自旋交叉过程中的协同效应。当很难获得配合物的单晶结构信息时，应用外延 X 射线精细结构分析(EXRFS)方法分析高、低自旋状态时配合物中心离子周围的配位环境就显得尤为有效。对于含铁离子的自旋交叉配合物而言，铁离子在不同自旋状态时穆斯鲍尔谱的同质异能位移和四极矩分裂都有差异，因此，穆斯鲍尔谱是研究铁系自旋交叉配合物的自旋交叉现象的最有效手段之一。

7. 自旋交叉现象在分子电子器件材料方面的展望

随着化学、物理以及材料科学工作者们对具有分子双稳性的化学体系的深入研究，人们逐渐认识到，分子双稳性现象的研究工作，不仅在基础研究方面具有重要的意义，而且在开发新一代的分子电子器件材料方面也具有广阔的应用前景。一些热诱导的自旋交叉配合物在 T_c 附近的很窄的温度范围内，其磁化率发生突变，利用这种性质可开发成快速热敏开关。特别是在 1984 年，Gütalich 等发现的光诱导自旋交叉效应(LIESST)后，这种可通过不同的光照射来开关不同自旋状态的特性，清楚地表明了光诱导自旋交叉效应在作为新型的光开关材料方面的应用价值。上世纪 90 年代末，Kahn 等发现了常温区具有较大热滞后效应的自旋交叉聚合物体系后，使得这类配合物作为信息储存功能材料的应用前景越来越受到广大科学工作者的关注。有些自旋交叉配合物的颜色随着自旋状态的转变而不同，比如低自旋状态时为紫色，高自旋状态则为白色。他们已提出设想，利用这一现象开发新一代分子显示器件[15]。

在世界各国科学工作者共同努力下，历经 70 年研究历程，尤其是近 10 多年来，自旋交叉现象方面的研究取得了长足的进展。以 Gütlich 为首的近 10 个欧洲研究小组已联手，以 TOSS(thermal and optical of switched spin state) 为名的攻关项目，已从欧共体获得近千万马克的基金资助。Kahn 等[1]也和法国电信局就合作开发这类配合物作为电话显示磁卡而达成协议。随着新的具有优良性能的自旋交叉化合物的被发现以及将此类材料制成相应的电子器件的技术方面问题一个个被克服，利用这类材料开发成分子电子器件必将实现[21]。

参考文献

[1] Kahn O, Martinez C J. Science, 1998, 279: 44.

[2] Fujita W, Awaga K. Science, 1999, 286: 261.

[3] (a) Cambi L, Cagnasso A. Atti. Accad. Naz. Lincei., 1931, 13: 809; (b) Cambi L, Szegoe L. Ber. Dtsch. Chem. Ges., 1931, 64: 259.

[4] Cambi L, Szegoe L, Cagnasso A. Atti. Accad. Naz. Lincei., 1932a, 15: 266; (b) Cambi L, Malatesta L, Ber. Dtsch. Chem. Ges., 1937, 70: 2067.

[5] Kênig E. Coord. Chem. Rev., 1968, 3: 471.

[6] Goodwin A. Coord. Chem. Rev., 1976, 18: 293.

[7] Gütlich P. Struct. Bonding, 1982, 44: 83.

[8] Toflund H. Coord. Chem. Rev., 1989, 94: 67.

[9] Gütlich P, Hauser A. Coord. Chem. Rev., 1990, 97: 1.

[10] Gütlich P, Hauser A, Spiering H. Angew. Chem. Int. Ed. Engl., 1994, 33: 2024.

[11] Lindoy L F, Livingstone S E. Coord. Chem. Rev., 1967, 2: 173.

[12] Bareforeld E K, Busch D H, Nelson S M Q. Chem. Soc. Rev., 1968, 22: 457.

[13] Kênig E. Prog. Inorg. Chem., 1987, 35: 527.

[14] Zarembovitch J, Kahn O. New J. Chem., 1991, 15: 181.

[15] Kahn O, Kroeber J. Jay C. Adv. Mater., 1992, 4: 718.

[16] Kêhler C P, Jokob R, Meissner E et al. J. Phys. Chem. Solids, 1990, 51: 239.

[17] Poganiuch P, Decurtins S, Gütlich P. J. Am. Chem. Soc., 1990, 112: 3270.

[18] Renovitch G A, Baker W A Jr. J. Am. Chem. Soc., 1967, 89: 6377.

[19] Haddad M S, Federer W D, Lynch M Y et al. J. Am. Chem. Soc., 1980,102:1468.

[20] Decurtins S, Gütlich P, Kêhler C P et al. Chem. Phys. Lett., 1984,105: 1～4.

[21] 游效曾，孟庆金，韩万书．配位化学的进展．北京：高等教育出版社，2000.

Abstract: The spin - crossover phenomena, in which some transition metal complexes exhibit a transition between a low - spin (LS) and a high - spin (HS) state, might be accompanied by other cooperative effects such as color change and large thermal hysteresis loop, etc. These complexes can be used as new types of molecular electronic device materials (thermal switch, optical switch and information memory medium) based on these cooperative effects. Therefore, spin - crossover complexes are an ideal molecular system in which a single molecule or molecular aggregation acts as an element of thermal switch, optical switch or information memory. The history and present situation for spin - crossover complexes are introduced in this paper briefly. The factors of influencing spin - crossover property, modern measurement technologies and the applications of the spin - crossover complexes in molecular electronic devices are also discussed, respectively.

Key Words: spin - crossover; molecular electronic device; molecular bistability

本文原载于《化学通报》，2002 年第 8 期

一种新的席夫碱配合物的合成、结构和磁性研究

近年来，对多核配位化合物的结构和磁性研究是成为配位化学、材料化学、材料物理领域中一个非常具有挑战性的课题。在过去几十年中，大量通过各种桥联配体桥联的配合物被合成。在这些桥联配体中，叠氮酸根离子被认为是在顺磁离子间传递磁相互作用最有效的配体。叠氮酸根离子配位的多样性决定它传递磁相互作用的多样性。采用 EE 还是 EO 方式，还与共存的配体的空间形状和静电作用有关。我们这里报道一种新的席夫碱配合物的合成，并研究了它的结构和磁性。

$[Cu_2L_2(N_3)]$的合成：水杨醛、二乙三胺和 $Cu(NO_3)_2$ 在乙醇中按摩尔比 1:1:1 混合，混合液回流约 2h，再加入 NaN_3，继续回流 1h，冷却，过滤，滤液挥发，得蓝色块状单晶。

配合物经元素分析和红外光谱表征，并通过四圆衍射测定其晶体结构。配合物属于单斜晶系，$P2_1/a$ 空间群，其晶体学参数为：$a=7.434\,0(1)$，$b=14.148(3)$，$c=14.664(3)$；$\beta=98.31(3)°$；$Z=2$；$V=1\,109.4(5)^3$；$Dc=1.352g/cm^3$；$\mu=0.090mm^{-1}$；$R=0.055\,5$，$Rw=0.091\,0$。

变温磁化率如图 1 所示，随着温度的降低，χ_M 值增大，在 8K 时达到最大值，然后随着温度的降低而迅速降低。室温下 $\chi_M T$ 值为 $0.815cm^3mol^{-1}$，比唯自旋双核铜的 $0.75cm^3mol^{-1}$ 稍大，在 300～60K 间，$\chi_M T$ 随温度降低而缓慢降低，60～2K 间，$\chi_M T$ 随温度降低而迅速降低。这是典型的三聚体中存在反铁磁偶合的特征。

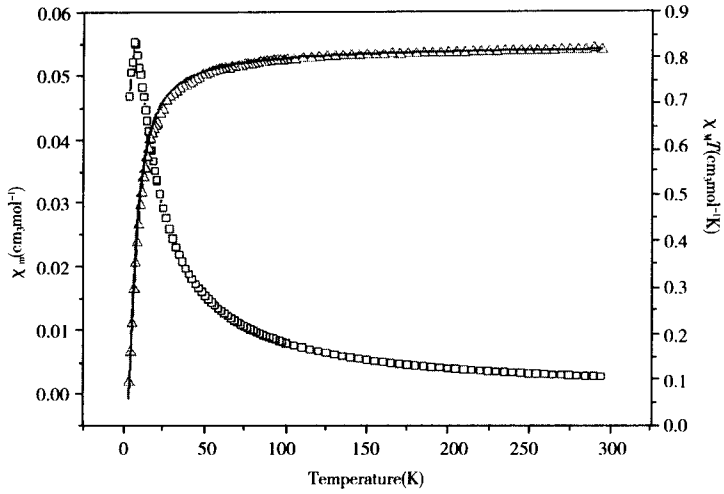


Figure 1 $\chi_M T$ product vs T (△) and χ_M vs T (□)
under an applied magnetic field of 1.0 T for $[Cu_2L_2(N_3)]$.
Solid lines represent the best fit of the data with the model described in the text.

参考文献

[1] Song, Y. ; Ohkoshi, S. ; Arimoto, Y. ; Seino, H. ; Mizobe, Y. ; Hashimoto, K. Inorg. Chem. 2003, 42, 1848

[2] Escuer, A. ; Kumar, S. B. ; Maunter, F. ; Vicente, R. Inorg. Chem. Acta 1998, 269, 313

[3] Holmes, S. M. ; Girolami, G. Mol. Cryst. Liq. Cryst. 1997, 305, 279

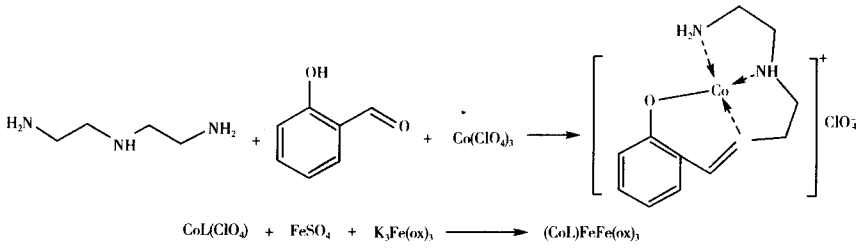
[4] Hibbs, W. ; Rittenberg, D. K. ; Sugiura, K. — I. ; Burkart, et al. Inorg. Chem. 2001, 40, 1915

[5] Tuczek, F. ; Solomon, E. I. Inorg. Chem. 1993, 32, 2850.

本文原载于《第五届全国配位化学会议论文集》

配位聚合物 $\{[CoL]Fe^{II}Fe^{III}(ox)_3 \cdot 1.5H_2O\}_\infty$ 的合成、波谱表征和磁学性质

二维层状结构的配位聚合物$[cation]Fe^{II}Fe^{III}(ox)_3\}_\infty$(其中 Cation=季胺盐、季膦盐)是一类重要的分子磁体[1-5]。由于它们有许多优点,特别是磁性可调性,即通过改变填充在阴离子层间的阳离子就能获得分子基铁磁体、亚铁磁体以及倾斜的反铁磁体[6],引起人们极大注意。但是这类分子基磁体的磁有序临界温度(T_c)低[7],常见阳离子也仅限于有机阳离子和$[FeCp_2^*]^+$、$[CoCp_2^*]^+$等金属茂阳离子[7-8]。根据分子场理论,提高 T_c 的有效途径之一是增强分子间的协同作用。基于这种思想,我们合成和表征了金属配合物阳离子 CoL^+(其中 L=水杨醛和等摩尔的二乙撑三胺缩合的 Schiff 碱)。由于配体 L 上的活泼 H 原子有可能与草酸根上的 O 原子形成氢键,增加了结构单元间协同作用,利用配位化学中有多种键所起的作用,分子具有丰富的空间结构,通过分子设计达到提高其 T_c 值的目的。本文合成和表征了 CoL^+ 金属配合物阳离子与$[Fe^{II}Fe^{III}(ox)_3]^-$阴离子形成的双金属二维层 5 状配位聚合物(Scheme1)$[CoL][Fe^{II}Fe^{III}(ox)_3]^- \cdot 1.5H_2O$,并对其磁性进行了研究。



Scheme 1 Synthetic routes of comples cation and layer coordination polymer

1. 实验部分

1.1 仪器和试剂

所有新化合物的C、H、N元素分析使用Perkin－Elmer240型元素分析仪测定。红外光谱使用Nicolet FT－IR AWATAR360光谱仪测定，样品与KBr磨均后压片，测量范围为400～4 000cm^{-1}。Mössbauer谱在美国Austin公司的S－600型谱仪上进行，在室温下采用等加速模式。放射源为20mCi的^{57}Co/Pd源，同质异能位移相对于α－Fe标定。变温磁化率使用SQUID MPMS－7磁强计测量。所用试剂均为分析纯，使用前未做进一步纯化.

1.2 原料的制备

$K_3[Fe(ox)_3]\cdot 3H_2O$按照文献[9]中的方法制备.

1.3 $CoL(ClO_4)\cdot 3H_2O$(1)的合成

在100mL的圆底烧瓶中，加40mL甲醇溶解，366mg$Co(ClO_4)_2\cdot 6H_2O$，边搅拌边逐滴加入103mg二乙撑三胺，加热回流20min后，滴加20mL含122mg水杨醛的甲醇溶液。混合溶液回流近30min后就有橙黄色微晶生成。继续回流40min，冷却后过滤。依次用少量甲醇、无水乙醚洗涤微晶状沉淀，真空干燥后，得产物344mg(产率82%)。元素分析结果C，31.51%；H，5.31%；N，10.01%。按分子式$C_{11}H_{22}N_3O_8ClCo$计算的理论值

C,31.55%;H,5.30%;N,10.04%。

1.4 配位聚合物[CoL]$Fe^{II}Fe^{III}(ox)_3\cdot 1.5H_2O$(2)的合成

在N_2气氛下,492mg$K_3[Fe(ox)_3]\cdot 3H_2O$,278mg $FeSO_4\cdot H_2O$溶解在30mL水和甲醇(体积比为1:1)混合溶剂中,室温下搅拌0.5h后,逐滴加入30mL含419mg配合物1的甲醇溶液,立即有黄褐色沉淀生成。滴加完毕,反应溶液过滤,用甲醇洗涤沉淀,真空干燥后,得产物567mg产率85%。元素分析结果C,30.52%;H,2.90%;N,6.27%;按化学式$C_{17}H_{19}N_3O_{14.5}Fe_2Co$计算的理论值:C,30.57%;H,2.87%;N,6.29%。

2. 结果与讨论

2.1 配合物1、2的合成

在热的甲醇中,摩尔比为1∶1∶1的$Co(ClO_4)_2\cdot 6H_2O$、二乙撑三胺和水杨醛一起回流即得到1产率高于80%。1中的C、H和N元素分析值与按分子式$CoL(ClO_4)\cdot 3H_2O$的计算值一致。

在N_2气氛下,水和甲醇混合溶剂中,摩尔比为1∶1∶1的$K_3[Fe(ox)_3]\cdot 3H_2O$,$FeSO_4\cdot H_2O$和1一锅反应得到高产率的2。2中的C、H和N元素分析结果与按化学式$C_{17}H_{19}N_3O_{14.5}Fe_2Co$计算的结果一致,表明在配位聚合物2中,平衡阳离子$[CoL]^+$、$Fe^{2+}$与$Fe^{3+}$的摩尔比是1∶1∶1,即,配位聚合物2可用结构简式$[CoL][Fe^{II}Fe^{III}(ox)_3]\cdot 1.5H_2O$表示。

2.2 配合物1、2的IR光谱表征

配合物1、2的IR光谱图分别示于图1和图2,一些特征官能团的IR振动频率归纳在表1中。

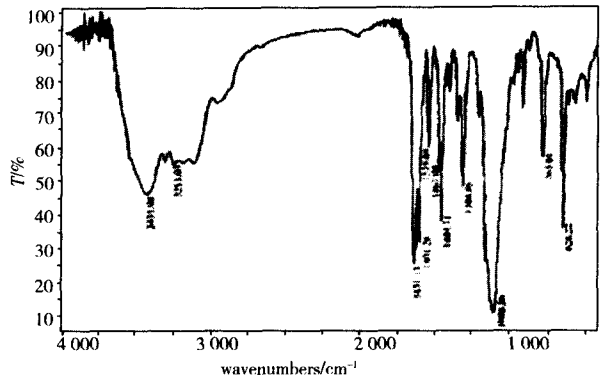


图 1　配合物 1 的红外光谱

Fig. 1　IR spectra of complex 1

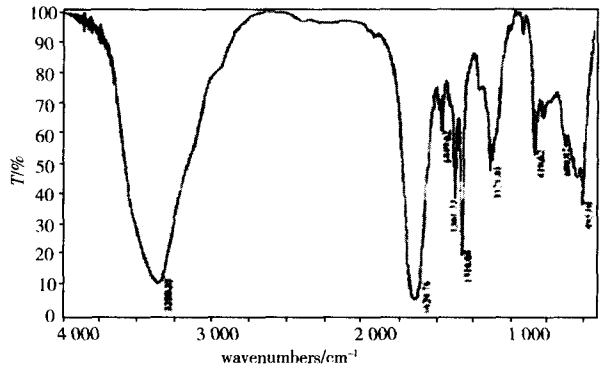


图 2　配合物 2 的红外光谱

Fig. 2　IR spectra of complex 2

表 1　配合物 1、2 的特征官能团的 IR 振动频率[10,11]

Table 1　Character Vibrating Frequency for 1 and 2

1		2	
IR/cm $^{-1}$	attribute	IR/cm $^{-1}$	attribute
3 431,3 253(m)	υ_{N-H},υ_{O-H}	3 350(m)	υ_{N-H},υ_{O-H}
3 017(w)	υ_{C-H}	3 010(m)	υ_{C-H}
2 865(w)	υ_{C-H}	2 875(m)	υ_{C-H}
1 631(s)	υ_{C-N}	1 629(s)	υ_{C-O}
1 601～1 449(m)	υ_{C-C}	1 611～1 445(m)	υ_{C-C}
1 145,1 120,1 089(s)	υ_{C-O}	819(m)	δ_{C-O}

表 1 中的结果清楚地呈现了苯环上的 υ_{C-H}、烷烃上亚甲基的 υ_{C-H}、Schiff 碱的 $\upsilon_{C=N}$特征峰，因而证明了配合物 1 中含二乙撑三胺和水杨醛形成的 Schiff 碱。在 1 100 - 1 140cm^{-1}的强吸收带归属为 ClO_4^- 的特征吸收带(υ_{Cl-O})。水杨醛的酚羟基配位时将失去质子，根据电荷平衡，在配合物 1 中，水杨醛和 ClO_4^- 的摩尔比只能是 1∶1。综上所述，Schiff 碱 L 是由 1∶1 摩尔比的二乙撑三胺和水杨醛缩合而成，而在配合物 1 中的 L 与 Co^{2+} 的摩尔比也应是 1∶1。

结构简式为[cation]$^+$[M$^{\text{Ⅱ}}$M$^{\text{Ⅲ}}$(ox)$_3$]的配合物，具有层状堆积结构，即[M$^{\text{Ⅱ}}$M$^{\text{Ⅲ}}$(ox)$_3$]$^-$形成蜂巢状阴离子层，一阶阳离子[cation]$^+$填充在阴离子层间[4]。此外，在草酸根配位的配合物中，草酸根的 υ_{as}(C=O)谱带和 δ(C=O)谱带的位置与其配位模式密切相关，因此，红外光谱技术是研究草酸根的配位模式的有力手段。草酸根单螯合配位模式的 υ_{as}(C=O)谱带、δ(C=O)谱带分别在 1 700cm^{-1}、800cm^{-1}左右有吸收[11]。若草酸根作为四齿配体，即桥联配位模式与过渡金属离子配位，那么相应的 υ_{as}(C=O)谱带红移，而 δ(C=O)谱带蓝移[12]。在 2 的红外光谱图中，υ_{as}(C=O)、δ(C=O)分别在 1 626cm^{-1}和 814cm^{-1}。上述结果表明，2 中的草酸根都是桥式配位的，即草酸根与 Fe^{3+}、Fe^{2+}形成了二维层状配位聚合物。

2.3 配位聚合物 2 的 Mössbauer 谱

^{57}Fe 的 Mössbauer 谱是研究 Fe 的价态和自旋态的最有效的方法之一[12]。为了确定二维层状配位聚合物 2 中含有 Fe^{2+}、Fe^{3+}，我们测定了 2 的室温 Mössbauer 谱，相应结果示于图 3。

显然，配合物 2 中含有两种不同状态的铁离子。应用 Origin (Version5.0)软件，对 2 中重叠的峰进行分峰拟合，分别得到两组峰，即(Ⅰ) $\delta = 0.44 mm \cdot s^{-1}$，$\triangle E_Q = 0.94 mm \cdot s^{-1}$；(Ⅱ) $\delta = 1.65 mm \cdot s^{-1}$，$\triangle E_Q = 2.45 mm \cdot s^{-1}$。较小的同质异能位移(和较小的四极矩分裂$\triangle E_Q$的双峰是高自旋 Fe^{3+} 离子的 Mössbauer 谱特征，较大的同质异能位移 δ 和较大的四极矩分裂$\triangle E_Q$的双峰是高自旋 Fe^{2+} 离子的 Mössbauer 谱特征[12]。

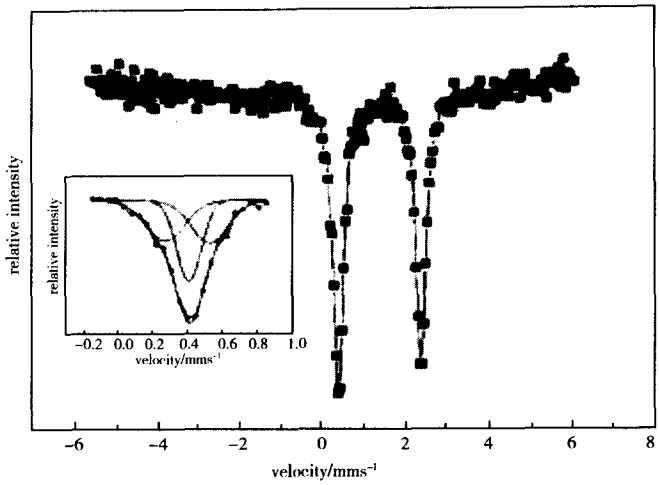


图 3　配合物 2 的 Mössbauer 谱

Fig. 3　Mössbauer spectra of complex 2

2.4　配合物 2 的磁学性质

我们测定了配合物 2 在 5～95K 温度范围内的变温磁化率，相应的 χ_m-T 和 $\chi_m T$-T 曲线分别见图 4。在 95K 时，配合物的 $\chi_m T$ 值为 0.008emu·K·mol^{-1} 远小于每个 $Co^{II}Fe^{II}Fe^{III}$ 单元的理论值（假定每个 Co^{II}、Fe^{II} 和 Fe^{III}"离子的 S 值分别为 3/2、2 和 5/2 这些离子间没有磁交换作用，那么相应于每个 $Co^{II}Fe^{II}Fe^{III}$ 单元的 χ_m-T 应为 7.25emu·K·mol^{-1}；随着样品温度的降低，χ_m-T 值逐渐减小，这些结果都显示了该配合物中比邻的自旋载体之间存在反铁磁交换作用。当样品温度降至大约 10K 时，$\chi_m T$-T 曲线出现了转折点，该转折点对应于 χ_m-T 曲线中的最低点。为了进一步研究该配合物在低温区的磁性，我们进一步测量了变磁场下的磁化强度（测量场从－50K 到 50kOe，测量温度为 5K），相应的 M－H 曲线示于图 5。插图中的磁滞环表明该配合物在低温时可能存在铁磁有序。但是外磁场达到 50kOe 时，该配合物也没有达到磁饱和。低温铁磁有序可能是亚铁磁或自旋倾斜造成的[13]。

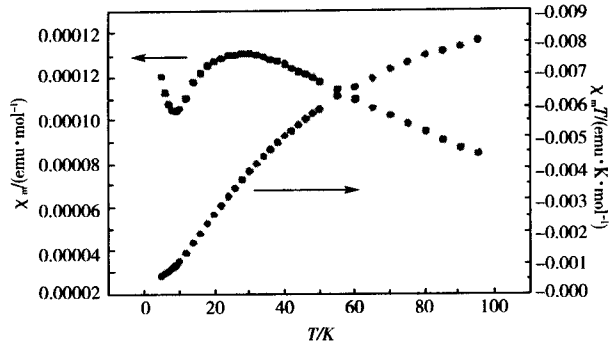


图 4 $\chi_m \sim T$ 和 $\chi_m T \sim T$ 曲线

Fig. 4 Plots of χ_m and $\chi_m T$ versus T for complex 2

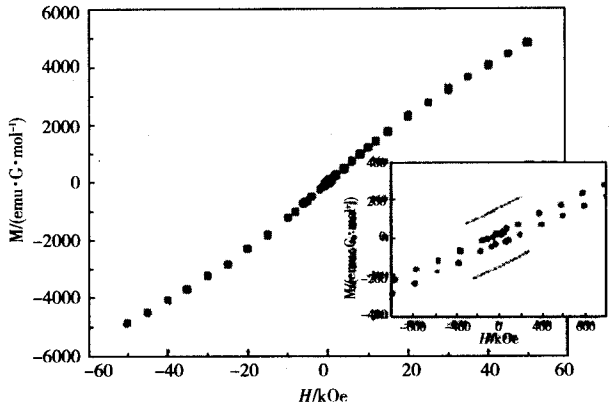


图 5 M－H 曲线(测量场－5kO$_e$ 到 5kO$_e$)，插图中显示磁滞环

Fig. 5 Plot of M versus H between 5kO$_e$ and －50kO$_e$ for complex 2, inset showing low field expanded part (hysteresis loop)

3. 结 论

我们合成了一种新的钴 Schiff 碱配合物 1，元素分析和红外光谱测定结果表明 Schiff 碱 L 是由 1∶1 的水杨醛和二乙撑三胺缩合而成，1 中 L^- 与 Co^{2+} 的摩尔比是 1∶1。CoL^+ 进一步与 Fe^{2+}、$[Fe(ox)_3]^{3-}$ 反应得到配合物 2，Mössbauer 谱清楚地表明配合物 2 中含有 Fe^{2+} 和 Fe^{3+} 两种价态的铁离

子，红外光谱表明该配合物具有二维层状结构。因此，2 是双金属层状配位聚合物。在该配合物中，比邻的自旋载体之间存在反铁磁交换作用。5K 时，该聚合物有弱的磁滞效应，表明该配合物在低温时可能存在铁磁有序，低温铁磁有序可能是亚铁磁或自旋倾斜造成的。

参考文献

[1] Bhattacharjee A. , Miyazaki Y. , Sorai M. Solid State Commun, 2000, 115, 639.

[2] Bhattacharjee A. , Miyazaki Y. , Sorai M. J. Phys. Soc. Jap. , 2000, 69, 479.

[3] Bhattacharjee A. , Feyerherm R . , Steiner M. J. Soc. Jap. , 1999, 68, 1679.

[4] Bhattacharjee A. J. , Matt. Sci. Lett. , 1996, 15, 102.

[5] Mathoniere C. , Nuttal C. J . , Carling S. G. , Day P. Inorg. Chem. , 1995, 35, 1201.

[6] Coronado E. , Galan - Macraos J. R. , Gomez - Garcia C. J. Synthetic Metals, 1999, 102, 1459.

[7] Coronado E. , Galan - Macraos J. R. , Gomez - Garcia C. J. Martinez - Agudo J . M. Synthetic Metals, 2001, 122, 501.

[8] (a) Coronado E. , Galan - Macraos J. R. , Gomez - Garcia C. J. Laukin V. Nature, 2000, 408, 447;

(b) Pellaux R. , Schmalle H. W. , Huber R. , Fisher P. , Hauss T. , Ouladdiaf B. , Decurtins S. Inorg. Chem. , 1997, 36, 2301.

[9] Baylar J. C. , Jones E. M. Inorg. Synth. , 1939, 1, 37.

[10] Tang Hui - Tong (唐恢同) Spectroscopic Identification of Organic Compound (《有机化合物光谱鉴定》), Beijing: Peking University Press, 1992.

[11] (a) Zhuang J. Z. Matsumoto N., Okawa H., Kida S. Chem. Lett., 1990, 87;
(b) Nakamoto K. Infrared Spertra of Inorganic and Coordination Compounds, 2nd ed., Wiley - Interscience: New York, 1970, p244.
[12] Coronado E., Galos J. R., Gomez - Garcia C. J., Martinez - Agudo J. M. Inorg. Chem., 2001, 40, 113.
[13] FENG Duan(冯端), ZHAI Hong - Ru(翟宏如). Metal Physics(金属物理学), Beijing: Science Press, 1998, p386

Coordination Polymer $\{[CoL][Fe^{II}Fe^{III}(ox)_3 \cdot 1.5H_2O]\}_\infty$: Syntheses, Spectra Characterization and Magnetic Properties

Abstract: A new Schiff base complex. $CoL(ClO_4) \cdot 3H_2O$ (1) {L represents condensed from equal molar ratio of salicylaldehyde and diethylenetriamine} was synthesized and characterized. Further, a new coordination polymer, $\{[CoL][Fe^{II}Fe^{III}(ox)_3] \cdot 1.5H_2O\}_\infty$ (2), was synthesized and characterized, where ox^{2-} = oxalate. The results of the IR and Mössbauer spectra of 2 revealed that the coordination polymer exists 2—D layer structure in the solid state, and anions layer was formed by $[Fe^{II}Fe^{III}(ox)_3]^-$ unit. The magnetic properties of 2 have been measured and the results indicate that there is magnetic ordering in the low temperature, which may arise from intermolecular ferromagnetic interactions or spin canted effects.

Key Words: bridging oxalate, coordination polymer, synthesis, spectra characterization, magnetic properties

本文原载于《无机化学学报》, 2003 年第 19 卷第 1 期

双金属层状配位聚合物 $\{[ML][Fe^{II}Fe^{III}(ox)_3]\cdot H_2O\}_\infty$ 的合成和波谱表征

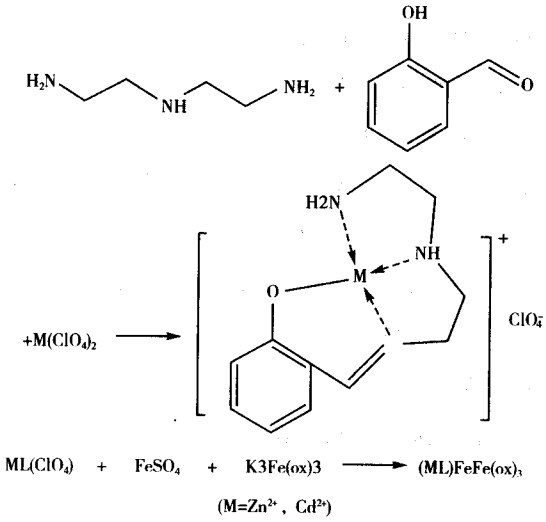
摘　要：合成和表征了两种新的 Schiff 碱配合物[$ZnL(ClO_4)\cdot 4H_2O$ (A)和 $CdL(ClO_4)\cdot 3H_2O$(B)]，其中 L=2－{[2－(Aminomethyl－amino)－ethylimino]－methyl}－phenol。A(或 B)、$FeSO_4\cdot 7H_2O$ 和 $K_3[Fe(ox)_3]\cdot 3H_2O$进一步反应，生成了配位聚合物$\{[ML][Fe^{II}Fe^{III}(ox)_3]\cdot H_2O\}_\infty$，其中 M=$Zn^{2+}$(C)或 Cd^{2+}(D)。红外光谱和 Mössbauer 谱测定结果表明，C 和 D 具有二维层状结构，其阴离子层由$[Fe^{II}Fe^{III}(ox)_3]^-$单元构成。

关键词：草酸根桥联；配位聚合物；合成；波谱表征

1. 引　言

近年来，人们对具有二维层状结构的配位聚合物 $A[Fe^{II}Fe^{III}(OX)_3]$(其中 A=季胺盐、季膦盐)的磁学性质产生了极大兴趣[1-5]。其重要原因之一是，通过改变填充$[Fe^{II}Fe^{III}(ox)_3]^-$阴离子层间的平衡阳离子可以调节这类层状配位聚合物的磁性，从而获得分子基铁磁体、亚铁磁体以及倾斜的反铁磁体[6,7]。研究结果表明，对这类具有二维层状结构的配位聚合物的研究，其阳离子仅限于有机阳离子和$[FeCp_2^*]^+$、$[CoCp_2^*]^+$等金属茂类阳离子[7]。最近，制备具有多种性质的分子基材料成为化学、物理学和材料科学领域中的热点之一，具有超导性的二维铁磁体以及具有强的二阶非线性的二维铁磁体均已见报道[8]。但是，至今还没有发现对具有发射荧光性质的铁磁体或亚铁磁体的研究。一些 Cd^{2+} 和 Zn^{2+} 的配合物具有发射蓝色荧光的性质[9]，如果在这类二维层状配位聚合物的阴离子层间插入能发射荧光的配合物阳

离子，那么有可能得到具有发光和铁磁双功能性质的分子基材料。鉴于此种设想，我们合成并表征了 ZnL^+ 和 CdL^+ 两种金属配合物阳离子，并进一步合成和表征了它们与 $[Fe^{II}Fe^{III}(ox)_3]^-$ 形成的双金属二维层状配位聚合物 $[ZnL][Fe^{II}Fe^{III}(ox)_3]\cdot H_2O$ 和 $[CdL][Fe^{II}Fe^{III}(ox)_3]\cdot H_2O$，研究了这两种配位聚合物的 Mössbauer 谱。配阳离子及层状配位聚合物的合成路线为：



2. 实　验

2.1　仪器和试剂

所有新化合物的 C、H、N 元素含量用 Perkin－Elmer 240 型元素分析仪测定。红外光谱使用 Nicolet FT－IR AVATAR 360 光谱仪测定，样品与 KBr 磨均后压片，测量范围为 400～4 000cm^{-1}。配位聚合物室温下的 Mössbauer 谱测试在 Austin－S 600 型等加速的 Mössbauer 谱仪上进行，20m$Ci^{57}Co$(Pd)为放射源，同质异能位移相对于 α－Fe 标定。合成反应中的所用试剂均为分析纯，使用前未作进一步纯化。

2.2 原料的制备

$K_3[Fe(ox)_3]\cdot 3H_2O$ 按照文献[10]中的方法制备．$Cd(ClO_4)_2\cdot 6H_2O$ 和 $Zn(ClO_4)_2\cdot 6H_2O$ 按照文献[11]中的方法制备。

2.3 $ZnL(ClO_4)\cdot 4H_2O$(A)和 $CdL(ClO_4)\cdot 3H_2O$(B)的合成

在 100mL 圆底烧瓶中，加入 40mL 甲醇溶解 372mg 的 $Zn(ClO_4)_2\cdot 6H_2O$，边搅拌边逐滴加入 103mg 的二乙烯三胺，加热回流 20min 后，滴加 20mL 含 122mg 水杨醛的甲醇溶液。混合溶液回流近 30min 后就有淡黄色微晶生成。继续回流 40min，冷却后过滤。依次用少量甲醇、无水乙醚洗涤微晶，真空干燥后，得产物 367mg(以原料二乙烯三胺计算，该反应产率为 83%)。元素分析结果：C，29.77%；H，5.48%；N，9.46%。按分子式 $C_{11}H_{21}N_3O_9ClZn$ 计算的理论值为：C，29.81%；H，5.46%；N，9.48%。用类似于制备配合物 A 的方法合成黄色配合物 B。以原料二乙烯三胺计算，反应产率为 82%。元素分析结果为：C，27.41%；H，4.63%；N，8.69%。按分子式 $C_{11}H_{22}N_3O_8ClCd$ 计算的理论值则为：C，27.46%；H，4.61%；N，8.73%。

2.4 配位聚合物的合成

$[ZnL][Fe^{II}Fe^{III}(ox)_3]\cdot H_2O$(C)的合成：在 N_2 气氛下，将 492mg $K_3[Fe(ox)_3]\cdot 3H_2O$、278mg $FeSO_4\cdot 7H_2O$ 溶解在 30mL 体积比为 1∶1 的水和甲醇中，室温下搅拌 30min 后，逐滴加入 30mL 含 443mg 配合物 A 的甲醇溶液，立即有深黄色沉淀生成。滴加完毕，继续搅拌 10min 后，过滤反应溶液，并用甲醇洗涤沉淀。最后真空干燥，得最终产物 565mg(以 $K_3[Fe(ox)_3]\cdot 3H_2O$ 原料计算，反应为产率 85%)。元素分析结果：C，30.59%；H，2.75%；N，6.27%；按化学式，$C_{17}H_{18}N_3O_{14}Fe_2Zn$，计算的理论值：C，30.68%；H，2.73%；N，6.31%．$[CdL][Fe^{II}Fe^{III}(ox)_3]\cdot H_2O$(D)的合成：用类似于制备 C 的方法合成 D，以 $K_3[Fe(ox)_3]\cdot 3H_2O$ 原料计算，反应产率高于 80%。元素分析结果为：C，28.61%；H，2.58%；N，5.87%。按化学式 $C_{17}H_{18}N_3O_{14}Fe_2Cd$ 计算的理论值为：C，28.66%；H，2.55%；N，5.90%。

3. 结果与讨论

3.1 配合物 A－D 的合成

将 $Zn(ClO_4)_2 \cdot 6H_2O$(或 $Cd(ClO_4)_2 \cdot 6H_2O$)溶解在热的甲醇中，然后依次滴加摩尔比为 1∶1∶1 的二乙烯三胺和水杨醛，回流过程中即得到浅黄色(黄色)微晶，以二乙烯三胺计算，A 和 B 的产率均高于 80%。元素分析结果和按分子式 $ZnL(ClO_4)_2 \cdot 4H_2O$($CdL(ClO_4)_2 \cdot 3H_2O$)的计算值一致。

在 N_2 气氛下，水和甲醇混合溶剂中，摩尔比为 1∶1∶1 的 $K_3[Fe(ox)_3] \cdot 3H_2O$、$FeSO_4 \cdot 7H_2O$ 和 A 或 B 反应得到 C 和 D. 元素分析结果与分别按化学式 $C_{17}H_{18}N_3O_{14}Fe_2Zn$(C)和 $C_{17}H_{18}N_3O_{14}Fe_2Cd$(D)计算的结果一致，表明在配位聚合物 C 和 D 中，平衡阳离子 $[ZnL]^+$(或 $[CdL]^+$)、Fe^{2+} 与 Fe^{3+} 的摩尔比是 1∶1∶1，即，配位聚合物 C 和 D 分别可用结构简式 $[ZnL][Fe^{II}Fe^{III}(ox)_3] \cdot H_2O$、$[CdL][Fe^{II}Fe^{III}(ox)_3] \cdot H_2O$ 表示。

3.2 配合物 A2D 的 IR 光谱表征

配合物 A－D 的 IR 光谱图分别示于图 1 和图 2，一些特征官能团的 IR 振动频率归纳在表 1 中。

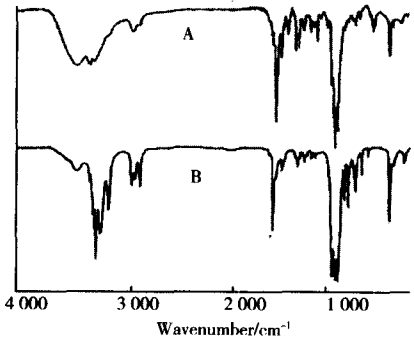


图 1 配合物 A 和 B 的红外光谱

Fig. 1 The infrared spectra of A and B

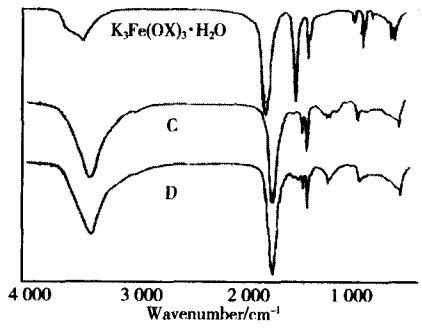


图 2 配合物 C、D 和 $K_3Fe(ox)_3 \cdot 3H_2O$ 的红外光谱

Fig. 2 The infrared spectra of C、D and $K_3[Fe(ox)_3] \cdot 3H_2O$

表 1　配合物 A－D 的特征官能团的 IR 振动频率[12,13]

Table 1　The character vibrating frequercies for A－D[12,13]

	IR/cm^{-1}	Functional group		IR/cm^{-1}	Functional group
A	3 433,3 328(m)	υ_{C-H}、υ_{O-H}	B	3431,3257(m)	υ_{C-H}、υ_{O-H}
	3 055(w)	υ_{OH}(phenyl)		3 039(w)	υ(phenyl)
	2 982(w)	υ_{OH}(alkyl)		2 939,2 863(w)	υ_{OH}(phenyl)
	1 642(s)	$\upsilon_{C=N}$		1 639(s)	$\upsilon_{C=N}$
	1 600～1 400(m)	υ_{OH}(phenyl)		1 600～1 400(m)	υ_{OH}(phenyl)
	1 120(s)	$\upsilon_{C=O}$		1 142(s)	$\upsilon_{C=O}$
C	3 369(m)	υ_{N-H}、υ_{O-H}	D	3 365(m)	υ_{N-H}、υ_{O-H}
	2 977(w)	υ_{OH}(phenyl)		3 011(w)	υ(phenyl)
	2 874(w)	υ_{OH}(alkyl)		2 865(w)	υ_{OH}(phenyl)
	1 646(s)	$\upsilon_{C=O}$		1 635(s)	$\upsilon_{C=O}$
	1 600～1 400(m)	υ_{OH}(phenyl)		1 600～1 400(m)	υ_{OH}(phenyl)
	820(s)	$\delta_{C=O}$		1 142(s)	δ_{C-O}

表 1 中的结果清楚地呈现了苯环上的 υ_{C-H}，烷烃上的亚甲基的 υ_{C-H}、Shiff 碱的 $\upsilon_{C=N}$特征峰，因而证明了配合物 A 和 B 中含二乙烯三胺和水杨醛形成的 Shiff 碱。在 1 120cm^{-1}～1 140cm^{-1} 的强吸收带归属为 ClO_4^- 的特征吸收带($\upsilon_{C=O}$)。Zn^{2+} 和 Cd^{2+} 的配位数一般不超过 6，水杨醛的酚羟基配位时将失去质子，根据电荷平衡，在配合物 A 和 B 中，水杨醛和 ClO_4^- 的摩尔比只能是 1∶1。综上所述，Shiff 碱 L 是由 1∶1 摩尔比的二乙烯三胺和水杨醛缩合而成，而在配合物 A 和 B 中的 L 与 M(M=Zn^{2+} 和 Cd^{2+})的摩尔比也应是 1∶1。

结构简式为$[cation]^+[M'^{II}M^{III}(ox)_3]^-$的配位聚合物，具有层状结构，即$[M'^{II}M^{III}(ox)_3]^-$形成蜂巢状阴离子层，一价阳离子$[cation]^+$填充在阴离子层间[4]。此外，在草酸根配体的配合物中，草酸根的 υ_{as}(C=O)和δ(C=O)谱带的位置与其配位模式密切相关。因此，红外光谱技术是研究草酸根配位模式的有力手段。单螯合草酸根的 υ_{as}(C=O)和 δ(C=O)分别在1 700 cm^{-1}、800cm^{-1}左右有吸收[13,14]；而作为四齿桥联配体的草酸根的υ_{as}(C=O)谱带将红移，δ(C=O)谱带将蓝移[13,14]。在 C 和 D 的红外光谱图中，C 的 υ_{as}(C=O)和δ(C=O)分别在 1 635cm^{-1} 和 818cm^{-1}，D 的 υ_{as}(C=O)和 δ(C=O)分别在 1 646cm^{-1} 和 820cm^{-1}。上述结果表明配合物 C 和 D 中的草酸根都是桥式配位的，即草酸根与 Fe^{3+}、Fe^{2+} 形成二维层状配位聚合物。

3.2　配位聚合物 C 和 D 的 Mössbauer

^{57}Fe 的 Mössbauer 谱是研究 Fe 的价态和自旋态的最有效的方法之一[15]。为了确定二维层状配位聚合物 C 和 D 中含有 Fe^{3+}、Fe^{2+} 两种不同价

态的离子，我们测定了 C 和 D 的室温 Mössbauer 谱。配合物 C 和 D 的 Mössbauer 谱极其相似，并且都显示了 Fe^{3+}、Fe^{2+} 的特征，代表性的 Mössbauer 谱示于图 3。应用 Origin(Version 5.0)软件，对配位聚合物 C 和 D 中重叠的峰进行分峰拟合，分别得到两组峰，即，配合物 C：(Ⅰ)δ=0.49mm/s，ΔE_Q=0.93mm/s；(Ⅱ)δ=1.69mm/s，ΔE_Q=2.47mm/s；配合物 D：(Ⅱ)δ=0.50mm/s，ΔE_Q=0.95mm/s；(Ⅱ)δ=1.68mm/s，ΔE_Q=2.48mm/s. 第一组双峰具有较小的同质异能位移 δ 和较小的四极矩分裂 ΔE_Q，是高自旋 Fe^{3+} 的 Mössbauer 谱特征；第二组双峰具有较大的同质异能位移和较大的四极矩分裂，是高自旋 Fe^{2+} 的 Mössbauer 谱特征。

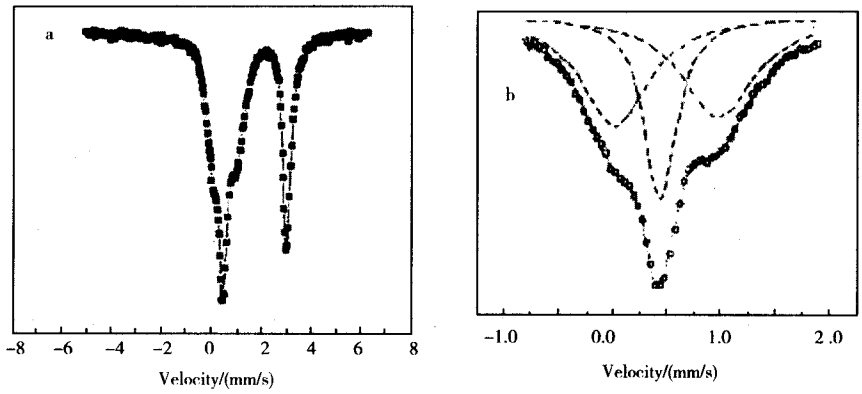


图 3 a. 配合物 C 的 Mössbauer 谱；
b. 多重峰的理论理论拟合曲线

Fig. 3 a. The Mössbauer spectra of C;
b. The theoretical fit curve of multi - peaks

4. 结 论

我们合成了两种 Schiff 碱配合物 A 和 B，元素分析和红外光谱测定结果表明 Schiff 碱 L 是由 1∶1 的水杨醛和二乙烯三胺缩合而成，A 和 B 中 L 与 M(M=Zn^{2+} 和 Cd^{2+})的摩尔比也是 1∶1。ML^+(M=Zn^{2+} 和 Cd^{2+})进一步与 Fe^{2+}、$[Fe(ox)_3]^{3-}$ 反应得到 C 和 D，红外光谱测定结果表明它们具有二维层状结构，Mössbauer 谱清楚地表明，配位聚合物 C 和 D 中都含有 Fe^{2+}、Fe^{3+}。因此 C 和 D 是双金属层状配位聚合物。

参考文献

[1] Bhattacharjee A, Miyazaki Y, Sorai M. Solid State Commun., 2000, 115:639

[2] Bhattacharjee A, Miyazaki Y, Sorai M. J. Phys. Soc. Jap., 2000, 69:479

[3] Bhattacharjee A, Feyerherm R, Steiner M. J. Phys. Soc. Jap., 1999, 68: 1679

[4] Bhattacharjee A. J. Matt. Sci. Lett., 1996, 15:102

[5] (a) Mathoniere C, Nuttal C J, Carling S G, Day P. Inorg. Chem., 1995, 35:1201

(b) Lu Guangsheng (罗广圣), Guo Shun (郭舜). Chin. J. Chem. Phys. (《化学物理学报》), 2001, 14:699

[6] Coronado E, Galvn - Mascarós J R, Gómez - García C J. Synthetic Metals, 1999, 102:1459

[7] Coronado E, Galán - Mascarós J R, Gómez - García C J, Martínez - Agudo J M. Synthetic Metals, 2001, 122:501

[8](a) Coronado E, Galán - Mascarós J R, Gómez - García C J, Laukhin V. Nature, 2000, 408:447

(b) Bónard S, Yu P, Audire J P, Rivière E, Clèment R, Guilhem J, Tchertanov L, Nakatani K. J. A m. Chem. Soc., 2000, 122:9444

(c) Bènard S, Yu P, Coradin T, Rivière E, Nakatani K, Cl ment R. Adv. Mater., 1997, 9:981

[9] Zhu H G, Strèbele M, Yu Z, Wang Z, Meyer H J, You XZ. Inorg. Chem. Commun., 2001, 4:557

[10] Baylar J C, Jones E M. Inorg. Synth., 1939, 1:37

[11] Ear L Mutterttes. Inorg. Synth., 1977, 10:30

[12] Tang Hui－tong (唐恢同). Spectroscopic Identification of Organic Compound (《有机化合物光谱鉴定》). Beijing (北京): Peking University Press (北京大学出版社). 1992. 7

[13] (a) Zhuang J Z, Matsumoto N, Ukawa H, Kida S. Chem. Lett., 1990, 87

(b) Nakamoto K. Infrared Spectra of Inorganic and Coor2dination Compounds, 2nd Ed.; WileyInterscience: NewYork, 1970. 244

[14] Chen Youcun (陈友存), Liu Guangxiang (刘光祥), Ren Xiaoming (任小明). Chin. J. Chem. Phys. (《化学物理学报》), 2002, 15: 153

[15] Coronado E, Galán－Mascarós J R, Gómez－García C J, Ensling J, Gütlich P. Chem. Eur. J., 2000, 6: 552

Syntheses and Spectra Characterization of Bimetallic Coordination Polymers with Layer Structure $\{[ML][Fe^{II}Fe^{III}(ox)_3 \cdot H_2O]\}_\infty$

Abstract: Two new Schiff base complexes, $ZnL(ClO_4) \cdot 4H_2O$ (A) and $CdL(ClO_4) \cdot 3H_2O$ (B), where L=2-{[2-(Aminomethyl-amino)-ethylimino]-methyl}-phenol, have been synthesized and characterized by elemental analysis and infrared spectra. Further, two new bimetallic coordination polymers, $\{[ML][Fe^{II}Fe^{III}(ox)_3 \cdot H_2O]\}_\infty$ were synthesized and characterized, in which ox^{2-} = oxalate, $M = Zn^{2+}$ (C) or Cd^{2+} (D). The bonds of $\nu_{as}(C=O)$, $\delta(C=O)$ were at 1635, 818 cm^{-1} for complex C and 1646, 820 cm^{-1} for complex D, respectively. The results of Mössbauer spectra of C and D revealed that there exist two kinds of valence ions. The two bimetallic coordination polymers feature the 2-D layer structure in the solid state, and their anions layer was formed by the $[Fe^{II}Fe^{III}(ox)_3]^-$ unit.

Key Words: bridged oxalate, coordination polymer, synthesis, spectra characterization

本文原载于《化学物理报》2003 年 16 卷第 2 期

多维分子基铁磁体 $Co(phen)_3[LiFe(ox)_3]$ 的合成与光谱表征

摘　要：合成具有较高居里温度的分子基磁体材料和寻求高的相转变温度 T_c 的分子基超导体一样，是当前分子材料领域中主要的研究方向．本文合成一种新的多维分子基铁磁体 $Co(phen)_3[LiFe(ox)_3]$，并用红外光谱表征其具有网络结构的配位聚合物。

关键词：多维；分子基铁磁体；设计；合成；草酸根桥联

分子铁磁体是指具有磁铁一样性质的分子化合物，它在相转变温度 T_c 下具有自发的磁化作用。目前研究的分子铁磁体主要为纯有机铁磁体和含金属的配合物铁磁体两大类。虽然早在 1963 年 Mc－Connell 就预言了有机化合物中存在着铁磁性相互作用，但是直到现在纯有机铁磁体的相转变温度只有 1.48K[1]。纯有机铁磁体由于在一般条件下，其有机自由基稳定性较差，而且也较难形成二维或三维有序的网络结构，这对于开发纯有机铁磁体是一个非常大的障碍。而且纯有机铁磁体大多都是结构没有确定的聚合物，不易溶于有机溶剂，所以缺乏再现性，难于应用。与此相对应，含有顺磁性金属离子的配合物，由于它所具有的特殊配位环境和配位结构的多样性，能够形成不同的网络结构的优点，正在不断地制备出具有较高相转变温度的金属配合物型铁磁体。因一维链状配合物作为基本单元组成宏观磁体的方法具有明显的局限性，要在一维链状配合物中较大幅度地提高相转变温度 T_c 是很难实现的，所以人们在研究一维分子基磁体的基础上着手进行二维和三维分子磁体的研究。将一维配合物单元扩展到多维及无限延伸的晶体是晶体磁工程的关键，同时多维分子基铁磁体的设计与合成是自然界向化学家的挑战。现在使用的磁材料（金属、合金、金属氧化物）是无机铁磁体，配合物型铁磁体是集无机铁磁体和纯有机铁磁体而成的一种全新的体系[2]。

由于分子铁磁体比离子型、合金类铁磁体具有更优良的性质，如不导电、比重小、透光性好、溶解性好、可塑性强、易于复合和加工等，很适合做航天材料、微波吸收材料、光磁开关、电磁屏蔽材料、磁记录材料和生物兼容材料等。然而，分子铁磁体的设计和合成是一项难度极大的工作，因为它违背了"电子倾向于配对"的自然趋势[3]。因此，寻找常温下的分子铁磁体是自然界向化学家的挑战。

1. 实验部分

试剂与仪器所用试剂均为市售分析纯试剂，未做进一步的纯化，金属钴的高氯酸盐和金属铜的高氯酸盐为实验室自制，红外光谱使用 Bruker 公司的 IFS66V 型 FT－IR 光谱仪，并用 KBr 压片法测定了该种配合物的红外光谱。

1.1 $K_3Fe(ox)_3$的合成[4]

称取 12g$K_2C_2O_4 \cdot H_2O$ 溶于 20mL 水中加热溶解，称取 3.2g$FeCl_3 \cdot 5H_2O$ 溶于 8mL 水中，使之完全溶解，将 $FeCl_3$ 溶液滴加到在近沸的 $K_2C_2O_4$ 溶液中，并且不断搅拌至澄清翠绿，浓缩，冷却得到翠绿色晶体，抽滤，用 10%的 HAc 洗涤一次，再用丙酮洗涤两次，干燥且避光保存。

1.2 Co^{2+}盐的处理

称取 2.81g $CoSO_4 \cdot 7H_2O$ 溶于适量的水，再逐滴加含 1.06g Na_2CO_3 的饱和的溶液，使两者恰好反应，生成紫红色的沉淀，过滤，将其置于小烧杯中，并加少许水，缓慢滴加 $HClO_4$ 至有极少量的沉淀为止，浓缩，冷却，得到紫红色的针状的 $Co(ClO_4)_2 \cdot 6H_2O$ 晶体，过滤，洗涤，干燥。

1.3 $Co(phen)_3[LiFe(ox)_3]$的合成

称取 386mg 的 $Co(ClO_4)_2 \cdot 6H_2O$ 晶体溶于适量的 1∶1 的乙醇水溶液，再取 594mg 的 1.10－啡罗啉溶于适量的乙醇，将两者混合，并且不断搅拌 20min，生成黄色的沉淀物，过滤，将沉淀物溶于 DMSO 呈棕黄色的溶液，向该溶液中加入含 143mg LiI 的 DMSO 溶液，不断搅拌 20min，再加入含 492mg 的 $K_3Fe(ox)_3$ 的 DMSO 溶液，有浅黄色的沉淀生成，搅拌 1h，抽滤，分别用水，乙醇，乙醚洗涤，真空干燥。该物质不溶于一般的有机溶剂。另

外，我们用同样的实验方法合成了灰色的物质 $Cu(phen)_3[LiFe(ox)_3]$，并对其红外光谱与 $Co(phen)_3[LiFe(ox)_3]$ 的红外光谱进行对照比较。

2. 结果与讨论

$[M(I)M(III)(ox)_3]^{2-}$ 一类物质形成蜂巢状阴离子层，阳离子 $Co(phen)_3^{2+}$ 填充在阴离子层间。此外，在草酸根配位的配合物中，草酸根的 $\upsilon_{as}(C=O)$ 谱带和 $\delta(C=O)$ 谱带的位置与其配位模式密切相关，因此，用红外光谱技术是研究草酸根的配位模式的有力手段。下面我们就对有关的配合物 $K_3Fe(ox)_3 \cdot 3H_2O$，$Co(phen)_3(ClO_4)_2$，$Co(phen)_3[LiFe(ox)_3]$，$Cu(phen)_3[LiFe(ox)_3]$ 进行红外光谱表征，红外光谱谱图如图 1－4 所示。在下面的四个配合物的红外光谱（IR）中，结晶水的 OH 振动峰出现在 3431cm^{-1} 左右，峰值分别为3 430cm^{-1}，3 431cm^{-1}，3 431cm^{-1}，3 432cm^{-1}，红外光谱图中草酸根单螯合配位模式的反对称伸缩振动频率 $\upsilon_{as}(C=O)$、弯曲振动频率 $\delta(C=O)$ 谱带分别在1 700cm^{-1}、800cm^{-1} 左右有吸收的特征峰值；若草酸根作为四齿配体，即桥联配位模式与过渡金属离子配位，那么相应的 $\upsilon_{as}(C=O)$ 谱带红移，而 $\delta(C=O)$ 谱带蓝移．在图 1 的 $K_3Fe(ox)_3$ 的红外光谱图中，$K_3Fe(ox)_3$ 的 $\upsilon_{as}(C=O)$、$\delta(C=O)$ 分别在1 715cm^{-1}，1 682cm^{-1}，1 644cm^{-1} 和 805cm^{-1}，而在图 $3Co(phen)_3[LiFe(ox)_3]$ 的红外光谱中，$\upsilon_{as}(C=O)$、$\delta(C=O)$ 分别在 1 707cm^{-1}，1 662cm^{-1} 和 872cm^{-1}，同样草酸根在图 $4Cu(phen)_3[LiFe(ox)_3]$ 的红外光谱中 $\upsilon_{as}(C=O)$、$\delta(C=O)$ 也分别在1 707 cm^{-1}，1 662cm^{-1} 和 872cm^{-1}，发生了较小的的位移，上述结果表明，该配合物中的草酸根是桥式配位的，即草酸根与 Fe^{3+}、Li^+ 形成了双金属网络结构配位聚合物[6]。

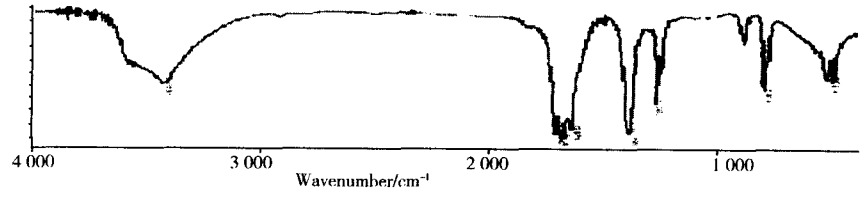


图 1　$K_3Fe(ox)_2$ 的红外光谱

在图 $2Co(phen)_3(ClO_4)_2$ 的红外光谱中，1 518cm^{-1}，1 425cm^{-1}，1 120 cm^{-1}，723cm^{-1} 则归属于 1，10－邻二氮菲的特征峰。在图 $3Co(phen)_3[LiFe$

$(ox)_3$]的红外光谱中明显可以观察到 1,10－邻二氮菲的特征峰为1 513 cm^{-1},1 421cm^{-1},732cm^{-1},在图 4Cu(phen)$_3$[LiFe$(ox)_3$]的红外光谱中同样可以明显地找到 1,10－邻二氮菲的特征峰为1 513 cm^{-1},1 421 cm^{-1},732cm^{-1},这暗示在合成的配合物中 1,10－邻二氮菲和 Cu^{2+},Co^{2+}发生了配位。阴离子 ClO_4^-的特征峰为1 146cm^{-1},1 120cm^{-1},1 096cm^{-1}[6],而在图 3 和图 4 的红外光谱中都没有这个特征峰,这说明了在配合物 Co(phen)$_3$[LiFe$(ox)_3$]和 Cu(phen)$_3$[LiFe$(ox)_3$]中不存在 ClO_4^-。

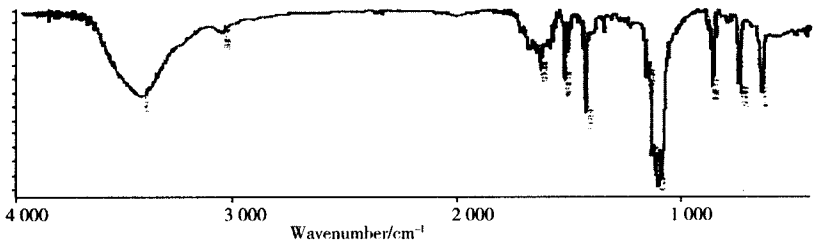


图 2　Co(phen)$_2$(ClO4)$_2$ 的红外光谱

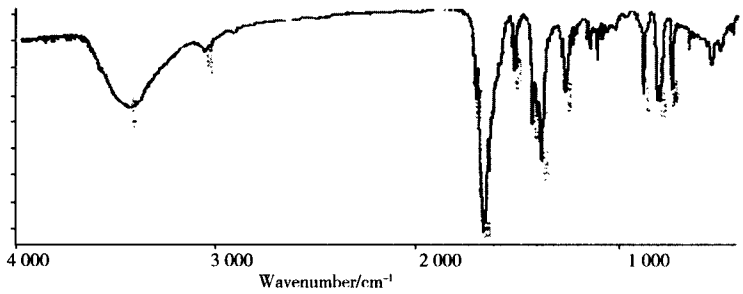


图 3　Co(phen)$_2$[LiFe$(ox)_1$]的红外光谱

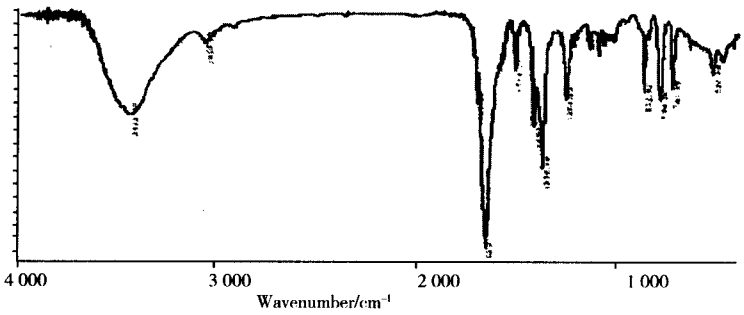


图 4　Cu(phen)$_2$[LiFe$(ox)_1$]的红外光谱

在比较图 3 和图 4 时，我们发现 $Co(phen)_3[LiFe(ox)_3]$的红外光谱和 $Cu(phen)_3[LiFe(ox)_3]$的红外光谱的特征峰值非常的接近，可见，两者属于同一类型的网状结构[7]的配位聚合物。

多维分子基磁体的设计与合成是一个跨学科的前沿课题，其研究成果不仅具有重要的理论意义而且具有极为广泛的应用前景。如$[Ru(bpy)_3][M_2^{II}(ox)_3]$(M 为第一过渡系金属离子)具有光、磁双方面功能，可用于光磁材料等。目前虽然利用改变抗衡离子、桥联配体、溶剂分子、顺磁中心、分子的手性等策略和方法可能增加维数和提高 T_c 温度，但随着化合物的维数增加，其化学、物理性质也有所改变，特别是变得不透明和难溶，失去了分子固有的化学特性。因此欲得到一个理想的分子基磁体实为自然界向化学家的一个新挑战。我们相信：在化学、物理、材料等学科的科学家的不懈努力下，随着实用分子基磁体的研制成功，它将在广泛的领域得到应用。

参考文献

[1] Chiareuim. , Novak N. A. , Rassat A. , et. al, A Ferromagnetic transit ion at 1. 48 K in an organic nitroxide[J]. 1963,363,147.

[2] 刘斌，杨光明，廖代正．功能材料，1997,28 (6),561.

[3] Kollmar C. , Kahn O. , Ferromagnetic spin alignment in molecular systems:an orbital approach [J]. A Res. ,1993,26,259.

[4] Bulgarevich S. B. , B ren D. V. , Movshovic D. Y. , Finocchiaro P. , Failla S. , Conformational invest Naralkylpyridiniumions by Cotton - Mouten effect method, J. Mo l. Struct. 1994,317:147.

[5] 陈友存，刘光祥，任小明．双金属层状配位聚合{$[NO_2BzQ\ 1][MCr(ox)_3]$}$_n$的合成、光谱表征和磁性研究．物理学报，2002,154.

[6] 唐恢同．有机化合物光谱鉴定[M]. 北京：北京大学出版社，1992.

[7] Regula S. , Silvio D. , Helen, S. E. , et. al. A Thermal Spin Transition in $[Co(bpy)_3][LiCr(ox)_3]$ (ox = bpy = 2, 2 - bipyridine) [J]. Chem. Eur. J. 2000. 6. 361.

Syntheses and Spectra Characterization of a New Multi - dimensional Molecule - based Ferromagnet: $Co(phen)_3[LiFe(ox)_3]$

Abstract: At present it is a main research direction in the molecule material field to synthesis molecule—based ferromagnet material with high curie temperature, which is the same as seeking molecule—based superconductor of high transition temperature (Te). The article tells the synthesis of a new molecule—based ferromagnet $Co(phen)_3[LiFe(ox)_3]$ and characterizes its net structure with IR spectra.

Key Words: multi - dimensional; molecule - based ferromagnet; design; synthesis; bridge - oxalated

本文原载于《安庆师范学院学报》2005 年第 11 卷第 4 期

基于席夫碱配合物的分子磁体：合成、结构和磁学性质

摘　要：合成了一种新的席夫碱配合物[NiL]ClO_4(1)，L为水杨醛与二乙烯三胺按1∶1摩尔比缩合的产物，晶体结构揭示在NiL^+单元中Ni^{2+}与1个O和3个N键合，配位构型近似为平面正方形。NiL^+和ClO_4^-间的氢键相互作用没有扩展成三维结构。配合物1是抗磁性的。在N_2气保护下，化合物1与$K_3[Fe(ox)_3]\cdot 3H_2O$、$FeSO_4\cdot 7H_2O$按摩尔比1∶1∶1反应得配位聚合物$[NiL][Fe^{II}Fe^{III}(ox)_3]$(2)。红外光谱结果表明，在配合物2中，$Fe^{II}$和$Fe^{III}$离子通过草酸根桥联形成阴离子层。变温磁化率测量结果表明，配合物2是反铁磁体，Neel温度为11K。温度高于65K，磁化率遵循Curie-Weiss定律，拟合磁化率给出Currie-Weiss常数和Weiss常数的最佳值分别为10.40(2)emu·K/mol，−22.9(4)K。

关键词：席夫碱；配位聚合物；晶体结构；磁学性质

近年来，分子磁体研究在理论和实验上都取得了可喜进展[1,2]，但迄今所研究的分子磁体的临界温度都非常低[3]。为了获得高转变温度(T_c)的分子磁体，需增强分子间的协同作用[4~7]。组成为$A[M'^{II}M^{III}(ox)_3]$(A为有机阳离子；ox为草酸根离子；M^{III}为Cr^{III}、Fe^{III}离子)的配位聚合物具有拟二维层状结构，二价的过渡金属离子(M'^{II})通过$[Cr^{III}(ox)_3]^{3-}$或$[Fe^{III}(ox)_3]^{3-}$连结成二维阴离子层，阳离子穿插于阴离子层间。这类配位聚合物长程磁有序的临界温度分布在6～43K范围内，已引起广泛的关注。阳离子A和$M'^{II}-ox-M^{III}$的组成变化可以使合成的一系列分子磁体表现出不同磁学性质，包括反铁磁性有序($M^{II}=Mn^{II}$，$M^{III}=Fe^{III}$)[8]，自旋玻璃态($M^{II}=Fe^{II}$，$M^{III}=Fe^{III}_{1-x}Cr^{III}_x$)[9]和短程的磁相关性($M^{II}=Cr^{II}$，$M^{III}=Cr^{III}$)[10]。配位聚合物的磁性多样性依赖于阳离子的性质。在利用氢键作用自组装分子磁体的研究中，我们发现分子磁体的临界温度(T_c)随着氢键

相互作用的增强而明显地提高[11]。用可与阴离子层形成氢键的阳离子代替 $A[M'^{II}M^{III}(ox)_3]$ 中的有机阳离子，分子间氢键作用可以将比邻的阴离子层连结成三维结构，因此增强了结构单元间的协同作用，其 T_c 值可望得到提高。本文设计合成了二乙基三胺水杨醛席夫碱阳离子 NiL^+ 配合物，将其与 $[Fe^{II}Fe^{III}(ox)_3]^-$ 阴离子进一步反应形成双金属二维层状配位聚合物 $[NiL][Fe^{II}Fe^{III}(ox)_3]$，研究了它的磁性。

1. 实验部分

1.1 试剂和仪器

所用试剂均为分析纯，直接使用不作进一步处理。Perkin－Elmer240型元素分析仪(美国)；Nicolet FT－IR AVATAR 360 红外光谱仪(美国)；Maglab2000 磁测量系统(英国)。

1.2 配合物 1 的合成

水杨醛、二乙三胺和 $Ni(ClO_4)_2$ 在乙醇中按摩尔比 1∶1∶1 混合后回流约 2h，冷却，抽滤。滤饼用乙醇、乙醚洗数次，真空干燥，得蓝色微晶状产物，产率 75%。元素分析 $C_{11}H_{16}ClN_3NiO_5$ 分析值(计算值)/%：C35.9(36.3)，H4.56(4.43)，N11.3(11.5)。红外光谱中在 1 089cm^{-1} 带归属为 υ(Cl—O)，1 626cm^{-1}、3 423cm^{-1} 带分别归属为 υ(C=N)和 υ(N—H)。

1.3 配位聚合物 2 的合成

在 N_2 气气氛下，将 492mg$K_3[Fe(ox)_3]\cdot 3H_2O$、278mg$FeSO_4\cdot 7H_2O$ 溶解在 30mL V(水)∶V(甲醇)=1∶1 混合液中，室温下搅拌 0.5h 后，滴加 30mL 含 419mg 配合物 1 的甲醇溶液，即有黄褐色沉淀生成。滴加完毕，过滤，用甲醇洗涤沉淀，真空干燥，产率 85%。元素分析 $C_{17}H_{16}N_3O_{13}Fe_2Ni$(计算值)%：C31.5(31.9)，H2.76(2.52)，N6.64(6.56)。红外光谱：中心在 1 654cm^{-1} 处的强宽峰，归属为 υ(C=N)+υ(C=O)。3 423cm^{-1} 和 820cm^{-1} 谱带分别为 υ(N—H)和 δ(C=O)。

1.4 配合物 1 的结构测定与解析

选取尺度为 0.20mm×0.10mm×0.10mm 的单晶，用 CAD4 衍射仪在

室温下收集强度数据。石墨单色化的 MoKαX 射线 λ＝0.071 073nm。SHELXTL 程序，直接法解析结构并全矩阵最小二乘法修正。理论加氢并精修。ClO_4^- 离子结构无序。晶体数据和修正结果见表 1。

表 1　化合物 1 在室温下的晶体学数据和精修结果

Table 1　Crystallographic data and refinement results of complex 1 at room temperature

Molecular formula	$C_{11}H_{16}ClN_3NiO_5$	V/mm^3	1403.7(5)
Molecular mass	364.43	Z	4
Space group	$P2_1/c$	μ/mm^{-1}	1.597
a/nm	0.891 20(18)	λ/nm	0.071 073
b/nm	1.335 3(3)	R_1	0.062 9
c/nm	1.192 0(2)	WR	0.167 2
β/(°)	98.29(3)		

$R_1=\sum(||F_o|-|F_c||)/\sum w(|F_o|^2-|F_c|^2)^2/\sum w(|F_o|^2)^2]^{1/2}$.

2. 结果与讨论

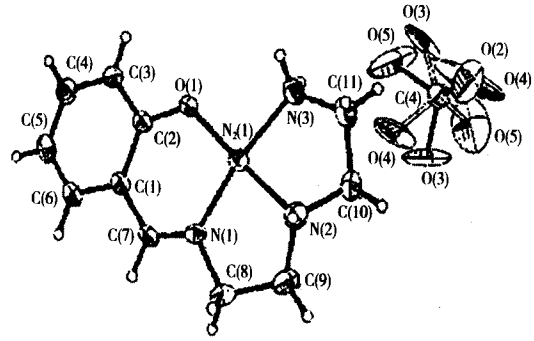
2.1　配合物 1 的结构描述

配合物 1 为单斜晶系[12]，$P2_1/c$ 空间群。不对称单元中含 1 个 NiL^+ 和 1 个高氯酸根离子。配合物 1 的 ORTEP 图示于 Scheme1。席夫碱配体 L^- 的 1 个 O 和 3 个 N 和 Ni^{2+} 离子配位，Ni—N 键长在 0.184 3(5)～0.193 6(6)nm 范围内，Ni—O 键长为 0.183 0(4)nm，O(1)—Ni(1)—N(1)、N(1)—Ni(1)—N(2)、N(2)—Ni(1)—N(3)以及 N(3)—Ni(1)—O(1)的键角分别为 96.8(2)°、86.5(3)°、86.5(3)°和 90.3(2)°。因此，Ni 离子偏离 N(1)、N(2)、N(3)、O(1)组成的配位平面 0.003 85(23)nm，表现为平面正方形配位几何。配位平面与苯环间的二面角仅 5.77(35)°。ClO_4^- 阴离子结构无序，氧原子的 2 个位置，占有率为 0.532 2、0.467 8。ClO_4^- 离子中的氧原子与阳离子中 NH_2/NH 中的氢原子之间存在氢键作用，但这种分子内的相互作用仅仅局限于相邻的阴阳离子间(Scheme 2)，并没有拓展成氢键网络(表 2)。

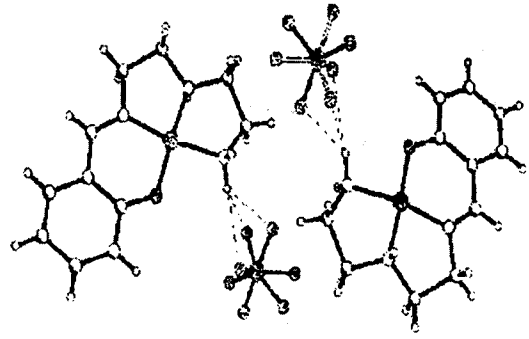
2.2　配位聚合物 2 的红外光谱

在配合物中，草酸根的 υ_{as}(C＝O)和 δ(C＝O)谱带的位置与其配位模式密切相关。因此，红外光谱技术是研究草酸根配位模式的有力手段。单螯

合草酸根的 υ_{as}(C=O)和 δ(C=O)谱带分别在 1 700cm^{-1}、800cm^{-1}左右有吸收峰；而作为四齿桥联配体的草酸根的 υ_{as}(C=O)谱带将红移，δ(C=O)谱带将蓝移[13]。在配合物 2 的红外光谱图中，υ_{as}(C=O)、δ(C=O)分别在1 654 cm^{-1}和 820cm^{-1}。上述结果表明，配合物 2 中的草酸根都是桥式配位的，草酸根与 $Fe^{Ⅲ}$，$Fe^{Ⅱ}$形成二维层状配位聚合物[13,14]。



Scheme 1 ORTEP of complex 1



Scheme 2 The H-bond interaction between the anion and the cation for complex 1

表 2 配合物 1 中氢键相互作用参数

Table 2 The H —bonding interaction pararmeters for complex 1

D—H	H—A	∠(D—H—A)/(8)	d(D—H—A)/mm
N(3)—H(3B)	H(3B)—O(2)^{i}	161.9	0.320 2(9)
N(3)—H(3B)	H(3B)—O(3)^{i}	139.9	0.331 0(12)
N(3)—H(3B)	H(3B)—O(5)^{i}	134.3	0.331 6(11)

Symmetry code $i=1-x,1-y,1-z$.

2.3 配合物 1 和配位聚合物 2 的磁性

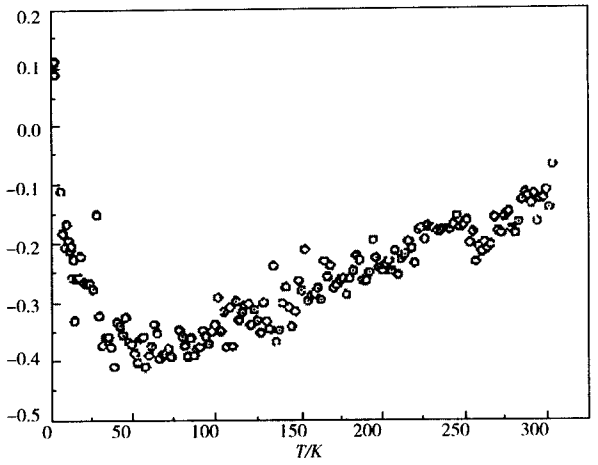


图 1 配合物 1 的 $\chi_m - T$ 关系图

Fig. 1 The plol of $\chi_m - T$ for complex 1

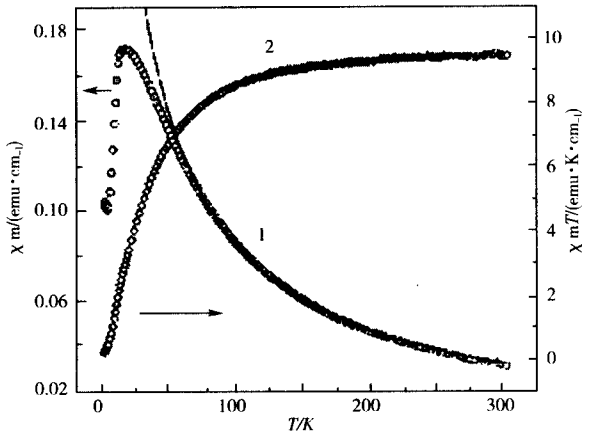


图 2 配位聚合物 2 的 $\chi_m T - T$ 和 $\chi_m - T$ 关系图

Fig. 2 The plots of $\chi_m - T(())$ and $\chi_m T - T(())$ for complex 2

配合物 1 的 $\chi_m - T$ 关系示于图 1。在 118～300K 范围内其为抗磁性。具有平面正方形配位构型的 Ni^{II} 离子的电子组态为 $[Ar]^{18}(3dxz)^2(3dyz)^2(3dz^2)^2(3dxy)^2(3dx^2-y^2)^0$，其总自旋 $S=0$，这是配合物 1 为抗磁性的原因。

配位聚合物 2 在 1.8～300K 温度的 χ_m-T 和 $\chi_m T-T$ 关系见图 2。χ_m 是每摩尔 $Ni^{Ⅱ}Fe^{Ⅱ}Fe^{Ⅲ}$ 单元的磁化率。配位聚合物 2 表现为反铁磁性交换作用的特征。温度低于 15K，磁化率显著降低，表明反铁磁有序开始。从 $d(\chi_m T)/dT-T$ 曲线的峰值求得反铁磁有序温度 $T_N=11K$(图 3)。

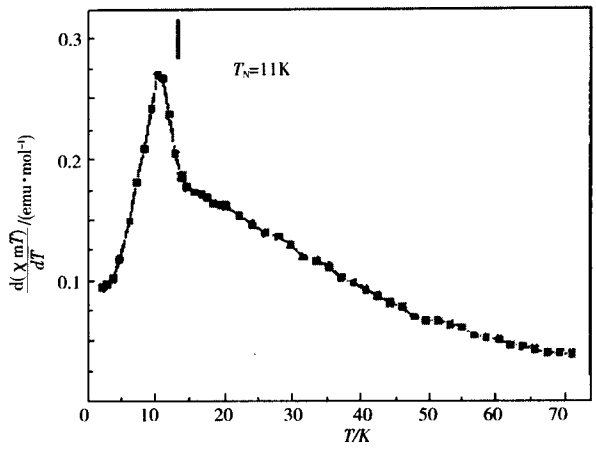


图 3　配位聚合物 2 的 $d(\chi_m T)/dT-T$ 关系图

Fig. 3　The plot of $d(\chi_m T)/dT$ versus T for complex 2

基于对配合物 1 的磁性分析，配位聚合物 2 中阳离子为抗磁性的，其磁性归于阴离子层的贡献。对一系列同类化合物的 Mössbauer 谱分析显示，A[$Fe^{Ⅱ}Fe^{Ⅲ}(ox)_3$]中的 $Fe^{Ⅱ}$ 和 $Fe^{Ⅲ}$ 都是高自旋态，即 $S(Fe^{Ⅱ})=2$、$S(Fe^{Ⅲ})=5/2$[8,14,15]。因此，每摩尔 $Ni^{Ⅱ}Fe^{Ⅱ}Fe^{Ⅲ}$ 单元的 μ_{eff}(唯自旋)值为 7.68μ_B。300K 时，配位聚合物 2 的 $\chi_m T$ 数值为9 141emu·K/mol，由公式 $\mu_{eff}=2\ 183(\chi_m T)^{1/2}$ 计算的 μ_{eff} 是 8.68μ_B。测量的 μ_{eff} 比唯自旋公式计算值大，归因于 FeⅡ和 FeⅢ离子轨道磁矩作用的贡献。用 Curries－Weiss 方程拟合配位聚合物 2 在 65～300K 间的磁化率，得到最佳拟合：Curries－Weiss 常数 C 和 Weiss 温度 θ 分别为 10.40(2)emu·K/mol 和－22.9(4)K，一致性因子 $R=9.6\times10^{-5}$($R=\sum_i[(\chi_m)_{obs}(i)-(\chi_m)_{calc}(i)]^2/\sum_i[(\chi_m)_{obs}(i)]^2$)。

参考文献

[1] Ding L, Zhang D Q, Zhang B, et al. Chin Chem Lett [J], 2000, 11: 749

[2] Miller J S, Epstein A J. Angew Chem Int Ed [J], 1994, 33: 385

[3] Gatteschi D, Carretta P, Lascialfari A. Physica B [J], 2000, 289～290: 94

[4] Gao S, Bai O, Yi L R. Acta Chim S in [J], 2000, 58: 1666

[5] Holmes SM, Girolami G S. J Am Chem Soc[J], 1999, 121: 5593

[6] Brinckerhoff W B, Zhang J, Miller J S, et al. Mol Cryst Liq Cryst A [J], 1995, 271: A207

[7] Mallah T, Thiebaut M, Verdaguer M, et al. Science [J], 1993, 262: 1 554

[8] Carling S G, Mathoniere C, Day P, et al. J Chem Soc Dalton Trans[J], 1996: 1 839

[9] Bhattachajee A, Iijima S, Mizutani F. J Magn Magn Mater[J], 1996, 153: 235

[10] Nutall C J, Bellitto C, Day P. Chem Commun. [J], 1995: 1 513

[11] Ren XM, Chen Y C, He C, et al. J C S Dalton Trans[J], 2002: 3915; Chen Y C, L iu G X, Xu H, et al. Russ J Coord Chem [J], 2003, 29: 251

[12] Sheldrick GM. SHELXTL, Structure Determination Software Programs, Version 5. 10. Bruker Analytical X－ray Systems Inc., Madison, Wisconsin, USA, 1997

[13] L iu G X, Ren XM, Xu H, et al. Chin Chem Lett[J], 2004, 15: 1 105

[14] Nakamoto K. Infrared Spectra of Inorganic and Coordination Compounds, 2nd Edn [M]. New York: Wiley Interscience, 1970: 244

[15] Zhuang J Z, Matsumoto N, 6 kawa H, et al. Chem Lett[J], 1990, 19: 87

Molecular Magnets Based on a Schiff—base Complex: Synthesis, Crystal Structures and Magnetic Properties

Abstract: A new schiff - base compound, $[NiL]ClO_4$ (1), was synthesized and characterized, where L represents the 1 : 1 condensation product of salicylaldehyde with diethyltriamine. The crystal structure of compound 1 shows that the Ni^{2+} ion in the NiL^+ moiety bonded with one O atom and three N atoms of the schiff - base ligand, L^-, and exhibits a near square coordination geometry. The H - bonding interaction between neighboring NiL^+ and ClO_4^- ions do not form H - bonding network. The temperature dependence of magnetic susceptibility (118 ~ 300 K) indicates that compound 1 is diamagnetic. The compound with stoichiometry of $[NiL][Fe^{II}Fe^{III}(ox)_3]$ (2) was prepared by mixing the aqueous solutions of compound 1, $K_3[Fe(ox)_3] \cdot 3H_2O$ and $FeSO_4 \cdot 7H_2O$ under N_2 atmosphere at ambient temperature. The IR spectrum of compound 2 illustrates that all the oxalate groups function as bridging groups, and compound 2 is actually a coordination polymer. The magnetic susceptibility measurement result at 118~300 K shows that this polymer possesses the anti-ferromagnetic ordering at below 11 K; the magnetic behavior above 60 K can be explained by the Curie - Weiss law, and the best fit for the magnetic susceptibility data at above 65 K gives a Curie - Weiss constant of 10.40 (2) emu K/mol and a Weiss temperature - 2219 (4) K, respectively.

Key Words: Schiff - base; coordination polymer; crystal structure; magnetic property

本文原载于《应用化学》,2005 年第 22 卷第 6 期

第二专题

自旋双稳分子磁体

具有平面型分子结构的$[M(mnt)_2]^-$配阴离子(M = transition metal ion; mnt^{2-} =maleonitriledithiolate)和具有Λ一型分子构象的苄基吡啶衍生物阳离子能形成阴阳离子完全分列的柱状堆积结构。在阴离子堆积柱内,$[M(mnt)_2]^-$配阴离子通过M…S…S…M、M…S…M等相互作用,形成自旋S=1/2的一维磁链,此类一维磁链配合物具有分子双稳性。$TCNE^-$($TCNQ^-$)等自由基分子离子与$[M(mnt)_2]^-$配阴离子具有相似的分子结构(二者都是平面型共轭体系,且每个分子的自旋S=1/2),因此,用$TCNE^-$($TCNQ^-$)等自由基分子离子替代$[M(mnt)_2]^-$配阴离子与苄基吡啶衍生物阳离子能形成阴阳离子完全分列的柱状堆积结构,相应的一维磁链化合物是潜在的具有分子双稳性的新体系。我们已开展两方面研究工作,首先立足于苄基吡啶衍生物的合成和结构表征,结合分子力学计算的结果,研究此类化合物中的各种弱相互作用,以及它们对分子堆积结构的影响,积累实验数据,为研究苄基吡啶衍生物阳离子和$TCNQ^-$、$TCNE^-$等自由基阴离子形成的一维分子基磁体奠定基础。我们开展的第二方面工作是,应用电化学方法制备并生长苄基吡啶衍生物阳离子和$[TCNQ]^-$,$[TCNE]^-$等自由基阴离子形成的一维分子基磁体,解析其结构。通过研究常压下的磁化率、优化出新的具有分子双稳性的一维分子基磁体。对新磁化率、磁比热和电导率等进行系统而深入的研究,探讨上述物理性质与压力,以及分子间的磁交换性质(磁交换常数J值的大小和符号)与自由基分子离子间重叠方式、各种短的堆积距离之间的关系。通过系统地改变平衡阳离子的分子构象,达到调节平衡阳离子的分子拓扑和体积大小,进一步实现控制自由基分子阴离子的堆积结构,以期获得具有分子双稳性的一维分子基磁性材料。

上述工作在本部分中收录了发表的学术论文10篇,其中被SCI收录8篇。

Molecule-Based Magnets with 1D Chain Structure of Bifurcated H-Bonding: Syntheses, Structure, and Magnetic Properties[1]

Abstract: Two complexes [PyH][Ni(Mnt)$_2$] (I) and [QlH][Ni(Mnt)$_2$](II) (Mnt^2 = maleonitriledithiolate, $[PyH]^+$ = pyridinium, $[QlH]^+$ = quinolinium) were synthesized and characterized by elemental analysis and IR spectra. ESR spectra of polycrystalline samples collected at room temperature are isotropic with g = 2.039 for I and anisotropic with g_z = 1.997, $g_y \approx g_x$ = 2.102 (g_{av} = 2.068) for II. The magnetic susceptibility data of I and II have been measured in the temperature range of 2~300 K. The results obtained suggest the antiferromagnetic coupling interactions between neighboring Ni^{3+} ions for I and ferromagnetic coupling interactions for II, respectively. Based on the crystal structure analysis of I, the magnetic properties of two complexes have been discussed.

Introduction

Recently, one-dimensional (1D) compounds have received an increasing interest because of their novel physical properties, such as Peierls transition, spin-Peierls transition, charge density wave (CDW) states, spin density wave (SDW) states, molecular bistability properties, etc. [1-4]. These 1D compounds have stimulated further theoretical investigations. In this area, the complexes containing $[Ni(Mnt)_2]^-$ anions are the most studied of the 1D transition metal complexes[5-7]. Previous works showed that

the geometry and size of the counterion strongly influence the stacking pattern of $[Ni(Mnt)_2]^-$ anions in the solid state and thus affect the physical properties of the relevant materials. Lately, we synthesized and structurally characterized a series of $[Cat]^+[Ni(Mnt)_2]^-$ complexes, where $[Cat]^+$ is the benzylpyridinium derivative. Preliminary results revealed the low-dimensional character in the structure and magnetism of these complexes. Furthermore, the stacking patterns of $[Ni(Mnt)_2]^-$ anion and magnetic properties of these materials can be tuned through systemic variation of the substituents in aryl rings [8, 9]. In order to obtain further information concerning the low dimensional nature of these complexes and the role of the counterion, we decided to study new compounds of this family containing $[Ni(Mnt)_2]^-$ anion. For this purpose, we selected the pyridinium derivatives, which have planar structures and a potential hydrogen bonding donor; therefore, a new type of stacking structure may exist [10]. In this paper, we report the syntheses and magnetic properties of two complexes.

Experimental

Disodium maleonitriledithiolate (Na_2Mnt) was prepared following the procedure described in [11]. Pyridinium chloride derivative was prepared by reacting pyridine derivative with one equivalent of diluted hydrochloric acid. A similar procedure of synthesizing $[Bu_4N]_2[Ni(Mnt)_2]$ was used to prepare $[PyH]_2[Ni(Mnt)_2]$ and $[QlH]_2[Ni(Mnt)_2]$ [11].

$[PyH][Ni(Mnt)_2](I)$[10]. A MeCN solution (10 cm^3) of I_2 (150 mg, 0.59 mmol) was slowly added to a MeCN solution (10 cm^3) of $[PyH]_2[Ni(Mnt)_2]$ (500 mg, 1.0 mmol) and the mixture was stirred for 20 min. Then, MeOH (80 cm^3) was added, and the mixture was allowed to stand overnight; the microcrystals formed 487 mg were filtered off, washed with MeOH and dried in vacuum. Yield of I was 86%.

For $C_{13}H_6N_5S_4Ni$:

anal. calcd. (%): C, 37.3; H, 1.44; N, 16.7.

Found (%): C, 37.1; H, 1.65; N, 16.5.

IR (cm^{-1}): 3205.1 s, 3170.3 s, 3087.4 m, 3073.5 s, 2213.9 sh, 2204.2 vs, 2159.9 sh, 1633.4 s, 1612.2 m, 1596.8 s, 1521.6 s, 1429.4 m, 862.1 w.

[QlH][Ni(Mnt)$_2$] (II). The procedure for preparing II was the same as in the case of I. Yield of II>85%.

For $C_{17}H_8N_5S_4Ni$

anal. calcd. (%): C, 43.5; H, 1.72; N, 14.9.

Found (%): C, 43.2; H, 1.91; N, 14.5.

IR (cm^{-1}): 3210.9 s, 3145.4 s, 3088.7 s, 3070.2 m, 2215.6 sh, 2209.3 vs, 1639.9 s, 1595.3 s, 1558.0 s, 1431.1 m, 869.7 w.

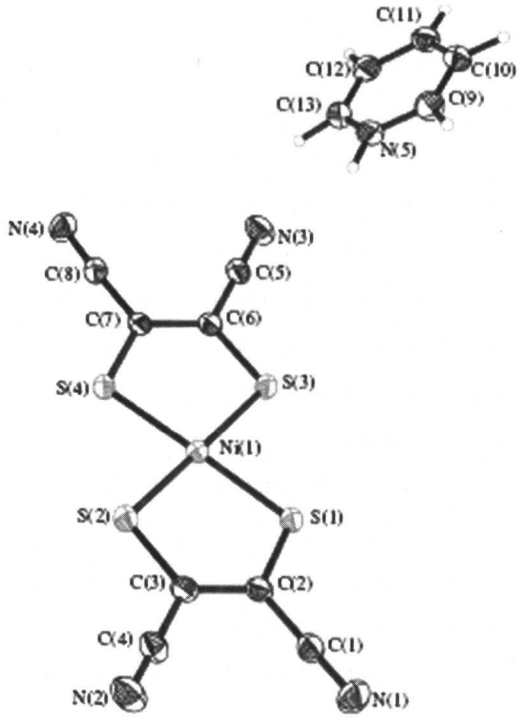


Fig. 1 ORTEP view of I with a 30% probability of thermal ellipsoids

Elemental analyses were performed on a Perkin—Elmer 240 analytical

instrument.

IR spectra were obtained with KBr pellets in the range of 4 000～400 cm^{-1} using a IFS66 VFT－IR spectrophotometer.

Magnetic susceptibilities of I and II were determined in the temperature range of 2～300 K on a MagLab system 2000 magnetometer, and diamagnetism was corrected using Pascal constants (1.6×10^{-4} emu mol^{-1} for and 1.8×10^{-4} emu mol^{-1} for II).

The ESR spectra were recorded from a polycrystalline sample on a (JEOL) JES－1XG spectrometer at 100 kHz modulation at room temperature. Mn^{2+} in MgO was used as a standard (ESR marker).

Results and Discussion

In the IR spectrum of the two complexes, the bands of υ (N－H) are very intense and appear at 3 205.1 and 3 170.3 cm^{-1} for I and 3 210.9 and 3 145.4cm^{-1} for II. The stretching vibrations of the CN group υ (CN) in the compounds with Mnt^{2-} usually give intense bands in the IR spectrum and in general are only weakly coupled by other vibrations of the molecule. Therefore, IR spectroscopy is suitable for studying Mnt^{2-}－containing complexes. In IR spectra, very intense characteristic υ (CN) bands appear at 2 204.2 cm^{-1} and have two shoulders at 2 213.9 and 2 159.9 cm^{-1} for I; the respective characteristic υ (CN) bands in II appear at 2 209.3 cm^{-1} and have a shoulder at 2 215.6 cm^{-1}. The multiplicity of CN vibrations results from the intermolecular interactions[12].

Crystals of complex I are monoclinic; space group $P2_1/c$. The ORTEP view with atomic numbering is shown in Fig. 1 [10]. The H-bonding interactions between donors (N-H of pyridine) and acceptors (CN of maleonitriledithiolate) in I are observed as depicted in Fig. 2. The contacts and angles of bifurcated H-bonding pairs are 2.95 for N(5)…N(3), 3.02Åfor N(5)N(4) (x, 1 + y, z), 132.3° for N(5)－H(5N)…N(3) , and 134.8°for

N(5)-H(5N)···N(4) (x, 1 + y, z). The H-bond interactions between anions and cations give rise to a zigzag chain of alternating cations and anions and lead to neighboring $[Ni(Mnt)_2]^-$ anions within an intrachain separating with larger distances. The packing diagram for I along b—axis is displayed in Fig. 3. The shortest Ni···Ni, Ni···S, and S···S distances are 6.39, 4.77, and 3.76Å within a chain and 4.28, 3.69, and 5.34Å between chains, respectively. These distances are larger than the corresponding sum of van der Waals radii of 3.26, 3.48, and 3.7Å, respectively [13]. Thus weak magnetic interactions between Ni^{3+} ions via the Ni(III)···Ni(III), Ni···S···Ni, or Ni···S···S···Ni coupling pathway are expected.

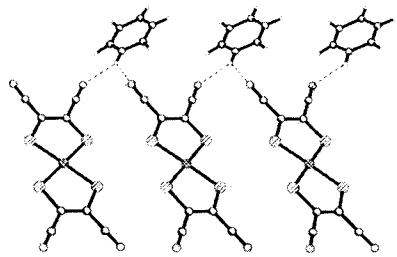


Fig. 2 One-dimensional anion chain formed by bifurcated H-bonding.

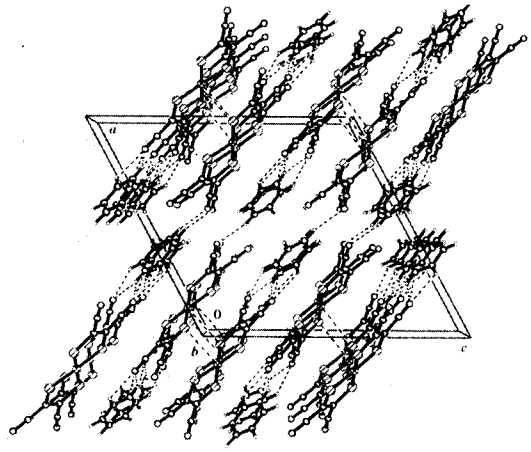


Fig. 3 Packing diagram viewed down the b—axis.

The polycrystalline ESR spectra of I and II were measured at room temperature and are displayed in Fig. 4. The ESR spectrum of I is almost isotropic, $g = 2.039$. However, the ESR spectrum of II is anisotropic, $g_z = 1.997$, $g_y \approx g_x = 2.102$ ($g_{av} = 2.068$).

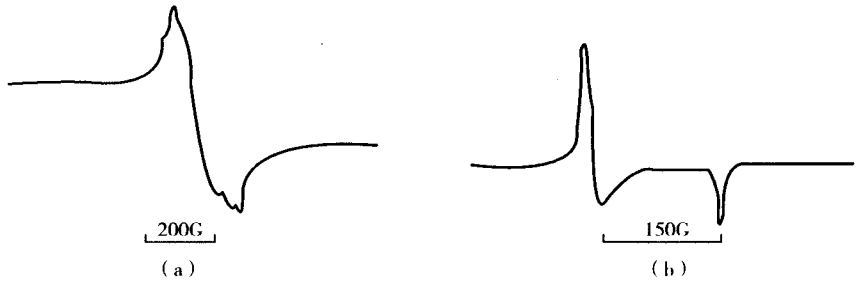


Fig. 4 ESR spectra of polycrystalline samples measured at room temperature for I (a) and II (b).

The magnetic susceptibilities of I and II at variable temperatures (2～300 K) were measured from their polycrystalline samples in a 10 kOe field. The corresponding plots of χ_m vs. T and $\chi_m T$ vs. T of I and II are shown in Fig. 5, where χ_m is the magnetic susceptibility per Ni(III) unit.

For I, the calculated $\chi_m T$ at 300 K, 0.294 emu K mol^{-1}, is somewhat less than the spin-only value expected for one noninteracting s = 1/2 metal center 0.375 emu K mol^{-1}. The $\chi_m T$ value decreases as the sample temperature is decreased in the temperature range of 300～80 K then drops to 0.003 emu K mol^{-1} at 80 K and remains almost unchanged below 80 K. These results suggest the antiferromagnetic coupling interactions between neighboring Ni^{3+} ions. Based on the crystal structural analysis, magnetic coupling interactions between $[Ni(Mnt)_2]^-$ anions through intermolecular H-bonding interactions can occur [14]. Thus, over the entire temperature range, the magnetic susceptibility data of I were analyzed as follows: at first, approximately, the Bonner Fisher model for a uniform chain of the s = 1/2 metal center[15] was used to simulate the magnetic exchange interactions within an intrachain, using Hamiltonian $\hat{H} = -2J \sum_{i-1}^{n} \hat{S}_i \hat{S}_{i-1} - g\beta$

$\sum_{i=1}^{n} H\hat{S}_i$ and the numerical expression[16]

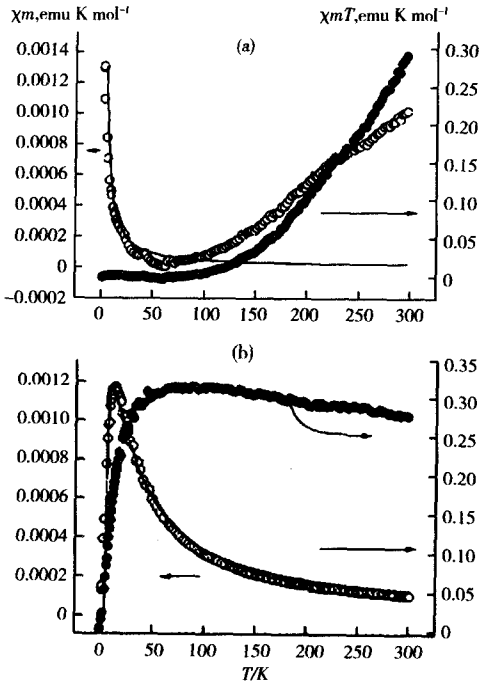


Fig. 5 Plots of $\chi_m T-T$ (●) and χ_m-T (○) of I (a) and II (b); solid lines are theoretical curves.

$$\chi_m^J=\frac{Ng^2\beta^2}{k_BT}$$

$$\times\frac{0.25+0.074975x+0.075235x^2}{1.0+0.9931x+0.172135x^2+0.757825x^3},$$

where $x=-J/k_BT$ A. molecular field correction [17], using

$$\chi_m^{J+J}=\frac{\chi_m^J}{1-(2zJ'/Ng^2\beta^2)\chi_m}+\chi_{TIP}$$

where z is the number of interacting neighbors, was further applied to account for the magnetic exchange interactions between chains. The parameters N, β, g, χ_{TIP}, and k_B have their usual meanings. With $g=2.039$, as determined from the polycrystalline ESR spectrum, least-squares analysis of the susceptibility data gives $J/k_B=-2.1$ K, $zJ'/k_B=0.54$ K, $\chi_{TIP}=5.7\times10^{-4}$ emu mol^{-1}, and($R=\sum_i(\chi_m^{obsd}-\chi_m^{obsd})^2/(\chi_m^{obsd})^2$). As can be seen

in Fig. 4, the results of fit are very poor, especially in the high temperature range; thus another magnetic coupling model needs to be considered.

For II, the calculated $\chi_m T$ at 300 K, 0.276 emu K mol^{-1}, is less than the spin-only value expected for one noninteracting $s = 1/2$ metal center (0.375 emu K mol^{-1}). The $\chi_m T$ value slightly increases as the sample temperature is decreased in the smple temperature range of 300~71 K, which shows that there exist weakly ferromagnetic coupling interactions between neighbor Ni^{3+} ions. The $\chi_m T$ value drops sharply below 80 K and almost reaches zero at 2 K; these results may follow from the competition of antiferromagnetic exchange interaction between magnetic interchains.

Assuming the crystal structure of II to be similar to that of I, the $\chi_m(T)$ data for II in the 2~300K temperature range were fit to the Baker equations with a molecular field correction; these equations were deduced from the ferromagnetic chain of $s = 1/2$ [18, 19]

$$\chi_m^{J+J'} = \frac{\chi_m^J}{1-(2J'/Ng^2\beta^2)\chi_m} + \chi_{TIP}, \tag{1}$$

$$\chi_m^J = \frac{Ng^2\beta^2}{4k_BT}\left[\frac{C}{D}\right]^{2/3} \tag{2}$$

$$C = 1.0 + 5.7979916y + 16.902653y^2 + 29.376885y^3 + 29.832959y^4 + 14.036918y^5, \tag{3}$$

$$D = 1.0 + 2.7979916y + 7.0086780y^2 + 8.653644y^3 + 4.5743114y^4,$$

where $y = J/2k_BT$ and the other parameters in the Eqs. (1)-(4) have their usual meaning. The best fit results were $J/k_B = 6.2$ K, $zJ'/k_B = -1.1$ K, $\chi_{TIP} = 6.9\times10^{-4}$ emu mol^{-1}, and the discrepancy factor $R = 2.7\times10^{-6}$ ($R = \sum i(\chi_m^{calc} - \chi_m^{obsd})^2/(\chi_m^{obsd})^2$) with $g = g_{av} = 2.068$ as determined from the polycrystalline ESR spectrum of II.

In conclusion, the variable temperature magnetic susceptibilities in the temperature range of 2~300 K and the powder ESR spectra at room temperature for two very different complexes with 1D structure were measured through intermolecular H-bonding. These results suggest that a lot of fac-

tors may influence the magnetic exchange interactions between neighbor Ni^{3+} ions for this type of $[Ni(Mnt)_2]^-$ containing complexes [6].

acknowledgments

This work was supported by the National Natural Science Foundation of china (project no. 20171001) and the Natural Science Foundation of Anhui Province (project no. 01012038) of China.

References

[1] Coomber, A. T., Beljonne, D., Friend, R. H., et al., Nature (London), 1996, vol. 380, p. 144.

[2] Manabe, T., Kawashima, T., Ishii, T., et al., Synth. Met., 2001, vol. 116, p. 415.

[3] Wei, J. H., Zhao, J. Q., Liu, D. S., et al., Synth. Met., 2001, vol. 122, p. 305.

[4] Fujita, W. and Awaga, K., Science, 1999, vol. 286, p. 261.

[5] Pullen, A. E., Pokhodnga, K. I., Faulmann, C., et al., Synth. Met., 1999, vol. 103, p. 2310.

[6] Pullen, A. E., Faulmann, C., Pokhodnga, K. I., et al., Inorg. Chem., 1998, vol. 37, p. 6714.

[7] Gama, V. P., Almeida, M., Henriques, R. T., et al., J. Phys. Chem., 1991, vol. 95, p. 4263.

[8] Ren, X. M., Lu, C. S., Liu, Y. J., et al., Transition Met. Chem., 2001, vol. 26, p. 136.

[9] Ren, X. M., Li, H. F., Wu, P. H., et al., Acta Crystallogr., Sect. C: Cryst. Struct. Commun., 2001, vol. 57, p. 1022.

[10] Ren, X. M., Lu, C. S., Wu, P. H., and Meng, Q. J., J. Chem. Crystallogr., 2001, vol. 31, p. 173.

[11] Davison, A. and Holm, H. R., Inorg. Synth., 19 vol. 10, p. 8.

[12] Ballester, L., Barral, M. C., Gutierrez, A., et al., Inorg. Chem., 1994, vol. 33, p. 2142.

[13] McCleverty, J. A., Prog. Inorg. Chem., 1968, vol. 10, p. 49.

[14] Ikorskii, V. N., Ovcharenko, V. I., Shvedenkov, Y. G., et al., Inorg. Chem., 1998, vol. 37, p. 4360.

[15] Bonner, J. C. and Fisher, M. E., Phys. Rev. A, 1964, vol. 135, p. 640.

[16] Estes, W. E., Gavel, D. P., Hatfield, W. E., and Hoggson, D., Inorg. Chem., 1978, vol. 17, p. 1415.

[17] Myers, B. E., Berger, L., and Friedberg, S. A., J. Appl. Phys., 1968, vol. 40, p. 1149.

[18] Baker, G. A., Rushbrook, G. S., Jr., and Gilbert, H. E., Phys. Rev. A, 1964, vol. 135, p. 1272.

[19] Deakin, L., Arif, A. M., and Miller, J. S., Inorg. Chem., 1999, vol. 38, p. 5072

本文原载于《俄罗斯配位化学》2003 年 29 卷第 4 期

Spontaneous magnetization below 7.7 K based on an extended 3 - D H-bonding network material: synthesis, crystal structure and magnetic properties

The structure of the complex [4 - aminopyridinium][Ni(mnt)$_2$], as determined by X - ray single crystal analysis, consists of 4 - aminopyridinium cations and [Ni(mnt)$_2$]$^-$ anions. The interactions between anions and cations via the bifurcated N(Py)- H···NC H-bonds give rise to a 1 - D zigzag chain of alternating cations and anions, and a 3 - D H-bonding network through further N(NH$_2$)- H···NC interactions. χ_{dc} and χ_{ac} have been measured down to 1.8 K and analysed, indicating the existence of a spin canting phenomenon. Below the critical temperature (around 7.7 K), the sample spontaneously magnetizes, and the hysteresis loop was observed at 1.85 K, corresponding parameters are as follows: H_c = 150 Oe and M_r = 7.9 emu mol^{-1}. The pathway of the exchange interaction in this complex via H-bonding is discussed in light of the crystal structure analysis.

Introduction

In recent years, the principles of supramolecular chemistry, in which a great deal of new concepts Concerning intermolecular non-covalent interactions such as H-bonding and π-π stacking interactions, have been introduced into the area of material science[1], and some have yielded materials exhibiting novel properties[2].

The preparation of molecular based magnets via the association of par-

amagnetic complex molecules through H-bonding interactions have attracted wide interest[3]. However, in this field little attention has been paid to the construction of $[M(mnt)_2]^-$ [M = Ni(III), Pd(III) and Pt(III)] with pyridinium derivatives, in which the CN groups of the mnt^{2-} ligand and H-N of the pyridinium derivatives may undergo H-bonding interactions. Actually, our primary work showed that there are strong bifurcated H-bonding interactions between these blocks[4]. Therefore, we might obtain 2 - D and 3 - D molecular magnet based on this class of building block if a reasonable pyridinium derivative is chosen. In this contribution, we report on the synthesis, crystal structure and magnetic properties of a molecular based magnet, [4 - aminopyridinium][$Ni(mnt)_2$], with an extended 3 - D H-bonding network.

Experimental

Materials

Disodium maleonitriledithiolate (Na_2mnt) was prepared following the procedure reported in the literature[5]. The pyridinium chloride derivative was prepared by reaction between pyridine derivative and one equivalent of dilute hydrochloric acid. A similar method to that reported for the synthesis of $[Bu_4N]_2[Ni(mnt)_2]$ [5] was used to prepare $[4-aminopyridinium]_2[Ni(mnt)_2]$.

Synthesis of [4 - aminopyridinium][$Ni(mnt)_2$] (1)

A MeCN solution (10 cm^3) of I_2 (150 mg, 0.59 mmol) was slowly added to a MeCN solution (10 cm^3) of $[4-aminopyridinium]_2[Ni(mnt)^2]$ (530 mg, 1.0 mmol) and the mixture was stirred for 20 min. MeOH (80 cm^3) was then added, and the mixture allowed to stand overnight; the 374 mg of microcrystals formed were filtered off, washed with MeOH and dried in vacuo (86% yield). Elemental analysis: calc. for $NiC_{13}H_7N_6S_4$: C,

35.96; H, 1.63; N, 19.36. Found: C, 35.81; H,1.72; N, 19.28%. IR (cm^{-1}): 3357.1s (υ_{N-H}), 3234.5s (υ_{N-H}), 2212.6vs ($\upsilon_{C\equiv N}$),, 1604.0s ($\upsilon_{C=N}$), 1475.7m ($\upsilon_{C=C}$), 1429.1m ($\upsilon_{C=-C}$),873.4w (υ_{C-S}).

Physical measurements

Elemental analyses were performed using a Perkin - Elmer 240 analytical instrument. IR spectra were obtained with KBr pellets in the 4000～400 cm^{-1} region, using an IFS66 VFT - IR spectrophotometer. Magnetic susceptibility was determined in the temperature range 2 - 285 K on a MagLab system 2000 magnetometer, and diamagnetism was corrected by Pascal's constants (2.0×10^{-4} emu mol^{-1}). The ESR spectra were recorded with a polycrystalline sample on a (JEOL) JES - 1XG spectrometer at 100 kHz modulation at room temperature. Mn^{2+} in MgO was used as a standard sample (ESR marker).

Data collection, structure solution and refinement

A brown red single crystal with dimensions of $0.3\times 0.2\times 0.2$ mm was mounted on a Siemens SMART CCD area detector with monochromated Mo - Kα radiation at room temperature. Crystal data collection parameters and refinement details are listed in Table 1. All computations were carried out via a PC - 586 computer using the SHELXTL - PC program package.[6] The structure was solved by direct methods and refined on F^2 by full-matrix least-squares methods. All the non-hydrogen atoms were refined anisotropically. Hydrogen atoms were placed in their calculated positions and refined following the riding model.

Table 1 Crystal data and structure refinement for I

Empirical formula	$C_{13}H7N_7NiS_4$
Formula weight	434,20
T/K	293(2)
Wavelength/Å	0.71073
Crystal system	Monoclinic

（续表）

Space group	$C2/c$
a/Å	41.3120(10)
b/Å	6.4570(10)
c/Å	12.9580(10)
β/°	93.730(10)
Volume/Å^3	3449.2(6)
Z	8
Absorption coefficient/mm^{-1}	1.616
F(000)	1752
Crystal size/mm^3	0.3×0.2×0.2
Reflections collected	8385
Independent reflections	3034[R(int)=0.0625]
Refinement method	Full-matrix least-squres on F^2
Data/restraints/parameters	3034//220
Goodness-of-fit on F^2	1.092
Final R indices[$I>2\sigma(I)$]	$R1$=0.0510, $wR2$=0.1496
R indices (all data)	$R1$=0.0543, $wR2$=0.1525

CCDC reference number 179243.

See http://www.rsc.org/suppdata/dt/b2/b204902c/ for crystallographic data in CIF or other electronic format.

Results and Discussion

Description of the structure

Complex 1 crystallizes in monoclinic space group C2/c. An ORTEP view with non-hydrogen atom labeling is shown in Fig. 1. There are two halves of non-equivalent $[Ni(mnt)_2]^-$ anions and a [4-aminopyridinium]$^+$ cation in the asymmetric unit cell. For two $[Ni(mnt)_2]^-$ anions, the Ni(1) and Ni(2) atoms are coordinated to four sulfur atoms and exhibit square-planar coordination geometry, respectively. The average Ni-S bond distances are 2.1441(9) Å in the anion containing the Ni(1) atom and 2.1457(9)Å in the anion containing the Ni(2) atom. The bond angles within the five-membered ring are 92.82(4)°for S(1)-Ni(1)-S(2) and 93.92(4)° for

S(3) - Ni(2) - S(3). These results agree well with those found in [Ni(mnt)$_2$]$^-$ complexes.[4] The anion containing the Ni(2) atom is almost planar, and all deviations from the four sulfur atoms are less than 0.06 Å. However, the CN groups for the anion containing the Ni(1) atom are bent away from the coordination plane defined by the four sulfur atoms, and the deviations are 0.125Å for the N(1) atom and 0.124Å for the N(2) atom, respectively.

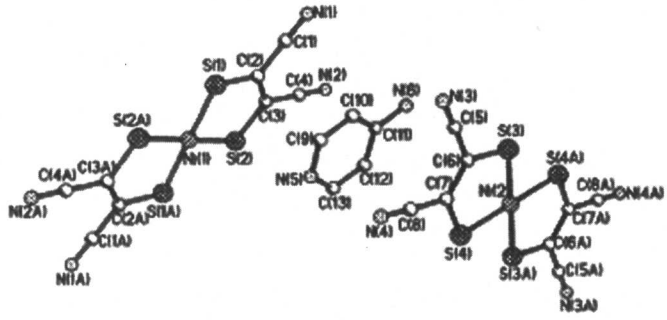


Fig. 1 ORTEP[14] view of 1 with atom labeling. Hydrogen atoms are omitted for clarity.

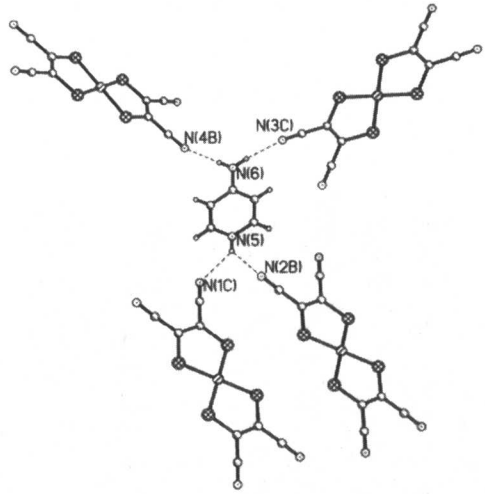


Fig. 2 H-bonding interactions between anions and cations for 1.

There are three H-bonding donors for 4 - aminopyridinium, and four H-bonding acceptors for [Ni(mnt)$_2$]$^-$; H-bonding interactions are thus expected between the anions and cations. Actually, the two types of strong H-bonding interactions observed in 1 are as depicted in Fig. 2, one exists

between the N atoms of the NH_2 groups and the N atoms of the CN groups of the mnt^{2-} ligands, and another bifurcated H-bonding between the N－H of the pyridinium and the CN groups of the mnt^{2-} ligands which is observed in some bipyridinium-containing compounds.[7] The corresponding distances and angles of H-bonding contacts are summarized in Table 2.

Table 2 Hydrogen bonds for 1(Å and °)

D···H···A	*d*(D···H)	*d*(H···A)	*d*(D···A)	(DHA)
N(5)－H(5A)···N(1)#3	0.86	2.35	3.030(5)	135.7
N(5)－H(5A)···N(2)#4	0.86	2.36	3.039(5)	136.6
N(6)－H(6A)···N(4)#5	0.86	2.17	3.019(5)	168.1
N(6)－H(6B)···N(3)#6	0.86	2.17	3.023(5)	170.4

Symmetry transformations used to generate equivalent atoms: #1: $-x+1/2,-y+1/2,-z+1$; #2: $-x+1,-y,-z+1$; #3: $x,-y+1,z+1/2$; #4: $x,-y,z+1/2$; #5: $x,y-1,z$; #6: $x,-y+1,z-1/2$.

The bifurcated H-bonding interactions between the CN groups and N－H of the pyridiniums give rise to a zigzag chain of alternating cations and anions, and the H-bonding interactions between the CN groups and the amino groups result in this complex forming an extended 3－D H-bonding network. The packing diagrams for 1 viewed down the *a*－ and *c*－axes are displayed in Fig. 3

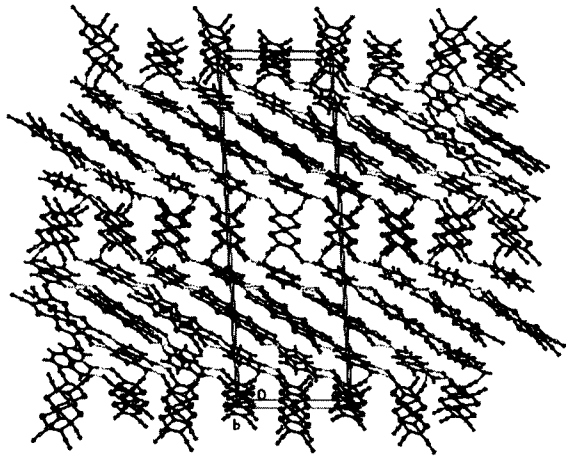


Fig. 3 Extended H-bonding network viewed down the *a* - axis, and showing two types of channels for 1.

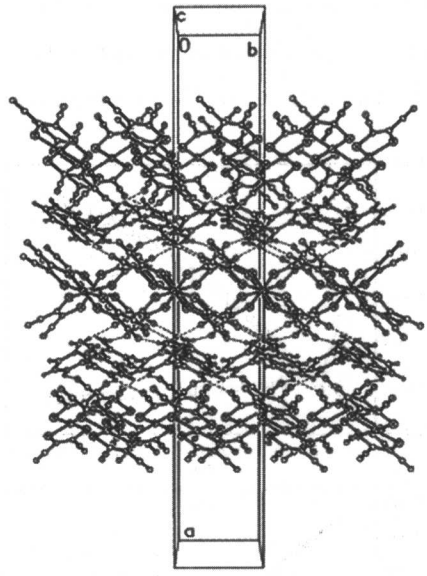


Fig. 4 Extended H-bonding network viewed down the a - axis.

and 4, respectively. Two types of channel are clearly shown in Fig. 3. The shortest Ni···Ni, Ni···S and S···S distances between neighboring $[Ni(mnt)_2]^-$ anions are 6.46, 4.86 and 3.81 . These distances are larger than the corresponding atom sums of van de Waals radii of 3.26, 3.48 and 3.7 Å, respectively,[8] so weak magnetic interactions between Ni(Ⅲ) ions via Ni(Ⅲ)···Ni(Ⅲ) or Ni···S···Ni or Ni···S···S···Ni exchange pathways are expected.

Magnetic properties

Fig. 5a shows the variation of χ_m and $\chi_m T$ with temperature for 1 measured in a field of 10 kOe, where χ_m denotes molar magnetic susceptibility and T temperature. The calculated $\chi_m T$ at 150 K, 0.224 emu K mol^{-1}, is less than the spin-only value expected for one non - interacting S = 1/2 (0.375 emu K mol^{-1}). The $\chi_m T$ value decreases as the sample temperature decreases, and the result indicates that there exist antiferromagnetic coupling interactions between neighboring Ni(Ⅲ) ions. It is noteworthy that the χ_m versus T curve undergoes an inflection around 16 K, and

the χ_m values depend on the external magnetic field below this temperature (as shown in Fig. 5b). This transition around 16 K may suggest that there is ferromagnetic ordering for 1 in the lower - temperature range.[9,10]

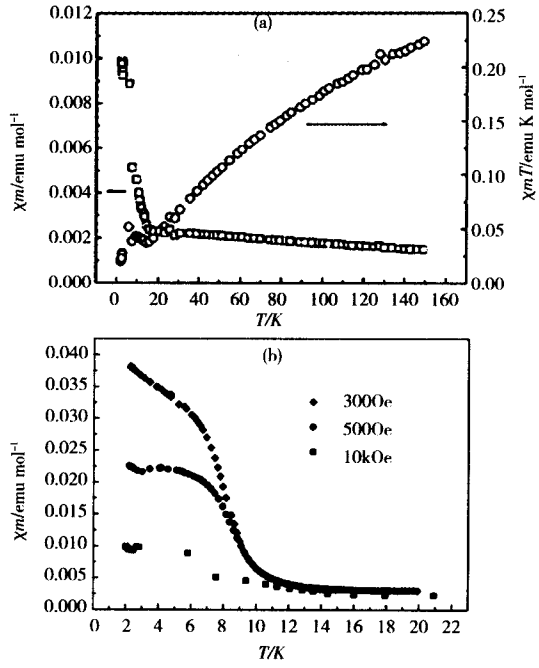


Fig. 5 (a) Variation with temperature of χ_m and $\chi_m T$ for 1 (dc field 10 kOe), and (b) the plots of χ_m at three values of applied field.

To confirm the appearance of magnetic ordering and determine the precise critical temperature, ac magnetic susceptibility measurements were performed. Typically, in a magnet containing net magnetic moments in the ordered state (for example, ferromagnet, ferrimagnet, or canted antiferromagnet), these measurements show a maximum in the in - phase signal (χ') near T_c and the out-of-phase signal (χ''starts to appear at temperatures just below T_c. In 1, χ'shows a maximum around 7.7 K indicating that the magnetic ordering may occur near this temperature, and a non-zero χ''was not observed below 7.7 K. In order to gain a deeper insight into the low - temperature magnetic behavior of 1, we performed χ_{ac} measurements as a function of temperature at different frequencies, and found the maximum of

χ' is independent on the frequency of ac-field, although χ'' signals are very weak which indicates that the ferromagnetic component is small due to very weak canting (Fig. 6). The FCM and ZFCM measurements (in a 300 Oe measured field) from 1.8 to 15 K for 1 show evidence of magnetic ordering, and a small but clear remnant magnetization is observed below ~7.7 K (Fig. 7). These results confirm long-range ordering is present.

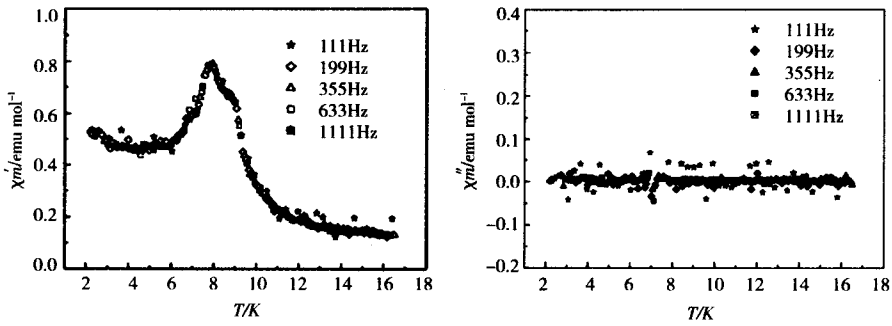


Fig. 6 Temperature dependence of ac-magnetic susceptibility measured at different frequencies, (Top: real part; Bottom: imaginary part).

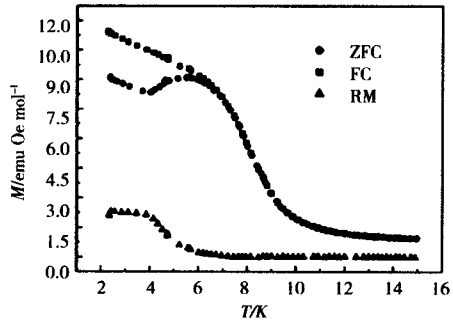


Fig. 7 Magnetization of 1 cooled in zero-field (ZFCM), a field of 300Oe (FCM) and remnant magnetization (RM), respectively.

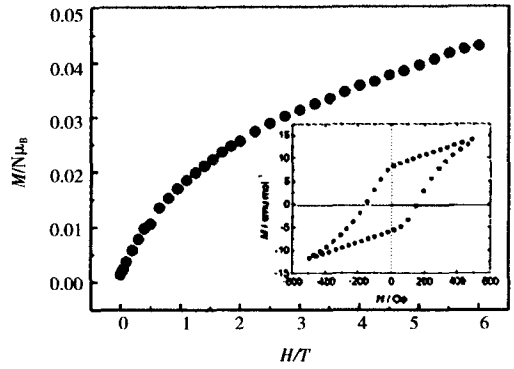


Fig. 8 Magnetization curve obtained at 1.85 K for 1. The inset shows the magnetic hysteresis loop with H_c = 150 Oe and M_r = 7.9 emu mol_1 at 1.85 K

Conclusions

A new system containing $[Ni(mnt)_2]^-$ anions has been structurally characterized and its magnetic behavior investigated. The H-bonding interactions between anions and cations give extended three - dimensional H-bonding networks. To the best of our knowledge, reports of the mnt^{2-} ligand acting as a H-bonding acceptor are rare. The various magnetic data for 1 are consistent with antiferromagnetic coupling between neighboring Ni (Ⅲ) ions with long - range ferromagnetic ordering below 7.7 K. We interpret these magnetic properties as a consequence of canted spin antiferromagnetism leading to weak ferromagnetism at low—temperature.[9,10] The analysis of the crystal structure of 1 indicated the shortest contacts of Ni…Ni, Ni…S and S…S between neighboring $[Ni(mnt)_2]^-$ anions are significantly larger the sums of the van de Waals radii of corresponding atoms, a magnetic exchange mechanism for 1 could thus involve interactions via the H-bonding network linking $[Ni(mnt)_2]^-$ anions.

Acknowledgements

The authors are grateful for the financial support of the National Natural Science Foundation of China (project no. 20171001 and 20125104), and the Natural Science Foundation of Anhui Province of China (project no. 01012038).

References

[1] (a) H. Saadeh, L. Wang and L. Yu, J. Am. Chem. Soc., 2000, 122, 546; (b) D. S. Lawrence, T. Jiang and M. Levett, Chem. Rev., 1999, 95, 2229.

[2] (a) G. B. Gardner, D. Venkataraman, J. S. Moore and S. Lee, Nature, 1995, 374, 792;

(b) D. Venkataraman, G. B. Gardner, S. Lee and J. S. Moore, J. Am. Chem. Soc., 1995, 117, 11600;

(c) M. Fujita, Y. J. Kwon, S. Washizu and K. Ogura, J. Am. Chem. Soc., 1994, 116, 1151;

(d) O. M. Yaghi, G. Li and H. Li, Nature, 1995, 378, 703.

[3] (a) Y. Pontillon, T. Akita, A. Grand, K. Kobayashi, E. Lelievre—Berna, J. Pé caut, E. Ressouche and J. Schweizer, J. Am. Chem. Soc., 1999, 121, 10126;

(b) A. Fragoso, M. L. Kahn, A. Castineiras, J. — P. Shtter, O. Kahn and R. Cao, Chem. Commun., 2000, 1547;

(c) D. G. Munno, D. Viterbo, A. Caneshi, L. Francese and M. Julve, Inorg. Chem., 1994, 33, 1585;

(d) D. G. Munno, W. Ventura, G. Viau, L. Francese and M. Julve, Inorg. Chem., 1998, 37, 1458;

(e)V. N. Ikorskii, V. I. Ovcharenko, Y. J. Shvedenkov, G. V. Romanenko, S. V. Fokin and R. Z. Sagdeev, Inorg. Chem., 1998, 37, 4360.

[4] X. M. Ren, C. S. Lu, P. H. Wu and Q. J. Meng, J. Chem. Crystallogr., 2002, 32, 173.

[5] A. Davison and H. R. Holm, Inorg. Synth., 1967, 10, 8.

[6] G. M. Sheldrick, SHELXTL, Structure Determination Software programs, version 5.10, Bruker Analytical X-Ray Systems Inc., Madison, WI, USA, 1997.

[7] A. L. Gillon, A. G. Orpen, J. Starbuck, X. M. Wang, Y. Rodríguez-Martín and C. Ruiz-Pérez, Chem. Commun., 1999, 2287.

[8] J. A. McCleverty, Prog. Inorg. Chem., 1968, 10, 49.

[9] (a) S. J. Rettig, R. C. Thompson, J. Trotter and S. Xia, Inorg. Chem., 1999, 38, 1360;

(b) S. J. Rettig, J. V. S nchez, A. Storr, R. C. Thompson and J. Trotter, J. Chem. Soc., Dalton Trans., 2000, 3931.

[10] S. R. Batten, P. Jensen, C. J. Kepert, M. Kurmoo, B. Moubaraki, K. S. Murray and D. J. Price, J. Chem. Soc., Dalton Trans., 1999, 2987.

[11] (a) O. Kahn, Molecular Magnetism, VCH publisher, New York, 1993;

(b) R. L. Carling, Magnetochemistry, Springer, Berlin, 1989.

[12] A. J. Banister, N. Bricklebank, I. Lavender, J. M. Rawson, C. I. Gregory, B. K. Tanner, W. Clegg, M. R. J. Elsegood and F. Palacio, Angew. Chem., Int. Ed. Engl., 1996, 35, 2533.

[13] N. Robertson, C. Bergemann, H. Becker, P. Agarwal, S. R. Julian, R. H. Friend, N. J. Hatton, A. E. Underhill and A. Kobayashi, J. Mater. Chem., 1999, 9, 1713.

[14] M. N. Burnett and C. K. Johnson, ORTEP-III, Report ORNL-6895, Oak Ridge National Laboratory, Oak Ridge, TN, 1996.

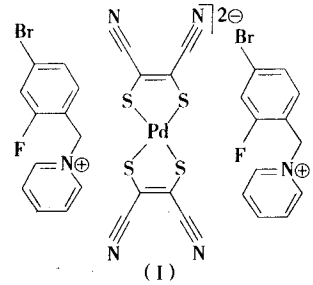
本文原载于《Dalton 英国皇家化学会》2002 年第 13 期

The 1 : 2 Bis(maleonitriledithiolato) - palladium(II)Complex of the N - (2 - fluoro - 4 - bromobenzyl)Pyridinium Cation

In the title salt, $(C_{12}H_{10}BrFN)_2[Pd(C_4N_2S_2)_2]$ or [N -(2 - fluoro - 4 - bromobenzyl) pyridinium]$_2$[Pd(mnt)$_2$], where mnt^{2-} denotes maleonitriledithiolate, the Pd^{2+} ion is coordinated by four S atoms of two mnt^{2-} ligands in a planar geometry. The asymmetric unit is composed of one N··· (2 - fluoro - 4 - bromobenzyl) pyridinium cation and one-half $[Pd(mnt)_2]^{2-}$ anion. The adjacent counter-cations form dimers by C_{py}- H···F_{Ar} hydrogen-bonding interactions. Anions and cations stack in alternating layers which are nearly parallel to the bc plane of the crystallographic unit cell.

Comment

Recently, one-dimensional (1 - D) compounds have been attracting widespread attention because of their novel physical properties, such as spin-Peierls transitions (Bray et al., 1975), spin-charge separation states (Lorenz et al., 2002), molecular bistabilities (Fujita & Awaga, 1999), and so on. Furthermore, more and more new quantum effects have been observed in 1 - D spin systems (Caneschi et al., 2001; Shiramura et al., 1998).



(I)

In current studies, we have developed a new class of [R - BzPy][Ni(mnt)$_2$] salt, where [R - BzPy]$^+$ represents aderivative of benzylpyridinium, as building blocks to construct a low-dimensional molecular solid (Ren, Meng, Song, Hu et al., 2002; Ren, Meng, Song, Lu et al., 2002; Xie, Ren, Song, Zhang et al., 2002; Xie, Ren, Song, Zou & Meng, 2002; Xie et al., 2003). We have found: (a) all [R - BzPy][Ni(mnt)$_2$] compounds stack with well separated columns of anions and cations in the solid state, in which [Ni(mnt)$_2$]$^-$ anions form a spaced 1 - D magnetic chain of s = 1/2 along the direction of the anion column; (b) the topology and size of the [R - BzPy]$^+$ ion, which is related to the molecular conformation of the [R - BzPy]$^+$ ion, can be modulated by systematic variation of the substituents in the aromatic rings, and so the stacking pattern of those complexes can be finely tuned by controlling the molecular conformation of the [R - BzPy]$^+$ ion; (c) The magnetic coupling interactions in these systems are very sensitive to intermolecular separations. A series of complexes with almost the same stacking patterns but slightly different intermolecular spacing has been obtained. The complexes exhibit magnetic diversity, and some reveal an unusual spin-Peierls-like phase transition. In order to further understand the relationship between magnetic properties and the stacking structures in these types of complexes, we have studied the complex [BrFBzPy]$_2$[Pd(mnt)$_2$], (I).

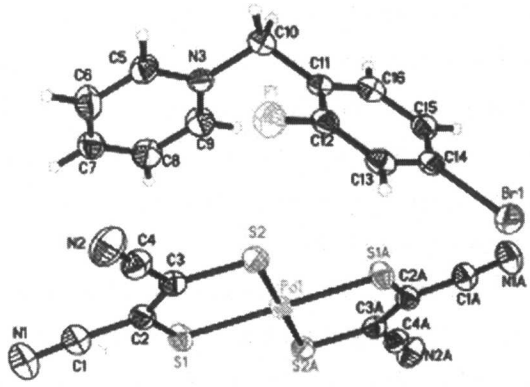


Figure 1 The cation and anion of complex (I), showing 30% probability displacement ellipsoids and the atom-numbering scheme.

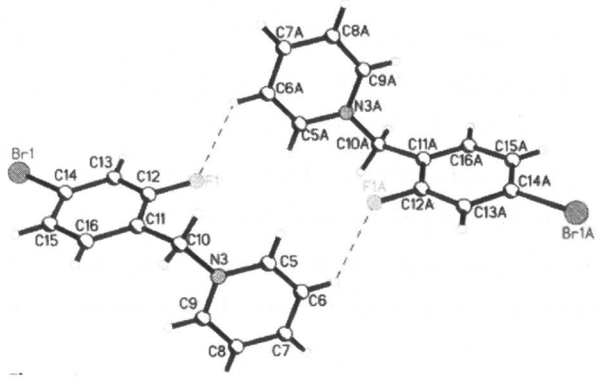


Figure 2 The hydrogen-bonding dimer formed by adjacent cations

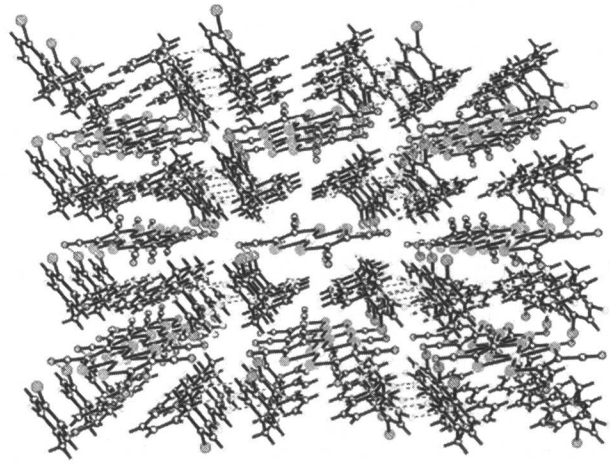


Figure 3 The layered packing of alternating anions and cations

The asymmetric unit of (I) is composed of one N-(2-fluoro-4-bromobenzyl)pyridinium cation and one-half $[Pd(mnt)_2]^{2-}$ anion (Fig. 1). The Pd^{2+} ion occupies an inversion center, surrounded by four S atoms of two mnt^{2-} ligands, and exhibits a square-planar coordination geometry. The Pd-S distances are in the range 2.2872 (11)-2.2941 (10)Å, with S-Pd-S angles of between 89.56 (3) and 90.44 (3)°(Table 1). These results are in agreement with those of corresponding $[Pd(mnt)_2]^{2-}$ complexes (Bois et al., 1998). The anion is almost planar, the N atoms of the CN groups being somewhat bent away from the plane, and atoms N1 and N2 deviate from the S4 plane by 0.64 (2) and 0.43 (2)Å, respectively. As for the cations, the pyridine and benzene rings twist with respect to each other, similar to the situation in an $[Ni(mnt)_2]^-$ series reported earlier by us (Ren, Meng, Song, Hu et al., 2002), and the dihedral angles between the reference plane, N3/C10/C11, and the benzene and pyridine rings are 65.73 (16) and 59.7 (3)°, respectively. Two adjacent cations dimerize through hydrogen-bonding interactions between F1 and C6 of a neighbouring molecule (Fig. 2). The anions and cations form alternating layers, which are nearly parallel to the bc plane of the crystallographic unit cell (Fig. 3).

Experimental

Disodium maleonitriledithiolate (Na_2mnt) was prepared following the procedure of Davison & Holm (1967). N-(2-Fluoro-4-bromobenzyl) pyridinium chloride was prepared by reacting 2-Fluoro-4-benzyl chloride with 1.5 equivalent of pyridine in refluxing acetone for 4 h. The white microcrystalline product was filtered off and washed with acetone and diethyl ether in turn; the yield is more than 86% after drying in vacuo. A similar method for synthesizing $[Bu_4N]_2[Pd(mnt)_2]$ (Davison & Holm, 1967) was used to prepare the title compound, (I). Well shaped, black single crystals suitable for X-ray analysis were obtained by diffusing diethyl ether into an acetonitrile solution of complex (I) for about 3 d.

Crystal data

$(C_{12}H_{10}BrFN)_2[Pd(C_4N_2S_2)_2]$	$Z=1$
$M_r=921.00$	$D_x=1.830Mg\ m^{-3}$
Triclinic, P1	Mo $K\alpha$ radiation
$a=7.1140(18)$Å	Cell parameters from 25
$b=11.035(3)$Å	reflections
$c=11.851(3)$Å	$\theta=3.1-27.5°$
$\alpha=69.564(4)°$	$\mu=3.24mm^{-1}$
$\beta=89.016(4)°$	$T=293(2)K$
$\gamma=74.151(4)°$	Block, black
$V=835.5(4)Å^3$	0.15×0.10×0.10mm

Data collection

Siemens CCD area-detector	2907 independent reflections
diffractometer	2348 reflections with $I>2\sigma(I)$
ω scans	$R_{int}=0.016$
A bsorption correction: empirical	$\theta_{max}=25.0°$
(*SADABS*: Sheldrick, 1996)	$H=-7\rightarrow8$
$T_{min}=0.665$, $T_{max}=0.728$	$k=-13\rightarrow13$
4372 measured reflections	$l=-13\rightarrow14$

Refinement

Refinement on F^2	H-atom parameters constrained
$R[F^2>2\sigma(F^2)]=0.030$	$w=1/[\sigma^2(F_o^2+(0.025P)^2]$
$wR(F^2)=0.065$	*where* $P=(F_o^2+2F_c^2)/3$
S=1.12	$(\Delta/\sigma)_{max}=0.001$
2907 reflections	$\Delta\rho_{max}=0.37e\ Å^{-3}$
214 parameters	$\Delta\rho_{max}=-0.47e\ Å^{-3}$

Table 1 Selected geometric parameters(Å,°)

Pd1-S1	2.2872(11)	Pd1-S2	2.2941(10)
S1-Pd1-S2	89.56(3)		

Table 2 Hydrogen—bonding geometry(Å,°)

D—*H*···*A*	*D*—*H*	*H*···*A*	*D*···*A*	*D*—*H*···*A*
C6—H6A···F1^{i}	0.93	2.40	3.079(4)	130

Symmetry code: (i) $2-x, 1-y, 2-z$.

All H atoms were placed in geometrically calculated positions (C—H = 0.93 and 0.97Å), with Uiso = 1.2Ueq(parent atom). Data collection: SMART (Siemens, 1996); cell refinement: SMART; data reduction: SAINT (Siemens, 1996); program(s) used to solve structure: SHELXS97 (Sheldrick, 1997); program(s) used to refine structure: SHELXL97 (Sheldrick, 1997); molecular graphics: SHELXTL.

This work was funded by the Chinese National Natural Science Foundation (project No. 20171001), the Education Commission of Anhui Province of China (project No. 2001kj162) and the Natural Science Foundation of Anhui Province of China (project No. 01012038).

References

[1] Bois, H., Connelly, N. G., Crossley, J. G., Guillorit, J. —C., Lewis, G. R., Orpen, A. G. & Thornton, P. (1998). J. Chem. Soc. Dalton Trans. pp. 2833—2838.

[2] Bray, J. W., Hart, H. R., Interrante, Jr. L. V., Jacobs, I. S., Kasper, J. S., Watkins, G. D., Wee, S. H. & Bonner, J. C. (1975). Phys. Rev. Lett. 35, 744—747.

[3] Caneschi, A., Gatteschi, D., Lalioti, N., Sangregorio, C., Sessoli, R., Venturi, G., Vindigni, A., Rettori, A., Pini, M. G. & Novak, M. A. (2001) Angew. Chem. Int. Ed. 40, 1760—1763;

[4] Davison, A. & Holm, R. H. (1967). Inorg. Synth. 10, 8—26.

[5] Fujita, W., Awaga, K. (1999). Science, 286, 261—262.

[6] Lorenz, T., Hofmann, M., Gruninger, M., Freimuth, A., Uhrig, G. S., Dumm, M. & Dressel, M. (2002) Nature (London), 418,

614－617.

[7] Ren, X. M., Meng, Q. J., Song, Y., Hu, C. J., Lu, C. S., Chen, X. Y. & Xue Z. L. (2002) Inorg. Chem. 41, 5931－5933.

[8] Ren, X. M., Meng, Q. J., Song, Y., Lu, C. S., Hu, C. J. & Chen, X. Y. (2002) Inorg. Chem. 41, 5686－5692.

[9] Sheldrick, G. M. (1996). University of Goèttingen, Germany.

[10] Sheldrick, G. M. (1997). SHELXTL. Version 5.10. Bruker Analytical X－ray Systems Inc., Madison, Wisconsin, USA.

[11] Shiramura, W., Takatsu, K., Kurniawan, B., Tanaka, H., Uekusa, H., Ohashi, Y., Takizawa, K., Mitamura, H. & Goto, T. (1998). J. Phys. Soc. Jpn, 67, 1548－1551.

[12] Siemens (1996). SMART and SAINT. Siemens Analytical X－ray Instruments Inc., Madison, Wisconsin, USA.

[13] Xie, J. L., Ren, X. M., Song, Y., Zou, Y. & Meng, Q. J. (2002) J. Chem. Soc. Dalton Trans. pp. 2868－2872.

[14] Xie, J. L., Ren, X. M., He, C., Song, Y., Meng, Q. J., Kremer, R. K. & Yao, Y. H. (2003) Chem. Phys. Lett. 369, 41－48.

[15] Xie, J. L., Ren, X. M., Song, Y., Zhang, W. W., Liu, W. L., He, C. & Meng Q. J. (2002) Chem. Commun. pp. 2346－2347.

本文原载于(*Acta Crystallogrphical Section E*)《国际晶体学报》2003 年 E59

3D H-bonding Networks Self－assembly from Pyridinium Derivatives and Bis (maleonitriledithiolato)Zincate(II)

Abstract: The two ion-pair complexes, $[pyH]_2[Zn(mnt)_2]$ (1) and $[4,4'-bipyH_2]$-$[Zn(mnt)_2]$ (2), were synthesized, where mnt^{2-} denotes maleonitriledithiolate, and $[pyH]^+$, $[4,4'-bipyH_2]^{2+}$ represent pyridinium and diprotonated 4,4′- bipyridinium, respectively. Their single crystal structures show that there are strong bifurcated H-bonding interactions between the cations of the pyridinium derivative and the $[Zn(mnt)_2]^{2-}$ anions in both 1 and 2. The bifurcated H-bonding interactions between the N H of the pyridiniums and the CN groups of the mnt^{2-} ligands give rise to a 2D layered H－bonding network, the adjacent layers come together in such way as mutual embrace to give a tight pack, thus 2D－hydrogen－bonding sheets further develop into 3D H-bonding networks through weak C－H…S and p…p stacking interactions in 1. As for 2, the cations and anions connect into several types of H-bonding macrorings ([2＋2], [3＋3] and [4 ＋ 4]), these H-bonding macrorings fuse to extend into 2D layered structure, the interpenetration between [3+3]and [4+ 4] type H-bonding macrorings in the adjacent layers give further rise to novel 3D extended H-bonding networks, in which there are clearly parallel stacks of cations and the chelate rings of anions.

1. Introduction

The scientific branches involved H-bonding are very diverse, and may

include biology, material science [1,2]. In recent years, the principles of supramolecular chemistry, in which a great deal of new concepts concerning intermolecular noncovalent interaction such as H-bonding interactions, have been introduced into the area of material science, and some have yielded materials exhibiting novel properties [2-4]. More recently, we have paid attention to the construction of planar $[Ni(mnt)_2]^-$ anions with pyridinium derivatives, in which there are strong bifurcated H-bonding interactions between the CN groups of mnt^- ligand and H N of pyridinium derivatives, 1D H-bonding chain consisting of $[Ni(mnt)_2]^-$ and pyridinium, and 3D H-bonding network based on $[Ni(mnt)_2]^-$ and 4 - aminopyridinium are obtained by changing H - bond donors[5]. These results motivate to further adjust H - bond acceptors with different topologic structure in order to get new H - bond supramolecular systems, so the $[Zn(mnt)_2]^-$ anion with tetrahedral geometry is considered to replace the square planar $[Ni(mnt)_2]^-$ as H - bond acceptor. In this contribution, we reported two compounds with novel H-bonding networks, and one of them is constructed of 3D interpenetration structure.

2. Experimental Section

2.1 General Procedures

Disodium maleonitriledithiolate (Na_2mnt) was prepared following the procedure in the literature[6]. Pyridinium chloride was prepared between pyridine and 1 equivalent of dilute hydrochloride acid, and 4,4′- bipyridinium chloride was prepared between 4,4′- bipyridine and 2 equivalent of dilute hydrochloride acid. Elemental analyses were performed with a Perkin - Elmer 240 analytical instrument. IR spectra with KBr pellets in 4000 - 400 cm^{-1} regions were obtained from an IFS66V FT - IR spectrophotometer.

$[Pyridinium]_2[Zn(mnt)_2]$ (1). A crude of 1 was prepared using the similar method for synthesizing $[Bu_4N]_2[Zn(mnt)2]$ [6], and then dis-

solved in MeCN. The crystals were obtained by the diethyl ether diffused into the MeCN solution of 1 for 3 days, and the yield is 80%. Elemental analysis calcd (%) for $C_{18}H_{12}N_6S_4Zn$ (505.95): C 42.7, H 2.39, N 16.6; found: C 42.5, H 2.40, N 16.3. IR spectrum (cm^{-1}): υ(CN), 2200.9s, 2154.6sh; n(CyC) of mnt22, 1484.3s.

[4,4′—Bipyridinium][Zn(mnt)$_2$] (2). The preparation procedure of 2 is similar to that of 1, and yield is 80%. Elemental analysis calcd (%) for $C_{18}H_{10}N_6S_4Zn$ (503.93): C 42.9, H 2.00, N 16.7; found: C 42.6, H 2.15, N 16.7. IR spectrum (cm^{-1}): υ(CN), 2197.1s, 2156.0sh; υ(C=C) of mnt^{2-}, 1488.9s.

All single crystals suitable for the X－ray structure analysis were obtained by diffusing diethyl ether into the MeCN solution of these complexes.

Table 1 Crystal data and structure refinement for 1 and 2

Complex	1	2
Empirical formula	$C_{18}H_{12}N_6S_4Zn$	$C_{18}H_{10}N_6S_4Zn$
Formula weight	505.95	503.93
Temperature(K)	293(2)	293(2)
Wavelength(Å)	0.71073	0.71073
Crystal system	Monoclinic	Monoclinic
Space group	$C2/c$	$C2/c$
Unit cell dimensions	a=7.3066(17)Å; b=13.447(3)Å; c=22.067(5)Å; β=93.677(4)°	a=64.729(7)Å; b=8.0310(10)Å; c=12.1800(10)Å; β=95.19°
Volume(Å^3)	2163.7(9)	6302.6(12)
Z	4	12
Density(calculated, g/cm^3)	1.553	1.593
Absorption coefficient (mm^{-1})	1.538	1.584
F(000)	1024	3048
Crystal size(mm^3)	0.25×0.20×0.20	0.15×0.10×0.10
Theta range for data collection (°)	3.17－24.99	1.90－27.01
Index ranges	$-8\leqslant h\leqslant 8$, $-15\leqslant k\leqslant 10$ $-26\leqslant l\leqslant 23$	$-74\leqslant h\leqslant 82$, $-10\leqslant k\leqslant 9$ $-15\leqslant l\leqslant 14$
Reflections collected	5182	17.630
Independent reflections	1904(R(int)=0.0674	6838(R(int)=0.0982)
Absorption correction	Empirical	Empirical
Max and min transmission	0.740 and 0.700	0.86 and 0.79
Refinement method	Full-matrix least-squares on F^2	Full－matrix least－squares on F^2
Data/restraints/parameters	1904/0/130	6838/0/393
Goodness-of-fit on F^2	1.065	1.024
Final R indices [I>2sigma(I)]	$R1$=0.0301, $wR2$=0.0796	$R1$=0.0679, $wR2$=0.1605
R indices (all data)	$R1$=0.0336, $wR2$=0.0811	$R1$=0.1449, $wR2$=0.1731
Largest diff. peak and hole	0.306 and －0.370 eÅ^{-3}	0.984 and －0.481 eÅ^{-3}

2.2 Structure determinations

Diffraction data on crystals of 1 and 2 were collected at 293 K with SMART area detector, and details of data collection are given in Table 1. All computations were carried out via a PC - 586 computer using the SHELXTL - PC program package[7]. The structures were solved by direct methods and refined on F^2 by full - matrix least - squares methods. All the nonhydrogen atoms were refined anisotropically. Hydrogen atoms were placed in their calculated positions and refined following the riding model.

3. Results and Discussion

3.1 Crystal structure of 1

The structure of 1 is composed of PyH^+ cations and $[Zn(mnt)_2]^{2-}$ anions. The Zn^{2+} ion occupies in a 2 - fold axis and is surrounded by four sulfur atoms of two mnt^{2-} ligands, and the coordination geometry of Zn^{2+} ion is a slightly distorted tetrahedron (the dihedral angle between two chelate rings is 89.62 (3)° in ZnS_4). The Zn - S distances range from 2.3106(7) to 2.3296(7)Å, the S Zn S angles range from 93.33(2) to 123.24(4)° (Table 2), these results are in agreement with that reported in literatures [8].

Table 2 Selected bond lengths (Å) and angles (°) for 1 and 2

Bond lengths		Bond angles	
Complex 1			
Zn(1)—S(1)	2.3106(7)	S(1)—Zn(1)—S(1)#1	123.24(4)
Zn(1)—S(1)#1	2.3106(7)	S(1)—Zn(1)—S(2)	116.82(3)
Zn(1)—S(2)	2.3296(7)	S(1)#1—Zn(1)—S(2)	93.33(2)
Zn(1)—S(2)#1	2.3296(7)	S(1)#1—Zn(1)—S(2)#1	116.82(3)
		S(2)—Zn(1)—S(2)#1	115.23(4)
Symmetry transformations used to generate equivalent atoms: #1 $-x, y, -z+1/2$			
Complex 2			
Zn(1)—S(2)	2.320(2)	S(2)—Zn(1)—S(4)	137.92(9)
Zn(1)—S(4)	2.3225(19)	S(2)—Zn(1)—S(1)	92.35(7)
Zn(1)—S(1)	2.329(2)	S(4)—Zn(1)—S(1)	101.31(7)
Zn(1)—S(3)	2.3349(19)	S(2)—Zn(1)—S(3)	103.38(7)

（续表）

Bond lengths		Bond angles	
Zn(2)－S(6)＃1	2.3229(19)	S(4)－Zn(1)－S(3)	92.27(7)
Zn(2)－S(6)	2.3229(19)	S(1)－Zn(1)－S(3)	138.52(9)
Zn(2)－S(5)＃1	2.3376(18)	S(6)＃1－Zn(2)－S(6)	136.59(12)
Zn(2)－S(5)	2.3377(18)	S(5)＃1－Zn(2)－S(5)＃1	92.67(6)
		S(6)－Zn(2)－S(5)＃1	102.42(6)
		S(6)＃1－Zn(2)－S(5)	102.42(6)
		S(5)＃1－Zn(2)－S(5)	138.57(11)

Symmetry transformations used to generate equivalent atoms: ＃1 $-x, y, -z+1/2$

Table 3　Hydrogen bonds for I and 2(Å and °)

D－H…A	d(D－H)	d(H…A)	d(D…A)	(DHA)
	Complex 1			
N(3)－H(3A)…N(2)＃2	0.86	2.26	2.938(3)	135.7
N(3)－H(3A)…N(1)＃3	0.86	2.64	3.196(3)	123.2
Symmetry transformations used to generate equivalent atoms:				
＃1－0$x, y, -z+1/2$; ＃2＝$x+1/2, -y+1/2, z+1/2$;				
＃3＝$-x+1, -y+1, -z+1$				
Complex 2				
N(5)－H(5A)…N(8)	0.86	2.28	2.918(9)	131.3
N(5)－H(5A)…N(7)＃2	0.86	2.34	2.995(9)	133.3
N(6)－H(6A)…N(3)＃3	0.86	2.23	2.943(8)	140.0
N(6)－H(6A)…N(4)＃4	0.86	2.36	2.972(9)	128.7
N(9)－H(9A)…N(2)＃5	0.86	2.30	2.924(9)	129.9
N(9)－H(9A)…N(1)＃6	0.86	2.42	3.078(9)	133.7
Symmetry transformations used to generate equivalent atoms:				
＃1＝$-x+1, y, -z+1/2$; ＃2＝$x, -y-1, z+1/2$;				
＃3＝$-x+3/2, -y-1/2, -z+2$; ＃4＝$-x+3/2, y-3/2, -z+3/2$;				
＃5＝$-x+1, -y, -z+2$; ＃6＝ $x+1, y, -z+3/2$				

There exist both H-bonding and $\pi\cdots\pi$ stacking interactions between anions and cations, and the H-bonding geometric parameters are summarized inTable 3. The near linear C－H…S weak H-bonding interactions exist between the pyridine rings and the S atoms of the mnt^{2-} ligands[9], in addition, there are very stronger bifurcated H-bonding interactions between the N－H of the pyridiniums and the CN groups of the mnt^{2-} ligands, and these bifurcated H-bonding interactions give rise to a 2D layered H-bonding network shown as Fig. 1, however, the PyH^{+} cations and pla-

nar $[Ni(mnt)_2]^-$ anions form only 1D H-bonding chain in [pyridinium][Ni $(mnt)_2$]. The π···π stacking interactions are observed between the pyridinium and adjacent chelate ring of anion (referred as Fig. S1 in Section 5), the dihedral angle between pyridinium and chelate ring of the anion is 10.8°, the center - to - center distance is 3.63Å, the shorter atomic separations are 3.51 of C(4)···C(5A), 3.72 of S(1A)···N(3A), 3.70 of S(1A)··· C(9A) and 3.52Å of C(2A)···C(5A) (symmetric code: A = X − 0.5; Y − 0.5 Z), respectively. The adjacent layers come together in such way as mutual embrace to give a tight pack (Fig. 2), thus 2D hydrogen-bonding sheets further develop into 3D H-bonding networks through weak C - H···S and π···π stacking interactions.

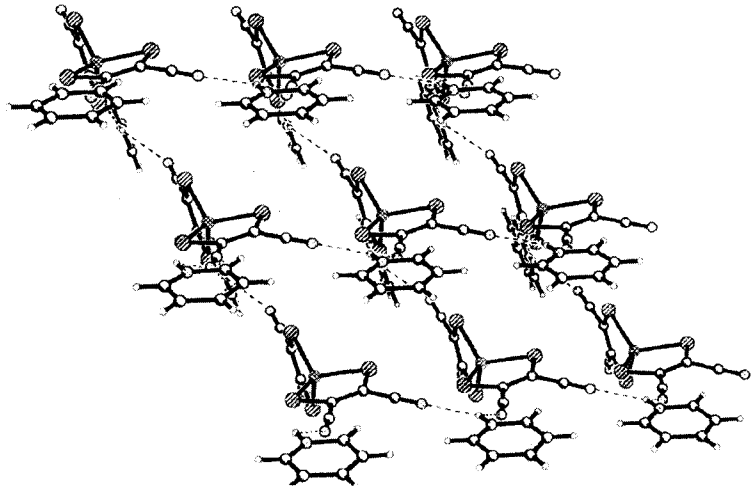


Fig. 1. Two−dimensional H-bonding network for 1.

3.2 Crystal structure of 2

Complex 2 crystallizes in the space group $C_{2/c}$; which is same as 1. The Zn(2) ion lies on a 2 - fold axis, the Zn(1) and Zn(2) ions exhibit greatly distorted tetrahedron coordination geometry unlike in 1 (the dihedral angles between two chelate rings are 59.16(8)° for Zn(1) - containing moiety, 38.67 (6)° for Zn(2) - containing moiety, respectively), and the corresponding bond lengths of Zn - S range from 2.320(2) to 2.3377(18)Å, the bond angles of S - Zn - S range from 92.27(7) to 138.57(11)° for both Zn

(1)- and Zn(2)- containing moieties (Table 2). As for the cationic moiety containing N(9), there is a 2 - fold axis, which is perpendicular to the C - C bond connecting two pyridyl rings. The two pyridyl rings in 4,4′- bipyridinum twist one another, the dihedral angles is 42.51(18)° for the entry containing N(5), and 50.99(17)° for the entry containing N(9), respectively, which are abnormally larger than the value in an isolated bipyridinium molecule (the torsional angles of isolated bipyridinium molecule is the range of 19 - 22°) [8].

One of structural features is H-bonding interactions between $[Zn(mnt)_2]^{2-}$ anions and $[4,4'-biPyH_2]^{2+}$ cations as 1, there exist very strong bifurcated H-bonding interactions between the N - H of the pyridiniums and the CN groups of the mnt^{2-} ligands, and the weak H-bonding interactions between the pyridine rings and the S atoms of the mnt^{2-} ligands (the contacts between H - atom of the bipyridine rings and the S - atom range from 2.72 to 2.97Å, which are compared with that in the literature [9]). It is worth to note that the 3D bonding networks pattern formed by anions and cations is different from that of 1, although the H-bonding interaction schemes between cation and anion for these two complexes are similar to each other. There are two types of [2 +2] molecular rings, that is, the two $[Zn(mnt)_2]^{2-}$ anions and two 4,4′- bipyridiniums construct into macrorings through intermolecular H-bonding interactions, one is two $[Zn(mnt)_2]^{2-}$ anions arranging side by side, another is two 4,4′- bipyridiniums arranging side by side (Fig. 3(a)). These [2 + 2] molecular rings further build into a wave - like 2D extended H-bonding network through the [3 +3] molecular rings with chair configuration (this [3 +3] molecular ring includes one anion contained - Zn(2), two anions contained - Zn(1) and three 4,4′- bipyridiniums), which is approximately parallel to crystallographic ac - plane (Fig. 3(a)). In addition, there are two types of [4 + 4] helical molecular rings formed by four $[Zn(mnt)_2]^{2-}$ anions and four 4, 4′- bipyridiniums, and they interpenetrate the wave - like 2D extended H-bonding network (Fig. 3(b)), a layer is developed by the fusing H-bonding macrorings described above. The adjacent layers interlock each other by

[3 + 3] and [4 +4] molecular rings to form 3D complex H-bonding networks, as displayed in Fig. 4. Another notable structural feature in 2 is clearly parallel stacks of the cations and the chelate rings of the anions (referred as Figs. S2 and S3 in Section 5), the typical values of the dihedral angles are 4.0 9.08, the center - to - center distances are 4.0Å, and some shorter atomic separations between overlap pairs range from3.50 to 3.70Å, which are listed in Tables S1 and S2 of Section 5. It appears that these stacking interactions between cations and the chelate rings of anions could be one of the dominant influences for both Zn(II) ions showing greatly distorted tetrahedral coordination geometry and the two pyridyl rings within a 4,4′- bipyridinium molecule exhibiting abnormal large dihedral angles, in other words, the crystal parking enfoces these distortions.

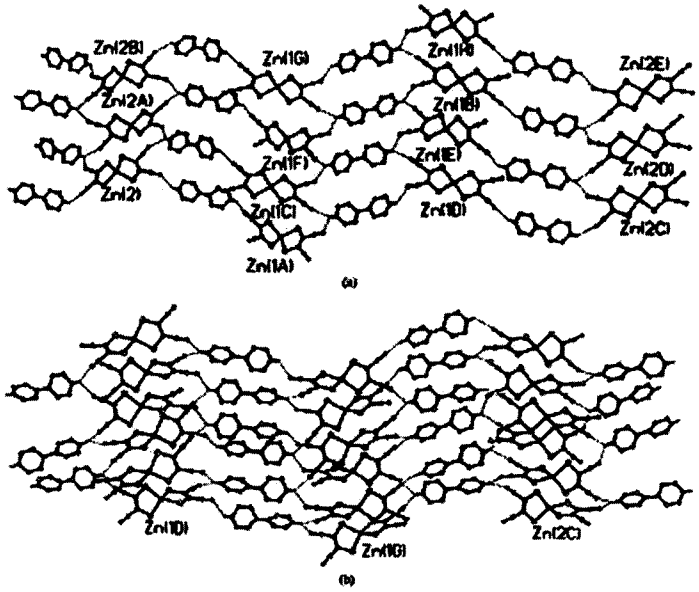


Fig. 3. H-bonding networks showing (a) [2+2] and [3+3] molecular rings; (b) [2+2], [3 +3] and [4+4] molecular rings.

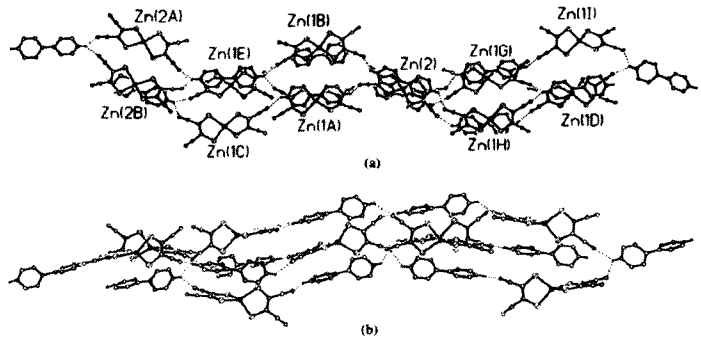


Fig. 4. Interpenetrating structure between [3+ 3] and [4+4] molecular rings (projecting along (a) (021) direction; (b) (012) direction).

4. Conclusions

In summary, the crystal structures of two ion-pair complexes, which consist of the derivatives of pyridinium and bis(maleonitriledithiolato)zincate(II), have been determined, and the results reveal that there exist strong bifurcation H-bonding interaction between CN of maleonitriledithiolate and NH of pyridinium like as the series of the derivatives of pyridinium and bis(maleonitriledithiolato) nickelate(III). However, the H-bonding interaction patterns between CN of maleonitriledithiolate and NH of pyridinium change from 1D chain to 2D network when the planar $[Ni(mnt)_2]^-$ anion of $[PyH][Ni(mnt)_2]$ replaced by tetrahedral geometry $[Zn(mnt)_2]^{2-}$ anion. The packing models between 1 and 2 are also different from each other, the 3D complex H-bonding networks of 2 are expected when two isolated pyridiniums are substituted by a 4,4′−bipyridinium, in fact, the several types of H-bonding macrorings in 2 fuse to extend into 2D layered structure, the interpenetration between [3+3] and [4+4] type H-bonding macrorings in the adjacent layers give further rise to novel 3D extended H-bonding networks. Another notable structural feature of these complexes are the stacking interactions between cations and the chelate rings of anions, these stacking interactions could be one of dominant reasons enforcing the

distortions of Zn(II) ionic coordination geometry in 2.

5. Supplemental Materials

Crystallographic data (excluding structure factors) for the structures reported in this paper have been deposited with the Cambridge Crystallographic Data Center as supplementary publications, and the CCDC numbers are from CCDC－201755 and CCDC－201756. Copies of the data can be obtained free of charge on application to CCDC, 12 Union Road, Cambridge CB21EZ, UK (Fax: ＋44－1223－ 336－033; e－mail:deposit@ccdc. cam. ac. uk)

Acknowledgements

This project was supported from the National Natural Science Foundation (project no. 20171001), the National Natural Science Foundation of Anhui Province of China (project no. 01012038).

References

[1] (a) T. Steiner, Angew. Chem. Int. Ed. 41 (2002) 48.
(b) H. W. Roesky, M. Andruh, Coord. Chem. Rev. 236 (2003) 91.
(c) T. Miyoshi, K. Takegoshi, T. Terao, Macromolecules 32 (1999) 8914.

[2] (a) Y. P. Cao, Y. Guan, J. Du, J. Luo, Y. X. Peng, C. W. Yip, A. S. C. Chan, J. Mater. Chem. 12 (2002) 2957.
(b) T. Akutagawa, T. Hasegawa, T. Nakamura, G. Saito, Cryst. Engng Commun. 5 (2003) 54

[3] M. Szafrański, A. Katrusiak, G. J. McIntyre, Phys. Rev. Lett. 89

(2002) 215507.

[4] (a) Z. Pajak, P. Czarnecki, J. Wasicki, W. Nawrocik, J. Chem. Phys. 109 (1998) 6420.

(b) Z. Pajak, P. Czarnecki, H. Maluszynska, B. Szafranska, M. Szafran, J. Chem. Phys. 113 (2000) 848.

(c) Z. Pajak, H. Maluszynska, B. Szafranska, P. Czarnecki, J. Chem. Phys. 117 (2002) 5303.

[5] (a) X. M. Ren, Y. C. Chen, C. He, S. Gao, J. Chem. Soc. Dalton Trans. (2002) 3915.

(b) X. M. Ren, C. S. Lu, P. H. Wu, Q. J. Meng, J. Chem. Crystallogr. 32 (2002) 173.

[6] A. Davison, H. R. Holm, Inorg. Synth. 10 (1967) 8.

[7] G. M. Sheldrick, SHELXTL, Structure Determination Software Programs, Version 5.10, Bruker Analytical X - ray Systems, Madison, WI, 1997.

[8] H. Xu, J. L. Xie, X. M. Ren, Y. C. Chen, Acta Crystallogr. Sect. E 58 (2002) m750.

[9] G. R. Lewis, I. Dance, J. C. S. Dalton Trans. (2000) 3176.

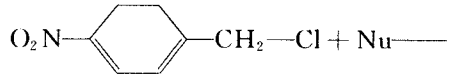
本文原载于(*Jounal of Molecular Struture*)《分子结构》2003 年 660 139－146

两种新型电荷转移盐的合成和光谱研究

摘 要：合成了两种新的有机盐[NO_2BzPy]Cl (1) 和[$NO_2BzPyNH_2$]Cl (2)，(1)[或(2)]与 K[TCNQ]$_2$进一步反应生成[NO_2BzPy][TCNQ]$_2$ (3) 和[$NO_2BzPyNH_2$][TCNQ]$_2$(4)。光谱数据表明：TCNQ 盐中存在 $TCNQ^0$和 $TCNQ^-$，并形成了一维 TCNQ 分子柱，且 $TCNQ^0$和 $TCNQ^-$之间存在相互作用，部分电荷从[TCNQ]$_2^-$向阳离子([NO_2BzPy]$^+$和[$NO_2BzPyNH_2$]$^+$)转移。

主题词：TCNQ；电荷转移盐；合成；表征

近年来，有机铁磁材料和超导材料的研究是材料领域中最具挑战性的课题，许多研究取得了巨大成功。另一方面，铁磁性和超导性共存于一个体系的却为数不多[1]，主要是因为这种类型配合物的分子设计是相当困难的。第一个被报道既有超导性又有磁性的配合物是(BEDT－TTF)$_4$(H_2O)[$Fe(C_2O_4)_3$(C_6H_5CN)[2]，此后又发现了 κ－$BETS_2Fe(Br_4)$[3]，但同时具有磁性和导电性的纯有机配合物却未见报道。TCNQ(7，7，8，8－四氰基对苯醌二甲烷)是一个强的电子接体，它可以和许多电子给予体形成电荷转移复合盐。由于 TCNQ 具有平面结构，当它形成复合盐时，可以按照一维方向形成分子柱，其间距小，能够形成 π－电子云重叠，因而能呈现较高的导电性，引起了人们的极大的兴趣。同时由 TCNQ 形成的电荷转移盐的磁性研究近来也成为研究热点之一[4,5]。本文通过有机盐与 K[TCNQ]$_2$合成了两种具有潜在磁性的电荷转移盐，并进行了表征。合成路线如图 1 所示：



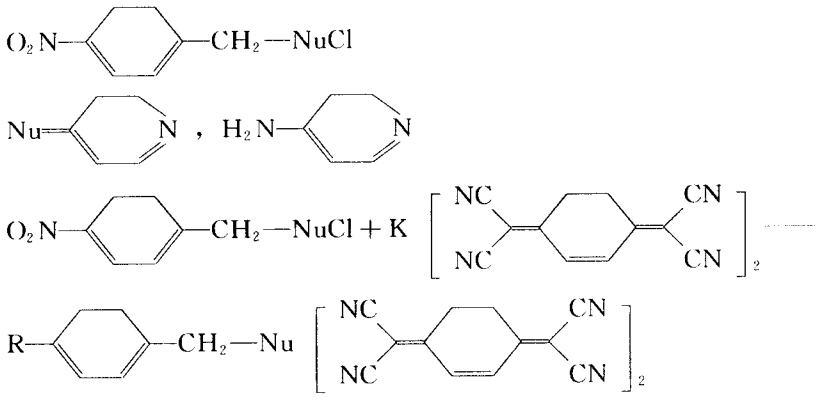


图 1

1. 实验部分

1.1 仪器和试剂

所有新化合物的 C，H，N 元素百分含量使用 Perkin－Elmer 240 型元素分析仪测定。红外光谱使用 Nicolet FT－IR AVATAR 360 光谱仪测定，样品与 KBr 磨均后压片，测量范围为 400～4000cm^{-1}。所用试剂均为分析纯，使用前未作进一步纯化。

1.2 原料的制备

K[TCNQ]$_2$按照文献[6]方法制备。

[NO_2BzPy]Cl (1) 的合成[7]：将对硝基苄氯 1.70 g 和吡啶 0.79 g 溶解在 40 mL 丙酮中，混合溶液回流 20 min 后就有白色微晶生成，继续回流 40 min，冷却后过滤，并依次用少量丙酮、无水乙醚洗涤微晶状沉淀，真空干燥后，得产物[NO_2BzPy]Cl 2.16 g（产率 87 %）。元素分析结果：C，57.21%；H，4.52 %；N，11.08 %。按化学式 $C_{12}H_{11}N_2ClO_2$ 计算的理论值：C，57.49 %；H，4.42 %；N，11.17 %。[NO_2BzPyNH_2]Cl (2) 的合成：用类似于制备(1) 的方法合成(2)，产率为 91 %。元素分析结果：C，54.05 %；H，4.61 %；N，15.77 %。按化学式 $C_{12}H_{12}N_3ClO_2$ 计算的理论值：C，54.25 %；H，4.55 %；N，15.82 %。

1.3 电荷转移盐的合成

[NO_2BzPy][TCNQ]$_2$(3) 的合成：称取 K[TCNQ]$_2$ 448mg 溶于 50 mL 近沸的无水乙醇中，然后加入 50 mL 含[NO_2BzPy]Cl 250 mg 乙醇溶液，混合液回流 8 h 后有浅绿色微晶生成，继续回流 40min ，冷却后过滤，并依次用少量乙醇、无水乙醚洗涤微晶状沉淀，真空干燥后，产物 509 mg（产率 73%）。元素分析结果：C ，69.11%；H ，3.12%；N ，22.34%。按分子式 $C_{36}H_{19}N_{10}O_2$ 计算的理论值：C ，69.34%；H ，3.07%；N，22146%。[NO_2BzPyNH_2][TCNQ]$_2$(4) 的合成：用类似于制备(3)的方法合成(4)，产率 75%。元素分析结果：C ，67.42%；H ，3.25%；N ，24.19%。按化学式 $C_{36}H_{20}N_{11}O_2$ 计算的理论值：C ，67.71%；H ，3.16%；N ，24.13%。

2. 结果和讨论

2.1 合成

K[TCNQ]$_2$ 的制备过程中，TCNQ 与 KI 反应在生成 $TCNQ^-$ 的同时，I^- 被氧化为 I_2。合成中 TCNQ 与 KI 的比例对反应产物的形式影响很大。加入物质的量的比为 1∶1 的 TCNQ 和 KI，反应生成的 I_2 和未反应的 I^- 形成 I_3^-，TCNQ 只有部分转化为 $TCNQ^-$，此时 TCNQ 与 $TCNQ^-$ 聚合成 $[TCNQ]_2^-$。

在无水乙醇溶剂中，摩尔比为 1∶1 的(1) 或(2) 和 K[TCNQ]$_2$ 反应得到产物(3) 和(4)。(3) 和(4) 的元素分析结果与分别按化学式 $C_{36}H_{19}N_{10}O_2$ 和 $C_{36}H_{20}N_{11}O_2$ 计算的结果相一致，表明这两种电荷转移盐中，有机阳离子([NO_2BzPy]$^+$ 或[NO_2BzPyNH_2]$^+$) 与 K[TCNQ]$_2$ 的摩尔比是 1∶1，即两种电荷转移盐分别可用结构简式[NO_2BzPy][TCNQ]$_2$ 和[NO_2BzPyNH_2][TCNQ]$_2$ 表示。

2.2 红外光谱

有机盐(1) 和(2) 在 1340～1350cm^{-1} 处均出现属于—NO_2 的吸收峰，在 1 620～1 662cm^{-1} 均出现了吡啶 C＝N 特征吸收峰。有机盐(2) 在 3 403.33 cm^{-1} 出现对氨基吡啶上 N—H 键伸缩振动。

图 1 是电荷转移盐(3) 的红外光谱，电荷转移盐(3) 和(4) 的红外光谱非常相似，它们的红外特征光谱数据见表 1 ，其简正模式按 Girlando－Pecile 标记[8,9]。在中性 TCNQ 中，C—N 仅在 2 220 cm^{-1}左右出现一个尖锐的单峰[8,9](见图 2)；在形成电荷转移盐之后，其电子振动模式引起红外解禁，在 2 210～2 180 cm^{-1}范围内出现了归属于 $TCNQ^-$的 Ag－2 或 Bu 振动模式，以及 $TCNQ^0$的 Bu 振动模式的二重吸收峰，表明 TCNQ 盐中存在电荷转移[10]。除了在 1 524～1 485 cm^{-1}，1 375～1 358 cm^{-1}，1 217～1 190 cm^{-1}和 845～806 cm^{-1}出现 TCNQ 固有的面内红外活性 Bu 带之外，同时还出现 6 个 Ag 吸收带，这些 Ag 吸收带在 TCNQ 中是非红外活性的，而在 $TCNQ^-$体系中却是红外活性的，它们的出现表明化合物中 TCNQ 间存在一定的相互作用[9]。在 810～799 cm^{-1}和 852～820 cm^{-1}出现的吸收带分别归属于 $TCNQ^-$和 $TCNQ^0$的 Bu－50 (CH 弯曲) 振动模式。因此可以推测，TCNQ 盐中存在 $TCNQ^0$和 $TCNQ^-$，并且形成了一维 TCNQ 分子柱[9]。

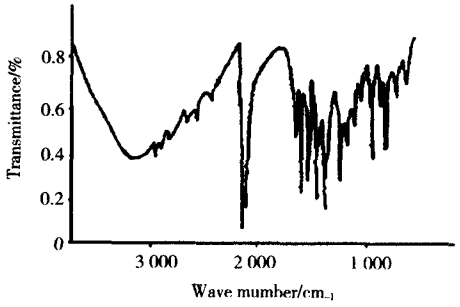


Fig. 1 IR spectra of charge transfer salt (3)

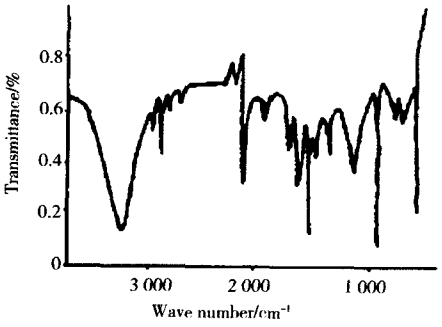


Fig. 2 IR spectrum of TCNQ

2.3 紫外光谱

测定了(3)，(4)和$[NO_2BzPyCl]^+K[TCNQ]_2$在乙腈溶剂中的紫外—可见光谱，如图3所示，(3)，(4)的光谱与$[NO_2BzPyCl]$和$K[TCNQ]_2$叠加的光谱非常相似，因此可以推测，TCNQ盐中由有机阳离子和$K[TCNQ]_2$复合而成的[6]。

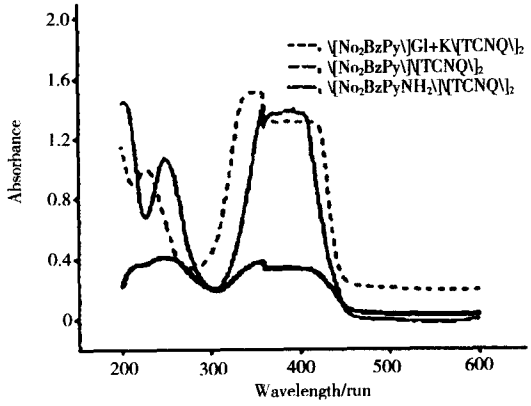


Fig. 3 UV-vis spectra of (3) ,(4) and $K[TCNQ]^{2+}[NO_2BzPyCl]$ in acteonitrile

2.4 电导率

电荷转移盐(3)，(4)的室温电导率分别为216×10^{-8}和312×10^{-8} $S\cdot cm^{-1}$。复合盐的室温下的电导率在$10^{-7}\sim10^{-9}S\cdot cm^{-1}$之间，属于有机半导体，它们的导电性可归结为TCNQ分子柱的形成和阳离子与TCNQ分子之间的部分电荷转移，但(4)的电导率大于(3)的电导率，这可能是由于对氨基吡啶上的氨基与TCNQ分子柱之间形成氢键造成的。

3. 结 论

我们合成了由TCNQ负离子和有机盐生成的电荷转移盐$[NO_2BzPy][TCNQ]_2$和$[NO_2BzPyNH_2][TCNQ]_2$，红外光谱和紫外光谱数据表明：TCNQ盐中存在$TCNQ^0$和$TCNQ^-$，并且形成了一维TCNQ分子柱，且$TCNQ^0$和$TCNQ^-$之间存在相互作用，部分电荷从$[TCNQ]_2^-$向阳离子($[NO_2BzPy]^+$和$[NO_2BzPyNH_2]^+$)转移。

表 1　电荷转移盐(3),(4)的红外光谱数据

	吸收峰归属	电荷转移盐(3)/cm^{-1}	电荷转移盐(4)/cm^{-1}
TCNQ 固有面内红外活性	C≡N 伸缩	2 185.30	2 195.96
	环外 C=C 伸缩	2 210.11	2 180
	环内 C—C 伸缩	1 519.84	1 517.54
	环外 C—C 伸缩	1 348	1 358
	C—H 弯曲	1 193.71	1 217.49
		836.25	838.57
TCNQ 活化吸收带	环内 C=C 伸缩	816.25	805
	环外 C=C 伸缩	1 596.65	1 541.85
	C—H 弯曲	1 325	1 305
		1 172	1 182.25
	环内 C—C 伸缩	1 040	1 045
	环内、外 C—C 伸缩	697.00	728.5

参 考 文 献

[1] Mukai K, Jinno S, Shimobe Y, Azuma N et al. Polyhedron., 2001, 20: 1537.

[2] Kurmoo M, Graham A W, Day P et al. J. Am. Chem. Soc., 1995, 117: 1209.

[3] Ojima E, Fujiwara H, Kato K et al. J. Am. Chem. Soc., 1999, 121: 5581.

[4] L I Jin shan, FENG Yi ji, MEN Zhenyu(李金山, 冯乙己, 门振宇). Chem. J. Chinese Univ. (高等学校化学学报), 1998, 19: 732.

[5] Zhao H, Heintz R A et al. Chem. Mater., 1999, 11: 736.

[6] Meby L R, Harder R J, Hertler W R et al. J. Am. Chem. Soc., 1962, 84: 3374.

[7] Bulgarevich S B, Bren D V et al. J. Mol. Stru., 1994, 317: 435.

[8] Girlando A, Pecile C. Spectrochim. Acta, Part A, 1973, 29: 1859.

[9] Bozio R, Girlando A. Pecile C. J. Chem. Soc., Faraday Trans. 2, 1975, 71: 1237.

[10] Inoune M , Inoune M B. J . Chem. Soc. , Faraday Trans. 2 , 1985, 81: 539.

Preparation and Spectroscopic Study of Two New Charge Transfer Salts

Abstract: TCNQ (TCNQ = tetracyanoquinodimethane) salts have good conductivity. The magnetic properties of substituted benzyl - pridiniums , such as ferromagnetism , antiferromagnetism and spin Peierls transition , have been widely investigated. In order to obtain some new materials with both conductivity and magnetism , two new organic salts , [NO_2BzPy]Cl (1) and [NO_2BzPyNH_2]Cl (2) , were synthesized and characterized. Furthermore , two new charge transfer salts , [NO_2BzPy] [TCNQ]$_2$(3) and [NO_2BzPyNH_2][TCNQ]$_2$ (4) were synthesized and characterized. The tested results of elementary analysis of charge transfer salts (3) and (4) were consistent with theoretical values , and the results of IR indicated that there exist TCNQ and TCNQ anions. One — dimensional molecular column of TCNQ has been formed. Partial charge transfer takes place from [TCNQ]$_2^-$ to cation.

Key Words: TCNQ; charge transfer salts; synthesis; characterization

本文原载于《光谱学与光谱分析》,2005 年第 25 卷第 3 期

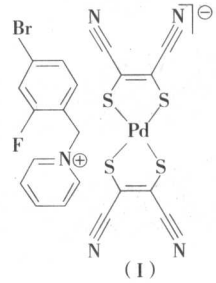
β – Phase of 1 – (4 – bromobenzyl)Pyridinium Bis(1,2 – dicyanoethene – 1,2 – dithiolato – κ^2S,S')Platinate(III)

The title compound, $(C_{12}H_{11}BrN)[Pt(C_4N_2S_2)_2]$, is a new polymorphic modification, viz. the β – phase; the α – phase has been published recently [Ren et al. (2004). Inorg. Chem. 43, 2569 – 2576]. In the β – phase, the anions and cations form segregated columnar stacks along the a axis, which is similar to the α – phase. Compared with the α – phase, the significant structural differences in the β – phase relate to the molecular conformation of the cation and the stacking architecture of both anions and cations.

Comment

Organic charge – transfer salts with segregated stacks are the subject of intensive study, due to their unusual properties in magnetism and conductivity (Coomber et al., 1996; Kawamura et al., 1997; Xie, Ren, Song, Zou & Meng, 2002; Xie, Ren, Song, Zhang et al., 2002; Xie et al., 2003). Recently, we reported the crystal structure of an ion-pair compound, 1 –(4′– bromobenzyl)pyridinium bis(maleonitriledithiolato)– platinate(III), which possesses segregated and regular stacks of cations and anions. Such an anionic stack behaves as a one-dimensional magnet with S = 1/ 2 and undergoes a magnetostructural transition at ca 260 K, which results from the instability of the one-dimensional electron gas (Ren et al., 2004). Here, we present the crystal structure of a new polymorph of the

title compound, (I) (Fig. 1), which we have called the β - phase. The α - phase corresponds to the crystal form reported earlier (Ren et al., 2004).



(I)

The β - phase crystallizes in a monoclinic space group, with one cation and one anion in the asymmetric unit. The anion, $[Pt(mnt)_2]^-$, shows a square-planar geometry (mnt is maleonitriledithiolate). The Pt—S bond lengths (Table 1) range from 2.249 (3) to 2.267 (3)Å. The S—Pt—S angles in the two chelate rings [89.79 (11) and 89.75 (11)°] are in good agreement with the values observed in the α - phase. In the cation, the plane formed by atoms N5/C14/C15 makes dihedral angles with the benzene and pyridine rings of 72.6 (15) and 104.6 (10)° respectively, while in the α - phase, the corresponding dihedral angles are 98.5 (6) and 93.1 (5)°. The dihedral angles between the benzene and pyridine rings in the β - and α - phases are 75.9 (4) and 114.1 (2)°, respectively. In the crystal structure of (I), the anions and cations stack into segregated columns along the a - axis (Fig. 2)

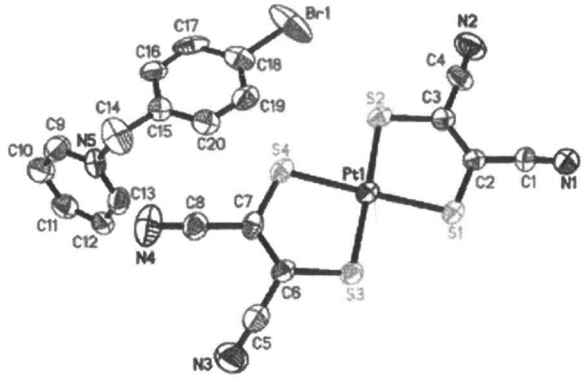


Figure 1 A view of (I), showing 30% probability displacement ellipsoids and the atom-numbering scheme. H-atoms have been omitted for clarity

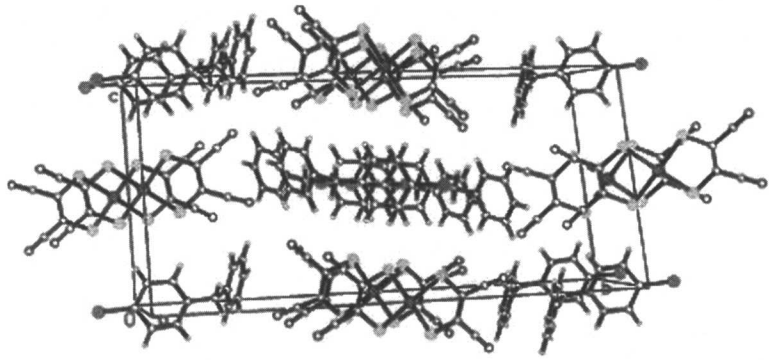


Figure 2 The crystal packing of (I), viewed approximately along the a axis.

There are remarkable differences in the crystal structures of the two polymorphs. The anionic stacks in the α - and β - phases are regular (Fig. 3a) and irregular (Fig. 3b), respectively. In the β - phase, two stacking patterns exist between adjacent anions, namely face - to - face overlap, and longitudinal and transverse offset. The face - to - face overlap involves an anionic pair containing atoms Pt1 and Pt1^{i}[symmetry code: (i) $1-x$, $2-y$, $1-z$], in which the distance between the Pt^{III} ions [3.4838 (8)Å] is comparable with that between the corresponding mean planes defined by the four coordinating S atoms [3.489 (3)Å]. The longitudinal and transverse offset involves an anionic pair containing atoms Pt1 and Pt1^{ii}[symmetry code: (ii) $2-x$, $2-y$, $1-z$], in which the distances between the Pt^{III} ions and between the corresponding mean planes are 4.3038 (9) and 3.6235 (4)Å, respectively. Within a cationic stack, neighbouring cations in the α - and β - phases are stacked in chair - conformation - like (Fig. 4a) and boat - conformation - like (Fig. 4b) fashions, respectively. In the β - phase, the anionic molecular planes in neighbouring stacks are inclined to each other with a dihedral angle of 27.73 (5)°[1.32 (5)°in the α - phase]. The dihedral angle between benzene rings in neighbouring cationic stacks is 21.94 (25)° [3.58 (18)°in the α - phase].

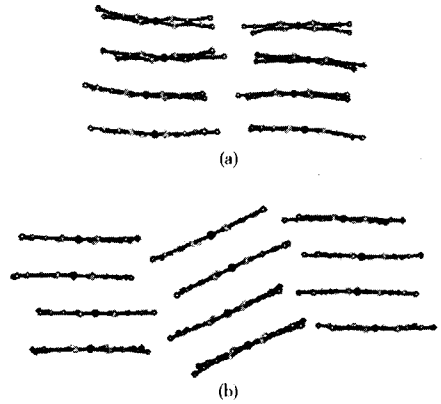


Figure 3 The anionic packing in (a) the α - phase and (b) the β - phase

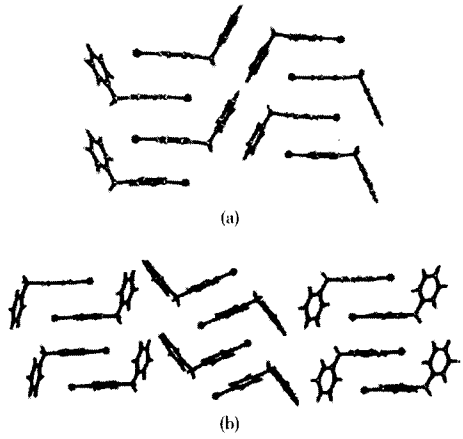


Figure 4 The cationic packing in (a) the α - phase and (b) the β - phase

With respect to the $[M(mnt)_2]^-$ - based compounds (M = Ni, Pd or Pt), their physical properties, such as conductivity and magnetism, are sensitive to the anionic stacking pattern. Therefore, the two polymorphs of (I) probably possess distinct conducting and magnetic behaviours, and such measurements are in progress.

Experimental

Disodium maleonitriledithiolate (Na_2mnt) was prepared following the

known procedure of Davison & Holm (1967). 1—(4—Bromobenzyl) pyridinium chloride was prepared by reacting 4—bromobenzylchlorine with 1.5 equivalents of pyridine in refluxing acetone for 4 h. The resulting product, containing white microcrystals, was filtered and washed with acetone and diethyl ether in turn, and then dried in vacuo, with a yield ca 80%. K_2PtCl_4, Na_2mnt and 1—(4— bromobenzyl) pyridinium chloride (equivalent molar ratio 1:2:2) were mixed in water. The red product which precipitated was separated, washed with water and then dissolved in MeCN. Iodine (1.5 molar equivalents) was added to the boiling solution with stirring. Five times the resulting volume of MeOH was then added and the mixture allowed to stand for 24 h. The microcrystals which formed were separated, washed with MeOH and dried in vacuo, with a yield ca 55%. A saturated MeCN solution of (I) at room temperature was placed in a refrigerator at 277 K for one week, and single crystals of (I) suitable for X-ray crystal structure analysis were obtained.

Crystal data

$(C_{12}H_{11}BrN)[Pt(C_4N_2S_2)_2]$	$D_x=2.046$Mg m^{-3}
$M_r=724.58$	Mo Kα radiation
Monoclinic, $P2_1/c$	Cell parameters from 851 reflections
$a=7.3814(8)$Å	$\theta=2.9-23.8°$
$b=26.180(3)$Å	$\mu=8.04$mm^{-1}
$c=12.6488(14)$Å	$T=293(2)$K
$\beta=105.739(2)°$	Block, black
$V=2352.7(5)$Å^3	0.20×0.15×0.10mm
$Z=4$	

Data collection

Bruker SMART CCD area-detector diffractometer	4851 independent reflections
	2886 reflections with $I>2\sigma(I)$
φ and ω scans	$R_{int}=0.097$
Absorption correction: multi-scan (*SADABS*; Sheldrick, 1996)	$\theta_{max}=26.5°$
	$h=-9\rightarrow9$

$T_{min}=0.24$, $T_{max}=0.45$
13418 measured reflections
$k=-32\rightarrow28$
$l=-13\rightarrow15$

Refinement

Refinement on F^2
$R[F^2>2\sigma(F^2)]=0.059$
$wR(F^2)=0.138$
$S=0.92$
4851 reflections
280 parameters
H—atom parameters constrained
$w=1/[\sigma^2(F_o^2)+0.0566P)^2]$
where $P=(F_o^2+2F_c^2)/3$
$(\Delta\sigma)_{max}=0.001$
$\Delta\rho_{max}=1.86$ eÅ^{-3}
$\Delta\rho_{mIN}=-1.58$ eÅ^{-3}

Table 1 Selected geometric parameters (Å,°)

Pt1—S4	2.249(3)	Pt1—S1	2.262(3)
Pt1—S2	2.255(3)	Pt1—S3	2.267(3)
S4—Pt1—S2	88.78(11)	S4—Pt1—S3	89.75(11)
S4—Pt1—S1	178.45(11)	S2—Pt1—S3	177.76(10)
S2—Pt1—S1	89.79(11)	S1—Pt1—S3	91.70(11)

All H atoms were placed in geometrically calculated positions and refined as riding, with C - H = 0.93—0.97Åand $U_{iso}(H) = 1.2U_{eq}(C)$. The residual electron density of 1.86 eÅ^{-3} and the deepest hole of - 1.58 eÅ^{-3} are situated at 1.04 and 1.74Åfrom Pt1, respectively.

Data collection: *SMART* (Siemens, 1996); cell refinement: *SMART*; data reduction: *SAINT* (Siemens, 1996); program(s) used to solve structure: SHELXS97 (Sheldrick, 1997a); program(s) used to refine structure: SHELXL97 (Sheldrick, 1997a); molecular graphics: SHELXTL (Sheldrick, 1997b); software used to prepare material for publication: SHELXL97.

The authors thank the Chinese National Natural Science Foundation (project Nos. 20171001 and 20371002) for financial support.

References

[1] Coomber, A. T., Beljonne, D., Friend, R. H., Bredas, J. L., Charlton, A., Robertson, N., Underhill, A. E., Kurmoo, M. & Day, P. (1996). Nature (London), 380, 144－146.

[2] Davison, A. & Holm, H. R. (1967). Inorg. Synth. 10, 8－26.

[3] Kawamura, T., Miyazaki, Y. & Sorai, M. (1997). Chem. Phys. Lett. 273, 435 438.

[4] Ren, X. M., Okudera, H., Kremer, R. K., Song, Y., He, C., Meng, Q. J. & Wu, P. H. (2004). Inorg. Chem. 43, 2569 2576.

[5] Sheldrick, G. M. (1996). SADABS. University of Göttingen, Germany.

[6] Sheldrick, G. M. (1997a). SHELXS97 and SHELXL97. University of Göttingen, Germany.

[7] Sheldrick, G. M. (1997b). SHELXTL. Version 5.10. Bruker AXS Inc., Madison, Wisconsin, USA.

[8] Siemens (1996). SMART and SAINT. Versions 4.0. Siemens Analytical X－ray Instruments Inc., Madison, Wisconsin, USA.

[9] Xie, J. L., Ren, X. M., He, C., Song, Y., Meng, Q. J., Kremer, R. K. & Yao, Y. H. (2003). Chem. Phys. Lett. 369, 41 48.

[10] Xie, J. L., Ren, X. M., Song, Y., Zhang, W. W., Liu, W. L., He, C. & Meng, Q. J. (2002). Chem. Commun. pp. 2346－2347.

[11] Xie, J. L., Ren, X. M., Song, Y., Zou, Y. & Meng, Q. J. (2002). J. Chem. Soc. Dalton Trans. pp. 2868－2872.

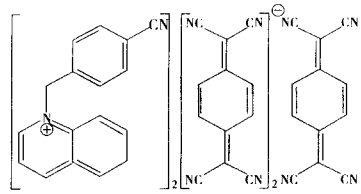
本文原载于(*Acta Crytallogrphica Section E*)《国际晶体学报》2005 E61

An Ion－pair Complex Composed of Two N－(4－Cyanobenzyl)Quinolinium Cations, Two 7,7,8,8－Tetracyanoquinodimethane Anions and One neutral 7,7,8,8－tetracyanoquinodimethane Molecule

In the title complex, $2C_{17}H_{13}N_2^+ \cdot 2C_{12}H_4N_1^- \cdot C_{12}H_4N_4$, a bound unit of two anions and one neutral TCNQ (TCNQ is7, 7, 8, 8 - tetracyanoquinodimethane) molecule is formed and adjacent units are displaced relative to each other along the direction of the shorter molecular axis of TCNQ. Completely segregated columnar stacks of TCNQ anions/molecules and cations are observed. Within an TCNQ column, the benzene rings are parallel to each other, the neutral TCNQ molecules lying on inversion centres. The centroid - to - centroid distance between adjacent aromatic rings is less than 4.2Å and $\pi - \pi$ stacking interactions are found.

Comment

The charge - transfer (CT) salt approach has been one of the most successful strategies for producing magnetically ordered compounds based on molecular building blocks (Jeffrey et al. ,2005). One of the most extensively used radicals in these studies has been the planar organic molecule 7, 7,8,8 - tetracyanoquinodimethane(TCNQ), since it shows a low reduction potential which makes it a suitable acceptor in charge-transfer processes. Another typical feature of this acceptor is its tendency to overlap its π - delocalised system with those of neighbouring molecules to form stacks with different degrees of electron delocalization (Alonso et al. , 2005).



(I)

Previous work has shown that molecular stacks of ion - pair complexes exhibit low - dimensional properties in some cases, which have interesting anisotropic magnetic, electronic and structural characteristics (Ren, Meng et al., 2002; Ren, Ma et al., 2003; Liu, Ren et al., 2005). Furthermore, the size and shape of the counter - cations play an important role in determining the ground - state properties of the resulting materials(Ren, Chen et al., 2002). As a result, ion - pair complexes consisting of the TCNQ anion and benzylquinolinium cations could offer the possibility of systematically studying the fundamental relationship between the stack structure and the size and steric properties of substituent groups. In this communication, we report the crystal structure of the title compound, (I).

The asymmetric unit of (I) is composed of one N -(4 - cyanobenzyl) quinolinium cation, one $TCNQ^-$ anion and one half of a centrosymmetric neutral TCNQ molecule (Fig. 1). This complex stacks into completely segregated columns of TCNQ anions/molecules and cations, as illustrated by the projection along the crystallographic b axis in Fig. 2. The cation and anion columns are linked by hydrogen-bonding interactions (Table 1). Within an anionic column, a strongly bound unit of $[(TCNQ)_3]^{2-}$ is formed, and adjacent units are displaced relative to each other along the direction of the shorter molecular axis of TCNQ. The benzene rings are parallel to each other. The centroid - to - centroid distances between adjacent aromatic rings are 3.809, 3.809 and 3.796Å(Fig. 3), indicating weak $\pi-\pi$ stacking interactions. The N -(4 - cyanobenzyl)quinolinium cations have a Λ - shaped conformation, and the dihedral angles formed by the C5/C8/N8 plane with the benzene and quinolinium rings are 10.56 (10) and 73.81 (10)°, respectively.

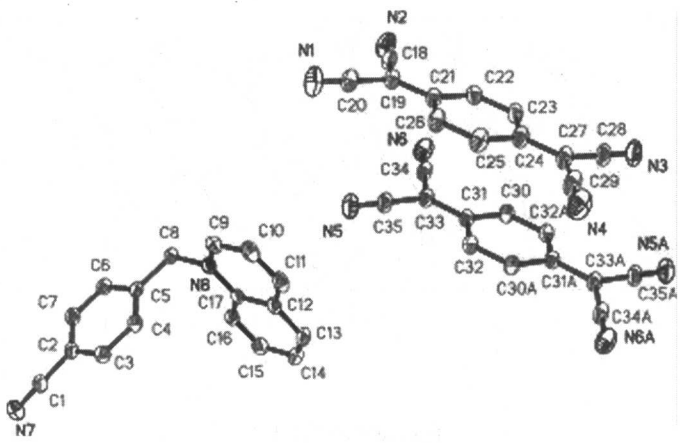


Figure 1 The cation, anion and centrosymmetric neutral TCNQ molecule of complex (I), showing 30% probability displacement ellipsoids and the atom-numbering scheme. [Symmetry code: (A) $1-x$, $1-y$, $-z$.]

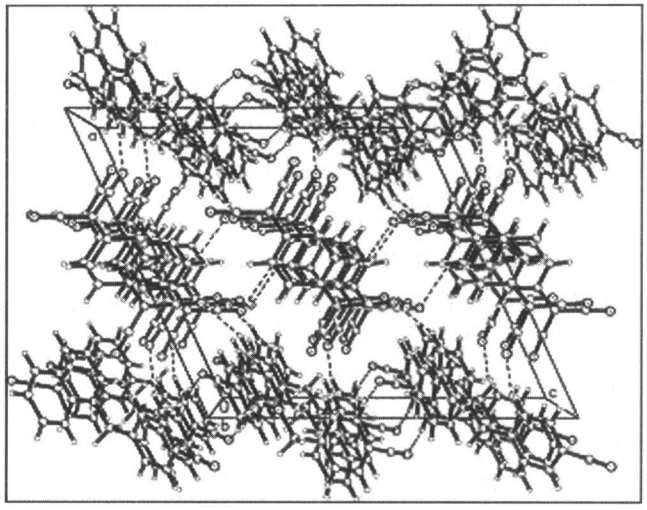


Figure 2 The cation, anion and centrosymmetric neutral TCNQ molecule of complex (I), viewed along the b-axis direction. Dashed lines indicate C – H···N hydrogen bonds.

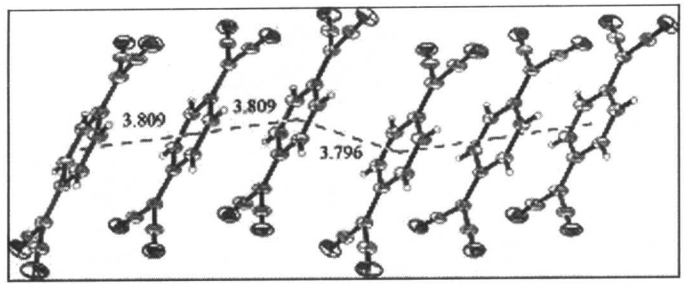


Figure 3 A side view of the one - dimensional anionic chain of (I). Distances are in Å

Experimental

N -(4 - Cyanobenzyl) quinolinium iodine was prepared by the direct combination of 1 : 1 molar equivalents of N -(4 - cyanobenzyl)- quinolinium chloride and NaI in a warm solution in acetone at 313 K. A white precipitate was formed (NaCl) which was filtered off, and a white microcrystalline product was obtained by evaporating the filtrate. 1 : 2 Molar equivalents of N -(4 - cyanobenzyl)quinolinium iodide and TCNQ were mixed directly in a solution in methanol, and the mixture was refluxed for 12 h. The violet - red microcrystalline product which formed was filtered off, washed with MeOH and dried in vacuo. Single crystals of (I) suitable for structure analysis were obtained by diffusing diethyl ether into an MeCN solution of (I).

Crystal data

$2C_{17}H_{13}N_2^+ \cdot 2C_{12}H_4N_4^- \cdot C_{12}H_4N_4$	$Z = 2$
$M_r = 1103.16$	$D_x = 1.346$ Mg m^{-3}
Monoclinic, $P2_1/c$	Mo Kαradiation
$a = 16.083\ (3)$Å	$\mu = 0.08$ mm^{-1}
$b = 10.8627\ (17)$Å	$T = 293\ (2)$ K
$c = 17.099\ (3)$Å	Block, dark green
$\beta = 114.327\ (3)°$	0.20×0.20× 0.15 mm
$V = 2722.0\ (7)$ Å3	

Data collection

Bruker SMART APEX CCD area—	14142 measured reflections
Detector diffractometer	5321 independent reflections
φ and ω scans	4175 reflections with $I>2\sigma(I)$
Absorption correction: multi-scan	$R_{int}=0.055$
(*SADABS*; Bruker, 2000)	$\theta_{max}=26.0$
$T_{min}=0.983$, $T_{max}=0.988$	
Refinement	
Refinement on F^2	H—atom parameters constrained
$R[F^2>2\sigma(F^2)]=0.056$	$w=1/[\sigma^2(F_o^2)+0.5287P]$
$wR(F^2)=0.138$	where $P=(F_o^2+2F_c^2)/3$
$S=1.05$	$(\Delta/\sigma)_{max}<0.001$
5321 reflections	$\Delta\rho_{max}=0.22$ eÅ^{-3}
388 parameters	$\Delta\rho_{min}=-0.21$ eÅ^{-3}

Table 1 Hydrogen-bond geometry (Å,)

D—H···A	D—H	H···A	D···A	D—H···A
C32—H32···N1i	0.93	2.58	3.220 (3)	126
C16—H16···N6ii	0.93	2.46	3.346 (2)	160
C11—H11···N3iii	0.93	2.58	3.426 (3)	151
C4—H4···N8	0.93	2.51	2.856 (2)	102
C3—H3···N7iv	0.93	2.58	3.435 (3)	154

Symmetry codes: (i) $-x+1$; $y-1/2$; $-z+1/2$; (ii) $-x$; $-y+1$; $-z$; (iii) $x+1$; $-y+1$; $-z$; (*iv*) $-x$; $-y$; $-z+1$.

All H atoms were placed in geometrically calculated positions, with C—H = 0.93Å, and refined as riding, with Uiso(H) = 1.2Ueq(C). Data collection: SMART (Bruker, 2000); cell refinement: SAINT (Bruker, 2000); data reduction: SAINT; program(s) used to solve structure: *SHELXS*97 (Sheldrick, 1997); program(s) used to refine structure: *SHELXL*97 (Sheldrick, 1997); molecular graphics:

SHELXTL (Bruker, 2000); software used to prepare material for publication: *SHELXTL*

This work was funded by the National Natural Science Foundation of China (project No. 20371002) and the Natural Science Foundation of An-

hui Province of China (project Nos. 2003kj253 and 2003jq153).

References

[1] Alonso, C., Ballester, L., Gutierrez, A., Perpinan, M. F., Sanchez, A. E. & Azcondo, M. T. (2005). Eur. J. Inorg. Chem. pp. 486 495.

[2] Bruker (2000). SADABS, SMART, SAINT and SHELXTL. Bruker AXS Inc., Madison, Wisconsin, USA.

[3] Jeffrey, A. C., Meredith, M. B., Hanusa, T. P., Wang, G. B., Brennessel, W. W. & Yee, G. T. (2005). Inorg. Chem. 44, 172—174.

[4] Liu, G. X., Ren, X. M., Kremer, P. K. & Meng, Q. J. (2005). J. Mol. Struct. 743, 125—133.

[5] Ren, X. M., Chen, Y. C., He, C. & Gao, S. (2002). J. Chem. Soc. Dalton Trans. pp. 3915—3918.

[6] Ren, X. M., Ma, J., Lu, C. S., Yang, S. Z., Meng, Q. J. & Wu, P. H. (2003). Dalton Trans. pp. 1345—1351.

[7] Ren, X. M., Meng, Q. J., Song, Y., Lu, C. S., Hu, C. J. & Chen, X. Y. (2002). Inorg. Chem. 41, 5686—5692.

[8] Sheldrick, G. M. (1997). SHELXS97 and SHELXL97. University of Göttingen, Germany.

本文原载于(*Acta Crytallogrphical Section E*)《国际晶体学报》,2006, o3256—o3258

Mixed – valence Molecular Magnets Based on $[TCNQ]_3^{2-}$ Building Block: Structures, Magnetic Properties and DFT Analyses

Ground states involving spatially inhomogeneous charge distributions have in recent years been observed in a wide range of novel electronic solids, particularly in reduced dimensions.[1] We focus our research interesting on the molecular magnets based on TCNQ radical ion. Such magnetic architectures posses a series of valences (for example, 0, −0.5 and −1) and easily assembly into a columar stack. It is possible to gain the molecular magnets with quasi – 1D structural and mixed – valence features.

Two mixed – valence magnets, $[Cat]_2[TCNQ]_3$ (Cat = 1 –(4′– cyanobenzyl)quinolinium (1) and 1 –(4′– cyanobenzyl)pyridinium (2)), exhibit similar stack structures and magnetic behaviors. Fig. 1 and 2 show ORTEP view and anionic parking diagram of 1, respectively.

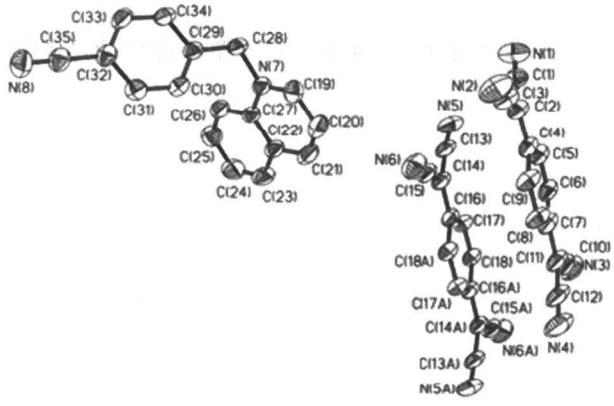


Fig 1 OPTEP View of 1 at 50% possibility ellipsoids

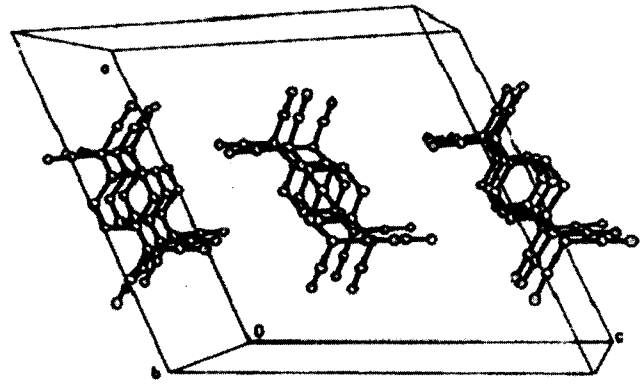


Fig 2 ORTEP view of 1 at 50% possibility ellipsoids Fig. 2 Packing structure of anions in

In conclusion, we prepare two mixed - valence compounds based on $[(TCNQ)3]^{2-}$ ions, which indicate similar stack structures. The magnetic behaviors were investigated by magnetic susceptibility measurements and DFT analyses.

(a) Y. Fagot—Revurat, M. Mehring and R. K. Kremer *Phys. Rev. Lett.* 2000, 84, 4176;

(b) J. C. Loudon, N. D. Mathur and P. A. Midgley *Nature* 2002, 420, 797;

(c) R. T. Clay, S. Mazumdar and D. K. Campbell *J. Phys. Soc. Jap.* 2002, 71, 1816.

本文原载于《加拿大国际学术会议(ICMM2006)论文集》

具有分子双稳性的一维自由基磁相变材料的研究

摘 要：具有分子双稳性的化合物是实现分子集合体作为新的光开关和信息存储元件的理想分子体系。本文研究了合成苄基吡啶衍生物，研究其分子构象与堆积的关系，并研究了构建一维分子基磁体，以及常温常压下的电学、磁学等性质。

主题词：自由基分子基磁体；分子双稳性；磁相变

具有分子双稳性的化合物包括过渡金属自旋交叉配合物和一些具有共轭分子结构和拟一维堆积结构的自由基化合物。目前，对过渡金属自旋交叉配合物尤其是含+2价Fe离子的自旋交叉配合物的研究，进行得广泛而深入，并已积累了大量的实验数据。应用超分子化学的原理，通过分子设计的方法，新的过渡金属的自旋交叉配合物体系不断被发现，同时，原有的自旋交叉配合物体系的性质不断被优化，比如，通过调控分子间的协同作用，调节自旋交叉配合物的高、低自旋态间的转变温度(Tc)，使之接近室温，增大相变(高、低自旋态转变)的热滞后环(the hysteresis loop)的宽度($\Delta Tc = Tc\uparrow - Tc\downarrow$)等。近年来，该领域中的研究工作已逐渐从纯基础研究向着应用基础研究的方向发展，如著名的磁化学家O. Kahn的研究小组多年来一直从事Fe^{2+}离子与三氮唑桥连配体形成的自旋交叉配位聚合物的研究，并得到了一系列具有优良性质的自旋交叉配位聚合物。基于这类自旋交叉配位聚合物在高、低自旋态时的颜色有很大的差异，并提出了如何把这类分子基磁性材料开发成电子显示器件、自旋开关器件等分子电子学器件的设计思想[1]。P. Gütlich领导的研究小组首先发现了过渡金属配合物光诱导自旋交叉现象(即光磁效应)。光诱导自旋交叉现象的研究揭示了自旋交叉配合物在热开关、光开关等分子电子学器件领域中的应用前景。

具有平面型分子结构的$[M(mnt)_2]^-$配阴离子(mnt^{2-} = maleonitrileodithiolate)和具有Λ－型分子构象的苄基吡啶衍生物阳离子能形成阴阳离子完全分列的柱状堆积结构。在阴离子堆积柱内,$[M(mnt)_2]^-$配阴离子通过M…S…S…M、M…S…M等相互作用,形成自旋$S=1/2$的一维磁链,此类一维磁链配合物具有分子双稳性[2]。TCNE (TCNQ)等自由基分子离子与$[M(mnt)_2]^-$配阴离子具有相似的分子结构(二者都是平面型共轭体系,且每个分子的自旋$S=1/2$),因此,用TCNE (TCNQ)等自由基分子离子替代$[M(mnt)_2]^-$配阴离子与苄基吡啶衍生物阳离子能形成阴阳离子完全分列的柱状堆积结构,相应的一维磁链化合物是潜在的具有分子双稳性的新体系,通过系统地改变平衡阳离子的分子构象,达到调节平衡阳离子的分子拓扑和体积大小,进一步实现控制自由基分子阴离子的堆积结构,以期获得具有分子双稳性的一维分子基磁性材料。

1. 苄基吡啶衍生物的合成及其分子构象——芳香环上取代基的性质之间关系的研究

具有平面型分子结构的TCNE、TCNQ等自由基分子是π轨道上的电子高度离域的共轭分子体系,比邻的自由基分子(π离子)间通过(轨道上电子间的相互作用,可形成具有一维电子结构的分子固体。通常,平衡阳离子的拓扑几何和体积的大小强烈影响着TCNE(或TCNQ)离子对化合物的堆积结构。构筑TCNE(或TCNQ)基的一维分子基磁体,要求TCNE (或TCNQ)与平衡阳离子必须形成完全分列的柱状堆积结构,即阴阳离子分别形成堆积柱。因而,选择合适的平衡阳离子对构筑TCNE(或TCNQ)基的一维分子基磁体就显得尤为重要。具有Λ－型分子构象的苄基吡啶衍生物(缩写为R－BzPy),其分子构象与其芳环上取代基的电子性质及其在环上的位置密切相关,因此,可以通过变化芳环上的取代基的性质,达到系统地改变苄基吡啶衍生物阳离子分子构象的目的,进而实现系统地调控苄基吡啶衍生物阳离子分子的拓扑几何和体积大小,最终实现构筑阴阳离子完全分列的TCNE(或TCNQ)基的一维分子基磁体的目标。

1.1 苄基吡啶(喹啉)衍生物的合成

对于该系列化合物的合成,本课题组已经探索了一系列的合成方法,并取得了比较好的实验结果,合成了一系列的苄基吡啶(喹啉)衍生物为下一

步的实验工作打下了良好的基础。

1.2 $[R-BzPy][TCNQ]_n$和$[R-BzQl][TCNQ]_n$的合成、结构和磁性研究：

我们在实验过程中，通过改变不同的条件生长出一系列适合单晶衍射的单晶体。我们测定了它们的晶体结构，研究了化合物 1－3 的磁学性质。1. [BrBzPy][TCNQ]2. [BrBzPy][TCNQ]$_2$3. [BrBzQl][TCNQ]$_2$.

1.3 基于 $R-BzPy^+$ ($R-BzQl^+$)和 $TCNQ^{n-}$ 的一维分子基磁体的研究

在 1 和 2 中，$[(TCNQ)_2]^-$ 和 $[TCNQ]^-$ 阴离子都堆积成四重亚单元，相邻的亚单元进一步构筑成 zig－zag 形阴离子堆积柱(Fig. 1)。在 1 中，晶体学上不等价的分子 A 和 B 分别与 $[TCNQ]^-$ 和 $[TCNQ]^0$ 分子的特征键长一致。红外光谱和分子轨道理论计算分析与结构分析结果一致。在 2 中，阳离子间通过氢键形成了超分子楼梯结构(Fig. 2)。

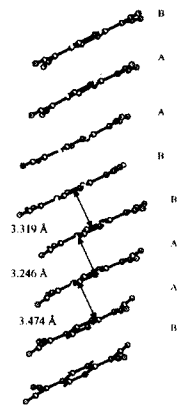


Fig. 1 The anionic stacking column with tetrad subunit in 1.

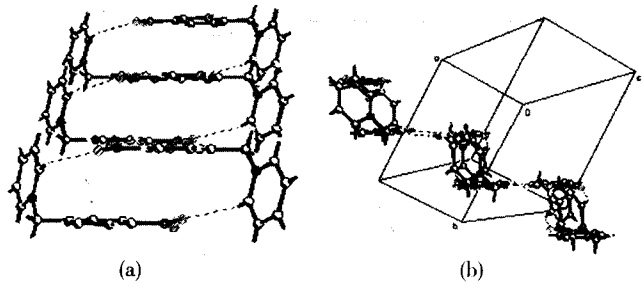


Fig. 2 Supramolecular staircase consisting of the cations of 1 -(4 - nitrobenzyl) pyridinium in 2 (a) the obverse view and (b) the side view of the supramolecular staircase.

1 和 2 的磁化率(2～350K)：顺磁性、反铁磁相互作用；

1 和 2 的室温 X - band EPR 谱：典型的自由基谱的特征。

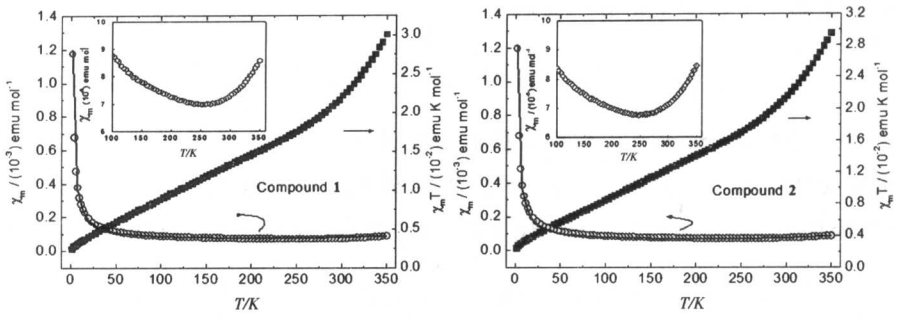


Fig. 3 Plots of the temperature dependence of magnetic susceptibility of 1 and 2.

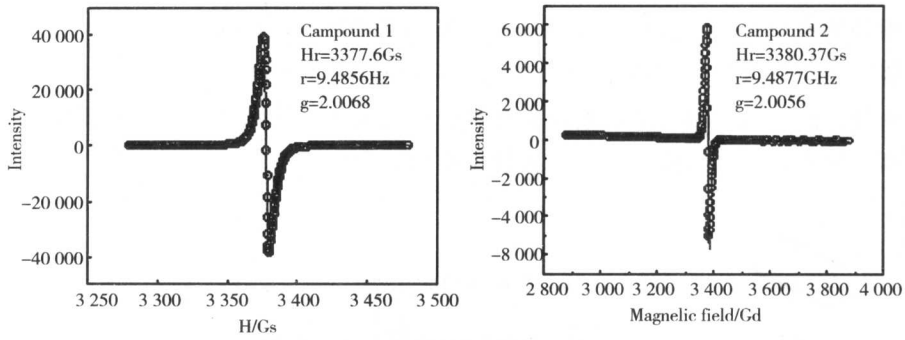


Fig. 4 X-band EPR spectra of 1 and 2, which exhibit the feature of radical signal.

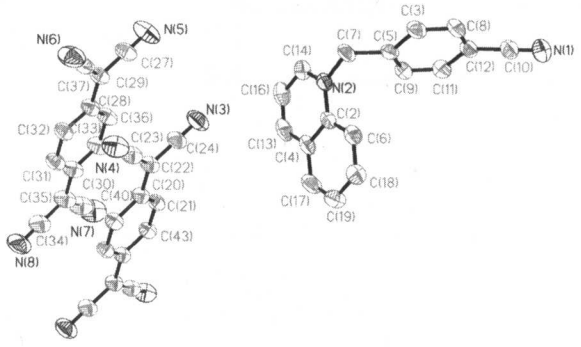


Fig. 5 Molecular structures of 4 (left) and 5 (right).

2. 苄基吡啶衍生物阳离子和 $TCNQ^-$($TCNE^-$)自由基阴离子形成的一维分子基磁体的研究

在第一步实验的基础上，应用电化学方法制备并生长苄基吡啶衍生物阳离子和$[TCNQ]^-$，$[TCNE]^-$等自由基阴离子形成的一维分子基磁体。

测定其晶体结构，结合分子力学、DFT 等理论方法，探讨苄基吡啶衍生物的芳香环上的取代基的性质(电子性质、空间位阻等)对此类离子对化合物的堆积结构的影响，从而在理论上和实验上为设计和制备新的具有分子双稳性的化合物体系积累实验数据。应用变温 IR、变温 Raman、变温 EPR 等波谱技术和变温磁化率、变温电导率测量等现代测试手段，对此类一维分子基磁体的分子双稳性以及各种协同效应进行深入和系统的研究。

2.1 基于$[M(mnt)_2]^-$的一维分子基磁体

用$[M(mnt)_2]^-$(M = Ni, Pd or Pt) 阴离子代替 $TCNQ^-$ 阴离子，得到了 3 种新化合物(6－8)。用不同的方法生长单晶，发现了$[Pt(mnt)_2]^-$化合物的 1 种新的晶相，测定了 6－9 的晶体结构[3－6]。

6 和 7 的结构和磁性：

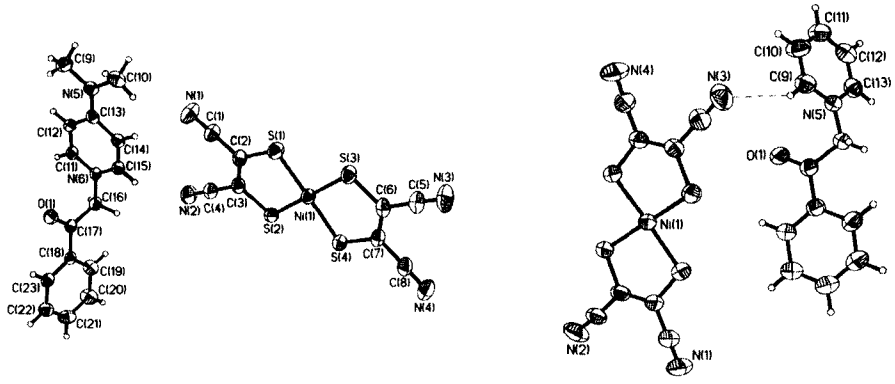


Fig. 6 Molecular structures of 6 (left) and 7 (right), which exhibits their magnetic feature。

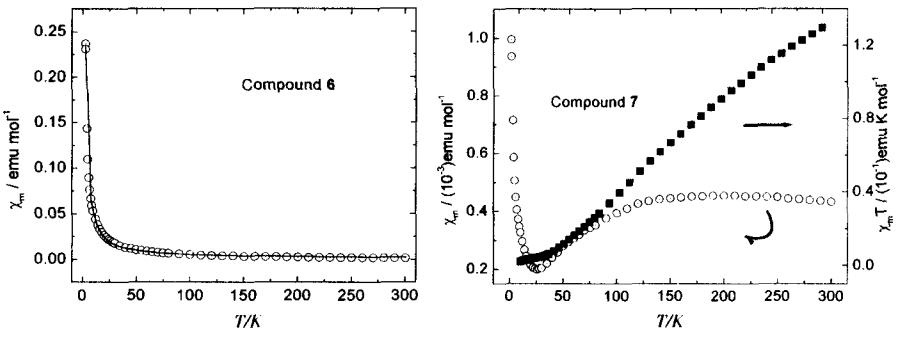


Fig. 7 Temperature dependences of magnetic susceptibility of 6 (left) and 7 (right).

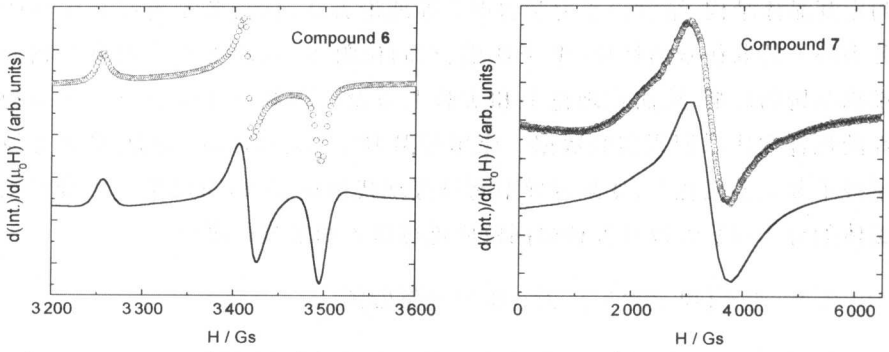


Fig. 8 EPR spectra of 6 (left) and 7 (right) at room temperature.

8 的结构和磁性：([FBzPy][Pd(mnt)$_2$]；FBzPy$^+$ = 1－(4′－fluorobenzyl)pyridinium)：

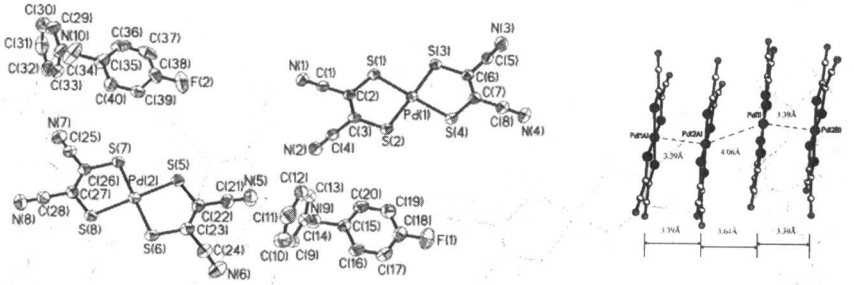


Fig. 9 Molecular and crystal structures of 8: [Pd(mnt)$_2$]$^-$ anions form columnar stack in which two kinds of anionic stacking patterns are found. The eclipsed plane over plane and two superimposed monomers rotated possess the distances of Pd…Pd as 3.69 and 4.06Å, respectively.

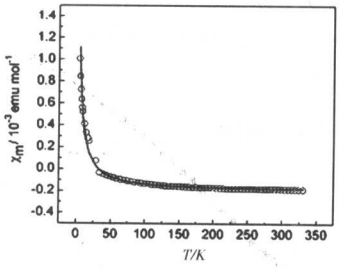


Fig. 10 Temperature dependence of magnetic susceptibility of 8 which shows very weak paramagnetism to indicate there exist strongly antiferromagnetic interactions within an anionic stack.

化合物 9 的同质异晶现象：化合物 9 的乙腈溶液缓慢挥发或降温分别得到 α 和 β 相晶体。在 α 相晶体中，室温时[Pt(mnt)$_2$]$^-$ 阴离子形成均匀的堆积柱，在 $T\approx269$K 时，晶体发生了磁结构相变。但是在 β 相晶体中，阴阳离

子分别形成了二聚的堆积柱(室温),其低温晶体结构和磁化率的测量正在进行之中。

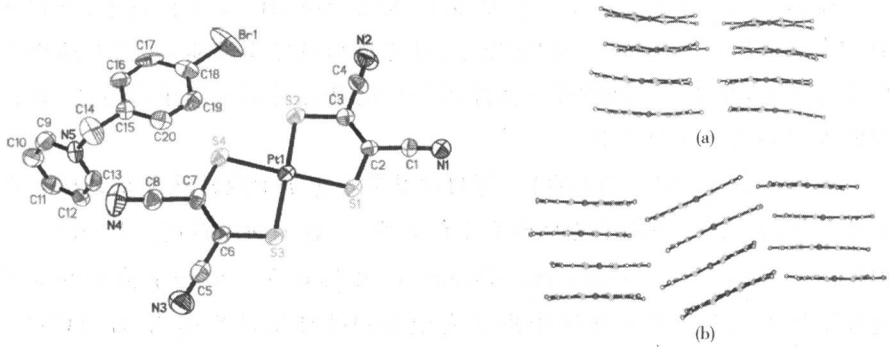
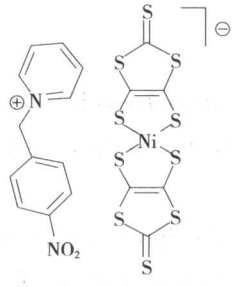


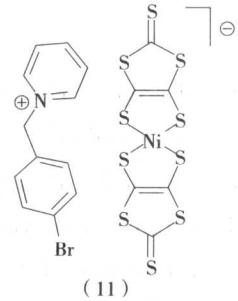
Fig. 11 Left: Molecular structure of 9; Right: Anionic stacks in (a) α and (b) β phase.

2.2 基于[Ni(dmit)$_2$]$^-$的自旋梯分子基磁体

鉴于[Ni(dmit)$_2$](dmit = 1, 3 - dithiole - 2 - thione - 4, 5 - dithiolate)与TCNQ在分子、电子结构上的相似性,用[Ni(dmit)$_2$]$^-$阴离子代替TCNQ$^-$阴离子,得到了2种新的自旋梯化合物(10和11),测定了它们的晶体结构,研究了其磁学性质[7]。



(10)



(11)

3. 高压下,TCNE$^-$(TCNQ$^-$)基的一维分子基磁体的磁、电学性质研究

TCNE$^-$(TCNQ$^-$)等自由基分子离子是共轭的分子体系,其π轨道上的电子高度离域化。比邻的自由基分子离子间的磁交换相互作用(分子轨道重叠、自旋极化)和自由基分子离子间重叠方式以及各种短的堆积距离密切相关。在此类一维分子基磁体中,堆积柱间和堆积柱内的分子间只存在

弱的 van de Waals 力等弱相互作用，外部静压力将会强烈影响分子间的堆积距离和重叠方式，因此，压力将会对此类一维分子基磁体的磁和电学性质产生深刻影响。在第二步工作的基础上，应用 SQUID 等实验技术，研究该类一维分子基磁体在高压下的磁化率、磁比热和电导率性质，探讨上述物理性质与压力，以及分子间的磁交换性质与自由基分子离子间重叠方式、各种短的堆积距离之间的关系。

如何控制 $TCNE^-$（$TCNQ^-$）等自由基分子离子形成柱状堆积结构是本申请工作的关键。我们的近期研究工作表明，具有平面结构的$[M(mnt)_2]^-$配阴离子（mnt^{2-} = maleonitrileodithiolate）和具有 Λ－型分子构象的苄基吡啶衍生物阳离子能形成阴阳离子完全分列的柱状堆积结构，而 $TCNE^-$（$TCNQ^-$）等自由基分子离子与$[M(mnt)_2]^-$配阴离子具有相似的分子结构（二者都是具有平面型分子结构的共轭体分子体系，且每个分子的自旋 $S=1/2$），因此，用 $TCNE^-$（$TCNQ^-$）等自由基分子离子替代$[M(mnt)_2]^-$配阴离子与苄基吡啶衍生物阳离子能形成阴阳离子完全分列的柱状堆积结构。

参考文献

[1] Light Induced Excited Pair Spin State in an Iron(II) Binuclear Spin - Crossover Compound, J. - F. Létard, O. Kahn, et al., J. Am. Chem. Soc. 1999, 121, 10630;

[2] A Novel Bis(trans－thiocyanate)iron(II) Spin - Transition Molecular Material with Bidentate Triaryltriazole Ligands and Its Bis(cis－thiocyanate)iron(II) High－Spin Isomer, D. Y. Zhu, X. Z. You et al., Chem. Mater. 2002, 14, 838.

[3] Unusual Magnetic Properties of One - Dimensional Molecule－Based Magnets Associated with a Structural Phase Transition, X. M. Ren, Q. J. Meng et al., Inorg. Chem. 2002, 41, 5686.

[4] Unusual Magnetic Property Associated with Dimerization within a Nickel Tetramer, X. M. Ren, Q. J. Meng et al., Inorg. Chem. 2002, 41, 5931.

[5] Peculiar Magnetic Behavior in Ion - pair Complex [1 — (4′ — fluorobenzyl)pyridinium] [Ni(mnt)$_2$] (mnt^{2-} = maleonitriledithiolate), J. L. Xie, X. M. Ren, Y. Song, W. W. Zhang, W. L. Liu, C. He, Q. J. Meng, Chem. Commun. (2002), 2346.

[6] Complicated Magnetic Behavior in One - dimensional Nickel(III) Chain Complex [1—(4′—cyanobenzyl)pyridinium][Ni(mnt)$_2$] (mnt^{2-} = maleonitriledithiolate), J. L. Xie, X. M. Ren, C. He, Z. M. Gao, Y. Song, Q. J. Meng, R. K. Kremer, Chem. Phys. Lett. 369 (2003), 41.

[7] Molecular Spin Ladders Self - assembly from [Ni(dmit)$_2$]— Building Blocks: Syntheses, Structures and Magnetic Properties, Y. C. Chen, G. X. Liu, Y. Song, H. Xu, X. M. Ren, Q. J. Meng, Polyhedron 24 (2005)2269.

Study on the Magnetic Phase Transition Materials of One-dimensional Organic Radical with Molecular Bistability

CHEN You - cun

(The school of chemistry and chemical engineering, Anqing Normal College, An Hui Anqing 246011, China)

Abstract: Molecular bistability complexes are an ideal molecular system because it can be used as new types of optical switch and information memory medium. In this paper, some syntehszed derivatives of bezylpyidinium and their relation to molecular configuration and molecular stack structure are studied. Then, for one-dimensional molecular based-magnets designed and synthesized, their magnetic and electronic properties under ordinary pressure and temperature are studied.

Key Words: radical molecule-based magnets; molecular bistability; Magnetic transition

本文原载于《安庆师范学院学报》2006 年第 3 期

Mixed-valence Molecular Magnets Based on $[TCNQ]_3^{2-}$ Building Block: Structures, Magnetic Properties and DFT Analyses

Abstract: Two radical compounds, $[CNQI]_2[(TCNQ)_3]$ (1) and $[CNPy]_2[(TCNQ)_3]$ (2) where $CNQI^+$ = 1-(4′-cyanobenzyl)quinolinium and $CNPy^+$ = 1-(4′-cyanobenzyl)-pyridinium, have been prepared and characterized structurally. In crystals of both 1 and 2, there are two crystallographic independent TCNQ species (labeled as TCNQ(A) and TCNQ (B)) in an asymmetric unit. The dihedral angle between the mean-molecular-planes of unit A and B, defined by the corresponding quinodimethane groups in TCNQ, is 0.9° in 1 versus 68.2° in 2. The unit A and B stack in the pattern…ABA…ABA…along b-axis in 1, while in two homogeneous types (…AA…and…BB…) along b-axis in 2, respectively. The typical magnetic characteristics in both 1 and 2 are: 1) strong AFM coupling interaction within a TCNQ stack leads to the $\chi_m T$ values at room temperature much smaller than expected spin-only value, 2) temperature dependent magnetic coupling behavior causes the plot of χm^{-1} versus T deviate from linearity. The IR spectra clearly show the existence of a mixed-valence state in both 1 and 2, namely, TCNQ (A) and (B) units possess the different negative charge. Even if 1 and 2 have the same molar ratio between countercation and TCNQ species (Cation:TCNQ = 2:3), their EPR spectra are significantly different. An isotropic signal with g = 2.0066 is observed in 1, while two sets of signals in 2, in which one is isotropic with g = 2.0062 and the other possesses five-fold hyperfine splitting structure that arise from the coupling between spins of electron and four equivalence nuclear of H-atoms in a quinodimethane group, with g = 2.0067 and A =

0.25 Gs. Calculations for charge distribution in TCNQ (*A*) and TCNQ (*B*) units were performed and the results disclosed the TCNQ (*A*) and TCNQ (*B*) units may be assigned to $TCNQ^{-1}$ and $TCNQ^{0}$ in 1, respectively, and $TCNQ^{-\delta}$ (where partial charge $\delta = 0.62-0.72$) in 2.

Key Words: TCNQ radical; mixed - valence; crystal structure; magnetic property; DFT calculation

1. Introduction

Mixed-valence molecular materials have attracted much attention because of their novel physical properties and possible application in molecular devices.[1] In such a molecular system, the procedure of charge disproportion or charge ordering may occur due to the spatially inhomogeneous charge distributions.[2,3] The transition from mixed-valence state to the stabilization of a charge-ordered state gives frequently rise to abrupt change in either the transport or the magnetic properties of the materials, which was observed in lots of organic electronic solids, such as DI - $DCNQI_2Ag$,[4] $[\{M_2(dta)_4I\}_\infty]$ (dta = $CH_3CS_2^-$, M = Ni, Pt);[5] tetrathiafulvalene derivatives of $TMTTF_2X$,[6] $(EDO-TTF)_2PF_6$,[7] $\beta''-(ET)_3X_2$,[8] $\theta-ET_2X$ and $\alpha-ET_2X$ [ET = bis(ethylenedithiotetrathiafulvalene)].[2,9-11] The common feature for these molecular solids is the system having a quarter-filled π - band, namely, there exists one electron or hole per two molecules.

TCNQ radical (TCNQ = 7,7,8,8 - tetracyanoquinodimethanide) possesses a series of variable valences (for example, 0, −0.5 and −1) due to the fine tunable degree of charge transfer and the columnar stack in a Donor - Acceptor compound, and thus it is possible to obtain the molecular magnets with quasi - 1D structure and mixed-valence feature. In this paper, we report the syntheses, crystal structures, IR spectroscopic and magnetic properties of two mixed - valence magnets, $[CNQI]_2[TCNQ]_3$ (1) and $[CNPy]_2[TCNQ]_3$ (2), where $CNQI^+$ = 1 -(4′- cyanobenzyl)quinolinium and $CNPy^+$ = 1 -(4′- cyanobenzyl)pyridinium, respectively.

2. Experiments

2.1 Chemicals and Reagents

All chemicals and solvents were reagent grade, and were used without further purification. 4 - cyanobenzyl chlorine is the product of Synica Chemicals. 1 -(4′- cyanobenzyl)quinolinium chloride (abbr. as [CNQl]Cl) and 1 -(4′- cyanobenzyl)- pyridinium chloride (abbr. as [CNPy]Cl) were synthesized following the published procedure.[12]

2.2 Physical measurements

Elemental analyses were performed with a Perkin - Elmer 240 analytical instrument. IR spectra were recorded on a Fourier Transform Infrared Spectrometer (170SX) (KBr pellet). Magnetic susceptibility data of 1 and 2 on polycrystalline sample were collected over the temperature range of 2 ~300K using a Quantum Design MPMS - 5S super - conducting quantum interference device (SQUID) magnetometer, and the diamagnetic corrections were made using Pascal's constants ($\chi 0 = 3.3$ emu. mol^{-1} for 1 and 2.8 emu. mol^{-1} for 2). 13 X - band EPR spectra of 1 and 2 were recorded on a Bruker 2000 — D — SRC spectrometer on polycrystalline material at room temperature and the microwave frequency is near to 9.7 GHz.

2.3 Syntheses of $[CNQI]_2[TCNQ]_3$(1) and $[CNPy]_2[TCNQ]_3$[2]

A modified procedure, described in reference [14], was utilized to prepare 1 and 2. Li(TCNQ)[15] (213 mg, 1.0 mmol) and [CNQl]Cl (283 mg, 1.0 mmol) (1 : 1 molar ratio) were mixed in water (40 mL) at room temperature, in heterogeneous phase, and stirred for ~ 2 h. The black precipitate formed was filtered off, washed with H_2O. The crude product was dissolved in MeOH (~15 mL) giving a clear solution. The violet - red crystals, which are suitable for X - ray analysis, were obtained after most solvent was evaporated. The crystals of 1 were collected by filtration,

washed with Et_2O, and dried in air. Yield: ~50%. Analysis Calc. for C35H19N8: C, 76.2%; H, 3.47%; N, 20.3% and found: C, 76.0%; H, 3.76%; N, 20.2%. IR spectra (cm^{-1}): 2227(m) 2199 (m), 2181 (vs), 2174 (vs) and 2156 (sh).

Compound 2 was prepared as that described in 1, starting from Li (TCNQ) and[CNPy]Cl in water. The yield of final product of crystals is about 52%. Analysis Calc. for $C_{31}H_{17}N_8$: C, 74.2%; H, 3.42%; N, 22.3% and found: C, 73.8%; H, 3.68%; N, 22.0%. IR spectra (cm^{-1}): 2233 (m), 2185 (vs), 2179 (sh), 2156 (vs).

2.4 X-ray Crystallography

Diffraction data of 1 and 2 were collected at 293 K on a Bruker SMART APEX CCD-based diffractometer with graphite-monochromatic Mo-Kα radiation. The structures were solved by direct method and refined on F^2 by full-matrix least-squares method using the SHELXTL-PC program package.[16] All non-hydrogen atoms were refined anisotropically. Hydrogen atoms were placed in their calculated positions and refined following the riding model. Crystal data for 1: $C_{35}H_{19}N_8$, M= 551.58, monoclinic, space group $P2(1)/c$, a = 16.083(3)Å, b = 10.8627(17)Å, c = 17.099(3)Å, β= 114.327(3)°, V=2722.0(7)^3, Z = 4, Dcalc= 1.346 gcm^{-3}, μ= 0.084 mm^{-1}, final R, R_w= 0.0521, 0.1327. 3856 observed reflections [$I > 2\sigma(I)$] out of 4781 unique (R_{int}= 0.0534), GOF= 0.913. Crystal data for 2: $C_{31}H_{17}N_8$, M= 501.53, triclinic, space group $P-1$, a = 7.314(2), b = 7.659(3), c = 25.131(8), α= 89.900(5)°, β= 89.450(5)°, γ= 64.846(5)°, V = 1274.2(7)^3, Z = 2, Dcalc = 1.307 gcm^{-3}, μ= 0.082mm^{-1}, final R, R_w= 0.0734, 0.2064. 3556 observed reflections [$I > 2\sigma(I)$] out of 4393 unique (R_{int}= 0.0511), GOF= 1.089.

2.5 Details of DFT Calculation

The whole non-modelized molecular structure of the real compounds were taken directly from the X-ray crystallography, and the unrestricted density functional theory (DFT) calculations with UB3LYP functional and

the 3 - 21G * basis set are performed using the GAUSSIAN 98 program[17] on the SGI 3800 workstation.

3. Results and Discussion

3.1 Descriptions of Crystal Structures

$[CNQI]_2[TCNQ]_3$ (1). Compound 1 crystallizes in a monoclinic system with space group $P2(1)/c$, and an asymmetric unit contains one and half TCNQ entries together with one $[CNQI]^+$ cation (Fig. 1a). For the sake of simple description, two crystallographic independent TCNQ molecules are represented as TCNQ (A) and TCNQ (B). The TCNQ (B) unit containing N(5) atom possesses a inversion centre, while the TCNQ (A) unit containing N(1) atom does not possess any symmetry. The mean molecular planes defined by the corresponding quinodimethane groups between TCNQ (A) and TCNQ (B) make 0.9 dihedral angle, indicating they are almost parallel to each other. The averaged lengths of chemically similar bonds in TCNQ (A) and TCNQ (B) units, summarized in Table 1, are somewhat different from each other, which are approximately close to $TCNQ^{-1}$ and $TCNQ^0$ entries, respectively.[18] Two TCNQ (A) and one TCNQ (B) molecules stack into a triad, and the triads further develop into a column in a pattern ···ABA···ABA···along b - axis (Fig. 1b). In a TCNQ column, the mean inter—planar separations within three different overlap pairs are 3.207Åfor AA, 3.311 Å for AB and 3.184 Å for BA pairs, respectively.

For the cation, the bond lengths and molecular conformation are in fare agreement with those in $[NO_2QI][Ni(mnt)_2]$,[19] and the dihedral angles between aromatic rings and the reference plane, C(28)/C(29)/N(7), are 10.6° for benzene, 73.8° for quinoline, respectively. There exist only van de Waals interactions between the neighboring anions and cations. $[CNPy]_2[TCNQ]_3$.. Compound 2 crystallizes in a triclinic system with space group $P-1$, and the asymmetric unit contains one and half TCNQ

moieties together with one $CNPy^+$ moiety (cf. Fig. 2a). Similar to 1, one of two crystallographic inequivalence TCNQ molecules possesses an inversion centre (which contains N(5)

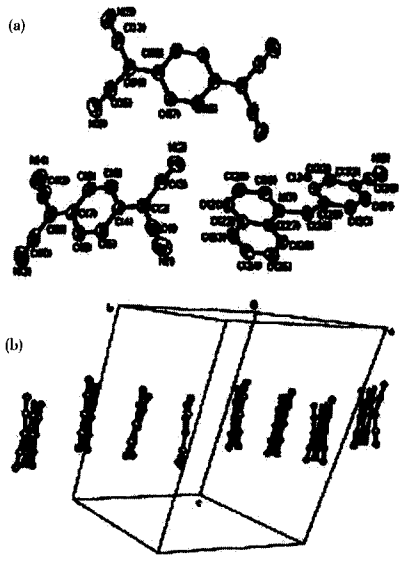
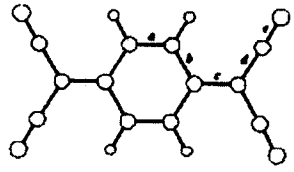


Fig. 1 (a)ORTEP view of 1 at 50% possibility ellipsoids (b) packing structure of amions showing atriad column in 1

Table 1 Averaged bond lengths (Å) of the TCNQ molecules in 1 and 2

The labeling systern is illustrated below



	a	*b*	*c*	*d*	*e*
TCNQ in 1(part A)	1.353	1.412	1.404	1.414	1.140
TCNQ in 1(part B)	1.344	1.425	1.383	1.421	1.140
TCNQ in 2(part A)	1.355	1.421	1.405	1.418	1.141
TCNQ in 2(part B)	1.347	1.418	1.398	1.412	1.142
[13c]$TCNQ^0$	1.346	1.448	1.374	1.440	1.138
[1]$TCNQ^{-1/3}$	1.350	1.435	1.393	1.430	1.140
[12b]$TCNQ^{-1/2}$	1.355	1.433	1.396	1.424	1.145
[13a]$TCNQQ^{-1}$	1.362	1.424	1.413	1.417	1.149

atom and is labeled as TCNQ (B)), and another does not possess any symmetry (which contains N(1) atom and is labeled as TCNQ (A)). The averaged lengths of chemically similar bonds in TCNQ (A) and TCNQ (B) units are listed in Table 1. It is worthy noting that it is difficult to assign the valence for two crystallographic independent TCNQ species from the metric bond parameters (the averaged bond lengths such as a, b, c, d and e; cf. Table 1), which is obviously different from that in 1. Another difference in the aspect of structural feature is the relative arrangement between TCNQ (A) and TCNQ (B) molecules. As shown in Fig. 2b, the mean molecular planes through the corresponding quinodimethane groups in A and B units make a dihedral angle of 68.2°, and TCNQ (A) and TCNQ (B) species form two types of TCNQ columns, respectively. Two different distances between mean - molecular planes are 3.121 and 3.338 Åin TCNQ (A)- type versus 3.771 and 3.771Åin TCNQ (B)- type columns. Separated by the cations, no short atomic contact is observed between the neighboring TCNQ columns. In $CNPy^+$ moiety, the dihedral angles between aromatic rings and the reference plane, C(24)/C(25)/N(7), are 77.9°for benzene, 129.3°for pyridine, respectively. And there are only weak van de Waals forces between neighboring $CNPy^+$ and TCNQ species.

3.2 Magnetic Susceptibilities and EPR Spectra

The temperature dependences of magnetic susceptibility are shown as the plots of $1/\chi m - T$ and $\chi mT - T$ for 1 and 2 in Fig. 3. To some extent, the magnetic behaviors of both 1 and 2 are similar to each other, and exhibit below features: 1) the χmT values at room temperature are much smaller than expected spin - only values, and upon cooling the χmT values decrease slowly in high temperature range while drop quickly in lower temperature, 2) there is no linear relationship between $1/\chi m$ and T. These characteristics indicate that there exist strong antiferromagnetic (AFM) coupling interactions within a magnetic TCNQ column and a temperature dependent magnetic coupling behavior. Obviously, the magnetic coupling interaction is stronger in the low temperature range than that in the high temperature

range. It is understandable that the temperature dependent magnetic coupling behavior in 1 and 2. For the planar molecule with extended electric structure, such as TCNQ and M(dithiolene)$_2$ species, spin polarization plays an important role in the intermolecular magnetic coupling interactions, and relatively small adjustments of the intermolecular arrangement

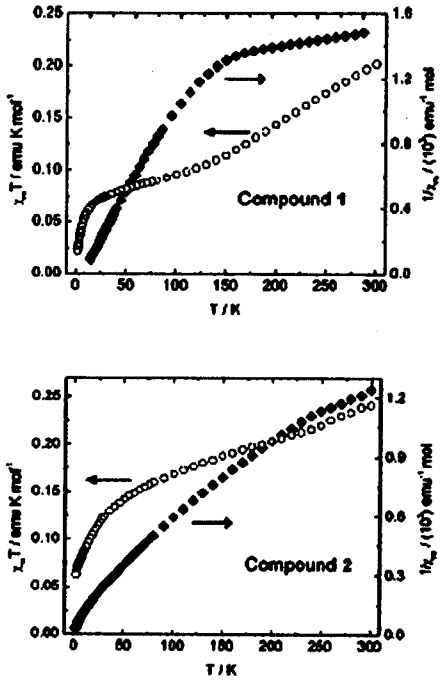


Fig. 3 Temperature dependences of magnetic susceptibility in the forms of $1/\chi_m - T$ and $\chi_m T - T$ for 1 and 2

(for example, a switch to an eclipsed rather than staggered arrangement) can easily change the magnetic coupling feature. Moreover, a variety of molecular arrangement can be easily reached with temperature change in such molecular crystals, since there are only weak intermolecular interactions. Therefore, the magnetic coupling nature is sensitive to the external perturbations (for example, temperature variation or pressure change).[20, 21]

Fig. 4 depicts EPR spectra of 1 and 2 with polycrystalline samples at room temperature. Compound 1 exhibits only one resonance signal even

though there exist two types of TCNQ species in solids. The typical radical EPR signal exhibits an isotropic feature without any sizable hyperfine structure observed. The resonance magnetic field, H_r, centered at 3481 G_s with a typical half-width at half-height of ~ 2 G_s, so the $g-$factors of 2.0066 was obtained. In spectra of 2, two sets of radical signals are observed. For one set, the resonance field centered at $H_r = 3480$ G_s with a half-width at half-height of ~ 3 G_s and the corresponding $g = 2.0062$, showing an isotropic characteristic. The other signal exhibits clearly five-folds hyperfine structure that might arise from the interactions between spins of electron and four equivalent hydrogen atomic nuclear ($IH=\frac{1}{2}$) in a quinodimethane group, and the corresponding g and A values are estimated as 2.0067 and 0.25 G_s, respectively.

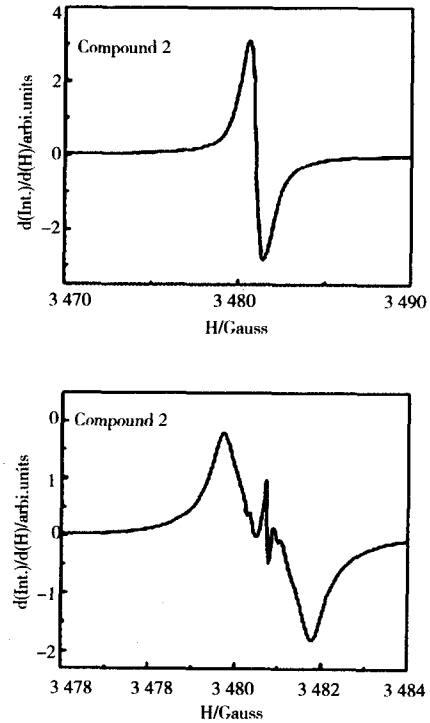


Fig 4 EPR spectra of 1 and 2 at room temperature

3.3 IR spectra and DFT calculations for spin and charge density distribution

For TCNQ species, the geometry varies with the electron population of the MO's, as expected. Thus it is possible to obtain an estimate of the molecular charge from the experimental geometry and IR spectra data. Actually, the relationship between geometric parameters in TCNQ species, IR spectra (especially the intense vibration band ν(CN) which displays in general no overlap with other vibration models)[22] and the degree of charge transfer has been investigated so far. However, in most cases the different analysis approaches do not consist with each other.[18a-d, 22, 23] Fig. 5 shows IR spectra of 1 and 2 which indicate the presence of two types of TCNQ species (ν(CN) for the neutral TCNQ molecule is usually higher than 2200 cm^{-1}), and one of them seems corresponding to $TCNQ^0$ species. This observation is approximately in agreement with the bonding length analyses for 1, but not for 2 (ref. Table 1). The reason to cause such a puzzle may arise from that each method is approximate and ignores some other effects, such as the influence of molecular packing on intermolecular geometry,[22, 23b]

In order to understand the charge distribution of TCNQ species in both 1 and 2, the DFT calculation for the valence assignment in a $[(TCNQ)_3]^{2-}$ unit was performed at UB3LYP/3-21G * level (one $[(TCNQ)_3]^{2-}$ unit includes two TCNQ (A) moieties and one TCNQ (B) moiety). The calculation results disclosed that two crystallographic independent TCNQ molecules have significantly different charges in 1. The total charge is −0.8264 for TCNQ (A), −0.8257 for symmetry generated TCNQ (A), and −0.3479 for TCNQ (B) units, that is, the negative charge is mainly localized on TCNQ (A) molecule. For 2, the total charge is −0.6565 for TCNQ (A), −0.6228 for the symmetry generated TCNQ (A), and −0.7208 for TCNQ (B) units, meaning the negative charges are almost distributed averagely on TCNQ (A) and TCNQ (B) molecules. The above results

consist approximately with EPR results of 1 and 2.

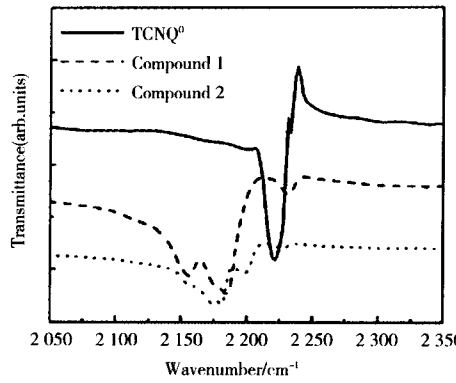


Fig 5 IR spectra for 1,2 and neutral TCNQ in the range of 2050—2350 cm^{-1} at room temperature, and spectra 1 and neutral TCNQ were shifted arbitrarily to transmittance values in order to clarify the figure

4. Conclusion and Remarks

In summary, we have investigated the crystal structural, magnetic property characterizations and theoretic analyses for two radical compounds based on the $[(TCNQ)_3]^{2-}$ unit. In crystals of both 1 and 2, an asymmetric unit in a cell includes two crystallographic independent TCNQ species (labeled as unit A and B). The unit A and B form a stack in the pattern…ABA…ABA…in 1, while two types of homogeneous columns (…AA…and …BB…) in 2, respectively. Temperature dependences of magnetic susceptibility revealed the magnetic features of strong AFM coupling interaction within a TCNQ stack and temperature dependent magnetic coupling behavior. The IR spectra clearly show the existence of a mixed-valence state in both 1 and 2, namely, the crystallographic inequivalent TCNQ (A) and TCNQ (B) units possess different negative charge and the values based on the analyses of IR spectra and bond lengths are approximately in agreement with each other for 1 but not for 2. EPR spectra exhibit two different reso-

nance signals in 2, however, only one resonance signal in 1 even though 1 and 2 have the same stoichiometry $[cation]_2[TCNQ]_3$. Further, DFT calculation for charge distribution performed in each crystallographic independent TCNQ species disclosed the TCNQ (A) and TCNQ (B) units may be assigned to $TCNQ^{-1}$ and $TCNQ^{0}$ in 1, and $TCNQ^{-\delta}$ (where partial charge $\delta = 0.62 - 0.72$) in 2.

5. Supplemental Materials

Crystallographic data (excluding structure factors) for the structures reported in this paper have been deposited with the Cambridge Crystallographic Data Center as supplementary publications, and the CCDC number is CCDC - 616746 and CCDC—607355 for 1 and 2, respectively. Copies of the data can be obtained free of charge on application to CCDC, 12 Union Road, Cambridge CB21EZ, UK (Fax: (+44) 1223—336—033; Email: deposit@ccdc. cam. ac. uk).

Acknowledgments

This project was financially supported by the National Natural Science Foundation of China (Grant Nos. 20171001 and 20371002), and the Natural Science Foundation of Education Commission of Anhui Province, China (Grant Nos. 044 - J - 04011, 2005hbz20 and 2006kj042a).

References

[1] T. Mochida, S. Yamazaki, S. Suzuki, S. Shimizu, H. Mori, Bull.

Chem. Soc. Jpn. 2003, 76, 2321 and therein references.

[2] H. Seo, J. Phys. Soc. Jpn. 2000, 69, 805.

[3] H. Seo, H. Fukuyama, Synth. Met. 2003, 135—136, 673.

[4] K. Hiraki, K. Kanoda, Phys. Rev. Lett. 1998, 80, 4737.

[5] M. Mitsumi, K. Kitamura, A. Morinaga, Y. Ozawa, M. Kobayashi, K. Toriumi, Y. Iso, H. Kitagawa, and T. Mitani/ Angew. Chem. Int. Ed. 2002, 41, 2767.

[6] (a) H. Seo, H. Fukuyama, J. Phys. Soc. Jpn. 1997, 66, 1249;
(b) F. Nad, P. Monceau, J. M. Fabre, Phys. Rev. B, 2000, 62, 1753;
(c) D. S. Chow, F. Zamborsky, B. Alavl, D. J. Tantillo, A. Baur, C. A. Merlic and S. E. Brown, Phys. Rev. Lett. 2000, 85, 1698.

[7] M. Sakata, M. Maesato, A. Ota, H. Yamochi, G. Saito. Synth. Met. 2005, 153, 393.

[8] T. Yamamoto, M. Uruichi, and K. Yakushi Phys. Rev. B, 2006, 73, 125,116.

[9] K. Miyagawa, A. Kawamoto, K. Kanoda, Phys. Rev. B, 2000, 62, 7679.

[10] H. Tajima, S. Kyoden, H. Mori, S. Tanaka, Phys. Rev. B, 2000, 62, 9378.

[11] K. Yamamoto, K. Yakushi, K. Miyagawa, K. Kanoda, A. Kawamoto, Phys. Rev. B, 2002, 65, 85,110.

[12] S. B. Bulgarevich, D. V. Bren, D. Y. Movshovic, P. Finocchiaro, S. Failla, J. Mol. Struct. 1994, 317, 147.

[13] R. L. Carlin, Magnetochemistry, Spring, Berlin, 1986. p. 3.

[14] P. F. Wang, G. X. Liu, and Y. C. Chen. Acta Crystallogr. Sect. E 2006, 62, O3256.

[15] L. R. Melby, R. J. Harder, W. R. Hertler, W. Mahler, R. E. Benson, W. E. Mochel, J. Am. Chem. Soc. 1962, 84, 3374.

[16] G. M. Sheldrick, SHELXTL, Structure Determination Software

Programs, Version 5. 10. Bruker Analytical X - ray Systems Inc., Madison, Wisconsin, USA, 1997.

[17] M. J. Frisch, et al. Gaussian 98, revision A. 11. 2; Gausian, Inc.: Pittsburgh, PA, 2001.

[18] (a) G. J. Ashwell, D. D. Eley, A. Harpper, A. C. Torrance, S. C. Wallwork, M. R. Willis, Acta Cryst. B 1977, 33 2258;
(b) G. J. Ashwell, S. C. Wallwork, S. R. Barker, P. I. C. Bertheir, Acta Cryst. B 1975, 31, 1175;
(c) R. E. Long, R. A. Sparks, K. N. Trueblood, Acta Cryst. 1965, 18 932;
(d) P. S. Flandrois and D. Chasseau Acta Crystallogr., Sect. B 1977, 33, 2744;
(e) G. X. Liu, X. M. Ren, R. K. Kremer, and Q. J. Meng J. Mol. Struct. 2005, 743, 125.

[19] X. M. Ren, C. S. Lu, Y. J. Liu, H. Z. Zhu, H. F. Li, C. J. Hu, Q. J. Meng Trans. Met. Chem. 2001, 26, 136.

[20] A. T. Coomber, D. Beljonne, R. H. Friend, J. L. Br das, A. Charlton, N. Robertson, Underhill, A. E. M. Kurmoo, P. Day, Nature 1996, 380, 144.

[21] Z. P. Ni, X. M. Ren, J. Ma, Z. D. Chen, J. L. Xie, C. L. Ni, Q. J. Meng, J. Am. Chem. Soc. 2005, 127, 14330.

[22] J. S. Chappell, A. N. Bloch, W. A. Bryden, M. Maxfield, T. O. Poehler, and D. O. Cowan J. Am. Chem. Soc. 1981, 103, 2442.

[23] (a) S. Flandrois, D. Chasseau, Acta Crystallogr., Sect. B, 1977, 833, 2744; (b) T. C. Urnland, S. Allie, T. Kuhlmann and P. Coppens J. Phys. Chem. 1988, 92, 6456.

本文已被 *Polyhedron*《多面体》杂志接收

第三专题

分子自旋梯磁体

具有平面型分子结构的金属二硫烯配合物阴离子$[M(dmit)_2]^{n-}$中，电子高度离域。比邻的阴离子间通过面对面的π…π堆积、肩并肩的S…S和错位的M…S相互作用，可形成具有梯状结构的分子基磁体。在这类离子对化合物中，平衡阳离子的拓扑几何强烈影响着化合物的堆积结构。因而，选择合适的平衡阳离子对构筑$[M(dmit)_2]^{n-}$基的分子自旋梯磁体就显得尤为重要。具有π－型分子构象的苄基吡啶衍生物，其分子构象与其芳环上取代基的电子性质及其在环上的位置密切相关，因此，可以通过系统地变化芳环上的取代基，达到调节苄基吡啶衍生物阳离子分子构象，进而实现系统地调控苄基吡啶衍生物阳离子分子的拓扑几何，最终实现构筑$[M(dmit)_2]^{n-}$基分子自旋梯磁体的目标。应用X－ray单晶结构测定等实验技术，分子力学计算等理论手段研究此类化合物中的各种弱相互作用，以及它们对分子堆积结构的影响。积累实验数据，为研究苄基吡啶衍生物阳离子和$[M(dmit)_2]^{n-}$阴离子形成的分子自旋梯磁体奠定基础。

磁电功能性基于具有开壳层电子结构的多硫烯配阴离子，此类配阴离子，易形成面对面二聚体，比邻的二聚体通过多硫烯配体侧位或端基上的硫原子之间的堆积作用，进一步形成梯状堆积结构。抗磁性的苄基吡啶衍生物阳离子，一方面，可防止多硫烯配阴离子形成二维或三维结构，另一方面，其分子构象的可调性有利于研究分子间的协同作用对堆积结构和材料的功能性的影响，实现功能材料的定向合成。空穴注入实际上是移去Femi面附近的部分电子，这要求电子载体分子应具有连续可变的价态，多硫烯配阴离子可满足这一要求。空穴注入不能改变自旋梯分子的晶体结构，二苯甲烷衍生物分子与苄基吡啶衍生物分子具有相似的分子结构，是此类分子自旋材料理想的空穴注入剂。通过分子设计、合成一系列分子自旋梯化合物、研究它们的性质，以及结构－性质－功能性之间的关系。

上述工作在本部分中收录了发表的学术论文6篇，其中被SCI收录4篇。

八面体配合物取代反应的反应动力学

摘 要:通过八面体配合物取代反应的可能机理及配合物的化学键理论对八面体配合物取代反应的活泼性进行具体分析,其实际值与理论值基本相符。

关键词:取代反应;反应机理

在配位反应中,通常发生旧的化学键的断裂和新的化学键的形成,因此从反应物到生成物的过程中,通常要发生反应物分子的靠近,分子间碰撞,原子改变位置直到生成新的化合物。配合物分子、原子、离子或基团在配合物反应的全部过程中分步反应的详尽历程叫做反应机理,取代反应是配合物中金属——配体键的断裂并代之以新的金属——配体键生成的一种反应,这种反应有两种类型,分别称为:亲核取代反应,简称 S_N 反应,亲电取代反应,简称 S_E 反应。在配位反应中亲电反应较少见,而亲核取代反应极为普遍,其反应机理主要有:离解机理、缔合机理及交换机理。

离解机理第一步是 M—X 键的断裂,原来的配合物[ML_nX]离解而失去一个配体 X,形成配位数比原配合物少一的中间配合物[ML_n],这一步是吸热过程,活化能大,反应慢。第二步是在中间配合物[ML_n]所空出的位置上,很快地与新的配体 Y 结合,形成新的 M—Y 键,这一步放热,反应快,总反应速率决定于第一步,速率方程可表示为:$\frac{d[ML_nY]}{dt}=k[ML_nX]$。反应速率与[$ML_nX$]的浓度成正比,而与 Y 的浓度无关,是对 ML_nX 的一级反应,这种反应是单分子亲核取代的反应,简称 S_{N1} 反应,其速率常数 k 的大小与 M—X 键的断裂难易有关,即与离去的配体 X 的性质有关,但与亲核试剂 Y 的种类和浓度无关。

缔合机理也包括两步：第一步是配合物[ML_nX]与亲核配体 Y 结合，形成比原配合物[ML_nX]的配位数多一的中间配合物[ML_nXY]，这一步慢，是决定速率的步骤。第二步是中间配合物[ML_nXY]不稳定，很快地离解生成[ML_nY]及 X。总反应速率方程可表示为$\frac{d[ML_nY]}{dt}=k[ML_nX][Y]$，反应速率决定于[$ML_nX$]与[Y]的浓度，在动力学属于二级反应。这种双分子亲核取代反应简称为 S_{N2} 反应。其速率常数 k 主要反映 M—Y 键形成的难易程度，与亲核配体 Y 的性质有很大的关系。

事实上配合物的取代反应的过程是复杂的，但共同点是发生了一个旧键的断裂和一个新键的形成，不同的机理只是这两类过程发生的时间上的差异，实际上很难设想 Y 取代 X 的反应中先彻底断裂 X 键，再配位 Y 键（或相反），反应过程中最可能的是 Y 接近的同时 X 逐渐离去，所以大部分的取代反应归之于交换机理。即配合物发生取代反应时新键的生成和老键的断裂同时进行，彼此相互影响，I 机理又可进一步分成 Id 机理和 Ia 机理。Id 机理的极限状态是 S_{N1} 机理即离解机理，Ia 机理的极限状态是 S_{N2} 机理即缔合机理。

配合物的取代反应速率差别很大，快的反应瞬间完成，慢的反应要几天，甚至几个月。所以把配合物分成活性配合物和惰性配合物。动力学上的活性配合物与惰性配合物与热力学上的稳定性不能混为一谈，这是两个不同的概念。虽然常常发现热力学上稳定的配合物在动力学上可能是惰性的，而热力学上不稳定的配合物往往是动力学上活性的，但实际上两者之间也没有必然的规律。例如 CN^- 离子与 Ni^{2+} 离子能形成稳定的配合物：$[Ni(H_2O)_6]^{2+}+4CN \rightleftharpoons [Ni(CN)_4]^{2-}+6H_2O$，其生成常数 β 约为 10^{22}，平衡大大偏向右方，说明 $[Ni(CN)_4]^{2-}$ 在热力学上是稳定的配合物，但是如果在此溶液中，加入 $^*CN^-$（用 ^{14}C 作标记原子），$^*CN^-$ 离子差不多立即就结合于配合物中。由此说明 $[Ni(CN)_4]^{2-}$ 是一个稳定的配合物，但从动力学角度考虑它是一个活性配合物。配合物的稳定性依赖于反应物与产物之间的能量差（反应能），而配合物的活性则依赖于反应物与过渡态之间的能量差（即活化能）。活化能大，则反应慢。

配合物的反应速率（即反应的活泼性）和反应机理的研究：一是为了把具有实用意义的配位反应最大效率投入生产；必须研究这一反应所遵循的

动力学方程和反应机理，从而获得必要的知识，设计工艺设备和流程。二是通过化学反应动力学的研究，寻找化学变化时从作用物到产物过程中所发生的各步反应模式，在广泛实验基础上概括反应微观变化时所服从的客观规律性。知道了一种反应机理能使我们了解反应的速率表现，而从反应的活泼性则可以给我们提供许多有关反应机理的信息，帮助我们对反应机理进行的判断。决定配合物动力学稳定性的主要因素是中心离子的电子层结构，大小和电荷。配位体的性质，键型。下面用几种化学键理论对其可能反应机理的反应活泼性作具体分析：

1. 简单静电理论

对于电价配键形成的配合物来说，其亲核取代反应机理和速率的主要因素是中心离子以及进入和离去配体的电荷和半径的大小。对于 S_{N1} 反应，如果中心离子 M 或离去配体 L 的半径越小，电荷越大，则 M—L 之间的键越牢固，M—L 键不易断开，不利于进行 S_{N1} 反应，S_{N1} 反应的速率就小。如果中心离子或离去配体的半径越大，电荷越小则 M—L 键越不牢固，M—L 键易断开，若按 S_{N1} 反应进行，则反应速率就大。例如：对下列两个 S_{N1} 反应来说，由于 Fe^{2+} 离子的半径为 0.76Å 比 Fe^{3+} 离子的半径 0.64Å 大，且 Fe^{2+} 电荷比 Fe^{3+} 的小，因此 $[Fe(H_2O)_6]^{2+}$ 进行水交换反应就比 $[Fe(H_2O)_6]^{3+}$ 来得快，同样 $[Co(NH_3)_5Br]^{2+}$ 的水合反应要比 $[Co(NH_{36}Cl]^{2+}$ 的快，因为 Br^3 离子半径(1.95Å)比 Cl^- 离子半径(1.85Å)大，因此 Co—Br 键比 Co—Cl 键更易断开。对于 SN_2 反应，设 Y 为进入配体，若 M—Y 键很牢固，则有利于 S_{N2} 反应的进行。进入配体的半径越小，负电荷越大，越有利于 S_{N2} 反应的进行，反应速率就大。在 S_{N2} 反应里，中心离子电荷数的增加有两方面的影响，一方面使 M—L 键不易断开，另一方面使 M—Y 键更易形成。究竟电荷数增加对反应速率有何影响要看两个因素相对大小而定。往往中心离子半径和电荷的增加使得进行 S_{N2} 反应的可能性增加。如果进入配体的半径很大，由于空间阻碍，进行 S_{N2} 反应的可能性减小，甚至不能进行。其他不参与取代反应的配体也会影响反应的速率，如果这些不参与取代反应的配体的负电荷很大，那么进入配体就会受到排斥而不容易进入，这样将有利于 S_{N1} 反

应而不利于 S_{N2} 反应的进行。

2. 内轨与外轨的配合物理论

对于内轨配合物来说，其取代反应速率决定于未成键的中心离子 $(n-1)d$ 轨道的电子分布情况，如果未成键的 $(n-1)d$ 轨道中至少有一个轨道是空的，这类型的配合物是活性配合物，如果未成键 $(n-1)d$ 轨道中，没有空的轨道(即每个轨道都已有至少一个电子)，则这类型的配合物是惰性配合物。

表 1 d^2sp^3 内轨型配合物

电子组态	分类	实例
$d^0d^0d^0(d^2sp^3)$	活性	Sc(Ⅲ) T(Ⅳ) V($\overline{\text{V}}$) Y(Ⅲ)
$d^1d^0d^0(d^2sp^3)$	活性	Ti(Ⅲ) V(Ⅳ) M_o($\overline{\text{V}}$)
$d^1d^1d^0(d^2sp^3)$	活性	Ti(Ⅲ) V(Ⅲ) M_o(Ⅳ)
$d^1d^1d^1(d^2sp^3)$	惰性	Cr(Ⅲ) V(Ⅱ) M_o(Ⅲ) M_n(Ⅳ)
$d^2d^1d^1(d^2sp^3)$	惰性	Cr(Ⅱ)(在 $Cr(CN)_6^{4-}$ 中)
$d^2d^2d^1(d^2sp^3)$	惰性	Fe(Ⅲ) Ru(Ⅲ) Ir(Ⅳ)
$d^2d^2d^2(d^2sp^3)$	惰性	Fe(Ⅱ)(在 $Fe(CN)_6^{4-}$ 中) Co(Ⅲ)

根据上述结论，八面体配合物取代反应按 S_{N2} 机理进行，是容易理解的。因为 d^0、d^1、d^2 型离子形成的八面体配合物中中心离子有空的 $(n-1)d$ 轨道，有利于接受第七个配体的电子对，形成配位数为七的中间配合物、有利于 S_{N2} 反应的发生，因此它们是活性的。d^3、d^4、d^5、d^6 型离子形成的内轨形八面体配合物中中心离子没有空的 $(n-1)d$ 轨道，第七个配体的加合有下列三种可能：

(1) 第七个配体的电子对加合到外 d 轨道(nd)上去。

(2) $(n-1)d$ 轨道中如有成单电子必须成对(只有 d^3、d^4 型有此可能)。

(3) $(n-1)d$ 轨道中的电子激发到较高的能级上去，以便空出 $(n-1)d$ 轨道来接受第七个配体的电子对。而这些过程都需要较高的活化能，因而

相应的反应慢，即相应的配合是惰性的。

对于 sp^3d^2 外轨型配合物，由于已经使用了外层 d 轨道，故一定有空的 d 轨道，可以推测这些配合物有一定活性。或用外轨配合物中的配位键较不稳定解释，它们一般比较容易失去一个配体而形成配位数为 5 的配合物作为 S_{N1} 反应的中间物，所以一般表现为活性配合物。

3. 配体场理论

八面体取代反应有两个机理 S_{N1} 及 S_{N2}，相应的八面体取配合物的过渡配合物分别是五配位和七配位的，随着空间构型的变化，配合物的稳定化能(CFSE)也发生了变化，这种变化直接影响了配合物的活化能。如果八面体配合物过渡到四角锥或五角双锥时，配合物的配位场稳定化能发生改变，这变化的部分是配位场效应对反应活化的贡献，叫做配位场活化能。所以可以据此粗略地判断配合物的动力学稳定性，因为配位场稳定化能的大小与过渡配合物的空间构型有关，故也可以由此确定反应机理究竟是 S_{N1} 机理还是 S_{N2} 机理。

在表 2 中，我们把初始配合物的 CFSE 减去过渡配合物的 CFSE 所得的配位场活化能用 $\triangle E$ 表示，$\triangle E_a$ 表示 S_{N1} 机理的配位场活化能，$\triangle E_a'$ 表示 S_{N2} 机理的配位场活化能。当 $\triangle E$ 为正值时，由于空间构型变化损失了配位场能量，反应需要额外增加能量，相应的活化能大，表现为惰性配合物。如 $\triangle E=0$ 或为负值则表现为活性配合物。从表 2 中还可以得出如下讨论：

表 2　S_{N1} 和 S_{N2} 机理的配位场活化能

	强　场					弱　场				
	八面体	四角锥	五角双锥	$\triangle E_a$	$\triangle E_a'$	八面体	四角锥	五角双锥	$\triangle E_a$	$\triangle E_a'$
d^0	OD_q	OD_q	OD_q	OD_q	OD_q	OD_q	OD_q	OD_q	OD_q	OD_q
d^1	4	4.57	5.28	−0.57	−1.28	4	4.57	5.28	−0.57	−1.28
d^2	8	9.14	10.56	−1.14	−2.56	8	9.14	10.56	−1.14	−2.56
d^3	12	10.00	7.74	2.00	4.26	12	10.00	7.74	2.00	4.26

（续表）

	强　场					弱　场				
	八面体	四角锥	五角双锥	$\triangle E_a$	$\triangle E'_a$	八面体	四角锥	五角双锥	$\triangle E_a$	$\triangle E'_a$
d^4	16	14.57	13.02	1.43	2.98	6	9.14	4.93	−3.14	1.07
d^5	20	19.14	18.30	0.86	1.70	0	0	0	0	0
d^6	24	20.00	15.48	4.00	8.52	4	4.57	5.28	−0.57	−1.28
d^7	18	19.14	12.66	−1.14	5.34	8	9.14	10.56	−1.14	−2.56
d^8	12	10.00	7.74	2.00	4.20	12	10.00	7.74	2.00	4.26
d^9	6	9.14	4.93	−3.14	1.07	6	9.14	4.93	−3.14	1.07
d^{10}	0	0	0	0	0	0	0	0	0	0

（1）d^0、d^5（弱场）、d^{10}，$\triangle E_a=0$，d^1 d^2 $\triangle E_a<0$ 强场，d^7、d^9 $\triangle E_a<0$，弱场 d^4、d^9 $\triangle E_a<0$，弱场 d^6、d^7 $\triangle E_a<0$，属于以上类型均应为活性配合物，其余则为惰性配合物。

（2）在强场情况 d^5、d^4、d^8、d^3、d^6 的 $\triangle E_a>0$ 且逐渐增大。（d^3 与 d^8 $\triangle Ea$ 相等），因而这些配合物均为惰性，且惰性的程度亦依上述次序递增，故 d^3 及弱场 d^6 结构的配合物 $[Cr(NH_3)_6]^{3+}$ 和 $[Co(NH_3)_6]^{3+}$ 的取代反应均很慢。

（3）在 d 电子数≥3 的情况下，几乎都是 $\triangle Ea<\triangle Ea'$，故 d 电子数≥3 的八面体配合物按 S_{N1} 机理取代的活化能比按 S_{N2} 的相对为小，故这些配合物按 S_{N1} 机理进行取代的可能性大．实验证明 d^7 构型配合物是活性的，其取代反应机理也是 S_{N1}。

把表 1、表 2 仔细加以比较，可以看出，强场中的 d^0d^6 或弱场中的 d^1d^3 构型，均相当于内轨配合物，其中只有 d^0d^2 构型为活性配合物，强场的 d^7d^{10} 和弱场的 d^4d^{10}（d^8 除外）构型，相当于外轨配合物，它们都有一定的活性，由此可见两轨理论和配位场理论基本上是一致的，但是对于 d^8 构型，两轨理论认为是活性的，而配位场理论认为是较惰性的。两者有分歧，实验事实说明 Ni^{2+}（d^8）八面体配合物比相同空间构型的 Mn^{2+}（d^5）、Co^{2+}（d^7）、Cu^{2+}（d^9）等配合物取代反应要慢。说明配体场理论有所进步。

4. 角重迭模型

根据巴索洛和皮尔逊提出的过渡金属配合物的相对动力学惰性或活性与中心金属 d 轨道的能量有关。具体地说，就是配离子由基态变为过渡态时，d 轨道能量的变化对取代反应的活化能有相当大的贡献，并且认为这种能量的损失与活化能成正比。应用这一方法原则上可以回答以下两个问题：(1)该配合物是动力学活性的还是惰性的？如果八面体的结构优先能(SPE)小于某个任选值，就可预测该配合物为活性的；而若 SPE 大于该任选值，则认为该配合物是惰性的。(2)可能的过渡态结构是什么？对于某一给定的 d 轨道占据方式，八面体结构同某一过渡态结构的能量差值若比同其他过渡态结构能量的差值都小，则反应将通过该过渡态进行。由于第一过渡系二价金属离子的八面体配合物的取代反应是按离解机理进行的。因此可认为其过渡态为三角双锥或四方锥结构。首先计算出过渡态的各 d 轨道的能量，并画出这两种过渡态结构的 d 轨道能级图。根据能级图算出各 d^n 组态的配合物的总 σ 电子稳定化能，再与八面体配合物的稳定化能相减，得到各 d^n 组态下的 SPE。假定八面体与五配位过渡态之间的能量差为 $1e$，或更小时，表示活化能低，配合物是活性的，相反，能量差值大于 $2e$，则表示配合物是惰性的。计算结果总结于表 3。这些理论预测与实验结果相当符合。

表 3 八面体配合物的惰性和活性的预测

d 电子组态			d^0	d^1	d^2	d^3	d^4		d^5		d^6		d^7		d^8	d^9	d^{10}
							低	高	低	高	低	高	低	高			
通过离解的反应活化	SPY 中间态	C_{4v}	惰性	惰性	惰性	惰性	惰性	活性	惰性	活性	惰性	活性	活性	活性	活性	活性	活性
	tby 中间态	D_{3h}	惰性	惰性	惰性	惰性	惰性	活性	惰性	活性	惰性	活性	活惰	活性	活惰	活性	活性

5. 分子轨道理论

前线轨道理论和分子轨道对称性守恒原理对化学反应进行的难易程度及产物构型起决定作用，使人们对反应动力学和反应机理的认识深入到了理解物质微观结构的一个新层次。双分子反应的轨道对称性规则如下：

(1) 关键性的轨道是反应物的最高已占轨道(HOMO)和最低空轨道(LUMO)，当两个反应物互相接近时，电子从 HOMO 流向 LUMO。

(2) 当两个分子互相接近起反应时，可以把它们的整体看作为一个大的准分子，这个准分子应属于某一对称点群。此时，就必须要求 HOMO 和 LUMO 都属于该点群的同一对称种类，也就是说一种反应分子的 HOMO 同另一种反应分子的 LUMO 的对称性要匹配，要有净重迭。

(3) HOMO 和 LUMO 的能量要相近(约在 6ev 范围内)。

(4) 当两个前线轨道都是成键 MO 时，则在反应过程中 HOMO 必须对应于要破裂的键，而 LUMO 对应于要生成的键。

如果在一个设想的基元反应中找不到一对轨道满足上述第 2、3、4 条规则时，则该基元反应为对称性禁阻反应，反应就难进行，反之为对称性允许的反应，反应就易进行。每一个基元反应都必须通过轨道对称性的检验。一个复杂反应，只有它所包括的基元反应均为对称性允许的反应时，方为对称性允许的，否则便是对称性禁阻反应，很难进行，要提高活化能。对于配合物的 S_{N2} 取代反应，上述规则是适用的，对于 S_{N1} 取代反应则也应有相应的轨道对称性规则。

影响动力学稳定性的因素很多，在具体观察问题的时候，应当综合考虑溶剂、配位体和取代试剂的性质，以及中心离子的电荷和半径等因素，不能单纯从中心离子的电子排布和配体场的作用来考虑。

参考文献

[1] 徐志国编．现代配位化学．Tt 化学工业出版社(第 1 版)

[2] 秦子斌编．配位化合物化学．武汉大学讲义

[3] 武汉大学、吉林大学编．无机化学．高等教育出版社(第 3 版)

[4] 傅献彩编．物理化学．高等教育出版社(第 2 版)

[5] 张祥麟编．配位化学．中南工业大学出版社(第 1 版)

本文原载于《安庆师范学院学报》,1998 年第 2 期

双－(2,2′－联吡啶)和二硫烯钌(Ⅱ)混配配合物合成、光谱表征和电化学性质

近20年来，多吡啶钌(Ⅱ)的配合物引起了人们极大的兴趣。这类配合物的光物理、光化学和电化学性质适合作为研究电子转移和能量迁移的超分子体系的建筑块，而且在光化学分子器件(PMDs)方面具有应用前景[1-5]。三-(2,2′-联吡啶)钌(Ⅱ)配合物，在可见光区具有强的金属到配体电荷转移吸收带，这种电荷转移跃迁涉及分子内的快速氧化－还原过程。当三-(2,2′-联吡啶)钌(Ⅱ)配合物中的一个2,2′-联吡啶分子被其他配体取代后，电荷转移激发态的氧化-还原性质明显受到影响[6-7]。通过改变钌(Ⅱ)中心周围的配体，可微调钌(Ⅱ)中心的氧化还原电位，进一步改变多联吡啶钌配合物的基态和激发态的光物理性质[7]。二硫烯负离子是一类良好的电子给体(见图1)，而且，通过改变二硫烯分子的取代基 R_1 和 R_2 即可调节二硫烯分子的给电子能力。因此，通过变化二硫烯分子的取代基就能系统地研究此类混配配合物的氧化-还原性质以及光物理和光化学性质。我们报道两种这类混配配合物的合成、光谱表征和电化学性质。

1. 实验部分

1.1 仪器和试剂

元素分析使用 Perkin－Elmer240C 型元素分析仪；红外光谱使用 BrukerIFS66V FT－IR 光谱仪，KBr 压片；电子光谱使用日本 Hitachi UV－

3 100光谱仪；所用试剂均为分析纯，循环伏安使用 EG&G 273 电化学分析仪，铂圆盘工作电极，铂片对电极，Ag－AgCl 参比电极，二茂铁作内标，溶剂 DMF 经 4Å 分子筛浸泡后再蒸馏。其他试剂使用前未被进一步纯化。

1.2 原料制备

cis－[Ru(bpy)$_2$]Cl$_2$ · 2H$_2$O，Na$_2$mnt 和 dmit(COph)$_2$分别按文献合成[8－10]，其中 mnt^{2-}、dmit^{2-}、dmit(COph)$_2$分别代表二腈基二硫烯、1,3－二硫杂环戊烯－2－硫酮－4,5－二硫烯和 4,5－(双－苯甲酰硫酯基)－1,3－二硫杂环戊烯－2－硫酮。

1.3 配合物合成

1. cis－[Ru(mnt)(bpy)$_2$]的合成

262mg(0.5mmol cis－[Ru(bpy)$_2$]Cl$_2$ · 2H$_2$O 和 100mg(0.54mmol) Na$_2$mnt 加到 100mL 单颈圆底烧瓶中，向该烧瓶加入 30ml 甲醇，悬浊液避光回流 2 小时。生成的微晶被过滤，先用甲醇洗涤至洗涤液近无色，再用少量乙醚洗，真空干燥。得产物 228mg，产率 82%。元素分析：计算值($C_{24}H_{16}N_6RuS_2$)：C,51.99；H,2.91；N,15.17。实验值 C,51.65；H,3.12；N,14.98。红外光谱(KBr 压片，cm^{-1})：2 194s，1 600m，1 460sh，1 452s，1 418s。电子光谱(nm,lgε)：293(4.96)，383(4.22)，506(宽峰)。

2. cis－[Ru(dmit)(bpy)$_2$](2)的合成

N$_2$保护下，20mL 含 108mg(2mmol)甲醇钠的甲醇溶液加到 219mg (0.54mmol)dmit(COph)$_2$的烧瓶中，室温搅拌 30 分钟，然后向烧瓶中加入 270mg(0.52mmol)cis－[Ru(bpy)$_2$]Cl$_2$ · 2H$_2$O 固体。悬浊液避光回流2.5 小时，过滤，用甲醇、丙酮和乙醚依次洗涤沉淀，真空干燥，得产物 218mg，产率 71.5%。元素分析：计算值($C_{23}H_{16}N_4RuS_5$)：C,45.25；H,2.64；N,9.18。实验值：C,44.98；H,2.85；N,8.87。红外光谱(KBr 压片，cm^{-1})：1 595m，1 457m，1 418m，1 405s，1 280s，1 070s。电子光谱 294(5.02)，385(4.43)，548(宽峰)。

2. 结果与讨论

2.1 配合物的组成

配合物 1 和 2 的 C、H 和 N 的含量分别和由化学式 $C_{21}H_{16}N_6RuS_2$ 和 $C_{23}H_{16}N_1RuS_5$ 计算值相符。

2.2 红外光谱

红外光谱特别适合研究含 mnt^{2-} 配体的化合物，因为 mnt^{2-} 的 CN 基伸缩振动在 2 200cm^{-1} 附近有很强的特征吸收。在配合物 1 的红外光谱中，具有很强吸收的 $\upsilon_{(CN)}$ 特征谱带位于 2 194cm^{-1}，1 400～1 600cm^{-1} 范围的吸收带归属为联吡啶的 $\upsilon_{(C=N)}$、$\upsilon_{(C=C)}$ 以及 mnt^{2-} 的 $\upsilon_{(C=C)}$[7,11]。在配合物 2 的红外光谱中，1 400～1 600cm^{-1} 吸收带归属为联吡啶的 $\upsilon_{(C=N)}$、$\upsilon_{(C=C)}$ 和 dmit 的 $\upsilon_{(C=C)}$，1 280 和 1 070cm^{-1} 归属为 $\upsilon_{(C-S)}$。

2.3 电子光谱

在 DMF 溶液中，配合物 1 和 2 的电子光谱如图 1 所示。紫外区 294nm 附近的吸收带归属为联吡啶分子内的 $\pi\rightarrow\pi^*$ 跃迁，380～500nm 的吸收带是 Ru(Ⅱ)和联吡啶之间的 $d\rightarrow\pi^*$ 跃迁[7]。波长大于 500nm 的宽带可能是从二硫烯的 S 负离子到 Ru(Ⅱ)离子之间的 LMCT 跃迁，或者是从二硫烯的 S 负离子到 2－2′-联吡啶的 π^* 的 LL′CT 跃迁。比较两种配合物的这一宽带，配合物 2 比配合物 1 明显红移，这一结果与 dmit 配体比 mnt 配体具有更强的给电子能力的事实是一致的。无论是配体与金属离子间的 LMCT 跃迁，还是电子接受配体与电子给予配体间的 LL′CT 跃迁，其谱带的位置与溶剂的性质密切相关。但是，由于两种配合物在多种有机溶剂中的溶解性都很小，因此我们仅测定了它们的 DMF，MeCN 和 Py 溶液中的紫外-可见电子吸收光谱，相应光谱数据列于表 1。配合物 1 和 2 中的电荷迁移谱带相应的 $1/\lambda$ 与溶剂的极性大小没有一致性关系。

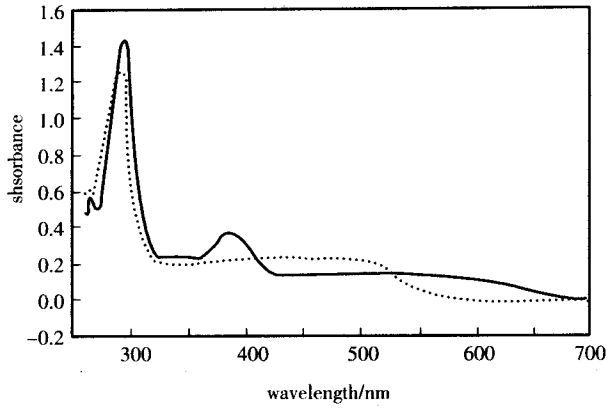


图 1　配合物 1 和 2 的紫外-可见光谱溶剂 DMF

Fig. 1　UV-visible spectra for 1 and 2(in DMF solution)

Dotted and solid lines srepresent 1 and 2, respectively

表 1　配合物 1 和 2 的电子吸收光谱数据

Table 1　Data of UV-visible Spectra for 1 and 2

	complex 1			complex 2		
	λ/nm(lgδ)			λ/nm(lgδ)		
	Ⅰ	Ⅱ	Ⅲ	Ⅰ	Ⅱ	Ⅲ
DMF	293(4.22)	385.5(.345)	505(3.54)	295(4.34)	384(3.75)	546(3.34)
MeCN	292(4.29)	380(3.51)	513.5(3.55)	295(4.35)	389(3.83)	551(3.36)
Py	293(3.89)	379.5(3.26)	503(3.24)	296.5(4.01)	341(3.66)	558(3.27)

2.4　氧化－还原性质

配合物 1 和 2 的 DMF 溶液的循环伏安曲线示于图 2，图 3a 和 3b 中最右端的一对可逆氧化还原波对应的是 Fe(Ⅲ)/Fe(Ⅱ)氧化-还原电对。扫描电势在－1500mV 到－1000mV 范围内，配合物 1 和 2 都有两个不可逆氧化波和两个不可逆还原波，它们相对于 Fe(Ⅲ)/Fe(Ⅱ)电对的电极电势列于表 2。E_1(Ox)归属为 Ru(Ⅲ)/Ru(Ⅱ)，E_2(Ox)以及 E_1(Red)、E_2(Red)可能是 Ru(Ⅱ)/Ru(Ⅰ)以及配体内的氧化－还原[7]。配合物 2 的 E_1(Ox)比配合物 1 相应的电极电势低，表明配合物 2 中的 Ru(Ⅱ)更容易被氧化成 Ru(Ⅲ)，

这可能是 dmit 比 mnt 更易将电子转移给 Ru(Ⅲ)以稳定三价钌所致，并与两种配合物电子光谱中的 LMCT 或 LL′CT 跃迁波长顺序一致。

表 2　配合物 1 和 2 的氧化-还原电极电势(相对于 Fe(Ⅲ)/Fe(Ⅱ)电对，单位：mV)

Table2　CV Data Versus Fe(Ⅲ)/Fe(Ⅱ)for 1 and 2(mV)

	E_1(Ox)	E_2(Ox)	E_1(Red)	E_2(Red)
complex 1	−450	−1188	−1574	−2034
complex 2	−483	−1073	−1595	−1933

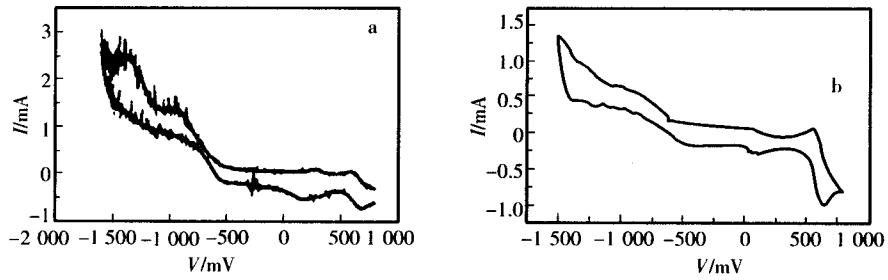


图 2　配合物 1 和 2 的循环伏安曲线(扫描速率：100mV·s^{-1})

Fig. 2　CV curves of 1 (a) and 2 (b) with scanning rates 100mV·s^{-1}

参 考 文 献

[1] Bruno G. ,Micol E. ,Schiavo S. L. ,Sinicropi M. S. Tresoidi G. J. Chem. Soc. Dolton Trans. ,1995,17

[2] Juris A. ,Balzani V. ,Barigelletti F. ,Campagna S. ,Belser P. ,Zelewsky A. B. Goord. Chem. Rev. ,1988,88,85

[3] Bolger J. ,Boder A. ,Gourdon G. ,Ishow E. ,Luuny J. P. J. Chem. Soc. Chem. Commun. ,1995,1799

[4] Belser P. ,Dux R. ,Baak M. ,Decoal L. L. ,Balzani B. Angew,Chem. , Int. Ed,Engl. ,1995,34,1100

[5] Harriman A. ,Odobel F. ,Sauvage J. P. J. Am. Chem. Soc. ,1995,117, 9461

[6] Kober E. M. , Caspar J. V. , Sullivan B. P. , Meyer T. J. Inorg. Chem. , 1985,24,3195
[7] Duan C. Y. , Lou Z. L. , You X. Z. , Thomas C. W. M. J. Coord. Chem. , 1999,46,301
[8] Sullivan B. P. , Salmon D. J. , Meyer T. J. Inorg. Chem. , 1978,17,3334
[9] Davusib A. , Holm H. R. Inorg. Synth. , 1967,10,8
[10] Steimecke G. , Sieler H. J. , Kirmse R. , Hoyer E. Phosphorus Sulfur 1979,7,49
[11] Nakamoto K. , Schlapfer C. W. Inorg. Chem. , 1975,14,1338

Synthesis, Spectra Characteriaztions and Electrochemistry Properties of the two Ru(Ⅱ) Complexes Consisting of Mixed Ligand Bpy and Dithiolene

Abstract : The two mixed ligand complexes, cis-[Ru(dmit)(bpy)$_2$](1) and cis-[Ru(mnt)(bpy)$_2$](2) (where mnt^{2-} is maleonitriledithiolate and $dmit^{2-}$ represents 4,5 - dimercapto - 1,3 - dithiole - 2 - thione), have been synthesized and characterized by element analysis and IR spectra. The electronie spectra of 1 and 2 in DMF solutions showed that the two complexes have broad absorption charge transfer bands [LMCT, i. e. charge transfer from dithiolate to Ru(Ⅱ)or LL′CT, that is, charge transfer from dithiolate to 2,2′-bipyridine] in the visibleregion. Compared with 1, the LMCT or LL′CT band for 2 shifts to low ferquency . The results of electrochemistry of the two complexes in DMF are consistent with that of the electronic spectra.

Key Words: Ruthenium(Ⅱ); mixed ligand complex synthesis synthesis characterization electrochemistry property

本文原载于《无机化学学报》2001 年第 17 卷第 4 期

分子基磁体[NCBzPy][Ni(dmit)$_2$]的合成、表征和磁学性质

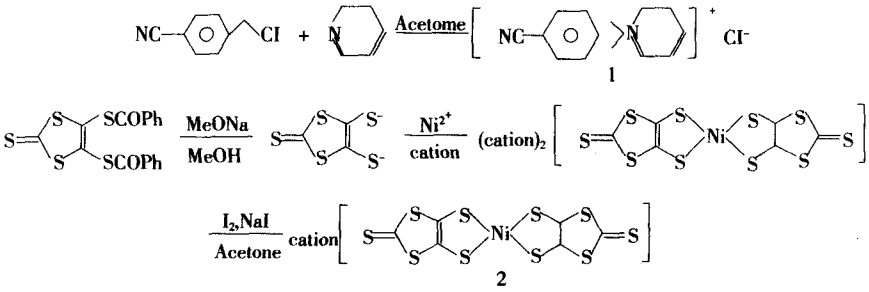
摘　要：合成了一种新的取代苄基吡啶盐[NCBzPy]Cl (1)，1 和 $NiCl_2$，$dmit^{2-}$ 反应生成分子基磁体[NCBzPy][Ni(dmit)$_2$](2)，其结构用元素分析、IR 和 UV 进行了表征。并测定了 2 在 2～300K 的变温磁化率，结果显示，相邻 Ni^{3+} 之间存在铁磁偶合作用。

关键词：分子基磁体；dmit；合成；磁性

Many new effects have been found for low dimensional spin systems in recent years[1~4]. Our interest is to construct quasi - one - dimensional molecule - based magnetic materials, formed by plate - like 1 ,3 - dithiole - 2 - thione - 4 ,5 - dithiolate (dmit) anionic metalcomplexes [M (dmit) $_2$]$^-$ (M = Ni^{3+} ,Pd^{3+} or Pt^{3+}) . The magnetic properties of these types of low - dimensional magnetic materials are associated with columnar crystallographic packing. More recently, we have developed a new class of [R - BzPy]$^+$ [Pt (dmit) $_2$]$^-$ salt, in which [R - BzPy]$^+$ represents aderivative of benzylpyridinium, as building blocks to construct a low - dimensional molecular solid, and have found that the topology and size of the [R - BzPy]$^+$ ion, which is related to its molecular conformation, can be modulated by systematic variation of the substituents in the aromatic rings. Therefore, the stacking pattern of these complexes can be finely tuned through controlling the molecular conformation of the [R - BzPy] $^+$ ion. This idea motivated us to prepare a series of complexes which exhibit magnetic diversity[5~8], with the goal of extending our research and under-

standing the relationship between magnetic properties and stacking structures. In this paper, [NCBzPy] Cl (1) and [NCBzPy] [Ni (dmit)$_2$] (2) were prepared and characterized.

1 was prepared by reacting 4 - cyano - benzyl chloride with 1. 5 equivalent of pyridine in refluxing acetone for 4h [white crystal, analysis (%), found (Calcd.) for $C_{13}H_{11}N_2Cl$: C, 67. 51 (67. 68) ; H, 4. 92 (4. 81) ; N, 12. 08 (12. 14)]. IR: δ= 3021 (C—H), 2225 (C≡N), 1642 (C = N) cm^{-1}. A solution of NaOMe dissolved in methanol was added to a methanol solution of dmit (COPh) $_2$. After stirring, a solution of $NiCl_2\ 6H_2O$ was added. After further stirring, a solution of 1 was added. The black precipitate was dissolved in an acetone solution of I_2. As the solution evaporated slowly, the black microcrystals 2 formed were separated, washed with acetone and dried in vacuo. Based on the experimental results, the stoichiomet ric equations are shown in Scheme 1.



Scheme 1

2. Yield : 78 %, m. p. 176 ℃～178 ℃. Elemental analysis of carbon, hydrogen and nitrogen were carried out with a model 2400 - Perkin - Elmer analyzer. Analysis(%), found (calcd.) for $C_{18}H_9N_2S_{10}Ni$: C, 34. 10 (34. 17) ; H, 1. 52 (1. 43) ; N, 4. 37(4. 43). Infrared spectrum was recorded from KBr pellets on Nicolet FT - IR A - VATAR 360 spectrometer. IR : υ= 3434～2957 (s, C - H), 2228 (sh, C ≡N), 1633(s, C = N), 1484 (m, C = C), 1347 (s, C - S), 1163 (w, C - C), 1050 (s, S - C - S), 1025 (s, C = S), 918 (w, C - S) cm^{-1}. Absorption spectra were monitored on a UV - 2401 UV - Vis spectrophotometer. Fig. 1 shows the char-

acteristic absorption peaks of the complex 2. There exist three peaks because the complex has a great π－conjugated system.

Magnetic susceptibilities of 2 was determined in the temperature range of 2 K～300 K on a MagLab system 2000 magnetometer, and the diamagnetism was corrected by Pascal's constants (1. 6 ×10 $^{-4}$emu • mol $^{-1}$). The corresponding plots of χ_m versus T and χ_m T versus T of 2 are shown in Fig. 2, where χ_m is the magnetic susceptibility per Ni (Ⅲ) unit. For 2, the calculated χ_m T at 300 K, 0. 260emu • K • mol $^{-1}$, is less than the spin—only value expected for one noninteracting s = 1/ 2 (0. 375emu • K • mol^{-1}). The χ_m T value slightly increases as the sample temperature decreases in the temperature range of 300 K～ 80 K, which shows that there exist weak ferromagnetic coupling interactions between neighbor Ni(Ⅲ) ions. The χ_m T value sharply drops below 80 K, and almost reaches zero at 2 K, these results may arise from antiferromagnetic exchange interaction competing between magnetic interchains.

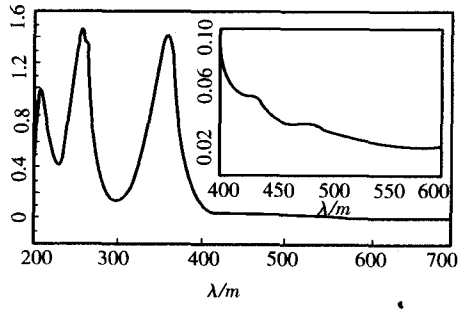


Fig. 1 UV-vis Spectra of 2

In conclusion the main goal of this work was to design molecular magnetic materials with stacking structures as mentioned in the introduction and study the relationship between magnetic properties and stacking structures. In this work a single crystal of 2 suitable for structure analysis was obtained and the relationship between magnetic properties and stacking structures was studied. The work and the relevant complexes are under investigation in our laboratory.

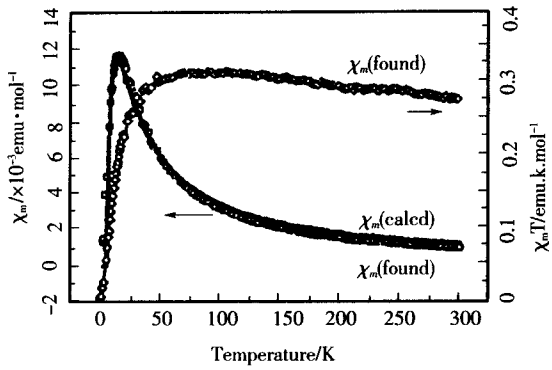


Fig. 2 The Functions of Temperature for 2

References

[1] Caneschi A, Gatteschi D, Lalioti N, et al. Cobalt (Ⅱ)-Nitronyl Nitroxide Chains as Molecular Magnetic Nanowires[J]. Angew Chem Int Ed, 2001, 40: 1760-1765.

[2] Wolf B, Zherlitsyn S, Schmidt S, Luethi B. Charge Carrier Doping in the Ni(dmit)$_2$ Simple Salts by Hydrogen-Bonding Pyridinium Cations[J]. Phys Status Solidi A, 2002, 189: 389-392.

[3] Mitsumi M, Kitamura K, Morinaga A, et al. Valence-Ordering Structures and Magnetic Behavior of Metallic MMX Chain Compounds, Kobayashi[J]. Angew Chem Int Ed, 2002, 41: 2767-2772.

[4] Lorenz T, Hofmann M, Grueninger M, et al. -Evidence for Spin-Charge Separation in Quasi-One-Dimensional Organic Conductors[J]. Nature, 2002, 418: 614-617.

[5] Liu G X, Xie J L, Ren X M, et al. 1-(2-Chlorobenzyl) pyridinium Bis(maleonitriledithiolato) Nickelate(Ⅲ)[J]. Acta Cryst, 2003, E59: m527-m529.

[6] Ren X M ,Meng Q J ,Song Y,et al . Unusual Magnetic Properties of One - Dimensional Molecule - Based Magnets Associated with a Structural Phase Transition[J] . Inorg Chem ,2002 ,41 :5686 — 5689.

[7] Xie J L ,Ren X M ,He C ,et al . Complicated Magnetic Behavior in One - Simensional Nickel (Ⅲ) Chain Complex[J] . Chem Phys Lett,2003 ,369 :41 — 43.

[8] Xie J L ,Ren X M ,Song Y,et al . Peculiar Magnetic Behavior in Ion - Pair Complex 1 -(4′- Fluoro benzyl) pyridinium] [Ni (mnt)$_2$] [J]. Chem Commun ,2002 :2346 — 2347.

Synthesis, Characterization and Magnetic Properties of Molecule - based Magnet [NCBzPy] [Ni(dmit) $_2$]

Abstract: A new substituted benzylpridiniums [NCBzPy]Cl was synthesized, futher, a molecule - based magnet [NCBzPy] [Ni (dmit) $_2$] was synthesized and characterized by elemental analysis, IR and UV spectra. Its magnetic susceptibility data has been measured in the temperature range of 2 K～300 K, and the result s indicated that there exist ferromagnetic coupling interactions between neighbor Ni (Ⅲ) ions.

Key Words: molecule - based magnet ; dmit ; synthesis ; magnetic property

本文原载于《合成化学》2004 年第 12 卷第 5 期

Self－assembly from 1D to 2D Molecular Magnets Based on $[Ni(dmit)_2]^-$ Building Blocks: Structures, Magnetic Properties and Spin Dimer Analyses

Recently, a great deal of research has been reported on conductivity and magnetic property of different types of bis－dithiolate metal complexes.[1] We focus our research interesting in the molecular magnets self－assembly from $[Ni(dmit)_2]^-$ ion, which exhibits the diversity of intermolecular interactions, such as intermolecularΠ－Π stack and side－by－side S···S interactions of $[Ni(dmit)_2]^-$ ions, so it is possible to gain the molecule－based magnets from 1D to 2D by modifying the stack structures of these types of compounds.

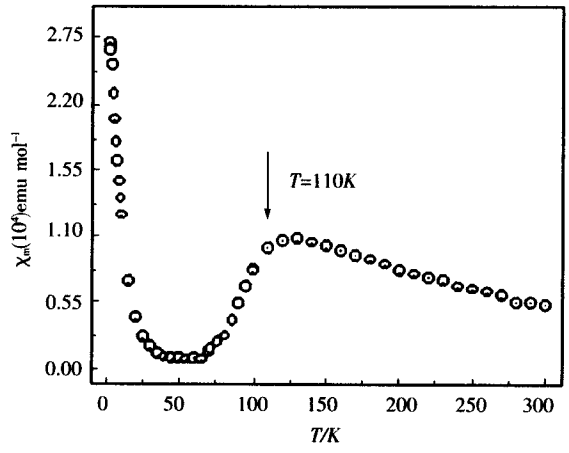


Fig. 1 plot of χm-T for 1(T_{sp} = 110K)

Two compounds, [1－(4′－R－benzyl)pyridinium][$Ni(dmit)_2$] (R = NO_2 (1) and Br (2)), reveal different stack structures and magnetic behav-

iors. $[Ni(dmit)_2]^-$ ions form a chain via side - by - side S···S interactions in 1, while a 2D structure in 2.

In conclusion, we used the counter - cation with modifiable molecular geometry to prepare two compounds based on $[Ni(dmit)_2]^-$ ions, which indicate different stack structures. The magnetic behaviors were investigated by magnetic susceptibility measurements and spin dimer analyses.

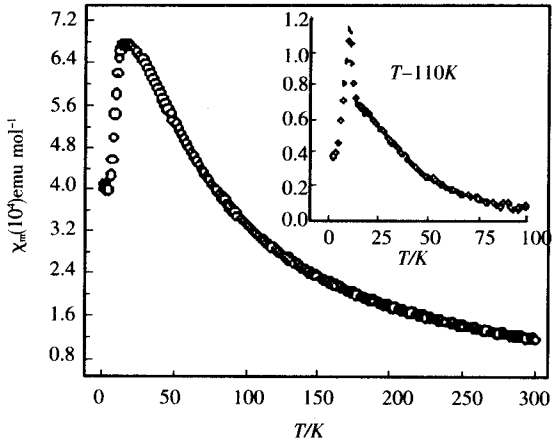


Fig. 2 plot of χm-T for 2(T_N = 10.9K)

(a) J. L. Xie, et al., Chem. Commun. 2002, 2346;

(b) A. T. Coomber, et al., Nature 1996, 380, 144;

(c) T. Autagawa, et al., Chem. Eur. J. 2001, 7, 4902.

本文原载于《日本国际学术会议(ICMM2004)论文集》

一维链状配合物[BrBzPy] [Ni(dmit)$_2$] 的合成和红外光谱研究

摘 要:合成了一种新的化合物[BrBzPy] [Ni (dmit) $_2$](1),并进行了红外光谱表征。晶体的结构结果表明它的空间点群为 $P2_1/c$,a=0.627 5(1) nm ,b= 1.743 8(3) nm,c = 2.283 9(3) nm,α = 90°,β= 9.187 (1) nm , γ = 90°,V = 2.497(7) nm^3, Z = 4,Mr = 700.57,D_C = 1.863 g · cm^{-3}。晶体中[Ni(dmit)$_2$] $^-$ 非常接近平面,共轭性相当显著,且成为一维链状结构。

主题词:Dmit ; 分子磁体; 红外光谱; 结构表征

分子磁学是近年来迅速发展的一个新兴前沿领域[1-3],它涉及化学、物理、材料和生命科学等诸多领域。自由基—金属一维链状配合物的合成和功能性研究已成为分子基材料的一个热点课题。20 世纪 80 年代中后期以来,各国科学家竞相研制分子基磁体,大大推动了分子磁学的发展[4]。由于一维配合物位于零维分子向多维聚合物过渡的结构区间,所以它兼具这两者的一些特点,如既具有扩展的磁结构体系,又保持了可溶性、可塑性和透光性等分子特性,特别是一维链状配合物还呈现出比三维磁性材料更为突出的量子力学效应。分子磁学的研究体系有多核金属配合物体系、自由基体系[5]和金属—自由基体系[6]。分子磁性理论的每一步跨越都将给材料科学、生命科学甚至计算机的发展带来革命性的影响,未来分子磁性理论的应用必将深远地影响我们的生活[7]。开发新型的非线性光学材料和优异的分子基铁电材料,特别是合成高 T_C 的分子铁磁体引起人们的关注。

1. 实验部分

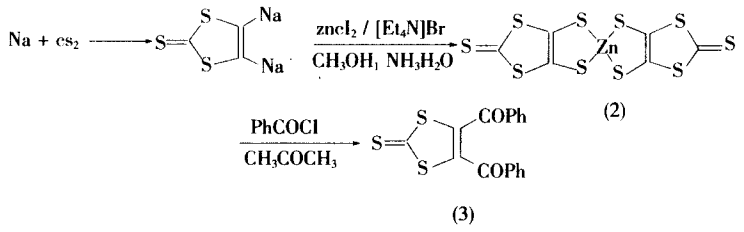
1.1 试剂和仪器

吡啶、氯化镍、无水甲醇、二硫化碳、二甲基甲酰胺、丙酮、氯仿(上海化学试剂公司),对溴苄基氯(美国),以上试剂为均为 AR 级,使用前没做进一步纯化。配合物(1)的化学组成由 PE－2400 元素分析仪确定,红外光谱使用 NicoletFTIR AVATAR 360 光谱仪,并用 KBr 压片法测定了该种配合物的红外光谱。

1.2 配合物的合成

1. $(PhCO)_2dmit$($dmit^{2-}$ = 2 - thioxo - 1,3 - dithiole - 4,5 - dithiolate)的合成[7]

配合物的合成如 Scheme 1 所示:



Scheme 1 The compound synthesis

将 DMF 滴加到 9mL CS_2 和 2g Na 组成的回流混合物中,溶液变红色,在浴温为 40℃的条件下回流 2h,加数滴绝对无水乙醇,溶液变暗红色,减压除去溶剂,用无水甲醇处理得血红色溶液,过滤,将溶液倒入一由 25mL 甲醇、25mL 氨水和 1g$ZnCl_2$ 组成的溶液中,析出红色沉淀,再加入含 2.7g [NBu_4]Br 的 12.5mL 水溶液,静置 18h,析出红色固体,过滤,用甲醇洗涤,真空干燥,得终产物为血红色固体(2)。将 35.67mL 左右 PhCOCl 边搅拌边滴加到 36.35g 化合物(2)溶于 133.76mL 丙酮经过滤得到的液体中,最终析出针状晶体,过滤得桔红色固体,用丙酮和无水甲醇洗涤至无色,真空干燥,

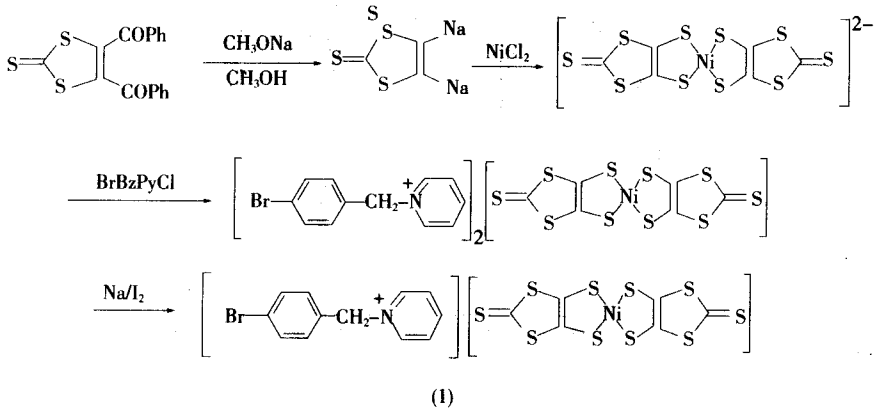
加入一定量氯仿，回流，稍冷，过滤，得棕红色液体，加入等体积的无水甲醇，析出黄色固体，再加热回流 0.5h，使固体全部溶解，冷却，放置过夜（约 18h），使之结晶，过滤，用甲醇，乙醇洗涤，得终产物桔黄色针状晶体(3)。

2. [BrBzPy]Cl(4)([BrBzPy]$^+$ =1 -(4′- Br - benzyl) Pyridinium)的合成

将 2.04g 对溴苄氯和 0.79g 吡啶溶解在 40mL 丙酮中，混合溶液回流 20min 后就有白色微晶生成，继续回流 40min，冷却后过滤，并依次用少量丙酮、无水乙醚洗涤微晶状沉淀，真空干燥后，得产物 2.29g[BrBzPy]Cl（产率 85%）。元素分析结果：C，48.55%；H，3.50%；N，5.07%。按化学式 $C_{11}H_9NClBr$ 计算的理论值：C，48.79%；H，3.33%；N，5.17%。

3. 配合物(1)的制备

制备过程见 Scheme 2 ：



(1)

Scheme 2 Preparation process

在氮气保护下，将 9 mmol CH_3ONa 和 20 mL CH_3OH 组成的溶液滴加到 2mmol $(PhCO)_2$dmit 中，搅拌 30min，溶液变成紫红色，再加入由 1mmol $NiCl_2 \cdot 6H_2O$ 和 20mL CH_3OH 组成的溶液，反应 20min，加入 2mmol BrBzPyCl，约 20min 后过滤，用甲醇洗涤，得墨绿色固体，用 60mL 丙酮溶解后，加入 Na/I_2(184/116mg)氧化溶液由墨绿色变亮绿色。自然挥发，大约需要 2 天时间即可获得适合 X 衍射分析的单晶。元素分析结果：C，48.55%；H，3.50%；N，5.07%。按化学式 $C_{11}H_9NClBr$ 计算的理论值：C，48.79%；H，3.33%；N，5.17%。

2. 结果与讨论

2.1 配合物(1)的红外光谱

配合物(1)的红外光谱[8]如图 1 所示，3 434～2 957cm^{-1}为苯环上和吡啶环上 C—H 伸缩振动，1 633cm^{-1}为吡啶环上 C=N 双键伸缩振动，1 484 cm^{-1}为苯环上和吡啶环上 C=C 双键的伸缩振动，1 163cm^{-1}为 C—C 的弯曲振动，826cm^{-1}为 C—Br 伸缩振动，1 352，918，473cm^{-1}为 C—S 伸缩振动，1 163 cm^{-1}为 C—C 伸缩振动，1 050cm^{-1}为 S—C—S 弯曲振动，1 025cm^{-1}为 C=S 双键的伸缩振动。红外光谱分析说明配合物(1)已形成[9]。

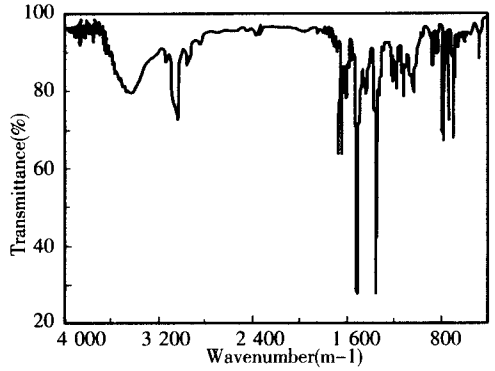


Fig. 1 Infrared spectrum of complex 1

2.2 配合物(1)的结构描述

X 射线单晶衍射显示，[BrBZPy][Ni(dmit)$_2$]为单斜晶型，Ni—S 键长在 2.1504 至 2.1707 范围内，两端的 C=S 键比典型的双键略长，其余的 C—S 键比典型的单键略短，C=C 比典型的双键略长，这种键长平均化的倾向及近完美的平面构型，说明[Ni(dmit)]$^-$具有较好的共轭性。经仔细比较，发现含 Ni 的内侧大五元环中的 C—S 键略短于不含 Ni 的外侧大五元环中的 C—S 键，图 1 中有两部分，一部分是[Ni(dmit)]$^-$阴离子，另一部分是取代的吡啶环阳离子。图 2 是标题配合物的分子结构。图 3 和图 4 是标题配合

物的晶胞堆积图，分别从 a 轴和 c 轴反映了配合物各原子之间的相互作用。阴离子形成双层堆积结构，与[NO_2BzPy][Ni(dmit)$_2$]的结构有所不同，阴离子部分形成一维链，层内不同离子间存在弱的 S—S 相互作用。图 4 是标题化合物的晶体结构，阴离子形成双层堆积结构，与[NO_2BzPy][Ni(dmit)$_2$]的结构有所不同，阴离子部分形成一维链，层内不同离子间存在弱的 S—S 相互作用。

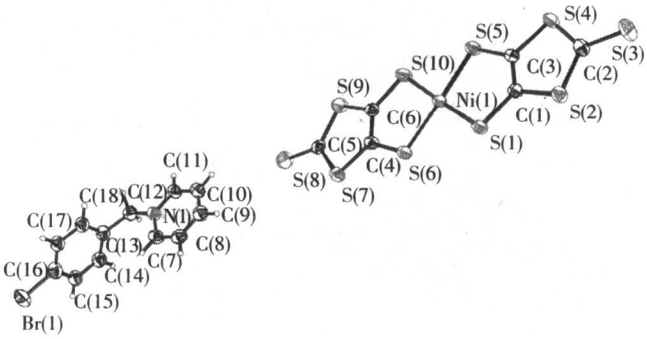


Fig. 2 Models of overlapping of [BrBzPy]$^+$ cation (left) and [Ni(dmit) 2]$^{2-}$ anion

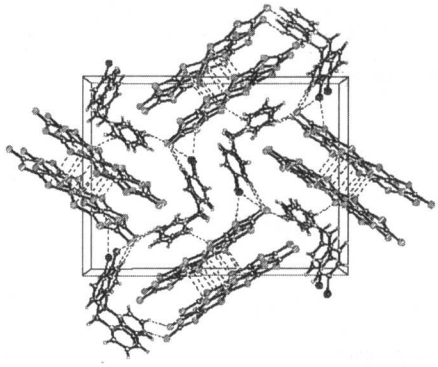


Fig. 3 Perspective view of [BrBzPy] [Ni (dmit)$_2$] down the a - axis, showing the alternating of anions and cations

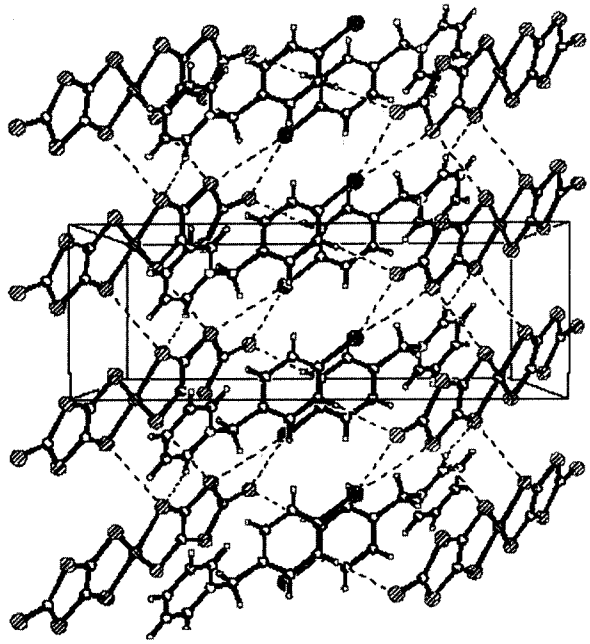


Fig. 4 Perspective view of [BrBzPy] [Ni (dmit)$_2$] down the c - axis, showing the alternating of anions and cations

综上所述，合成了一种链状配合物[BrBzPy][N(dmit)$_2$]，用元素分析和IR进行了表征，结构数据显示，该化合物阴离子部分形成了一维链状结构。化合物的导电性和磁学性质正在研究中。

参 考 文 献

[1] Kahn O. Molecular Magnetism. New York : VCH Publishers, 1993.

[2] Kahn O. Adv. Inorg. Chem. , 1996, 43 : 179.

[3] GAO En - qing, LIAO Dai - zheng(高恩庆，廖代正). Chem. J. Chin. Universities(《高等学校化学学报》), 1999, 20 : 1179.

[4] Chiarelli R, Novak M A, Russat A. Nature, 1993, 363 : 147.

[5] Kahn O. Struct . Bond. , 1987, 68 : 89.

[6] Miller J S. Inorg. Chem. ,2000,47 : 4392.

[7] DAI Yao - dong, YU Zhi (戴耀东,余智). Ziran Zazhi (《自然杂志》), 2002,24 (1) : 15.

[8] WU Xiao - yuan, ZHANG Han - hui, HUANG Chang - cang, SUN Rui - qing, YANG Qi - yu, LIN Zhi - hua (吴小园,张汉辉,黄长沧,孙瑞卿,杨齐渝,林志华). Spectroscopy and Spectral Analysis(《光谱学与光谱分析》),2004,24 (6) : 694.

[9] XIAO Li - ren, GAO Feng, TANG Jie - yuan, ZHANG Wen - gong(肖荔人,高锋,唐洁渊,章文贡). Spectroscopy and Spectral Analysis(《光谱学与光谱分析》),2004,24 (6) : 756.

Synthesis and Infrared Spectroscopic Study of 1 - D Magnetic Chain Compound Based on [BrBzPy] [Ni(dmit) $_2$]

Abstract : The synthesis and functional study of one - dimensional free radical - metal chain compound has been a hotspot task in molecule material, especially in composing high T_C molecule ferromagnet. A new compound [BrBzPy] [Ni(dmit)^2] has been prepared and characterized. The crystal structure at room temperature was determined. The crystal is triclinic with space group $P2_1/c$, a = 01627 5(1) nm , b = 11743 8(3)nm, c = 21283 9 (3) nm, $\alpha = 90°$, $\beta = 91187\ (1)°$, $\gamma = 90°$, V = 2. 497 (7) nm^3, Z = 4, Mr = 700. 57, and D_C = 11863 g · cm^{-3}. The planar $[Ni(dmit)_2]^-$ is nearly perfect, which shows that it has good conjugate characteristic and is a 1 - D magnetic chain compound.

Key Words: dmit ; molecular magnets ; infrared spectra ; structure characterization

本文原载于《光谱学与光谱分析》,2006 年第 26 卷第 1 期

Molecular spin ladders self-assembly from $[Ni(dmit)_2]^-$ building blocks: Syntheses, structures and magnetic properties

Abstract: Two ion-pair compounds, consisting of 1-(4′-R-benzyl) pyridinium ($[RBzPy]^+$, R = NO_2 (1) and Br (2)) and $[Ni(dmit)_2]^-$ ($dmit^{2-}$ = 2-thioxo-1,3-dithion-4,5-dithiolato), have been synthesized and structurally characterized. The anions of $[Ni(dmit)_2]^-$ stack into dimers, which further construct into two-leg ladder through terminal S···S interactions in 1, lateral S···S interactionsin 2. The weak H—bonding interactions of C-H···Swere observed in 2, while only weak van de Waals interactions between anion and cations in 1. The magnetic susceptibilities measured in 2-300 K indicate AFM exchange interaction domination both two compounds. A peculiar magnetic transition at —100 K was observed in 1. An AFM ordering below —11 K was found in 2, and the best fit to magnetic susceptibility above 45 K in this compound, using a dimer model with $s = 1/2$, give rise to $\Delta/k_B = 36.1$ K, $zJ = -0.91$K, $C = 3.2 \times 10^{-3}$ emu K mol^{-1} and $\chi_0 = -4.0\ 10^{-6}$ emu mol^{-1} with g of 2.0 fixed.

2005 Elsevier Ltd. All rights reserved.

Key Words: Bis(2-thioxo-1,3-dithion-4,5-dithiolato) nickelate compound; crystal structure; magnetic property; spin ladder

1. Introduction

Recently, a great deal of research has been reported on conductivity

and magnetic property of different types of bis－dithiolate metal complexes [1]. In our previous research, using benzylp－yridinium derivatives ($[RBzPy]^+$) as the counter－cation of $[M(mnt)_2]^-$ (M = Ni, Pd and Pt), a series of ion－pair compounds with segregated columnar stacks of cations and anions have been prepared [2 6]. The quasi－one－dimensional magnetic nature of these compounds was attributed to intermolecular porbital interactions within the anionic columns. Furthermore, for some compo－unds, spin－Peierls－like transition was observed[1a,4,5a]. More presently, we are devoted to our research interesting on the molecular magnets selfassembly from $[Ni(dmit)_2]^-$ ion due to its molecular and electronic structure resemble $[Ni(mnt)_2]^-$ ion, which is expected to obtain new series of molecular magnets with peculiar magnetic phase transition via incorporating the benzylpyrid－inium derivatives into $[Ni(dmit)_2]^-$ spin system. Herein, we report syntheses, crystal structures, and magneticproperties of two compounds consisting of $[Ni(dmit)_2]^-$ and benzylpyridinium derivatives.

2. Experiments

2.1 Physical measurements

Elemental analyses were performed with a Perkin－Elmer 240 analytical instrument. Magnetic susceptibility data on polycrystalline sample were collected in 2－300 K using a MagLab system 2000 magnetometer.

2.2 Syntheses of $[NO_2BzPy][Ni(dmit)_2]$ (1) and $[BrBzPy][Ni(dmit)_2]$ (2)

1 and 2 were prepared according to the procedure described in [7], elemental Anal. Calc. for $C_{18}H_{11}N_2NiO_2S_{10}$: C, 32.4; H, 1.66; N, 4.20. Found: C, 31.9; H, 1.70; N, 4.18% for 1, and Anal. Calc. for $C_{18}H_{11}BrNiS_{10}$: C, 30.9; H, 1.58; N, 2.00. Found: C, 30.7; H, 1.68; N, 1.96% for 2. The single crystals suitable for X－ray analysis were obtained by disper-

sing Et_2O into MeCN solution of 1 for one week.

2.3. X-ray crystallography

Diffraction data of 1 was collected at 293 K on a CAD4 with Mo Kα radiation. The structure of 1 was solved by direct method and refined on F^2 by full-matrix least-squares method using the SHELXTL program package[8]. All non-hydrogen atoms were refined anisotropically. Hydrogen atoms were placed in their calculated positions and refined following the riding model. Crystal data for 1: $C_{18}H_{11}N_2NiO_2S_{10}$, M = 666.60, triclinic, space group $P\bar{1}$, a = 9.3500(19)Å, b = 11.780(2)Å, c = 11.860(2)Å, α = 80.16(3)°, β = 89.52(3)°, γ = 76.04(3)°, V = 1248.3(4) Å^3, Z = 2, D_{calc} = 1.773 g cm^{-3}, μ = 1.635 mm^{-1}, final R, R_w = 0.0450, 0.1034. 3601 observed reflections [$I > 2\sigma(I)$] out of 4370 unique (R_{int} = 0.0154), GOF = 0.984.

3. Results and discussion

3.1 Descriptions of crystal structures

1. $[NO_2BzPy][Ni(dmit)_2]$ (1)

The ORTEP view of 1 in an asymmetric unit and the packing structure projected along c-axis are shown in Fig. 1(a) and (b). The bond lengths and angles in $[Ni(dmit)_2]^-$ anionic moiety are in good agreement with the reported compounds[1d]. The bond lengths in $[NO_2BzPy]^+$ moiety are close to the values in $[NO_2BzPy][Ni(mnt)_2]$ [4], and the dihedral angles between aromatic rings and the reference plane, C(13)/C(12)/N(1), are 67.0° for benzene ring, 88.2° for pyridine ring, respectively.

Two neighboring anions, which molecular planes are approximately perpendicular to a-axis, stack plane-to-plane with each other to form a dimer, the inter-planar distance (the anionic molecular plane is defined by

coordination S atoms) is 3.72Å, the nearest S···S contacts are 3.69Å between S(3) and S(10)^{i}, 3.74Å between S(2) and S(8)^{i} (symmetry code: i = 1 − x, 1 − y, 1 − z).

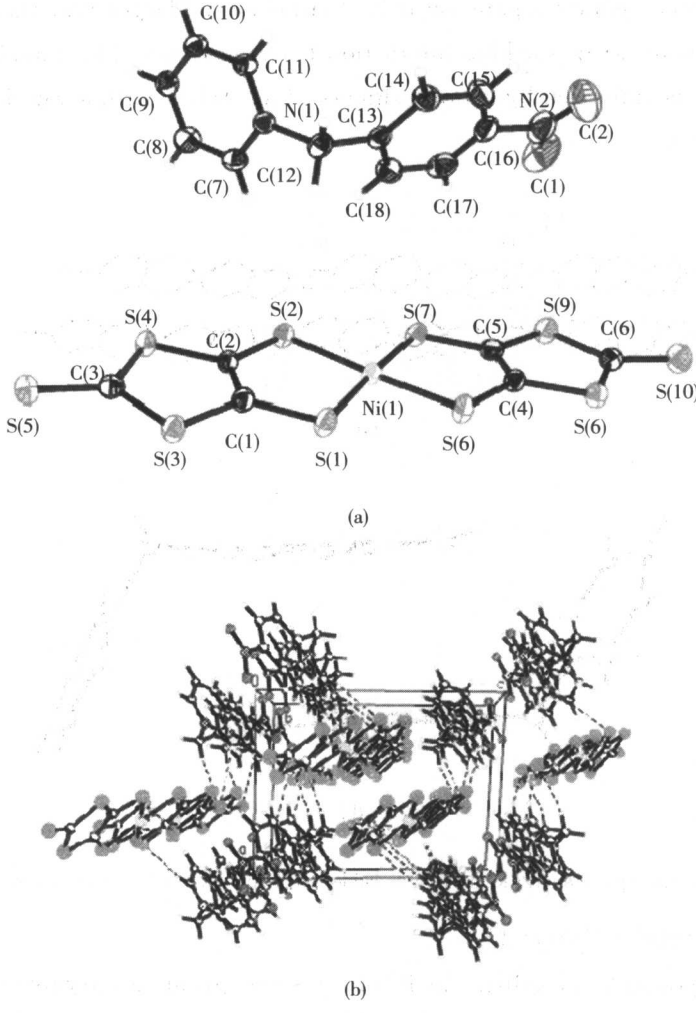


Fig. 1. (a) ORTEP drawing of 1 with 30% possibility ellipsoids and (b) the packing structure projected along c - axis

This dimer develops further into two - leg ladder via terminal S···S interactions along b - axis [the shorter S···S separations are S(10)···S(4)j =

3.52Å, S(8)···S(4)^{j} = 3.38Å, S(8)···S(5)^{j} = 3.69 Å (symmetry code: j = x, 1 + y, z)] (cf. Fig. 2(a)). Two neighboring[NO_2BzPy]$^+$ cations dimerize in a fashion of a chair - like conformation as illustration in Fig. 2(b). These distances of center - to - center between two benzene rings is 4.50 and the inter - planar separation is 3.59, they are so larger that there is no any significant π···π stacking interaction between them. The anionic two - leg ladder is embraced by cationic dimers (Fig. 1(b)) with a van de Waals interactions.

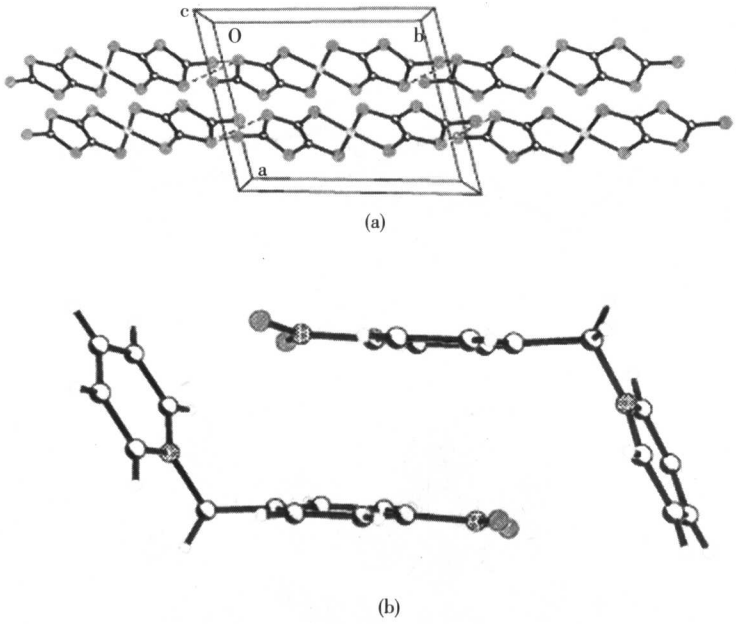


Fig. 2. (a) Spin ladder(the diction of ladder leg is parallel to b-axis of cation in 1)

2. [BrBzPy][Ni(dmit)$_2$] (2) [7]

Compound 2 crystallizes in P2(1)/c space group, an asymmetric unit contains a couple of anion and cation. The bond parameters in anion moiety are very similar to that in 1, and those in [BrBzPy]$^+$ moiety are closed to the values in [BrBzPy][Ni(mnt)$_2$] [4]. Compared with 1, the Molecular geometry of [BrBzPy]$^+$ exhibits distinct difference from [NO_2BzPy]$^+$. The dihedral angles between aromatic rings and the reference plane, C(13)/C

(12)/N(1), are 106.3° for benzene ring, 160.5° for pyridine ring, which are departures far from 90°. Two adjacent anions are eclipsed to overlap as a dimer as in 1, whereas the correspondence inter-atomic separations and inter-playnar distance are much less than that in 1 [Ni(1)···Ni(1)^{i} of 3.51Å, S(1)···S(10)^{i} of 3.57Å, S(5)···S(6)^{i} of 3.49Å (symmetry code: i = −x, 1 − y, − z) and the inter−plane distance of 3.49Å]. The lateral S···S interactions between neighboring anionic dimmers lead them to form a two−leg ladder (Fig. 3(a)). Two−leg ladders are held together by intermediate cations via non−normal C H···S H−bonding interactions to construct into 3D network (Fig. 3(b)) [7].

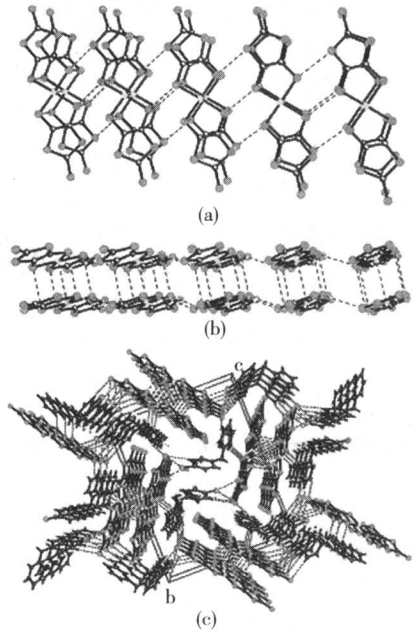


Fig. 3. (a) and (b) Spin ladder of $[Ni(dmit)_2]^-$ anions viewed along different directions (c) molecular packing diagram projected along a−axis in 2.

3.2 Magnetic properties

The temperature dependences of magnetic susceptibility for 1 and 2 are shown in Figs. 4 and 5. With respect to 1, χ_m increases slowly as temperature goes down, and drops sharply below ~110 K to reveal a magnetic tran-

sition, the transition temperature is determined as 100.3 K in plot of d ($\chi_m T$)/dT versus T (inset of Fig. 4). Above 110 K, AFM exchange interaction between neighboring spins dominates. Below 110 K, χ_m drops exponentially as temperature decreases to illustrate there is a spin energy gap in low - temperature phase. A paramagnetic Curie tail in low temperature region is attributed to the magnetic impurities of uncoupled spins. Based on crystal structural analysis, we try to fit magnetic susceptibility data in high - temperature phase by the exchange model, an isolated spin dimmer of s = 1/2 or a spin ladder in high temperature limit, but all efforts fail.

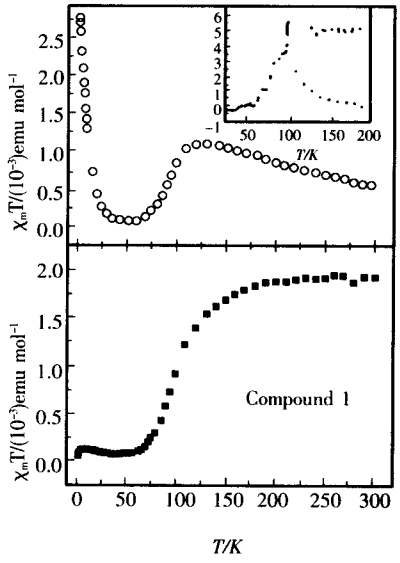


Fig. 4. Plots of χ_m- Tand $\chi_m T$-T of 1($T_\varphi \approx 100.3$k)

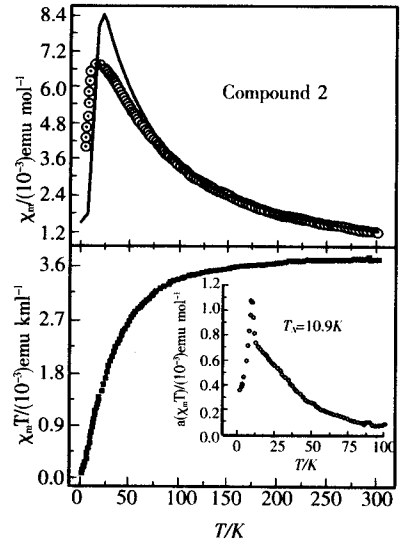


Fig. 5. χ_m- Tand $\chi_m T$- of 2 as a function of T($T_N \approx 10.9$k), open circle (χ_m); experiment data; solid line (χ_m); theoretically reproduced with the fit parameters.

The magnetic susceptibility of 2 increases as temperature deceases, and reaches a maximum with $\chi_m = 6.73 \times 10^{-3}$ emu mol^{-1} at 16.5 K, and then abruptly drops to indicate the character of antiferro magnetic ordering. Theoretically, the long - range magnetic ordering cannot occur in a 1D magnetic system, as for 2, the weak H - bonding interactions to connect spin ladders and cations into 3D network were observed, which provide the possible magnetic exchange paths between spin ladders to lead to long - range

magnetic ordering [5b,9]. The χ_m value of 4.07×10^{-3} emu mol^{-1} at 2 K is somewhat less than 2/3 the value at the temperature at which it is a maximum. TN is estimated as 10.9 K corresponding to the peak temperature in plot of $d(\chi_m T)/dT - T$ (inset of Fig. 4). From the viewpoint of structure, the magnetic coupled interaction is much larger within a dimmer than between dimers, the formula of χ_m, thereby, in paramagnetic phase can be expressed below:

$$\chi_m = \frac{\chi_{dimer}}{[1-(zJ'/Ng_2\beta^2)\chi_{dimer}]} + \frac{C}{T} + \chi_0 \qquad (1)$$

and

$$\chi_{dimer} = \frac{Ng^2\pi\mu_B^2}{k_BT} \cdot (3+\exp(\triangle/k_BT))^{-1} \qquad (2)$$

in Eq. (1), the first term is a contribution from a dimer of s = 1/2 based on spin Hamiltonian $H = -2J\hat{S}_1 \cdot \hat{S}_2$, in which $\triangle$ ($=2|J|$) is the energy gap between singlet and triplet spin state, and the coupled interaction between neighboring dimers is further treated using molecular field theory [10]. C/T and χ_o show the contribution from the magnetic impurity and the sum of diamagnetic and possible van Vleck paramagnetic parts, respectively. The best fit magnetic susceptibility above 45 K to Eq. (1) gives rise to $\triangle/k_B = 36.1$ K, $zJ = -0.91$ K, $C = 3.2\times10^{-3}$ emu K mol^{-1} and $\chi_m = -4.0\times10^{-6}$ emu mol^{-1} with g of 2.0 fixed.

4. Conclusion and remarks

Summarily, we have represented the crystal structural and magnetic susceptibility characterri zation for two compounds consisting of $[Ni(dmit)_2]^-$ and benzylpyridinium derivative. The anions in two compounds stack into dimers, and these dimers further construct into two - leg ladders viaterminal S···S interactions in 1, and by lateral S···S interactions in 2. The two—leg ladders are held together by cations through weak H—bonding interactions of C - H···S in 2, while only weak van de Waals interactions are present in 1. The $\chi_m(T)$ in 2 - 300K indicated that AFM exchange in-

teractions dominate both 1 and 2. A spin－Peierls－like transition occurs in 1 at ～100 K. An AFM ordering below－11 K was found in 2, and its magnetic behavior in paramagnetic phase can be demonstrated as a spin dimer of $s = 1/2$. In order to clarify the nature of the peculiar magnetic transition in 1 and AFM ordering in 2, further structural determination in low－temperature phase and DSC/Cp measurements around the transition temperature for 1, and AC magnetic susceptibility measurement for 2 are in progress.

Acknowledgement

This project was financially supported from the National Natural Science Foundation of China (Grant Nos. 20171001 and 20371002).

Appendix A. Supplementary data

Crystallographic data (excluding structure factors) for the structures reported in this paper have been deposited with the Cambridge Crystallographic Data Center as supplementary publications (CCDC－250087 of 1). Copies of the data can be obtained free of charge on application to CCDC, 12 Union Road, Cambridge CB21EZ, UK (fax: +44 1223 336 033; e-mail: deposit@ccdc.cam.ac.uk) or on the web http://www.ccdc.cam.ac.uk). Supplementary data associated with this article can be found, in the online version at doi:10.1016/j.poly.2005.03.082.

References

[1] (a) J. L. Xie, X. M. Ren, Y. Song, W. W. Zhang, W. L. Liu, C. He, Q. J. Meng, Chem. Commun. 2346 (2002);
(b) A. T. Coomber, D. Beljonne, R. H. Friend, J. L. Bre′das, A. Charlton, N. Robertson, A. E. Underhill, M. Kurmoo, P. Day, Nature 380 (1996) 144;

(c) I. D. Parker, R. H. Friend, P. I. Clemenson, A. E. Underhill, Nature 324 (1986) 547;
(d) T. Autagawa, T. Hasegawa, T. Nakamura, T. Inabe, J. Am. Chem. Soc. 124 (2002) 8903.

[2] X. M. Ren, C. S. Lu, Y. J. Liu, H. Z. Zhu, H. F. Li, C. J. Hu, Q. J. Meng, Trans. Met. Chem. 26 (2001) 136.

[3] X. M. Ren, H. Okudera, R. K. Kremer, Y. Song, H. Cheng, Q. J. Meng, P. H. Wu, Inorg. Chem. 43 (2004) 2569.

[4] X. M. Ren, Q. M. Meng, Y. Song, C. S. Lu, C. J. Hu, Inorg. Chem. 41 (2002) 5686.

[5] (a) J. L. Xie, X. M. Ren, C. He, Z. M. Gao, Y. Song, Q. J. Meng, R. K. Kremer, Chem. Phys. Lett. 369 (2003) 41;
(b) J. L. Xie, X. M. Ren, Y. Song, Y. Zou, Q. J. Meng, J. Chem. Soc., Dalton Trans. 2868 (2002);
(c) J. L. Xie, X. M. Ren, S. Gao, W. W. Zhang, Y. Z. Li, C. S. Lu, C. L. Ni, W. L. Liu, Q. J. Meng, Y. G. Yao, Eur. J. Inorg. Chem. 2393 (2003).

[6] X. M. Ren, H. Okudera, J. L. Xie, Q. J. Meng, J. Mol. Struct. 733 (2005) 119.

[7] W. J. Tong, L. Liu, Q. J. Meng, Y. Z. Li, Acta Cryst. E 58 (2002) m724.

[8] G. M. Sheldrick, SHELXTL, Structure Determination Softwareprograms, Version 5.10. Bruker Analytical X－ray Systems Inc., Madison, WI, USA, 1997.

[9] X. M. Ren, Y. C. Chen, C. He, S. Gao, J. C. S. Dalton Trans. 3915 (2002).

[10] C. J. O_Connor, Prog. Inorg. Chem. 29 (1982) 203.

本文原载于 Polyhedron(《多面体》)杂志 2005 第 24 期 2269－2273